Molecular mechanisms of cellular dysfunction caused by a tauopathy-associated fragment

Dakkak, Dina

Awarding institution:
King's College London

Molecular mechanisms of cellular dysfunction caused by a tauopathy-associated fragment

Dina Dakkak

This thesis is submitted in fulfilment of the degree of

Doctor of Philosophy

Department of Basic and Clinical Neuroscience
King's College London
Institute of Psychiatry, Psychology and Neuroscience

Declaration

I hereby declare that, with the exception of Figure 4-1, all of the work presented in this thesis is my own.

Dina Dakkak
July 2018

Publications arising from this thesis

Guo, T., Dakkak, D., Rodriguez-Martin, T., Noble, W., & Hanger, D. P. (2019). A pathogenic tau fragment compromises microtubules, disrupts insulin signaling and induces the unfolded protein response. *Acta Neuropatho. Commun.*, *7*(1), 2.

Acknowledgments

This thesis, along with my entire PhD journey, has been the most significant undertaking of my career, and I could not have made it through without the help and support of my family, mentors and friends.

My entire family has been the best support system and I don't know how to begin to thank them. To my incredibly nurturing mother, who has always put our happiness and wellbeing above her own, thank you for constantly pushing me to pursue my career and go after what I want no matter what. You were always there to console me when times were really tough, and I could not be more appreciative. To my father, my rock, you have taught me from a very young age the importance of education and working hard, and I could not have made it through this PhD without your advice, love and support. To my sister and brother, thank you for being there when I needed to vent my frustrations and for always being my number one cheerleaders.

I would like to thank both of my supervisors for shaping me into the scientist that I am today. To my first supervisor Diane Hanger, it was a great pleasure and opportunity to work in your laboratory. Thank you for the great deal you have taught me, for being incredibly understanding, and for encouraging me to keep going and not get disheartened when experiments didn't go according to plan! To my second supervisor, Wendy Noble, thank you for all of your advice and contributions throughout the three years and for reminding me (particularly towards the end) that there is a light at the end of the tunnel.

A huge thank you to Patricia Gomez Suaga, who has been a remarkable mentor and has taught me a lot about autophagy. Her perspective and feedback on my work has helped me (and my thesis) come a long way. I would also like to thank Tong Guo on his continuous input and contributions to my work and for always encouraging me to think outside the box and for pushing me to pursue hypotheses I was sceptical about. In addition I would like to thank Maria Jimenez Sanchez on all of her contributions and advice on my work.

I would not have made it through this PhD without my two lab mums Beatriz Gomez Perez-Nievas and Elizabeth Glennon. Thank you both for teaching me a lot of what I know

in the lab and for constantly giving me advice on my career and life in general. I will really miss our very dramatic chats!

I would additionally like to acknowledge George Chennell, Dawn Lau, Gabor Morotz, Sebastien Paillusson and Aurelio Vazquez de la Torre Cervera, for their help around the lab. A big thank you to Rebecca Gresham for being the most incredible lab manager, in spite of me often forgetting to wear my lab coat! Thank you to all past and present members of Team Tau.

Throughout my PhD I supervised two BSc students, Damandeep Rathore and Matthew Worssam, and one MSc student, Kanwal Ahmed. I would like to thank all of my students for their help; it was a great privilege to supervise all three of them.

This PhD has allowed me to gain the most supportive group of friends. Natalia Yankova, Sarah Freckleton and Chun Hao Wong, thank you all for being there for me whenever I needed you and for making our times in the lab much more entertaining and memorable. I will greatly miss our binge eating sessions and tea breaks in the meeting room. I would additionally like to acknowledge Sarah Freckleton for proof reading some of my chapters.

Finally I would like to thank some of my other friends, Aizza Malik, Liane Al Baba, Rawan Jaber and Nidaa Alataba for always cheering me on and for consoling me when I needed it.

Abstract

Tauopathies are a group of neurodegenerative diseases characterised by cognitive and motor dysfunction, and pathological aggregates of abnormally phosphorylated and cleaved tau, a microtubule associated protein. Whilst the cause of these pathological changes is unknown, it is likely to be a combination of toxic gain-of-function acquired by aggregated tau, along with a loss of normal function of tau. This laboratory previously identified a form of cleaved tau (Tau35) in post-mortem human tauopathy brain and has developed animal and cell models expressing Tau35 to investigate molecular mechanism underlying tauopathy. These models include a transgenic mouse expressing Tau35 in low amounts, and Chinese hamster ovary (CHO) cells stably expressing Tau35 (CHO-Tau35) or full-length human tau (CHO-FL). This thesis aims to determine how Tau35 affects molecular mechanisms involved in tau metabolism, including the unfolded protein response (UPR) and autophagic/lysosomal degradation.

In aged Tau35 mice, there was evidence of a toxic gain of function, including increased tau phosphorylation at disease-relevant epitopes in multiple brain regions. In addition, Tau35 mice exhibit activation of the UPR in specific brain regions. In CHO-Tau35 cells, a significant reduction in basal autophagy was identified, which was not apparent in either untransfected CHO cells or in CHO-FL cells expressing full-length tau, suggesting that Tau35 expression results in defective autophagy. Under conditions that stimulate autophagy, CHO-Tau35 cells exhibited a reduced capacity to activate mTOR-mediated autophagy and reduced autophagic flux. Conversely, expression of Tau35 promoted activation of autophagy through an mTOR-independent mechanism. Furthermore, inhibition of glycogen synthase kinase-3 rescued the defective autophagy in CHO-Tau35 cells. Notably, CHO-Tau35 cells exhibited a reduction in the number of lysosomes, as well as defective lysosomal functionality and a deficit in lysosome biogenesis compared to CHO-FL and untransfected CHO cells.

Taken together, these findings suggest novel mechanisms through which the presence of Tau35, a tau fragment associated with the development of human tauopathy, exerts a detrimental effect on cells and provides insights into the significance of protein degradation systems in the development of tauopathy.

Table of Contents

List of abbreviations

Abbreviation	Definition
3-MA	3-Methyladenine
AD	Alzheimer's disease
AEP	Asparagine endopeptidase
ALS	Amyotrophic lateral sclerosis
AMBRA	Activating molecule in BECN1-regulated autophagy protein
AMPK	AMP-activated protein kinase
ANOVA	Analysis of variation
ApoE4	Apolipoprotein E4
APP	Amyloid precursor protein
APS	Ammonium persulfate
ATF4	Activating transcription factor 4
ATF6	Activating transcription factor 6
Atg1	Autophagy related protein 1
Atg10	Autophagy related protein 10
Atg101	Autophagy related protein 101
Atg12	Autophagy related protein 12
Atg13	Autophagy related protein 13
Atg14	Autophagy related protein 14
Atg3	Autophagy related protein 3
Atg4	Autophagy related protein 4
Atg5	Autophagy related protein 5
Atg7	Autophagy related protein 7
Atg8	Autophagy related protein 8
Atg9	Autophagy related protein 9
Aβ42	Amyloid beta peptide (42 amino acids)
BACE1	Beta-site APP-cleaving enzyme 1
BCA	Bicinchoninic acid
Bcl-2	B cell lymphoma 2
Bcl-XL	B cell lymphoma XL

Abbreviation	Definition
3-MA	3-Methyladenine
Bin1	Bridging integrator-1
BiP	Binding immunoglobulin protein
BME	Beta mercaptoethanol
BODIPY	Dipyrromethene boron difluoride
BSA	Bovine Serum Albumin
CaMK	Ca^{2+}-calmodulin dependent protein kinase
CBD	Corticobasal degeneration
Cdk5	Cyclin dependent kinase 5
cDNA	Complementary deoxyribonucleic Acid
CHO	Chinese hamster ovary
CHOP	CCAT-enhancer binding-proteins homologous protein
CK1	Casein kinase 1
CLEAR	Coordinated lysosomal expression and regulation
CMA	Chaperone mediated autophagy
CNS	Central nervous system
CO_2	Carbon dioxide
CSF	Cerebrospinal fluid
DAPK	Death-associated protein kinase
DMSO	Dimethyl sulfoxide
DNA	Deoxyribonucleic Acid
DTT	1,4 Dithiothreitol
EDTA	Ethylenediaminetetraacetic Acid
EGFP	Enhanced Green Fluorescent Protein
EGTA	Ethylene Glycol Bisoxyethylenenitrilo)tetraacetic acid
eIF2α	Eukaryotic initiation factor 2 α
ER	Endoplasmic Reticulum
ERK	Extracellular Signal-Regulated Kinase
ESLB	Extra strong lysis buffer
FACS	Fluorescence-Activated Cell Sorting
FAK	Focal Adhesion Kinase

Abbreviation	Definition
3-MA	3-Methyladenine
FBS	Fetal Bovine Serum
FIP200	FAK family kinase-interacting protein of 200
FL	Full length
FSC	Forware scatter
FTDP-17	Frontotemporal dementia and parkinsonism linked to chromosome 17
FTLD	Frontotemporal lobar degeneration
GAPDH	Glyceraldehyde 3-phosphate dehydrogenase
GFP	Green Fluorescent Protein
GM1	Monosialotetrahexosylganglioside
GSK3 α/β	Glycogen synthase kinase 3 α/β
H3	Histone 3
HBSS	Hanks' Balanced Salt Solution
HD	Huntington's disease
HEK293	Human embryonic kidney 293
HEPES	N-2-Hydroxyethylpiperazine-N'-2-Ethanesulfonic acid
HOPs	Homotypic fusion and vacuolar sorting
HPRT	Hypoxanthine phosphoribosyltransferase
ICC	Immunocytochemistry
IRE1	Inositol-requiring enzyme 1
JNK	C-Jun N-terminal kinase
KDa	Kilodalton
LAMP	Lysosome-associated membrane protein
LB	Luria-Bertani broth
LBPA	Lysobisphosphaditic acid
LC3	Microtubule-associated protein 1 light-chain 3
LRRK2	Leucine rich repeat kinase 2
LSD	Lysosomal storage disorder
MAP	Mitogen Activated Protein
MAPK	Mitogen-Activated Protein Kinase

Abbreviation	Definition
3-MA	3-Methyladenine
MAPT	Microtubule-associated protein tau
MCOLN1	Mucolipin subfamily, member 1
MEK	Methyl Ethyl Ketone (Butanone)
MHC	Major Histocompatibility Complex
miRNA	Micro RNA
mRNA	Messenger RNA
MT	Microtubule
MTB	Microtubule binding
mTOR	Mammalian target of rapamycin
mTORC1	Mammalian target of rapamycin complex 1
N_2	Nitrogen
NAADP	Nicotinic acid adenine dinucleotide phosphate,
NaCl	Sodium chloride
NaF	Sodium fluoride
NBR1	Neighbor of BRCA1 gene
NCLs	Neuronal ceroid lipofuscinoses
NFT	Neurofibrillary tangle
NIH	National Institute of Health
NPC	Nuclear pore complex
P62/SQSTM1	Sequestosome 1
p70S6	Ribosomal protein S6
p70S6K	Ribosomal protein S6 kinase beta-1
PBS	Phosphate Buffered Saline
PCR	Polymerase Chain Reaction
PD	Parkinson's disease
PE	Phosphatidylethanolamine
PFA	Paraformaldehyde
PHF	Paired helical filament
PI3K	Phosphatidylinositol 3-Kinase
PiD	Pick's disease

Abbreviation	Definition
3-MA	3-Methyladenine
PKA	Protein kinase A
PKB	Protein kinase B
PKC	Protein kinase C
PKR	Protein kinase RNA
PP1	Protein phosphatase 1-induced
PS1	Presenilin 1
PSA	puromycin-sensitive aminopeptidase
PSP	Progressive supranuclear palsy
PTEN	Phosphatase And Tensin Homolog (Mutated In Multiple Advanced Cancers 1)
PTP	Protein Tyrosine Phosphatase
Rab5	Ras related protein 5
Rab7	Ras related protein 7
RFP	Red fluorescent protein
RNA	Ribonucleic Acid
SAPK	Stress-Activated Protein Kinase
SDS	Sodium dodecyl sulphate
SEM	Standard error of mean
SH3	Src Homology 3
SNAP	synaptosomal associate protein
SNARE	Soluble N-ethylmaleimide-sensitive factor attachment protein receptor
SSC	Side scatter
TAE	Tris base, acetic acid and EDTA
TAOK	Thousand-and-one amino acid kinases
TBS	Tris-buffered saline
TDP-43	TAR DNA-binding protein 43
TEMED	N,N,N’,N’tetramethylethylendiamine
TFEB	Transcription factor EB
TNF	Tumor Necrosis Factor

Abbreviation	Definition
3-MA	3-Methyladenine
TOR	Target of rapamycin
TPK	Tau protein kinase
TRAIL	Tumor Necrosis Factor Related Apoptosis Inducing Ligand
TRPM2	Transient receptor potential
UHP	Ultra high purity
ULK1	Unc-51 like autophagy activating kinase
UPR	Unfolded protein response
UPS	Ubiquitin-proteasome system
UV	Ultraviolet
UVRAG	UV radiation resistance-associated gene protein
V-ATPase	Vacuolar H+ ATPase
VEGF	Vascular Endothelial Growth Factor
VPS	Vesicular protein sorting
WB	Western blot
WT	Wild-type
XBP1	X-box binding protein 1

List of figures

List of tables

Chapter 1 Introduction

1.1 Tau gene and protein

Human tau is a microtubule-associated protein encoded by the *MAPT* gene located on chromosome 17 (17q21). *MAPT* consists of 16 exons, although exons 0 and 14 are transcribed but not translated. *MAPT* pre-RNA is differentially spliced in a manner correlating with stages of neuronal maturation and neuronal types (see below) (Wang et al., 2007).

Tau has an N-terminal acidic projection domain that, when is bound to microtubules, extends from the surface of the microtubule and a C-terminal domain encoded by exons 9 to 13, which contains the microtubule-binding region of tau (Goedert and Jakes, 1990). In human brain, alternative splicing of tau mRNA at exons 2 and 3 (in the N-terminal region) and exon 10 (in the C-terminal half of tau) gives rise to six different tau isoforms. Differential splicing of exons 2 and 3 leads to 2N tau isoforms being under-represented (9% of total human CNS tau), unlike 0N and 1N tau (comprising 37% and 54% of human CNS tau, respectively). (Goedert and Jakes, 1990). These tau isoforms differ from one another by the presence or absence of a 29- or 58-amino acid insert at the N-terminus of the protein. Isoforms containing 0, 1 (encoded by exon 2) or 2 (encoded by exons 2 and 3) inserts are termed 0N, 1N and 2N, respectively. Another difference between the tau isoforms is the inclusion or exclusion of a 31-amino acid microtubule-binding repeat sequence encoded by exon 10. Exclusion of the sequence encoded by exon 10 gives rise to tau isoforms (3R) bearing three microtubule binding repeats (MTBs), whereas the inclusion of the sequence leads to the expression of isoforms with four MTBs (4R) (Panda et al., 2003; Wray et al., 2008) (Figure 1-1). In healthy individuals, 3R and 4R tau isoforms are present in an approximately equal ratio. Tau is predominantly found in neurons. It is present at much lower levels in glia and in interstitial fluid, and barely detectable amounts in astrocytes and oligodendrocytes (Goedert, 2004; Wang and Mandelkow, 2016).

Tau expression is developmentally regulated. The shortest tau isoform (0N3R) comprising 352 amino acids, is expressed early in development and also in adult human brain. However, 4R tau isoforms are expressed solely in adult brain. The 0N3R tau isoform has a

molecular weight of 48 kDa on SDS-PAGE while the longest tau isoform, 2N4R, comprising 441 amino acids runs at 67 kDa (Crowther et al., 1989; Lee, 2001). 2N4R tau contains 80 Ser or Thr residues, 56 negatively charged acidic (Asp or Glu) residues, 58 positively charged basic (Lys or Arg) residues and 8 aromatic (5 Tyr and 3 Phe) residues (Wang and Mandelkow, 2016).

Within adult neurons, tau is found primarily in axons, with barely detectable amounts present in dendrites and nuclei (Forman et al., 2004; Wray et al., 2008). However, in young neurons, tau is found to be more evenly distributed between the neurites and cell body (Papasozomenos and Binder, 1987; Sultan et al., 2011). The relative proportions of tau isoforms present in different brain regions differs between animal species. For instance, in humans the amount of 0N3R tau is lower in the cerebellum than it is in other brain regions (Boutajangout et al., 2004; Trabzuni et al., 2012). In addition, murine 3R tau isoforms are only transiently expressed in the neurons of foetal and new-born mice. On the other hand, in adult mouse brain, the three isoforms of 4R tau are almost exclusively expressed (Kosik et al., 1989).

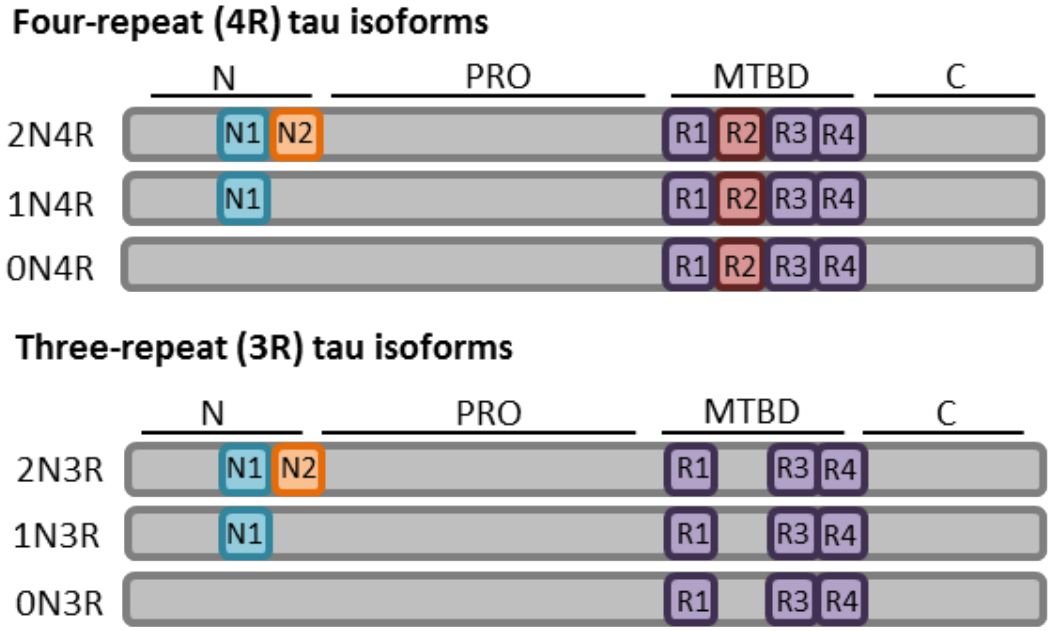

Figure 1-1 Domains of tau protein and alternative splicing in the human CNS: The six human brain tau isoforms are generated through alternative splicing of exons 2, 3 and 10. These tau isoforms differ according to the presence of 0, 1 or 2 amino-terminal inserts (0N, 1N or 2N, respectively) and the presence of microtubule-binding repeat R2, encoded by exon 10, yielding 3 or 4 carboxy-terminal repeat domain (3R or 4R, respectively) tau species (adapted from (Guo et al., 2017)).

1.1.1 **Relating tau structure to its functions**

Tau is hydrophilic and is found as an unfolded protein in its native state and is stable under acidic conditions and at high temperatures. However in solution, tau shows a preference to adopt a paperclip-like conformation, in which the N-terminal, C-terminal and the repeat domains all approach each other (Jeganathan et al., 2006). Tau is overall a basic protein, however, the ~120 N-terminal residues are predominantly acidic, and the ~40-residue C terminus has an overall neutral charge (Goedert and Jakes, 1990). Tau has four distinct domains: an acidic projection region towards the N-terminus; a proline-rich region in the centre of the molecule; a microtubule-binding region, which contains either three or four carboxy-terminal repeat domains which facilitates the binding between microtubules and

the C-terminal tail (Figure 1-1) (Mandelkow et al., 1996). All of these structural features are vital for tau to carry out its proper function. Tau is known to be bound to microtubules and stimulate microtubule assembly in cell-free reactions (Shahani and Brandt, 2002). Studies have demonstrated that tau is capable of promoting microtubule nucleation, growth, and bundling (Shahani and Brandt, 2002), as well as greatly reducing the dynamic instability of microtubules (Shahani and Brandt, 2002).

The N-terminal domain of tau projects away from microtubules, allowing tau to bind to other components in the cell. The N-terminal region of tau can interact with cell membranes. This region of tau is involved in regulating microtubule dynamics, the attachment and/or spacing between microtubules and other cell components, without binding to microtubules directly (Chen et al., 1992). For example, N-terminally truncated tau fragments showed altered microtubule interactions, even in the presence of an intact microtubule binding domain (Matsumoto et al., 2015). The N-terminal portion of tau additionally binds to the C terminus of the p150 subunit of the dynactin complex. This promotes the association of the microtubule motor dynein with membranous cargoes such as organelles (Magnani et al., 2007). Much remains unknown regarding the specific functions of the N-terminal inserts in tau, although these sequences appear to influence the distribution of tau because 0N, 1N, and 2N tau isoforms each show distinct subcellular localisations in mouse brain (Magnani et al., 2007).

The proline-rich domain of tau harbours seven Pro-XX-Pro (PXXP) motifs, providing potential recognition sites for Src homology-3 (SH3)-containing proteins including the Src family of protein kinases, such as Lck, Fgr, and Fyn, bridging integrator 1 (Bin1), the p85α regulatory subunit of phosphatidylinositol 3-kinase (PI3K). This domain also serves additional functions including regulating actin binding and the assembly of microtubules (He et al., 2009), as well as being a key DNA and RNA interacting site, which may explain the presence of tau in the nucleus (Bukar Maina et al., 2016).

Very little is known about the function of the C-terminal region of tau, However, a few studies suggest that changes within this region such as phosphorylation might have an impact on the other domains of tau, thereby influencing their interactions with other

proteins and their availability for phosphorylation (Connell et al., 2001); Reynolds et al, 2008).

1.1.2 **Functions of axonal, dendritic and nuclear tau**

In the axon, tau interacts with microtubules via its repeat-domain and flanking regions. Tau is therefore able to act as a stabiliser of microtubules, as well as a regulator of the dynamic instability of microtubules that leads to the reorganisation of the cytoskeleton (David et al., 2002; Davies et al., 1997). Once tau is bound to microtubules, it can form a local hairpin conformation through the interaction of residues 269-284 and 300-310, which contain the hexapeptide motifs ^{273}VQINK^{280} and ^{306}VQIVYK^{311} (Bhaskar et al., 2005). These two motifs are vital for tau aggregation, thereby implying that the stability of microtubules delays the aggregation of tau. Tau can additionally influence the function of motor proteins dynein and kinesin. Dynein functions as a retrograde transporter moving cargoes towards the cell body, whereas kinesin transports cargoes in an anterograde direction towards axon terminals (de Barreda and Avila, 2010). Tau has an inhibitory effect on both of these proteins by competing with them and binding to microtubules, slowing anterograde and retrograde axonal transport (de Barreda and Avila, 2010). This inhibition of transport leads to the build-up of multiple cargoes such as mitochondria. In addition, tau is able to regulate the release of cargo vesicles from kinesin by the activation of protein phosphatase (PP) 1 and glycogen synthase kinase-3β (GSK3β) through the N-terminus of tau (de Silva et al., 2006).

Work conducted on cultured rat neurons with a knockdown of tau led to an inhibition of neurite formation. In contrast the overexpression of tau facilitated neurite formation (Deming et al., 2016). This study highlights the importance of tau in the elongation and maturation of axons. To date, the physiological functions of the small amounts of tau present in the dendrites have not been well established. Dendritic tau may be involved in synaptic plasticity as synaptic activation leads to the translocation of endogenous tau to the post synaptic compartments from the dendritic shaft in acute hippocampal slices (Ding et al., 2008).

Tau has been detected in the nuclei in a variety of different cell types such as neurons, fibroblasts and neuroblastoma cells (Dixit et al., 2008; Dolan and Johnson, 2010). It is

hypothesised that tau is required to maintain the integrity of genomic DNA, cytoplasmic RNA and nuclear RNA (Violet et al., 2014). In vitro gel-retardation experiments clearly demonstrated that tau has the capacity to bind to AT-rich satellite DNA sequences directly (Sjoberg et al., 2006). Interaction of tau with DNA has been reported to be aggregation-dependent so that aggregated tau loses its capacity to interact with DNA. Since nuclear tau has also been found in neurons from patients with Alzheimer's disease (AD), aberrant nuclear tau could affect the nucleolar organisation during the progression of AD (Sjoberg et al., 2006).

1.2 Tauopathies

The tauopathies are a group of heterogenous dementias characterised clinically by cognitive and motor dysfunction, and pathologically by aggregates of highly phosphorylated and cleaved tau protein that become redistributed from the axons into the cell bodies and dendrites of nerve cells (Wang et al., 2010). In these disorders, tau deposits likely begin to accumulate many years prior to the onset of clinical symptoms; making early diagnosis immensely challenging (Golde et al., 2011). The causes underlying disease onset in these disorders remains unclear. However, it is likely to include a combination of toxic gain-of-function acquired by tau aggregation, along with a loss of normal function of tau. Most tauopathies exhibit a sporadic onset, however there is also a genetic predisposition for the development of some tauopathies. The group of disorders comprising the tauopathies includes AD which is the most prevalent and well characterised member, as well as other neurodegenerative disease including corticobasal degeneration (CBD), progressive supranuclear palsy (PSP), Pick's disease (PiD) and frontotemporal lobar degeneration (FTLD-tau) (Spillantini and Goedert, 2013). Interestingly, the tau profile detected on western blots in these diseases is greatly variable (Figure 1-2) and allow the partial biochemical discrimination of some tauopathies (Figure 1-2).

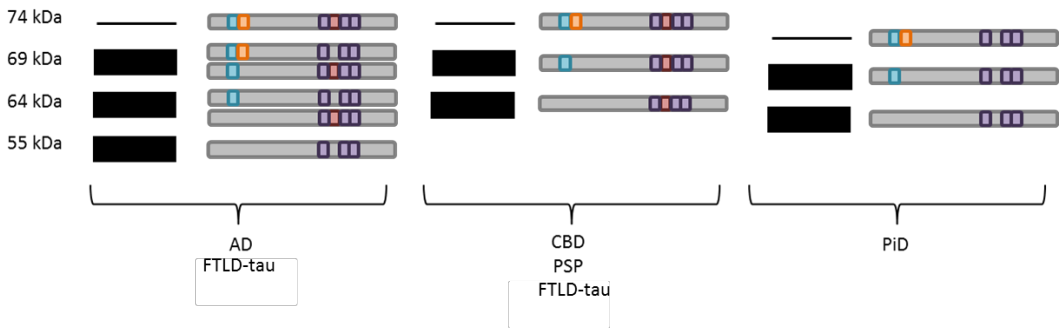

Figure 1-2 Schematic representation of the banding pattern of tau isoforms in different tauopathies: AD contains both 4R and 3R tau isoforms, tau pathology in PSP and CBD contains mainly 4R tau, while in PiD mainly 3R tau is present. In FTLD-tau the pattern is more varied with some cases containing both 3R and 4R tau, and others characterised by predominantly 4R or 3R tau. (adapted from (Buee et al., 2000)).

1.2.1 **Alzheimer's disease**

AD is an age-related condition with a higher propensity in the elderly (Misiak et al., 2013). Approximately 6% of the population and 50% of people over the age of 90, with 800,000 people in the UK affected by this disorder (Wimo et al., 2013). It is predicted that AD will affect 1 in 85 people globally by 2050, making it a global epidemic (Brookmeyer et al., 2007).

There are two major hallmarks of AD (summarised in Table 1-1). The first of these is the formation of amyloid plaques, whereby amyloid precursor protein (APP) can be split by either α secretase and then γ secretase or in tandem by β secretase and γ secretase (Crump et al., 2013). As a result, amyloid beta (Aβ) peptides of different lengths are formed. The peptide created from 42 amino acids (Aβ 42) has greater cytotoxicity and is deposited in amyloid plaques. This form of Aβ accumulates during AD (Figure 1-3) (Kuperstein et al., 2010). The second typical lesion of AD is the neurofibrillary tangle (NFT), made up of paired helical filaments (PHF) comprising highly phosphorylated tau (Goedert, 2004). In AD, as in healthy human brain, both the 3R and 4R tau isoforms are present in an equal ratio. Studies by Braak (Braak and Braak, 1991) were the first of their kind to develop a staging pattern of AD which was based on the neuropathological similarities in the

pattern of NFT spreading in AD brains. They categorised their observations into six primary stages. They additionally correlated brain pathology to disease severity and clinical phenotypes. The robust consistency in NFT spreading provide the basis for a now widely used diagnostic tool for AD. Primarily, NFTs are observed in the transentorhinal/peripheral cortex (Braak stage I), followed by the CA1 region of the hippocampus (Braak stage II). Subsequently, these structures accumulate in the subiculum of the hippocampus (Braak stage III), then amygdala, thalamus and claustrum (Braak stage IV). Finally, in the late stages of disease, NFT pathology spreads to the isocortical areas, with associative areas affected first (Braak stage V), followed by the primary sensory, motor and visual areas (Figure 1-3) (Braak stage VI) (Braak and Braak, 1991; Hyman et al., 1984).

Table 1-1 Summary of the two hallmarks of AD

Pathology	**Amyloid plaques**	**Neurofibrillary tangles**
Precursor	Amyloid precursor protein (APP)	Tau protein
Enzymes involved in the pathology	β-secretase and γ-secretase	Phosphorylation by a wide group of kinases and cleavage by proteases (discussed below in section 1.3)
Consequence of the precursor processing	Formation of amyloid beta created from 42 amino acids, oligomerization into amyloid plaques	Increased phosphorylation of tau, lowering of tau solubility, loss of tau affinity for microtubules
References	(Jankowsky et al., 2004; Korte et al., 2012)	(Boutajangout et al., 2011; Reddy, 2011)

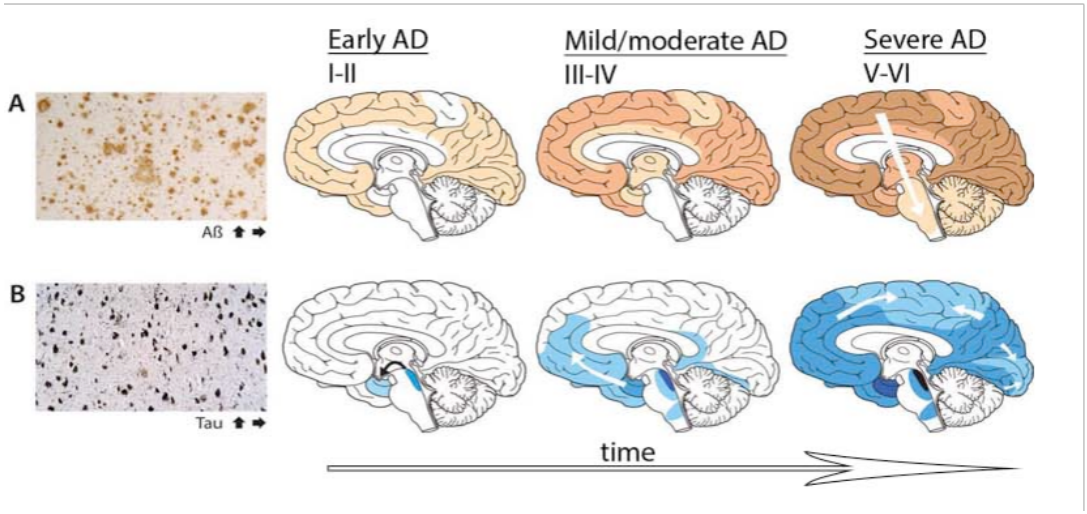

Figure 1-3 The accumulation of Aβ and tau in AD brain: A Brain section of β-amyloid (Aβ) plaques labelling which first appear in the neocortex, followed by the cortex and finally subcortical regions. B Brain section of paired helical filaments (PHF) and neuropathological staging of severity. NFT load in early AD (Braak stages I-II) occurs first in the locus coeruleus and trans entorhinal area (CA1, subiculum and entorhinal cortex). followed by spreading to neighbouring limbic system regions such as the amygdala and hippocampus in later stages of mild/moderate AD (Braak stages III and IV) and finally to connected neocortical brain regions and rest of the brain in late stage severe AD (Braak stages V-VI) as indicated by arrows (Jucker and Walker, 2011).

1.2.2 **Corticobasal degeneration**

CBD is a rare progressive neurodegenerative tauopathy that usually presents as a movement disorder in the clinic. In contrast to healthy control and AD brain, this disease is a 4R tauopathy, meaning that the proportion of 4R tau exceeds that of 3R tau. This disease is associated with a wide variety of motor, sensory, behavioural and cognitive symptoms including but not limited to rigidity, limb dystonia, focal reflex myoclonus and postural/action tremor, symptoms that can also occur in other tauopathies (Ludolph et al., 2009). This clinical heterogeneity between CBD and other tauopathies makes differential diagnosis difficult and accurate identification of the disorder usually occurs post-mortem (Kouri et al., 2011). Important neuropathological features of CBD include cortical and nigral atrophy; microscopically there are numerous swollen cortical neurons as well as tau-

immunoreactive astrocytic plaques not observed in other tauopathies (Ludolph et al., 2009).

1.2.3 **Progressive supranuclear palsy**

PSP is another relatively uncommon neurodegenerative disease. According to the NIH reported prevalence is only about three to six in every 100,000 people worldwide. It is characterised clinically by parkinsonian symptoms together with other features, including postural instability, downward gaze supranuclear palsy, dysarthria and dysphagia (Steele et al., 1964). Pathologically, as with other tauopathies, the brains of PSP patients contain deposits of highly phosphorylated and aggregated tau. Unlike in AD, in post-mortem brains of PSP patients, tau is found to be formed predominantly into straight filaments (PSP-tau) in neurons and glia as opposed to forming PHFs. A classical and unique feature of PSP is the presence of fibrous aggregates of insoluble tau in tufted astrocytes (Bergeron et al., 1997). These tau-positive structures are present in the pallidum, subthalamic nucleus, substantia nigra, pons and other subcortical structures. Unlike in AD, where PHF-tau appears on western blots as a triplet of 68, 64 and 62 kDa and an additional band of 72 kDa, in PSP, tau appears as a doublet exhibiting bands at 68 and 64 kDa (Figure 1-2) (Flament et al., 1991). Like CBD and unlike AD, in PSP there is an increase in the ratio of 4R to 3R tau, making it a 4R tauopathy. In contrast to CBD, there are specific cleaved fragments of tau in PSP brain lacking the N-terminus that could be used to exclusively identify the disease (Arai et al., 2004). In addition, the cerebrospinal fluid (CSF) from PSP patients harbours reduced amount of C-terminally cleaved tau; an additional unique feature compared to other tauopathies (Borroni et al., 2007; Brandt et al., 2005; Reimann, 2017).

In post-mortem brains of PSP patients, tau is found to be in straight filaments in neurons and glia. Conversely, in AD, tau is primarily found as paired helical filaments (PHF) that make up the neurofibrillary tangles, which are typical lesions of the disease (Goedert, 2004). Other differences include a variation in the ratio of the six tau isoforms in the tauopathies. In PSP and CBD brains, there is an increase in 4R tau.

1.2.4 **Pick's disease**

PiD is a rare disorder characterised by progressive dementia and personality deterioration. Early clinical symptoms include frontal disinhibition. Neuropathologically, this disease shows gliosis, neuronal loss, circumscribed atrophy of the frontal, frontotemporal, and frontoparietotemporal cortices and of ballooned neurons as well as Pick bodies, which are spheroidal aggregates of highly phosphorylated tau in neurons (Ludolph et al., 2009). Pick bodies are more abundant in the hippocampus compared to the neocortex (Delacourte et al., 1996). Within the hippocampus, Pick bodies are apparent in granular cell neurons of the dentate gyrus, in the CA1 region of the hippocampus, subiculum and entorhinal cortex, whereas in the neocortex, they are mainly found in layers II and VI of the temporal and frontal lobes (Avila et al., 2004; Robert and Mathuranath, 2007). Biochemical analyses of Pick's disease by western blotting using phospho-specific tau antibodies showed the presence of three bands distinctive to the disease; a doublet of tau at 55 and 64 kDa, and a third, fainter band at 69 kDa (Botez et al., 1999). Further studies indicated that Pick bodies and the tau doublet at 55 and 64 kDa are not labeled with immunological probes directed against the sequence encoded by exon 10 indicating only 3R tau isoforms aggregate into Pick bodies, making this a 3R tauopathy (Braak et al., 1999). Contrasting with PSP and CBD, in Pick's disease 3R tau is more abundant than 4R tau isoforms (Rockenstein et al., 2015).

1.2.5 **Frontotemporal lobar degeneration**

FTLD is a term for the group of non-Alzheimer degenerative dementias with focal cortical neuronal loss and gliosis (McKhann et al., 2001). The most common FTLD is associated with TAR DNA-binding protein 43 (TDP-43) pathology (FTLD-TDP), with tauopathies (FTLD-tau) being slightly less common (Wider and Wszolek, 2008). As described above, there is preferential accumulation of 3R or 4R tau in various tauopathies, providing a biochemical sub-classification. The classifications of the most common forms of FTLD-tau compared to AD are summarised in Table 1-2.

Table 1-2 Classifications of the most common subtypes of FTLD-tau (Adapted from (Mackenzie et al., 2010))

Disorder	Affected brain regions	Major clinical features
4R tauopathies		
CBD	Cortex and basal ganglia	Focal cortical syndrome and parkinsonism
PSP	Basal ganglia, brainstem and cerebellum	Atypical parkinsonism
FTLD-tau	Cortex, basal ganglia and brainstem	Focal cortical syndrome and parkinsonism
3R tauopathies		
PiD	Cortex and limbic lobe	Dementia and focal cortical syndromes
FTLD-tau	Cortex, basal ganglia and brainstem	Dementia and focal cortical syndromes
3R-4R tauopathies		
AD	Cortex and limbic lobe	Dementia
FTLD-tau	Cortex and limbic lobe	Dementia and psychosis

1.3 Post-translational modification of tau

Tau can undergo multiple post-translational modifications, some of which may lead to changes in tau conformation. These modifications include phosphorylation, isomerisation, glycation, nitration, addition of β-linked N-acetylglucosamine (O-GlcNAcylation), acetylation, oxidation, polyamination, sumoylation, ubiquitylation and proteolytic cleavage or truncation (Lee et al., 2001; Reyes et al., 2008; Rodriguez-Martin et al., 2013). Tau phosphorylation, acetylation and truncation, in particular, are associated with the development of tauopathy.

1.3.1 Tau phosphorylation

The phosphorylation of tau has been the most widely investigated conformational change in relation to neurodegeneration (Hanger et al., 2009a). Tau contains 85 phosphorylation sites, including 45 serine (53% of phosphorylation sites of tau), 35 threonine (41%) and 5 tyrosine (6%) residues (Figure 1-4) (Hanger et al., 2009a). In AD, tau is abnormally

phosphorylated at many sites, mostly within the microtubule-binding repeat and flanking domains. These phosphorylation sites are of diagnostic value because several antibodies against Alzheimer tau recognise these motifs, including antibodies AT8, PHF1, and AT100, amongst others (Hanger et al., 2009b; Simic et al., 2016).

Under pathological conditions, there is a marked elevation in tau phosphorylation in all tauopathies. This results in a reduced affinity of tau to bind to microtubules, which leads to destabilisation of the cytoskeleton, particularly in neurons. Tau phosphorylated at Ser262, Ser293, Ser324 and Ser356 (each located in one of the four microtubule-binding repeats), and at Thr214, Thr231 and Ser235 (lying outside the microtubule-binding domain) leads to the dissociation of tau from the microtubules (Drewes et al, 1995; Ksiezak-Reding et al 2003). Ultimately the tau that detaches from the microtubules undergoes self-aggregation, forming oligomers and higher order tau aggregates (von Bergen et al., 2000). The phosphorylation of tau in the proline-rich domain disrupts its microtubule assembly activity and induces a slight increase in the propensity of tau to self-aggregate (Eidenmuller et al., 2001). However, phosphorylation of the C-terminal region of tau dramatically increases the ability of tau to self-aggregate (Liu et al., 2007)

In AD, abnormal phosphorylation of tau occurs prior to the appearance of NFTs (Braak and Braak, 1995). The expression of a pseudo-phosphorylated tau construct in neural cells reproduces structural and functional aspects of AD (Fath et al., 2002). Moreover, overexpression of pseudo-phosphorylated tau dramatically decreases microtubule interactions and disrupts the microtubule network, thereby exerting neurotoxic effects (Cho and Johnson, 2004a; Gong and Iqbal, 2008; Zhang et al., 2009b).

In addition to the loss of microtubule binding ability and formation of toxic or oligomeric tau species, elevated tau phosphorylation can induce a neurodegenerative phenotype through alternative mechanisms. Primarily an increase in phosphorylated tau leads to tau mis-sorting from axons into the somatodendritic compartment, compromising axonal microtubule integrity and resulting in synaptic dysfunction (Hoover et al., 2010; Ittner and Götz, 2011). In addition, increased tau phosphorylation can have an impact on tau degradation. For example, tau phosphorylated on Ser262 or Ser356 is unable to undergo

degradation by the proteasome as the phosphorylation event prevents the recognition of the protein by the C terminus of heat shock protein 70-interacting protein-heat shock protein 90 (CHIP-HSP90) complex (Wyttenbach, 2004). In support of this view, inhibition of autophagy in neurons resulted in a three-fold accumulation of phosphomimic tau compared with wild type tau, and endogenous tau was unaffected; indicating that autophagy is the primary route for clearing phosphorylated tau in neurons (Rodriguez-Martin et al., 2013).

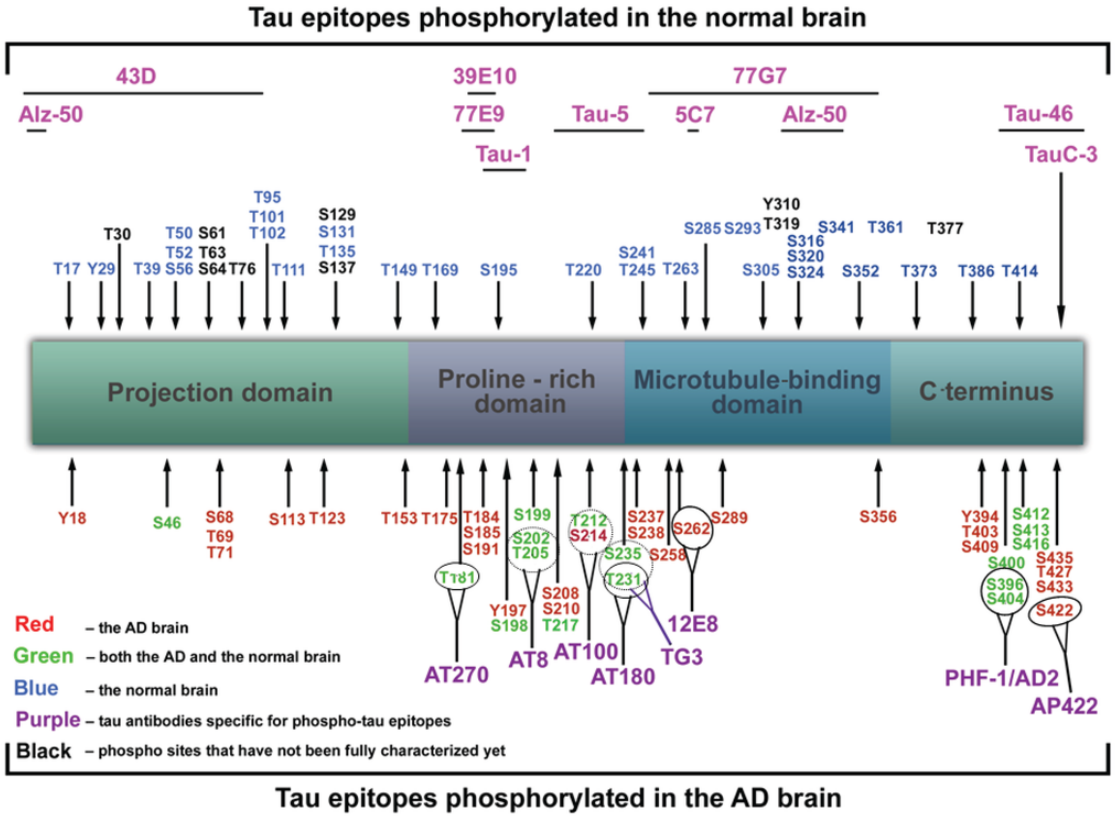

Figure 1-4 Putative phosphorylation sites on tau and epitopes specific for major tau antibodies: A schematic representation of the phosphorylation sites of tau. Sites marked in red indicate amino acids phosphorylated in AD brain, green in both AD and normal brain, blue in normal brain, and black refers to phosphorylation sites that have not been fully characterised yet. Tau antibodies specific for phospho-tau epitopes are shown in purple, while pink denotes antibodies specific for non-phosphorylated tau epitopes (Simic et al., 2016).

One possibility behind the accumulation of phosphorylated tau in the tauopathies could be due to elevated kinase activity, such as GSK3, cyclin-dependent kinase 5 (CDK5) and/or microtubule-affinity regulating kinase (MARK), amongst others such as the thousand-and-one amino acid kinases (TAOKs) 1 and 2 (Giacomini et al., 2018). In conjunction, a decrease in the activity of tau phosphatases such as PP1, PP2A and PP2B may also contribute to an increase in the phosphorylation of tau (Billingsley and Kincaid, 1997).

1.3.1.1 Tau kinases

Tau is a target of multiple protein kinases. Tau protein kinases can be grouped into three classes: proline-directed protein kinases (PDPK), protein kinases non-PDPK and tyrosine protein kinases (TPK). PDPK are kinases that phosphorylate serine and threonine preceding a proline residue (S/TP motif). Examples of such enzymes include GSK3, extracellular signal-regulated kinases 1 and 2 (ERK1/2) (discussed in more detail below), cyclin-dependent protein kinase-5 (CDK5) and mitogen-activated protein kinases (MAPK) such as p38 and c-Jun N-terminal kinases (JNK) (Hanger et al., 2007; Tenreiro et al., 2014).

The C-terminal portion of tau contains the KXGS motifs Figure 1-5 which can be phosphorylated by kinases such as the MARK, Ca^{2+}-calmodulin dependent protein kinase II (CaMKII), protein kinase A (PKA) and TAOKs (Hanger et al., 2007; Tavares et al., 2013). Phosphorylation of KXGS motifs can reduce interaction between tau and microtubules and may constitute an early event in the pathogenesis of tauopathy (Biernat and Mandelkow, 1999; Nishimura et al., 2004).

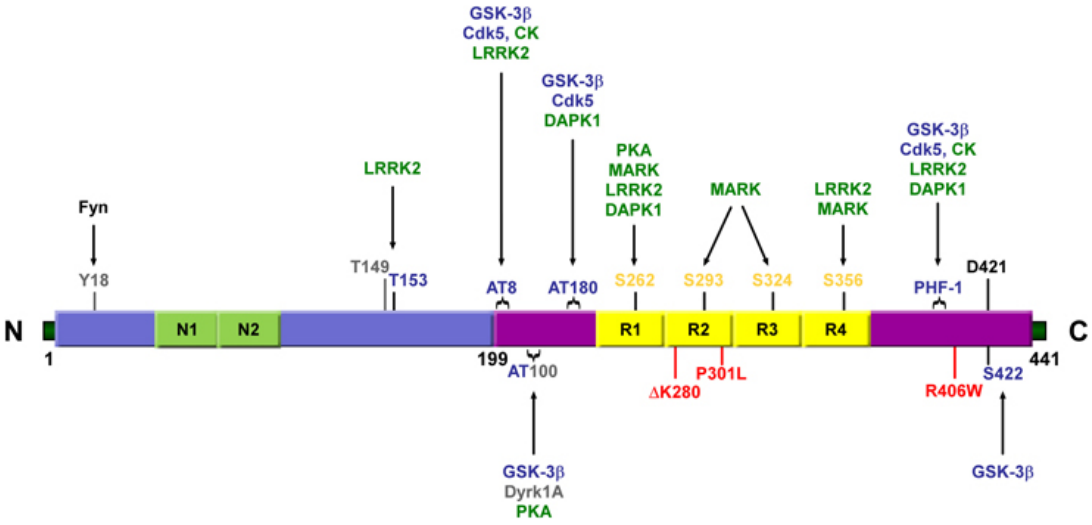

Figure 1-5 Schematic representation of residues that can be phosphorylated in the longest isoform of tau: Illustration of tau as being phosphorylated by tau kinases. KXGS motifs (shown in yellow text), and other sites (represented in grey) can be phosphorylated by proline-directed kinases (blue) and non-proline directed Ser/Thr kinases (green). Antibody epitopes AT8, AT100, AT180, and PHF-1 comprise dual and triple serine/threonine residues (indicated by brackets). GSK3: Glycogen synthase kinase 3β/a, Cdk5: Cyclin-dependent kinase5; CK1: casein kinase 1, MARK: MT affinity-regulating kinase; LRRK2: leucine-rich repeat kinase2; DAPK: Death-associated protein kinase; Dyrk1A: dual-specificity protein kinase 1, SAPK: stress-activated protein kinase, PSK: TAOKs (Tenreiro et al., 2014).

There are two major isoforms of GSK3; α and β, which are encoded by different genes, but share approximately 85% sequence homology (Woodgett, 1991). Alternative splicing of GSK3β at exon 8A generates two isoforms β1 and β2 (Woodgett, 1991). The β1 isoform is the more abundant form of GSK3β (Mukai et al., 2002). The β2 isoform of GSK3 is found in neuronal soma while the β1 isoform is found both in neuronal soma and in axons (Mukai et al., 2002). GSK3 phosphorylation can be catalysed by several protein kinases including protein kinase cAMP-dependent (PKA) (Fang et al., 2000), protein kinase B (PKB) (Cross et al., 1995), protein kinase C (PKC) (Goode et al., 1992), p70S6K/p85S6 kinase, p90-ribosomal S6 kinase (Sutherland et al., 1993). P70S6K/p85S6 kinase and p90-ribosomal S6

kinase are activated in response to Akt/protein kinase B (PKB) and MAPK (p38 and ERK1/2), respectively.

Several lines of evidence link the activation of GSK3 with the development of tauopathy. Tau phosphorylation by GSK3 has been identified at 42 sites, with 29 of these being phosphorylated in AD brain (Hanger et al., 2009b). In AD patients, GSK3β was found to co-localise with NFT (Yamaguchi et al., 1996), and the active form of GSK3β (phosphorylated at tyrosine 216) increases in the frontal cortex of AD brains (Leroy et al., 2007). GSK3β phosphorylates tau at Thr231 and primes the C-terminus of tau for subsequent phosphorylation, promoting NFT formation (Cho and Johnson, 2004b; Rudrabhatla and Pant, 2010). In a study in cultured neurons, lithium (an inhibitor of GSK3β activity) reduced the phosphorylation of tau, enhanced the binding of tau to microtubules, and promoted microtubule assembly (Marchand et al., 2015). GSK3 inhibition also induces pro-survival signals through increased activity of the autophagy/lysosomal networks (Marchand et al., 2015). An additional study done in transgenic mice showed that the inhibition of GSK3β reduces tau phosphorylation (Caccamo et al., 2007; Engel et al., 2006; Nakashima et al., 2005), tauopathy and neurodegeneration (Noble et al., 2005), blocks NFT formation (Engel et al., 2006; Leroy et al., 2010) and rescues neuronal loss (Serenó et al., 2009)

ERK1 and ERK2 exhibit 83% homology and they regulate cell division, growth, proliferation, cell migration, cell differentiation, and apoptosis (Guise et al., 2001). ERK1/2 becomes activated by dual phosphorylation at Thr202 and Tyr204 for ERK1 and at Thr184 and Tyr186 for ERK2 (Roux and Blenis, 2004). This activation occurs through the activity of the upstream MAP kinase kinase (MEK). The increased phosphorylation of tau in AD has been proposed to involve the activation of ERK. A study carried out by Pei et al, found that increasingly phosphorylated (activated) MEK1/2 and ERK1/2 were present in the initial stages of neurofibrillary degeneration in the projecting neurons in AD brain (Pei et al., 2002). Further work revealed that the accumulation of phosphorylated MEK1/2 and ERK1/2 was initiated in the cytoplasm of pretangle neurons and correlated with the progressive development of neurofibrillary tangles (Pei et al., 2002).

1.3.1.2 Tau phosphatases

Tau phosphatases belong to PPP group, which dephosphorylates either serine and threonine residues (PP1, PP2A, PP2B and PP5) and PTP group, which dephosphorylate tyrosine residues (PTEN). Physiologically in the human brain, without the development of a neurodegenerative pathology, PP2A accounts for more than 70% of cellular phosphatase activity in the brain (Liu et al., 2005a). PP2A dephosphorylates tau and is implicated in the regulation of tau phosphorylation. PP2A activity is decreased by approximately 50% in AD brain, which could contribute to increased tau phosphorylation (Liu et al., 2005b).

Interestingly, the inhibitory phosphorylation of PP2A at Tyr307 is stimulated by the activity of GSK3β. These data provide a strong link between PP2A and GSK3β and suggest that the inactivation of PP2A could be due to the GSK3 (Yao et al., 2011; Zhang et al., 2008). In addition, *In vivo* studies showed that PP2A inhibition induces an increase in tau phosphorylation and spatial memory deficits (Zhang et al., 2008), and these effects are reversed by the addition of acetyl-l-carnitine (Yin et al., 2010). Moreover, PP2A inhibition by okadaic acid in rats increases tau phosphorylation in neurons and impairs spatial memory retention (Sun et al., 2003).

1.3.2 **Tau acetylation**

Unlike phosphorylation, which involves serine, threonine and tyrosine residues, acetylation involves lysine residues and acetylation has been suggested to be an early step in the aggregation of phosphorylated tau (Fontaine et al., 2015). Tau acetylation is elevated in patients with AD and this event prevents degradation of phosphorylated tau (Min et al., 2010). This study also found that, when looking at the frontal cortex of patients with varying degrees of AD, the patients at earlier stages had high levels of acetylated tau, and it wasn't until the later stages of the disease that increasingly phosphorylated tau was detected (Min et al., 2010). This suggests that tau acetylation may precede the phosphorylation of tau and NFT formation (Min et al, 2010). Furthermore, a recent study by Cohen et al (2011) used mass spectrometric analysis in cell and mouse models to demonstrate that tau acetylation at specific lysine residues (especially K280) inhibits tau function by disrupting microtubule binding, as well as promoting the aggregation of phosphorylated tau (Cohen et al., 2011; Russell et al., 2014). However, another study. found that KXGS motifs, located in the microtubule-binding domain of tau, were

hypoacetylated in people with AD, as well as in mouse models, suggesting an opposite relationship where decreased acetylation of tau increases vulnerability to tau phosphorylation (Cook et al., 2014a). Together, these contradictory results demonstrate that although acetylation does appear to play a role in the development of AD, the nature of that role is not well understood and requires further investigation. Perhaps, the different interactions between post-translational modification of tau at different sites could explain these different results, as they evidently have a complex relationship. Further, due to the complex relationships of post-translational modification of tau, it has been suggested that the degree of tau acetylation may also influence the extent of tau ubiquitination (Marcus and Schachter, 2011).

1.3.3 **Tau truncation**

In addition to highly phosphorylated and aggregated tau, truncated tau has additionally been reported in tauopathies including AD, PiD, CBD and PSP. These fragments can lack either the N- and C-termini of tau, or both (Garcia-Sierra et al., 2008). Specifically, a caspase-cleaved tau species (cleaved at D13 by caspase-6 and at D421 by caspase-3), termed **Δ**tau,, has previously been reported. This fragment of tau is recognised by an antibody specific to this fragment, which labels NFTs in the CA1 layer of the hippocampus in AD (Garcia-Sierra et al., 2008). Several other lines of evidence reveal the role of truncated tau in the development of a neurodegenerative phenotype. For example, tau truncated at Asp421 colocalises with tangles in AD brain as well as in a number of transgenic mouse models of AD, which may indicate that the generation of this tau fragment may be an early event in tangle formation (Basurto-Islas et al., 2008; Horowitz et al., 2004). A further study revealed that the mutation of Ser422 in full-length tau to glutamate (S422E), which mimics a permanent state of phosphorylation, prevents caspase cleavage at Asp421 (Guillozet-Bongaarts et al., 2006). These findings support the view that caspase degradation of tau can be inhibited by phosphorylation of residues adjacent to the caspase cleavage site (Hanger and Wray, 2010). Additional studies reveal that while both increased tau phosphorylation and truncation are found in NFTs in AD, cleavage occurs following tau phosphorylation (Guillozet-Bongaarts et al., 2005; Mondragón‐Rodríguez et al., 2008). Conversely, tau cleavage has been suggested to drive aggregation of tau and any associated disease-modifying proteins, leading to a loss of tau function. Supporting

this statement is the fact that truncated protein fragments can form the initial seeds required for aggregation and appear to be upstream in the proteopathic cascade that occurs in neurodegenerative disease (Zilka et al., 2006a). Some of the truncated tau fragments that may be involved in the development of human tauopathies are summarised in Table 1-3.

Table 1-3 Tau fragments identified in human brain that may be involved in the development of human tauopathy (Adapted from (Guo et al., 2017)).

Tau fragment (residues)	Tauopathy	Pathology	References
C-terminally cleaved tau (40–53kDa)	AD brain	Synaptic dysfunction	(Sokolow et al., 2015)
Delta tau (A15-D421)	AD brain	Tangle formation, amyloid plaques, synaptic dysfunction, tau filament formation	(Fasulo et al., 2000)
NH_2-tau (E45-R230)	AD brain ALS brain Control brain	Neurodegeneration phenotype	(Amadoro et al., 2011)
(I151-A391)	AD brain	Tangle formation	(Filipcik et al., 2012)
(Q124-L441)	Control brain	Increased acetylation and detyrosination of tubulin	(Garg et al., 2011)
(A125- R230)	AD brain Control brain	Elevated levels of phosphorylated and aggregated tau	(Garg et al., 2011)
Tau35 (E187-441), 33–37kDa)	PSP brain CBD brain	Tau pathology, cognitive and motor dysfunction	(Bondulich et al., 2016)
Tau-CTF24 (L243-L441)	PSP brain CBD brain	Tau pathology, synapse loss	(Matsumoto et al., 2015)

A particular study found a significantly higher numbers of phospho-tau positive NFTs when compared with cleaved tau in Braak III, IV and V brains. Consistent with these findings, in a double transgenic mouse model (Tet／GSK-3β／VLW) overexpressing GSK-3β and tau with a triple FTLD-tau mutation (VLW) with AD-like phenotypes, it was apparent that there were elevated levels of tau phosphorylated at sites Ser199⁄Ser202/Thr205, when compared to the levels of truncated tau (Mondragon-Rodriguez et al., 2008).

Nonetheless, the role of truncated tau in neurodegeneration has multiple roles as illustrated by an array of findings. The presence of a 17 kDa tau fragment (Tau_{73-315}) was identified in cerebellar granule neurons undergoing apoptosis as a result of caspase-3 and calpain-mediated cleavage (Canu et al., 1998). In parallel, a different 17 kDa tau fragment (Tau_{45-230}) was found in hippocampal neurons treated with Aβ (Park and Ferreira, 2005).

N-terminally truncated tau has additionally been linked with the development of tauopathy. The NH2-tau fragment (Tau_{26-230}), was identified in human SH-SY5Y cells undergoing apoptosis and in the hippocampus of 15 month-old AD11 transgenic mice, exhibiting AD-like pathology (Corsetti et al., 2008). Moreover, more recently, a C-terminal tau fragment ($Tau_{243-441}$), termed Tau-CTF24, was found in the Tg601 mouse model of 4R tauopathy (Matsumoto et al., 2015). A 35 kDa C-terminal tau fragment ($Tau_{187-441}$) lacking the N-terminus of tau, but containing all four microtubule-binding repeats (4R), was found to be solely present in 4R tauopathies such as PSP (Wray et al., 2008). Subsequent characterisation of this fragment by low-level expression in a transgenic mouse model, revealed progressive cognitive and motor deficits, as well as aggregated and increasingly phosphorylated tau (Bondulich et al., 2016).

Tau can be cleaved by a variety of proteolytic enzymes including caspases, cathepsins, calpains, thrombin and puromycin-sensitive aminopeptidase. Caspases and cathepsins are discussed briefly below.

1.3.3.1 Caspases

Tau can be cleaved by caspases at three distinct sites, residues Asp25, Asp348 and Asp421, of which Asp421 is the preferred cleavage site (Guo et al., 2004). The consensus sequence

at Asp421 is recognised by caspases-3 and -7 and mutation of this residue to glutamate inhibits caspase-mediated tau proteolysis (Chung et al., 2001). In addition, Asp421 in tau is targeted by caspases-1, -6, and -8, generating tau fragments that are approximately 5 kDa smaller than full-length tau due to the removal of C terminus (Gamblin et al., 2003). To date, truncation of tau at Asp421 by caspases has been validated both *in vitro* and *in vivo*, and appears to be directly related to the development of tau pathology (Amadoro et al., 2010). Studies corroborate this observation as a tau fragment cleaved at Asp421 by caspase-3 is found in rodent primary cultured neurons (Garwood et al., 2011), and htau transgenic mice (Noble et al., 2009). The presence of these caspase-cleaved tau products in AD brain was identified using antibodies TauC3 and α-ΔTau, which are specific for caspase-cleaved tau (Gamblin et al., 2003).

1.3.3.2 Cathepsins

Cathepsins are synthesised in membrane-bound ribosomes as N-glycosylated precursors. Subsequently, they are transferred into the endoplasmic reticulum (ER) and later into the Golgi complex. During transport to the Golgi complex, pro-cathepsins (inactive) acquire modification of their carbohydrate moieties, which includes the formation of the mannose 6-phosphate (M6P) residues and are transported to late endosomes. Upon fusion with late endosomes, the dissociation of ligands occurs (Nakanishi, 2003). The major part of the enzyme is then transported to the lysosome where the pro-peptides of the cathepsins are removed due to the acidic environments of late endosomes and lysosomes. Thus active cathepsins are formed (Zhang et al., 2009a).

Lysosomal dysfunction has been demonstrated in aged brain, leading to leakage into the cytoplasm of lysosomal enzymes (Lloyd-Evans and Haslett, 2016). The cathepsins are a group of lysosomal proteases. Cathepsin D is an aspartyl protease that has been most associated with the development of tauopathy (De Strooper, 2010). Several groups have shown *in vitro* that tau is cleaved by cathepsin D between amino acids 200 and 257, resulting in the generation of a 29 kDa tau species (Bendiske and Bahr, 2003). Defects in the activity of cathepsin D have additionally been reported in several studies on AD. The presence of C-terminally truncated tau has been reported in the brains of CLN10 (cathepsin D null) mice (Khurana et al., 2010). Moreover, the complete loss of cathepsin D in patients has been shown to lead to a devastating form of a lysosomal

neurodegenerative disorder that is autosomal recessive and can manifest in early childhood, causing neuronal ceroid lipofuscinosis (Steinfeld et al., 2006). The pH optimum of cathepsin D is narrow and is within the range of ~pH3.1–3.5. The extremely narrow pH optimum means that cathepsin D will likely become less functional with age as the pH of lysosomes is elevated (Cuervo and Dice, 2000). Consequently, there is, therefore, a clear association between loss of optimal function of this enzyme and common neurodegenerative diseases of ageing.

The role of other cathepsins in relation to neurodegeneration has also been suggested, in particular cathepsins B and L (Felbor et al., 2002). In human neuroblastoma cells inducibly expressing tau, disruption of lysosomes with chloroquine results in inhibition of tau degradation and the appearance of tau aggregates (Wang et al., 2009). This study also implicated the involvement of cathepsins B and L in generating two amyloidogenic tau fragments in a cell model of tau aggregation expressing a tau fragment, $tau_{RD}\Delta K280$ (microtubule binding repeats with ΔK280 mutation). These findings imply that cathepsins B and L may play a role in tau aggregation (Hamano et al., 2008a; Wang et al., 2009). Moreover, in cathepsin $B^{-/-}/L^{-/-}$ mice, a large degree of brain atrophy was observed. This was due to apoptosis of select neurons in the cerebral cortex and the cerebellar Purkinje and granule cell layers. Neurodegeneration in the mice was accompanied by pronounced reactive astrocytosis and is preceded by an accumulation of ultrastructurally and biochemically unique lysosomal bodies in large cortical neurons and by axonal enlargements (Felbor et al., 2002).

1.4 Mouse models of tauopathy

Transgenic rodents have been used to investigate pathogenic mechanisms in diseases of the CNS, and animal models of disease are vital for pre-clinical investigations of potential therapeutic strategies (Noble et al., 2010). There are now a multitude of animal models that aim to investigate different disease-associated proteins and their post-translational modification in relation to the neurodegenerative tauopathies. Several strategies have been used to create such models including overexpression of individual wild-type or mutant tau isoforms, knock-in of human tau or knock-out of rodent tau, regulatable expression of mutant human tau and over-expression of the entire wild-type mouse or human *MAPT* gene (Noble et al., 2010) Most existing transgenic mouse models of

tauopathy rely on over-expression of wild-type or mutant forms of tau. While these models provide useful insight on the mechanistic understanding of tau, they do not mimic the levels of tau expression in human tauopathies., which usually exhibit only modest changes in steady state levels of tau. For example, a number of different mouse lines expressing P301L mutant tau have been created (McGowan et al., 2006). The expression of 0N4R tau with the P301L mutation under the control of the mouse prion promoter, leads to the build-up of increasingly phosphorylated and insoluble tau (van Swieten et al., 2004). Moreover, NFTs and Pick-body like inclusions form from 4.5 months of age in the brainstem and spinal cord of P301L tau mice (Lewis et al., 2000). These changes are accompanied by progressive motor and cognitive abnormalities (Lin et al., 2003). The P301S mutation causes the formation of NFTs and glial tangles containing straight tau filaments. In contrast to P301L mice, the overexpression of 0N4R or 1N4R tau with the P301S mutation, results in accelerated neurofibrillary pathology (Allen et al., 2002; Yoshiyama et al., 2007).

Melis et al (2015) generated two mouse models of tauopathy over-expressing tau. L66 mice model the FTLS-tau spectrum of diseases, and these animals over-express human *MAPT* cDNA containing two point mutations (equivalent to P301S and G335D). L66 mice have abundant tau pathology distributed throughout the brain, with a high proportion of affected neurons seen in the hippocampus and entorhinal cortex. The pathology is neuroanatomically static and declines with age. The second mouse model: L1 expresses a truncated 3-repeat tau fragment which constitutes the bulk of the PHF core in AD corresponding to residues 296–390. These mice model cognitive changes seen in AD (Melis et al., 2015). L1 mice display a much weaker histopathological phenotype in comparison with L66 mice, but show evidence of tau spreading that resembles the Braak staging of AD. Behaviourally, the mice exhibit minimal motor deficits but shows severe cognitive impairments (Melis et al., 2015).

However, a mouse model that does not depend on excessive over-expression of tau was generated by McMillan et al (2011). In this model, mice express at approximately twice the amount of endogenous tau, a 4R tau truncation construct, lacking the C-terminus as it terminates at residue E391. These mice exhibit a sufficient build-up of insoluble and

phosphorylated tau to generate a “pre-tangle”-like pathology (McMillan et al., 2011). Importantly however, these mice failed to show accumulation of tangles and no cognitive studies were conducted on these animals, which significantly limits the validity and characterisation of this potential model of tauopathy.

A 35 kDa tau fragment that is highly phosphorylated at the C-terminus and lacking the N terminus was identified in PSP brain (Wray et al., 2008). This tau fragment contained all four MTB domains of tau and was found in the brains of PSP, CBD, and FTDP-17 patients, but was absent from AD brain (Wray et al., 2008). Based on these findings, Tau35 mice were generated by targeted insertion of Tau35, which is controlled by the human tau promoter at the *Hprt* (hypoxanthine phosphoribosyl transferase) locus on the X chromosome (Bondulich et al., 2016). This tau fragment has a haemagglutinin (HA) tag that allows its discrimination from endogenous mouse tau. Tau35 mice differ from many other models of tauopathy that over-express mutant forms of tau. This particular mouse model expresses a human tauopathy-associated 35 kDa tau fragment at a level that is <10% of endogenous mouse tau (Bondulich et al., 2016).

Tau35 mice exhibit age-related limb clasping, kyphosis and a reduced life span (Bondulich et al., 2016). This is consistent with other mouse models of tauopathies (Lalonde and Strazielle, 2011; Laws and Hoey, 2004; Wu et al., 2012). Tau35 mice show a loss of hindlimb grip strength as well as a progressive clasping of either their hindlimbs or all four limbs. In addition, abnormal spine curvature is seen in Tau35 mice and the kyphotic index is reduced, demonstrating progressive, age-related kyphosis (Bondulich et al., 2016). Tau35 mice additionally had a reduced latency to fall from the rotarod, which decreases with age, possibly caused by reduced muscle strength and motor ability. Furthermore, Tau35 mice exhibit spatial learning and hippocampal-dependent memory deficits. These changes in learning and memory were apparent in the Morris water maze. No differences were found in non-associative short-term memory, olfaction or anxiety (Bondulich et al., 2016). These mice additionally showed a reduced median survival of 717 days, compared to 788 days in WT mice (Bondulich et al., 2016).

Tau35 expression also alters the intrinsic excitability of CA1 pyramidal neurons in mice, leading to an induction of higher cell capacitance and rise of action potential rate (Tamagnini et al., 2017). Tau35 accumulation leads to hyperexcitability and hypoexcitability at polarised and depolarised potentials, respectively (Tamagnini et al., 2017). Moreover findings indicate that Tau35 mice exhibit a significant increase in short-term facilitation of the synaptic response without changing long-term synaptic plasticity (Tamagnini et al., 2017).

1.5 Protein degradation mechanisms

The abnormal protein inclusions present in several neurodegenerative diseases contain a large amount of misfolded or unfolded proteins, which leads to organelle stress. Consequently, this group of disorders is often referred to as diseases of protein misfolding (Ciechanover and Kwon, 2015). Several studies have reported that neuronal death in AD and PD originates in the ER, which is the organelle that is responsible for regulating correct protein folding, assembly, secretion and the formation of protein complexes (Matus et al., 2008).

1.5.1 Tau degradation

The ubiquitin–proteasome system (UPS) and the autophagy-lysosomal system are the two major pathways responsible for the degradation of intracellular proteins. Initially tau was considered to be primarily a proteasomal substrate (Lee et al., 2013). However, more recently studies found that the UPS may not be the primary degradation machinery for endogenous tau (Brown et al., 2005; Feuillette et al., 2005). It is now well established that tau is a substrate for the autophagy-lysosomal system. Using an inducible mouse neuroblastoma N2a cell model of tauopathy expressing the repeat domain of Tau with a FTLD-tau mutation (Tau RD ΔK280), it was shown that the autophagy-lysosomal system can efficiently degrade both soluble mutant tau as well as tau aggregates (Wang et al., 2009). In addition, inhibition of autophagy leads to enhanced aggregation and cytotoxicity of mutant tau (Krüger et al., 2012). Using an inducible N2a cell line expressing the full-length wild-type isoform hTau40, it was further demonstrated that autophagy can also degrade full-length tau (Wang et al., 2009). Phosphorylation in the repeat domain, which regulates the affinity of tau for microtubules, does not alter its sensitivity to autophagy–lysosomal degradation (Wang et al., 2009).

An additional study found that soluble PHF-tau isolated from human AD brain was not degraded by the proteasome but instead it inhibited proteosomal activity (Keck et al., 2003). Moreover, in a different study, tau was degraded by the proteasome *in vitro*, but not in primary neurons or in neuroblastoma cells (Brown et al., 2005). In the latter systems, tau proteins in a variety of forms had been reported to be degraded through the autophagy-lysosome system. Inhibitors of various autophagy processes, such as ammonium chloride, chloroquine, and 3-methyladenine (3-MA), delayed tau degradation and enhanced the formation of high molecular weight species of tau (Hamano et al., 2008b). On the other hand, rapamycin facilitated the degradation of insoluble forms of tau in a Drosophila model (Berger et al., 2007). These findings therefore suggest that while tau is degraded by the proteasome in some instances, it is predominantly degraded via the autophagy and lysosomal system.

1.6 The ubiquitin proteasome system (UPS)

The UPS has received particular attention in the study of neurodegenerative disorders due to its role as a critical regulator of proteostasis. The function of the UPS is to rid cells of misfolded, defective, and aggregation-prone proteins, which have been found to accumulate in neurodegenerative diseases (Ciechanover and Brundin, 2003). The pathway is predominantly responsible for the clearance of short-lived, damaged, and misfolded proteins in the nucleus and cytoplasm (Ciechanover and Brundin, 2003).

In the UPS, proteins are committed to degradation by their ligation to ubiquitin (Hershko, 1991). An enzymatic cascade composed of ubiquitin activator, conjugase, and ligase catalyse the covalent attachment of ubiquitin to a substrate protein. Ubiquitin is conjugated via its carboxy-terminal Gly to an internal Lys residue or, less commonly, to the free N-terminus of the substrate (Dantuma and Bott, 2014). At least three rounds of ubiquitylation lead to the formation of a polyubiquitin chain (Figure 1-6). This acts as a signal for the proteasome, which in turn can go on to perform its degradative function through its 20S catalytic core (Bedford et al., 2010). The proteasome unfolds substrates, breaking them up into short peptides (Bhattacharyya et al., 2014). The peptides are then released and are rapidly processed into amino acids by cellular aminopeptidases and recycled (Reits et al., 2003).

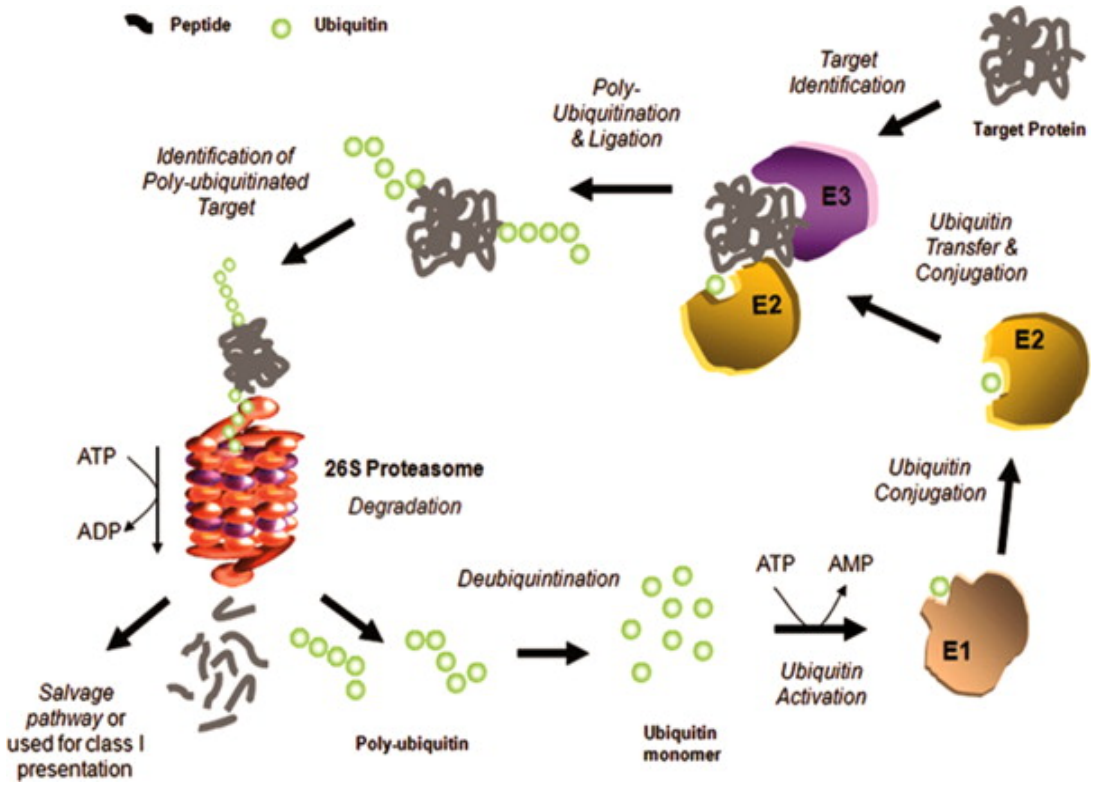

Figure 1-6 Schematic diagram of the ubiquitin proteasome system (UPS): The UPS involves at least three enzymes (E1, E2, and E3). These catalyse the addition of ubiquitin to lysine residues on the substrate protein. Polyubiquitinated substrates are subsequently identified by the proteasome or proteasome associating protein, and the ubiquitin removed by deubiquitinases and the substrate unfolded and translocated in the 20S core for proteolysis (Suh et al., 2013)

The initial clue for the pathological link between tau and the UPS was derived from the observation of co-localisation and accumulation of ubiquitin in PHFs and NFTs (Morishima-Kawashima et al., 1993). Subsequently, it was shown that blocking the activity of the 20S catalytic core inhibits tau degradation in transfected SH-SY5Y cells expressing exogenous human tau (David et al., 2002). It is thought that the ubiquitination of tau weakens its microtubule-binding affinity, similar to the effects of tau phosphorylation. PHF-tau isolated from human AD brain was also found to co-immunoprecipitate with various proteasome subunits (Keck et al., 2003), further supporting a role for the UPS in tau degradation.

1.7 Autophagy and lysosomal degradation

Unlike the UPS, the autophagy/lysosomal pathway is primarily responsible for degrading long-lived proteins and organelles such as mitochondria, that are unnecessary or even detrimental for cell survival (Damme et al., 2015). There are three main types of autophagy (Figure 1-7); macroautophagy (herein referred to as autophagy), microautophagy, and chaperone-mediated autophagy. In starved organisms, autophagy prolongs survival through providing necessary energy and dietary components by the recycling of intracellular proteins and organelles (Metaxakis et al., 2018).

Induction of autophagy initiates the formation of an isolation membrane (phagophore). Phagophore formation involves the localisation of autophagy proteins to pre-autophagosomal structures (Nixon and Yang, 2011). The phagophore elongates sequestering protein aggregates, lipid droplets and organelles and finally closes off to form a double-membrane vesicle, the autophagosome. During maturation, autophagosomes can fuse with late endosomes (Rab7-positive structures), generating a hybrid organelle called an amphisome, or can directly fuse with lysosomes forming an autolysosome. Finally, acidic hydrolases such as cathepsin D degrade the sequestered content (Figure 1-7) (Deng et al., 2017; Kang et al., 2011).

Phagophore membrane formation occurs through a beclin-1-dependent mechanism, positioning beclin 1 as a marker of early autophagy activation. Beclin-1 is a novel Bcl-2-homology (BH)-3 domain only protein (Czabotar et al., 2014). Increasing evidence suggests that nuclear factor (NF)-κB, E2F transcription factors (E2F) and microRNAs (miRNAs) are involved in regulation of beclin-1 expression in autophagy (Kang et al., 2011). Upon autophagy stimulation, beclin-1 is released from Bcl-2 at the ER, forms complex with UVRAG/AMBRA (ultra-violet radiation resistance-associated gene/activated molecule in beclin 1 regulated autophagy/) (Figure 1-7) (Kang et al., 2011).

More than 30 evolutionarily conserved autophagy related genes (Atgs) have been identified and shown to play a vital role in phagophore formation and elongation of the autophagosome (Mizushima, 2007). The activation of Atg13 is particularly important for this step. This protein is negatively regulated by the mammalian target of rapamycin

complex 1 (mTORC1) and interacts with the mammalian homolog of yeast Atg1 kinase complex (ULK1) complex to facilitate early autophagy (Jung et al., 2010). Once the phagophore forms, there are two ubiquitin-like systems that are key to autophagy progression. The first is the Atg5– Atg12 conjugation and the LC3 (microtubule-associated protein 1A/1B-light chain 3) processing step (Axe et al., 2008; Hayashi-Nishino et al., 2009; Yla-Anttila et al., 2009). In the first of these systems, Atg7 activates Atg12 in an ATP-dependent manner by binding to its C-terminal Gly. Atg12 is then transferred to Atg10, that potentiates the linkage of Atg12 to Atg5. Conjugated Atg5 – Atg12 complexes in pairs with Atg16L dimers to form a multimeric Atg5 – Atg12 – Atg16L complex that associates with the extending phagophore. The association of Atg5 – Atg12 – Atg16L complexes is thought to induce curvature into the growing phagophore (Figure 1-7) (Kirkin et al., 2009).

The autophagy pathway is additionally regulated by the autophagy substrate p62/sequestosome 1 (p62/SQSTM1). P62 is involved in the degradation of protein aggregates and cytoplasmic bodies via selective autophagy through its PB1 (Phox/Bem 1p), LIR (LC3 interacting), and UBA (ubiquitinated protein aggregates) domains to maintain homeostasis in the cell (Lin et al., 2013). P62 binds Atg8/LC3 through a region termed the LC3-interacting region. p62 along with its PB1 partner, NBR1 (neighbor of BRCA1 gene 1), have been proposed to regulate the packing and delivery of polyubiquitinated, misfolded, aggregated proteins and damaged organelles for their clearance through autophagy (Kirkin et al., 2009). In addition, evidence reveals that p62 regulates cell survival, as the disposal of toxic aggregates is essential for the prevention of cell death in several pathological situations in which p62 is a component of these aggregates (Figure 1-7) (Zatloukal et al., 2002).

Autophagosome formation is dictated by the processing of LC3B, which is encoded by the mammalian homologue of Atg8. Upon autophagy induction, LC3B is cleaved by Atg4; a cysteine protease, to generate LC3B-I. The carboxyterminal glycine exposed by Atg4-dependent cleavage is then activated in an ATP-dependent manner by Atg7 (Kabeya et al., 2000). Activated LC3B-I is then transferred to Atg3. Subsequently, phosphatidylethanolamine (PE) is conjugated to the carboxyl glycine of activated LC3B-1 to generate LC3B-II. Recruitment and integration of LC3B-II into the growing phagophore is

dependent on Atg5–Atg12 (Kabeya et al., 2000). LC3B- II is found on both the internal and external surfaces of the autophagosome, where it plays a vital role in both autophagosome membrane formation and in selecting cargo for degradation. The synthesis and processing of LC3 is markedly increased during autophagy, making it a robust indicator of levels of autophagy in cells (Barth et al., 2010). It has previously been shown that both LC3-I and LC3-II interact with microtubule-associated proteins and this facilitates their association with microtubules (Figure 1-7) (Wang and Mandelkow, 2012a).

In the context of autophagosomal-lysosomal fusion, pleckstrin homology domain–containing protein 1 functions as a tethering factor by simultaneously binding both to LC3 on autophagosomal membranes via an LC3-interacting region and to the homotypic fusion and vacuolar sorting (HOPS) complex on the lysosomal membrane (McEwan et al., 2015). The Atg14 protein also acts as a tether between autophagosomes and lysosomes by interacting with syntaxin 7 (STX7) and synaptosomal associate protein 29 (SNAP29), which are soluble N-ethylmaleimide-sensitive factor attachment protein receptors (Q-SNAREs), located on the autophagosomal membrane. Consequently, the two structures fuse and form an autolysosome (Figure 1-7) (Diao et al., 2015).

Ultimately, upon fusion, the ∼60 acid hydrolases within the lysosome digest all classes of macromolecules, such as proteins, lipids, nucleic acids, and carbohydrates.(Chapel et al., 2013). Afterwards, the end products of lysosome-mediated digestion are actively or passively transported by integral membrane proteins of the lysosomal membrane to the cytoplasm, where they are utilised in biosynthetic reactions (Jezegou et al., 2012; Liu et al., 2012).

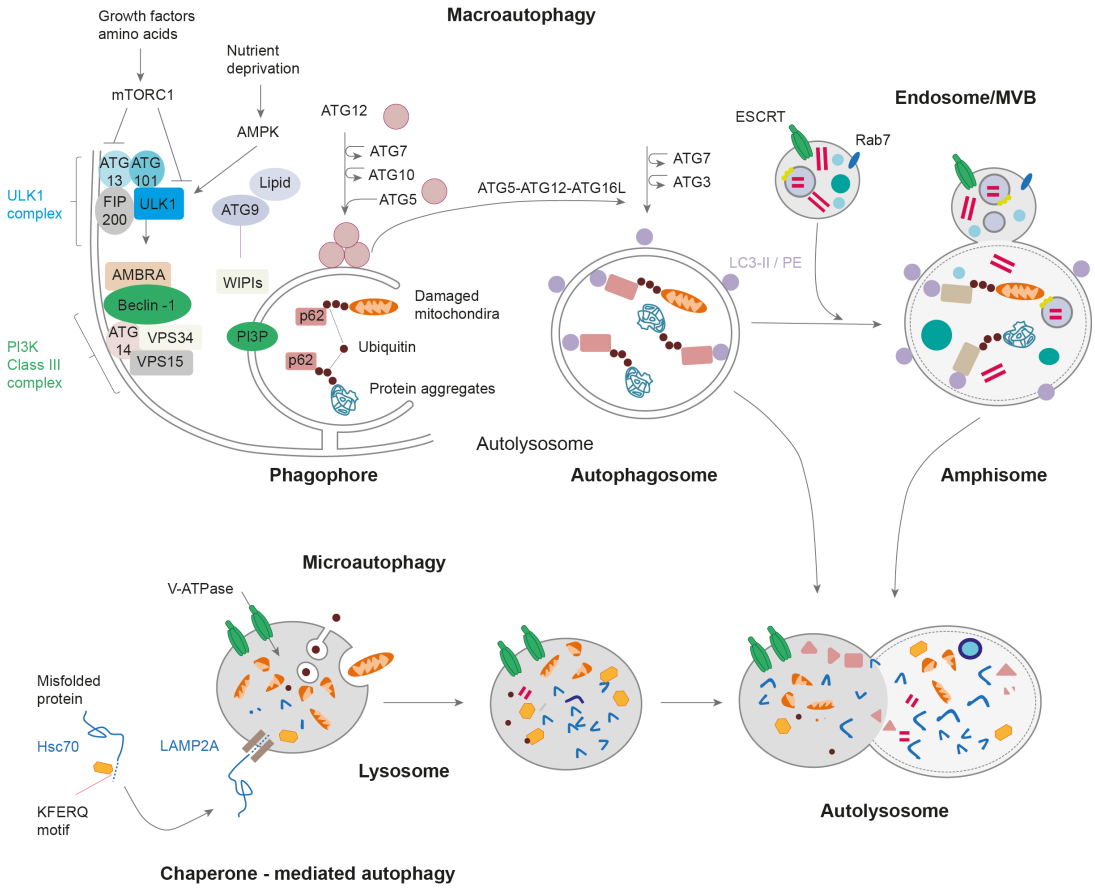

Figure 1-7 Schematic diagram of macroautophagy, microautophagy and chaperone-mediated autophagy: Summary of microautophagy, chaperone-mediated autophagy, and macroautophagy. Macroautophagy begins with cargo recognition and the formation of a phagophore that matures into autophagosomes. Autophagic cargo may include material incorporated via endocytosis and transported via endosomes and multivesicular bodies for lysosomal degradation. The autophagosome can fuse with an endosome to generate an amphisome, which fuses with a lysosome leading to an autolysosome. However, the autophagosome can fuse directly with the lysosome also generating an autolysosome. The lysosomes maintain an acidic pH through the proton (H+) vacuolar ATPase (V-ATPase) and are characterized by their expression of lysosomal associated membrane proteins (LAMP). Macroautophagy is inhibited by mTORC1 activation and activated AMPK via phosphorylation of ULK1 complex that includes ATG13, ATG101, and focal adhesion kinase (FAK) family kinase-interacting protein of 200 kD (FIP200). The next complex involved in autophagosome formation is the PI3K complex, which includes beclin 1, AMBRA, ATG14,

and VPS 34 and VPS15. ULK1 phosphorylates AMBRA1, enabling the PI3K class III complex to relocate from the cytoskeleton to the phagophore and generate PI3P. PI3P catalyses the conjugation of ATG5 and ATG12 (in the presence of ATG7 and ATG12); attachment of the ATG5/ATG12/ATG16 complex induces the conjugation of LC3 to PE. The cargo selectivity for protein of aggregates or damaged organelles such as mitochondria involves one or several cargo receptors, including the ubiquitin-binding adaptor protein p62/sequestosome 1.

1.8 Regulators of autophagy

Autophagy is shown to be mainly regulated through a wide range of upstream metabolic pathways and food consumption. Such pathways additionally affect ageing as well as age-related neurodegenerative diseases. Such pathways include but are not limited to, mTORC1, the ULK1 complex, AMPK and ERK pathways as well as transcription factor EB (TFEB) and GSK3.

1.8.1 Mammalian target of rapamycin complex 1 (mTORC1)

mTOR is a serine/threonine kinase, which is a master regulator of cellular metabolism and promotes cell growth in response to environmental cues (Jung et al., 2010). mTOR forms two distinct signaling complexes; mTORC1 and mTORC2, of which the mTORC1 complex is relevant to autophagy (Kim and Guan, 2015). mTORC1 integrates nutrient and growth factor signaling to promote anabolic metabolism, such as protein synthesis and lipid synthesis, and to inhibit catabolic pathways, such as lysosome biogenesis and autophagy (Kim and Guan, 2015). The mTORC1 complex comprises mTOR, G protein β-subunit-like protein (GβL), proline-rich Akt substrate of 40 kDa (PRAS40), and the regulatory-associated protein of TOR (raptor). Notably, rapamycin solely binds to mTORC1, and inhibits mTORC1-mediated phosphorylation of ribosomal S6 kinase (Kim et al., 2002). Notably, mTORC1 deficiency has been shown to resemble rapamycin treatment, which activates autophagy (Figure 1-8) (Kim et al., 2002).

Under nutrient-rich conditions, mTORC1 negatively regulates autophagy by phosphorylating ULK1/2 and Atg13, thereby inhibiting the kinase complex (Figure 1-8) (Ganley et al., 2009; Hosokawa et al., 2009). Moreover, under such conditions, PRAS40 is phosphorylated by protein kinase B (PKB or Akt) and dissociates from raptor to activate mTORC1. In response to starvation, the mTORC1-dependent phosphorylation sites in ULK1/2 are rapidly dephosphorylated, and ULK1/2 then autophosphorylates and phosphorylates Atg13 and FIP200 (an ULK-1 interacting partner) (Hosokawa et al., 2009). Therefore, under nutrient rich conditions, mTORC1 activation inhibits autophagy activation. Conversely, upon starvation, mTORC1 activity is inhibited, thereby activating autophagy.

1.8.2 **AMP-activated protein kinase (AMPK)**

AMPK is a serine/threonine kinase that is the major energy-sensing kinase that activates a wide variety of catabolic processes. The phosphorylation of a conserved threonine residue (Thr172) in the activation loop of the catalytic α-subunit by upstream kinases such as LKB1 and Ca^{2+}-activated Ca^{2+}-calmodulin-dependent kinase kinase β (CaMKKβ), is a prerequisite for the activity of AMPK (Hawley et al., 2005; Woods et al., 2005). The increased phosphorylation of AMPK at Thr172 has been associated with increased autophagy activation as it was shown to correlate with rises in the levels of LC3-II in colorectal cancer cells (Sueda et al., 2016).

AMPK and mTORC1 both regulate the vesicular protein sorting 34 (VPS34) (an ATG14L-associated) complex, a class III PI3K whose activity is crucial for autophagosome formation (Jung et al., 2010). VPS34 forms multiple complexes and has critical roles in cellular vesicle trafficking and autophagy induction (Figure 1-8). Under starvation conditions, AMPK activates the pro-autophagy VPS34 complex by phosphorylating beclin-1. AMPK additionally leads to the phosphorylation of Thr163/Ser165 of the VSP34 complex, which acts to inhibit autophagy. On the other hand, mTORC1 phosphorylates ATG14L in the VPS34 complex and inhibits the lipid kinase activity of VPS34, providing another mTORC1-mediated mechanism in autophagy inhibition (Alers et al., 2012).

1.8.3 **The mammalian homologue of Atg1, ubiquitin like kinase (ULK1) complex**

The ULK1 complex plays a central role in autophagy induction. The mTORC1 complex, functions in part, by phosphorylating Ser758 (Ser757 in mouse) of ULK1 and inhibiting ULK-1. On the other hand, AMPK, a positive regulator that stimulates autophagy in response to energy depletion, directly regulates autophagy through phosphorylating and activating ULK1 (Figure 1-8) (Egan et al., 2011). mTORC1-dependent phosphorylation appears to antagonise AMPK activity by preventing the physical association of AMPK with ULK1 (Figure 1-8) (Kim et al., 2011). mTORC1 phosphorylation of ULK1 at Ser757 disrupts the physical interaction between AMPK and ULK1 thereby inhibiting autophagy. These findings highlight the physiological role of ULK1 phosphorylation by AMPK. In contrast the phosphorylation of ULK1 at Ser317, Ser555 and Ser777 by AMPK, mediates the translocation of ULK1 and activates autophagy and mitophagy (Tian et al., 2015). mTORC1

is also able to inhibit ULK1 stability by inhibitory phosphorylation of AMBRA1 (Nazio et al., 2013).

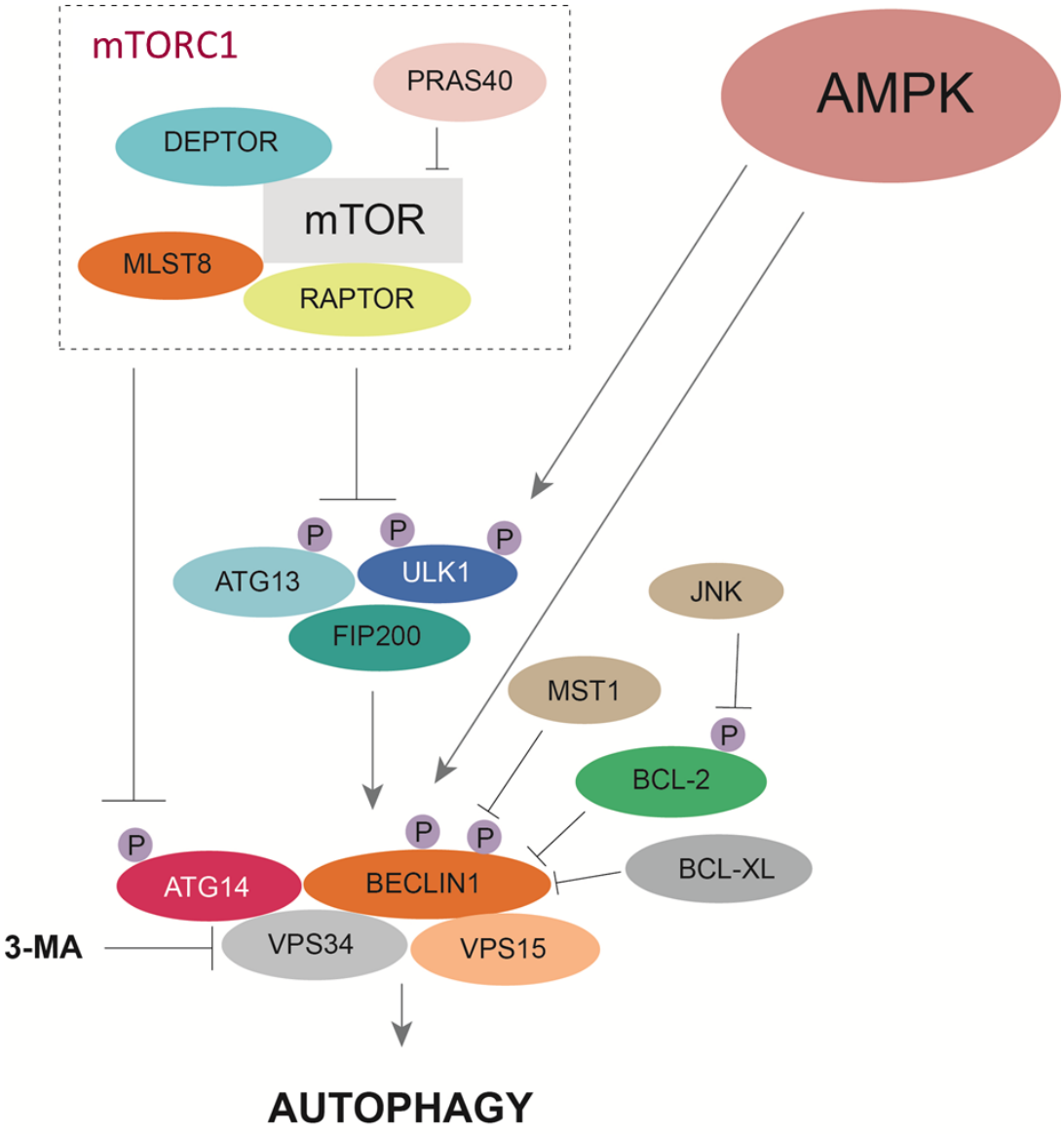

Figure 1-8: Schematic representation of the role of mTORC1, AMPK and the ULK1 complex in autophagy activation: Activated mTORC1 phosphorylates ATG13, ULK1, and ATG14 to inhibit autophagy. AMP-AMPK activates autophagy by directly phosphorylating ULK1/2 and beclin 1. BCL-2 and BCL-XL bind to beclin 1 to inhibit autophagy. JNK phosphorylates BCL-2 to prevent its interaction with beclin 1, whereas MST1 phosphorylates beclin 1 to increase its interaction with BCL-2 and BCL-XL, inhibiting autophagy. 3-MA inhibits VPS34 and suppresses autophagy.

1.8.4 **Transcription factor EB (TFEB)**

Transcription factor EB (TFEB) is considered to be the master regulator of autophagy, since it regulates the expression of genes required for autophagosomal and lysosomal biogenesis (Napolitano and Ballabio, 2016). TFEB is a basic helix-loop-helix leucine zipper transcription factor (Roczniak-Ferguson et al., 2012b). It binds to a promoter motif responsible for coordinating the expression of lysosomal genes; the coordinated lysosomal expression and regulation (CLEAR) network. This comprises of genes involved in autophagy, lysosomal biogenesis, lysosomal exocytosis, endocytosis, and membrane repair (Palmieri et al., 2011). Once bound, TFEB results in autophagosome formation and autophagosome–lysosome fusion (Figure 1-9) (Settembre et al. (2011). In addition, TFEB augments cellular clearance through lysosomal exocytosis, a process mediated by activation of the lysosomal Ca^{2+} channel transient receptor potential (TRPM2), also known as Mucolipin-1 (Medina et al., 2011; Xiao et al., 2015a).

Under normal conditions, TFEB is located in the cytoplasm. However, conditions of stress, such as starvation/autophagy activation, result in the translocation of TFEB to the nucleus, where it promotes the transcription of its target genes (Martina et al., 2014). The activation state of TFEB and its phosphorylation state at Ser142 and Ser211 are directly correlated. The phosphorylation of TFEB is facilitated either by ERK2 or mTORC1 (Figure 1-9). When TFEB is in the cytoplasm, it can often be found on the surface of lysosomes. Under nutrient-rich conditions, mTORC1 binds to the TFEB on the lysosomal surface, thereby facilitating its phosphorylation and cytoplasmic sequestration. Inhibiting mTORC1 with torin 1 results in TFEB nuclear accumulation (Settembre et al., 2012).

TFEB also regulates its own expression through a starvation-induced autoregulatory loop (Settembre et al, 2013). The TFEB promoter contains multiple CLEAR elements. TFEB itself binds to these elements, leading to additional TFEB expression (Settembre et al., 2013). Moreover, Mucolipin-1 leads to TFEB dephosphorylation and its ultimate nuclear translocation due to an increase in local Ca^{2+} levels, which activates calcineurin (a protein phosphatase) (Medina et al., 2015).

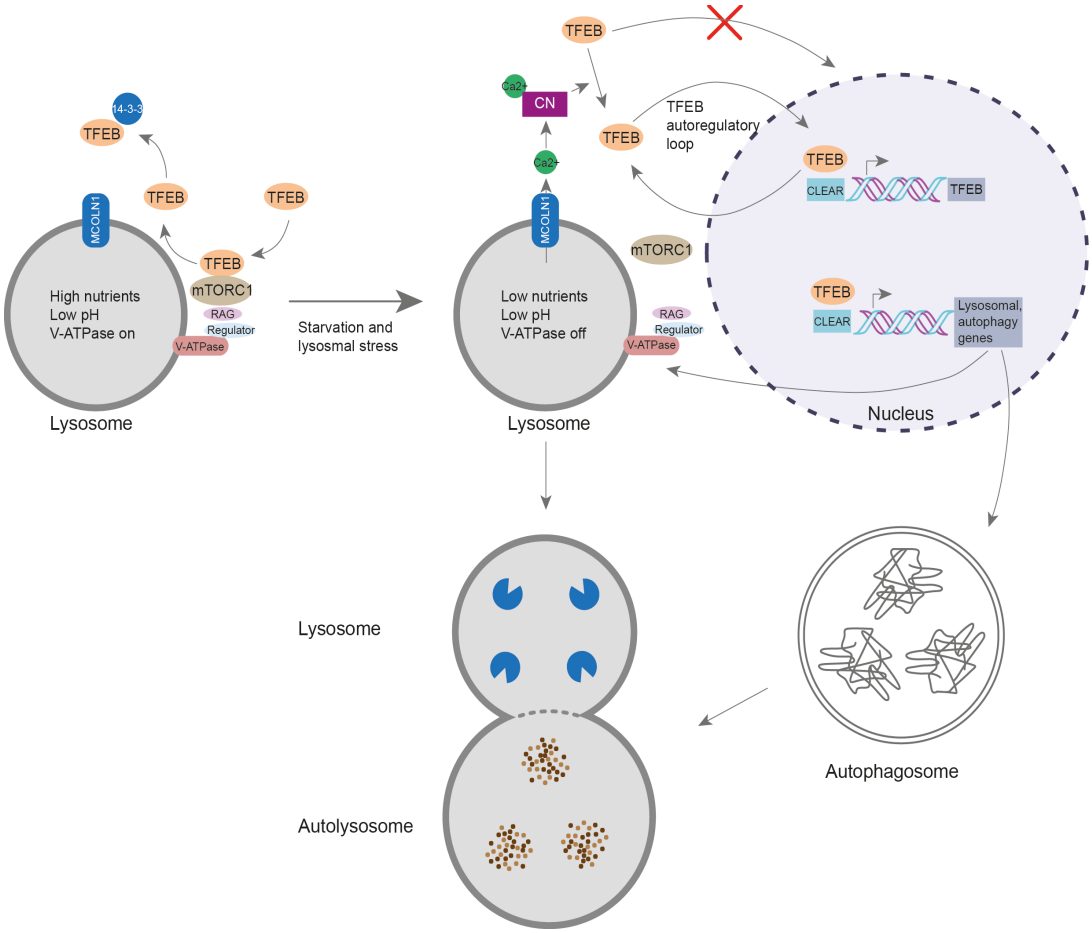

Figure 1-9 Role of TFEB in autophagy/lysosomal degradation: In nutrient-rich conditions, the V-ATPase, Ragulator, and Rag GTPases form an active complex that binds tomTORC1 at the lysosomal surface and activates it. mTORC1 then phosphorylates TFEB which leads to is cytoplasmic sequestration. Under starvation conditions and lysosomal stress, mTORC1 is released from the lysosomal surface and inactivates it. Because mTORC1 can no longer phosphorylate TFEB, the unphosphorylated TFEB translocates to the nucleus to bind to the CLEAR sequence of its target genes, leading to the upregulation of autophagy and lysosomal genes. The TFEB gene also has numerous CLEAR sequences in its promoter, and thus TFEB upregulates its own expression in an autoregulatory loop. Another positive feedback loop deals with Mucolipin-1, that is a transcriptional target of TFEB. Mucolipin-1 creates high Ca^{2+} concentration near the lysosomal surface. The higher Ca^{2+}concentration then activates the phosphatase calcineurin, which dephosphorylates TFEB, promoting its activation.

1.9 Autophagy and disease

Several reports find a strong association between ageing and downregulation or deregulation of autophagic activity (Metaxakis et al., 2018; Nixon, 2013; Rubinsztein et al., 2007). A role for autophagy in the clearance of protein aggregates has been suggested for several proteins, including β-amyloid, α-synuclein, tau, prion protein and huntingtin (Casarejos et al., 2011; Sarkar et al., 2007b). In neurodegenerative diseases, autophagy dysfunction arises at various points along the pathway, giving rise to distinct pathologic patterns with different implications for modulating autophagy as a therapy (Nixon, 2013). This dysfunction is observed in many neurodegenerative diseases (summarised in Table 1-4). Studies in human brain reveal downregulation of Atg5, Atg7, and beclin 1 autophagy genes (Lipinski et al., 2010), as well as an increased mTOR activity, accompanied by a decline in Atg proteins in brains of aged rodents (Ott et al., 2016). In addition, in AD brain, autophagic vacuoles accumulate without degradation of their contents by lysosomes (Nixon et al., 2005a; Yu et al., 2004), suggesting autophagic dysfunction. A series of dysfunctions that can occur in the autophagy pathway in various neurodegenerative diseases are outlined in Table 1-4.

Table 1-4 Summary of autophagic deficits in neurodegenerative diseases (Adapted from (Nixon et al., 2013)).

Autophagic deficit	Neurodegenerative disease	Proposed autophagy defect
Substrate sequestration and autophagosome formation	Parkinson's disease	Rab1A-mediated Atg9 mislocalisation (Winslow et al., 2010)
	Huntington's disease	Mutant huntingtin-mediated aggregation of beclin-1 or mTOR; impaired engagement of cargo by autophagosomal membrane (Shibata et al., 2006)
	Lafora's disease	Decreased autophagosome formation via mTOR upregulation (Aguado et al., 2010)
Substrate recognition, selective autophagy	Amyotrophic lateral sclerosis (ALS)	*SQSTM1* (p62) mutations (Fecto and Siddique, 2011)
	Inclusion body myopathy, Paget's disease of the bone and frontotemporal dementia (IBMPFD)	*VCP* (p97) mutations lead to decreased autophagosome maturation and mitophagy (Ritz et al., 2011; Tresse et al., 2010)
	Parkinson's disease	PINK and parkin mutations lead to impaired mitophagy; *LRRK2* mutations lead to decreased CMA; mutation or duplication of synuclein-encoding genes leads to decreased CMA (Alvarez-Erviti et al., 2010)
Autophagosome-lysosome-endosome fusion	Lower motor neuron disease	Dynactin (*DCTN1*) mutations lead to impaired autophagosome and lysosome transport (Ferrucci et al., 2011)

	ALS	Dynactin mutations; mutant ALS2-mediated Rab5 suppression (Otomo et al., 2011)
	Spinal and bulbar muscular atrophy	Mutations in dynein motor complex components (for example, *DYNC1H1*) (Ferrucci et al., 2011)
	Frontotemporal dementia	*CHMP2B* mutation leads to impaired amphisome formation (Ganley et al., 2011)
Lysosomal digestion	Alzheimer's disease	Presenilin 1 (*PSEN1*) mutations cause a deficiency in V-ATPase, leading to increased lysosome pH; ApoE4 variant or Aβ leads to increased LMP; *APP* mutations or duplications, increased cholesterol or the ApoE4 variant lead to activation of Rab5 or Rab7 activation and substrate overload in lysosomes (Cataldo et al., 2004; Glabe, 2001)
	Parkinson's disease	Duplications or mutations of synuclein genes or *ATP13A2* mutation lead to lysosome pH elevation and hydrolase inhibition; MPTP treatment leads to increased LMP; β-glucosidase (*GBA*) mutation leads to decreased lysosomal hydrolytic activity (Sardi et al., 2011)
Lysosomal storage disorders	Neuronal ceroid lipofuscinoses (NCLs)	*CLN3* mutation leads to decreased autolysosome maturation; cathepsin D mutation leads to decreased proteolysis (Siintola et al., 2006)
	Niemann-Pick type C (NPC)	*NPC1* mutation leads to decreased proteolysis from stored lipid (Elrick, 2002)
	Mucolipidosis type IV	MCOLNl (*TRPML1*) mutations lead to a lysosomal pH elevation (Curcio-Morelli et al., 2010)
	Gaucher's disease	β-glucosidase (*GBA*) mutation leads to decreased lysosomal hydrolysis (Sardi et al., 2011)

Disruption in early autophagy has been shown to be linked to the development of AD. APP transgenic mice with a heterozygous deletion of beclin 1 have an increase in Aβ plaque deposition, neuronal loss, and the accumulation of abnormal lysosomes containing electron-dense material (Pickford et al., 2008b). These findings indicate that autophagy plays a central role in APP transport and metabolism, as well as the degradation of APP metabolites (Jaeger and Wyss-Coray, 2010).

Increased mTOR activation is linked to several neurogenetic disorders characterised by abnormal synaptic plasticity (Gipson and Johnston, 2012). Using 3xTg-AD mice, it was shown that increased mTOR signaling correlated with tau accumulation. There was an overt correlation between genetically increasing mTOR signaling and elevated tau levels and phosphorylation. Moreover, the reduction of mTOR signaling with rapamycin ameliorates tau pathology and rescues motor deficits, suggesting that mTOR signaling regulates tau phosphorylation (Caccamo et al., 2013a; Meske et al., 2008).

Dysregulation of the ULK1 complex has previously been associated with the development of neurodegeneration. For example, ULK1 kinase activity is deregulated in Huntington's disease (HD) (Sarkar and Rubinsztein, 2008). In addition, increased mTOR independent ULK1 activity via phosphorylation of p62/SQSTM1 while ULK1 mediated ATG14/Beclin-1 phosphorylation is decreased in Huntington's disease (Wold et al., 2016). Moreover, CBD and PSP brains show abnormal accumulation of p62, as well as LC3 and colocalisation of both LC3 and p63 with phosphorylated tau (Piras et al., 2016a). In addition, *in vivo* work on P301S tau mice showed that stimulation of autophagy reduced the amount of tau aggregates and improved nerve cell survival (Schaeffer et al., 2012a).

A mouse model with tissue-specific knockdown of Atg7 in the CNS showed accumulation of inclusion bodies in autophagy-deficient neurons, however no changes in proteasome function were evident (Komatsu et al., 2006). Inclusion bodies were increasing in size and number with age leading to vast neuronal loss in comparison to controls. These mice were dead within 28 weeks of birth revealing the adverse effect of Atg7 knockdown on life span (Komatsu et al., 2006).

Taken together, these results highlight the vitality of the autophagic pathway for the survival of neural cells and that inadequate level of autophagy can lead to the pathogenesis of neurodegenerative disorders.

The mislocalisation of proteins including TFEB has been reported in several neurodegenerative diseases including AD, PD, HD and ALS (Barber *et al,* 2010; Nunomura *et al,* 2006). TFEB has been proposed as a key component in the degradation of highly phosphorylated and misfolded tau (Polito et al., 2014) and activation of TFEB by fisetin, a naturally occurring flavonol, increases degradation of phosphorylated tau in neurons (Kim et al., 2016). In addition, enhancing the activation of autophagy lysosomal pathway through exogenous TFEB expression in the brains of P301L tau mice dramatically reduces tau pathology, neurodegeneration, and behavioural deficits (Polito et al., 2014). The proposed mechanism of action in this study operates via a TFEB–PTEN (phosphatase and tensin homolog)–Akt–mTOR–TFEB feedback regulatory loop. As such, TFEB activates autophagy through upregulation of PTEN and inhibition of Akt and mTOR, which further activates TFEB (Polito et al., 2014). On the other hand, the role of TFEB in the development of neurodegeneration has been shown to have both positive and negative effects. On the one hand, the cytoplasmic sequestration of TFEB could result in deficiency in the clearance of accumulated, potentially toxic proteins. On the other hand, TFEB could be upregulated in response to lysosomal stress resulting from a pre-existing insult such as mutation or dysfunction in other components of the autophagy pathway (Martini-Stoica et al., 2016a).

There are likely to be numerous mechanisms that could explain the altered subcellular distributions of proteins such as TFEB in degenerating neurons. A key mechanism for which there is increasing evidence is impairment in nucleocytoplasmic transport. The role of the nuclear pore complexes and nuclear transport has been investigated in a number of human diseases. The importin family of proteins control he import of proteins into the nucleus and comprises importin α and β (Pemberton and Paschal, 2005). Zhu and colleagues examined the localisation of importin-α1 in post mortem AD cases and found that there was little to no importin-α1 in NFT or amyloid plaques in hippocampal CA1 neurons, compared to the cytoplasmic localisation of importin-α1 in age-matched control

brain (Lee *et al,* 2008). Importin-α is a key player in nucleocytoplasmic transport and the mislocalisation of this protein can have profound impacts on cell survival (Lee *et al,* 2008).

Lysosomal dysfunction is apparent in AD, PD and HD. Recent findings indicate that different neurodegenerative diseases exhibit varying amounts of lysosomal associated membrane proteins (LAMP 1 and LAMP2) in comparison to controls. Studies of CSF from people with PD show significant decreases in both LAMP1 and LAMP2 compared with control CSF (Boman et al., 2016). In contrast, CSF from people with CBD showed increases in LAMP1 and LAMP2 compared to controls (Boman et al., 2016). Lysosome size also correlates with normally functioning lysosomes. Work by Yang and colleagues using TgCRND8 (APP overexpressing) mice indicated that enlarged autolysosomes in this model are filled with incompletely digested autophagic substrates, reflecting inefficient degradation by lysosomal hydrolases compared to controls. Furthermore, lysosome fractions isolated from the brains of TgCRND8 mice contain abnormally high levels of LC3-II, ubiquitinated proteins and Aβ (Yang et al., 2011). Moreover, it has been shown that experimentally induced lysosomal dysfunction triggers the development of characteristic features of the aged human brain. These include proliferation of endosomes–lysosomes, increased tau phosphorylation, production of tau protein fragments resembling those found in NFTs, and the accumulation of 16–30 kDa tau fragments (Oyama et al., 1998; Zhang et al., 2009a). Cathepsin D inhibitors block the formation of phosphorylated tau fragments in AD hippocampus (Bi et al., 2000). In addition, recent evidence showed that the autophagic-lysosomal system also plays a role in the clearance of tau, whereas dysfunction of this system results in the formation of tau insoluble aggregates in lysosomes (Hamano et al., 2008b).

1.10 The unfolded protein response (UPR)

The UPR pathway is an adaptation to organelle stress and this is activated when the normal function of the ER is disrupted by intrinsic or extrinsic insults, in order to prevent ongoing protein synthesis upon accumulation of unfolded proteins (Schonthal, 2012). Activation of the UPR involves the upregulation of genes encoding chaperones such as immunoglobulin heavy-chain binding protein (BiP), foldases, and proteins involved in the degradation of ER localised proteins by the proteasome (Matus et al., 2008).

A growing body of evidence shows an association of the UPR pathway with the development of both genetic and sporadic forms of neurodegeneration, including AD and PD (Imaizumi et al., 2001). This pathway has also been identified as a key player in the pathology in models of neurodegeneration such as prion disease (Halliday and Mallucci, 2014). The function of the UPR is to enhance the protein folding capacity of the ER and this can be activated by amino acid deprivation, viral replication and the presence of unfolded proteins (Radford et al., 2015).

The UPR has three main arms, comprising inositol requiring enzyme 1 (IRE1), protein kinase RNA (PKR)-like ER kinase (PERK) and activating transcription factor 6 (ATF6) (Figure 1-10). When cells are not stressed, BiP is bound to IRE1, PERK and ATF6, thereby inhibiting activation of the UPR pathway (Halliday and Mallucci, 2014). Upon accumulation of misfolded/unfolded proteins, these three proteins dissociate from BiP as the misfolded/unfolded proteins bind to and sequester BiP. Therefore, the three branches of the UPR can be active and it has been shown that all three branches of the UPR can be simultaneously activated when there is excessive ER stress (Wu and Kaufman, 2006). The more immediate initiation of the pathway is through the activation of PERK, which is followed by the slower activation of the other two arms, IRE1 and ATF6. Activation of PERK results from its autophosphorylation, which causes the subsequent phosphorylation of eukaryotic initiation factor 2α (eIF2α) and has the effect of reducing protein synthesis to counteract the increased load on the ER (Smith and Mallucci, 2016). This phosphorylation has two outcomes: either a repression in protein translation which stops protein synthesis of most proteins, or conversely the upregulation of activating transcription factor 4 (ATF4) which is involved in the regulation of protein folding genes such as C/EBP homologous protein (CHOP) which eventually leads to apoptosis (Figure 1-10) (Radford et al., 2015).

The accumulation of unfolded proteins causes the cytoplasmic domain of ATF6 to translocate from the ER to the Golgi apparatus. Once it reaches the Golgi, ATF6 is cleaved by site 1 and site 2 proteases at the transmembrane site into a 50 kDa fragment. The cleavage event results in the formation of nuclear activated ATF6 (nATF6) which is then transported to the nucleus where it activates central UPR genes (Figure 1-10) (Smith and Mallucci, 2016)

The presence of unfolded proteins in the cell leads to the trans-autophosphorylation of IRE1, resulting in its activation. Subsequently, IRE1 goes on to activate the splicing of mRNA that encodes X-box binding protein 1 (XBP1). sXBP1 is a transcription factor that directly targets genes that facilitate the refolding and degradation of misfolded proteins, including ER chaperones such as Grp78/BiP, Grp58, Grp94, ER-associated degradation (ERAD) components (Figure 1-10) (Ron and Hubbard, 2008). The aforementioned splicing event results in the alteration of the reading frame of the XBP1 mRNA, forming a transcription factor that regulates multiple UPR related genes as well as genes involved in redox metabolism and autophagy (Halliday and Mallucci, 2014).

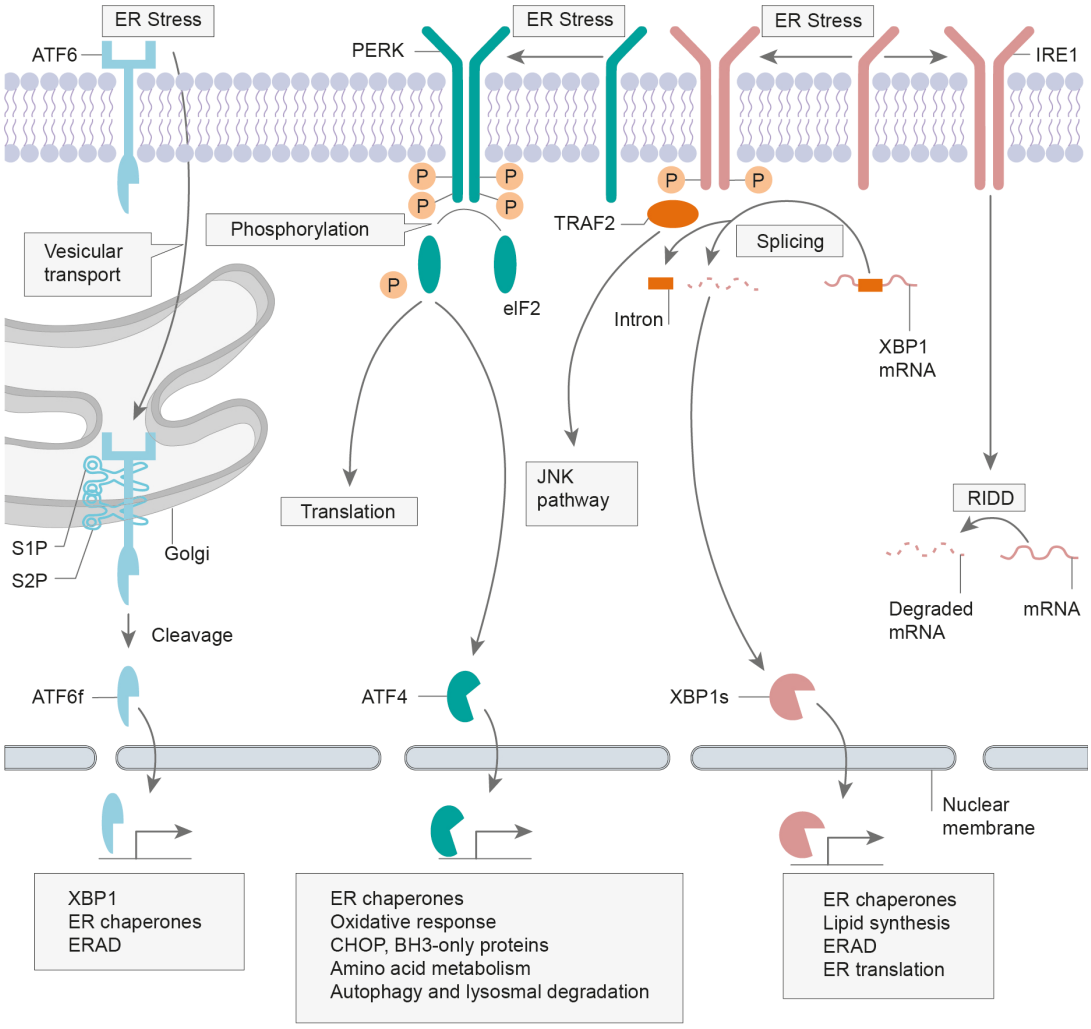

Figure 1-10 Schematic representation of the three arms of the UPR: The three branches of the unfolded protein response (UPR) pathway. The binding of unfolded proteins to BiP causes the dissociation and activation of PERK, IRE1 and ATF6. Activation of the PERK branch leads to the phosphorylation of eIF2α which leads to reduced protein synthesis through activation of CHOP. Activation of IRE1 leads to alternative slicing of XBP1 causing transcription of chaperones and ERAD protein. ATF6 is cleaved forming nATF6 leading to the expression of UPR target genes (adapted from (Hetz and Mollereau, 2014)).

Once the UPR is activated, the ultimate outcome will depend on the levels of stress. Thus, mild ER stress will lead to an adaptive ER response, whereby cells return to their normal physiological state. On the other hand, chronic ER stress can prove to be a burden on the cell thereby leading to cell death (Hetz and Mollereau, 2014). Therefore, acute activation of the UPR appears to be a protective mechanism adopted by cells, however prolonged UPR activation is detrimental to cell health and survival. Consequently, increasing links are being drawn between UPR activation and neurodegenerative diseases such as AD, PD, HD and ALS (Hoozemans et al., 2012). In agreement with these findings, a close association has been proposed between the occurrence of neurodegeneration and the upregulation of ER stress markers in animal models of AD, PD, ALS and HD (Mercado et al., 2013; Vidal et al., 2011).

In a *Drosophila* model of AD, the enforced expression of active XBP1 was shown to protect against amyloid-β toxicity, possibly through reduced release of Ca^{2+} from the ER (Casas-Tinto et al., 2011). Furthermore, using genetic mouse models of AD (APPswe/PS1dE9) that express familial Alzheimer's disease–related mutant APP and mutant presenilin 1 (*PS1*) with a deletion of exon 9), ablation of PERK in the brain improved memory impairment (Ma et al., 2013a). In contrast, another study proposed that phosphorylation of eIF2α in AD occurs through RNA-activated protein kinase (PKR; also known as eIF2αK2) rather than PERK. However, to date these findings have not been confirmed (Lourenco et al., 2013).

Increased activation of the UPR has additionally been correlated with tau pathology. In AD, it is suggested that UPR activation may precede pathogenesis of the disease (Nijholt et al., 2012b). In a specific study in AD brain, increase in UPR markers closely correlated with the presence of phosphorylated tau and GSK3β (Nijholt et al., 2012b). This suggests that prolonged UPR activation in neurons may be involved in detrimental tau phosphorylation (Hoozemans et al., 2009).

1.11 Apoptosis

Apoptosis (programmed cell death) is activated as a final resort of the cell to deal with an irreparable amount of damage. Initiation of this pathway commences with the activation

of caspases, a process that is very tightly regulated by the Bcl-2 family of proteins. This family of proteins is composed of pro- and anti-apoptotic proteins that are defined by the presence of up to four conserved domains ((Matus et al., 2008),

1.11.1 **Apoptosis and autophagy**

It was shown by Wirawan et al. (2010) that beclin-1 and PI3K, two components of the autophagy-inducing complex, are direct substrates of caspases. The cleavage of beclin-1 and PI3K by caspases (caspases 3, 7 and 8) was observed in response to different inducers of the intrinsic (mitochondrial) and extrinsic (death receptor-mediated) pathways of apoptosis (Wirawan et al., 2010). Moreover, c-Jun N-terminal kinase (JNK1) or ERK-mediated phosphorylation of Bcl-2, or DAPK-mediated phosphorylation of beclin-1 regulate dissociation of beclin-1 and Bcl-2/Bcl-XL during autophagy (Tang et al., 2010; Wei et al., 2008). Such observations highlight a possible crosstalk between autophagy has additionally been shown in HeLa that the overexpression of Bax (activates the intrinsic pathway of apoptosis) and TRAIL (a death receptor ligand) in Hela cells leads to the caspase-mediated cleavage of beclin 1 (Cho et al., 2009; Lao et al., 2009). However, recent studies indicate that active caspase-8 can be degraded by autophagy. This further implies the existence of a feedback mechanism that cross-regulates autophagy and apoptosis (Hou et al., 2010).

Beclin-1 is unable to neutralise the anti-apoptotic function of Bcl-2, which is exerted at the mitochondrial membrane. Concurrently, Bcl-2 or Bcl-XL reduces the pro-autophagic activity of beclin-1 (Pattingre et al., 2005). Interestingly, ER-localised Bcl-2, but not mitochondrial-localised Bcl-2, inhibits autophagy, which is consistent with the notion that ER-associated class III PI3K activity may be crucial in the nucleation of autophagosome formation (Pattingre et al., 2005). In addition to the apoptosis-associated cleavage of beclin-1, there is an additional apoptotic-associated cleavage of more autophagic proteins including Atg5 and Atg4D by caspase-3. Similar to the cleavage of beclin-1, cleavage of Atg5 inactivates autophagy. Conversely Atg4D cleavage generates a fragment with increased autophagic activity (Galluzzi et al., 2010), indicating that this may be an important regulatory mechanism in coordinating the activity of autophagy and apoptosis.

1.11.2 **Apoptosis and the UPR**

Under pathological conditions, the protective effect of sXBP1 is masked by the build-up of pro-apoptotic factors, thereby driving activation of apoptosis. All three branches of the UPR have been implicated in ER stress-induced apoptosis. Firstly, the activation of CHOP by PERK/eIF2α phosphorylation ultimately drives the cell to apoptosis. Moreover, Both CHOP and JNK control the activation of pro- and anti-apoptotic Bcl-2 proteins by increasing the expression of pro-apoptotic Bak and Bax, resulting in permeabilisation of the outer mitochondrial membrane and execution of the intrinsic apoptotic process (Dhanasekaran and Reddy, 2008; Jager et al., 2012). In addition, IRE1 can elicit the activation of apoptosis signal-regulating kinase 1(ASK1)/JNK. ASK1-deficient cells have been shown to be resistant to ER stress-induced apoptosis, as well as JNK activation, indicating that ASK1 acts upstream of the site of JNK activation (Kadowaki et al., 2005).

IRE1 is additionally able to activate caspase-12 (Kim et al., 2006). Caspase-12 is synthesised as a pro-enzyme and solely responds to ER stress, as shown by studies that revealed that caspase-12 deficient cells are resistant to ER stress-induced apoptosis, but not apoptosis induced by alternative stimuli (Kaneko et al., 2003). IRE1 within the cytosol recruits TRAF2, which interacts with caspase-12, resulting in the formation of the IRE1/TRAF2/caspase-12 complex and subsequent cleavage of activated caspase-12 (Yoneda et al., 2001). These mechanisms all result in downstream caspase activation and elicit the execution of ER stress-induced cell death (van der Kallen et al., 2009).

1.12 Aims and objectives

Since the identification of the Tau35 fragment in brains of 4R tauopathies including PSP, CBD and FTLD-tau (Wray et al., 2008), extensive work has gone into characterising the effects of this form of truncated tau (see Figure 1-11) and establishing the role of tau fragmentation using cell and animal models (Bondulich et al., 2016).

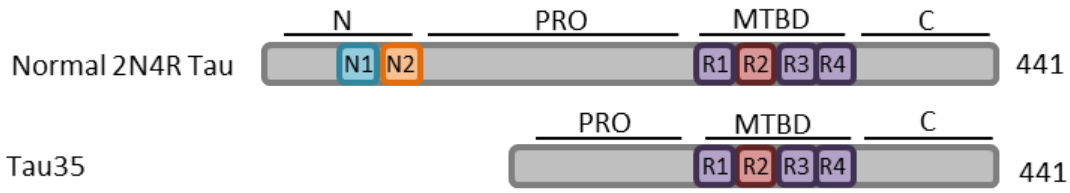

Figure 1-11 Schematic representation of Tau35 compared to 2N4R tau: 2N4R tau (amino acids 1-441) contains two inserts (N1, N2), followed by proline-rich domain and the MT binding domain, consist of four MTB repeats (R1-R4). Tau35 (amino acids 187-441) retains the majority of the proline-rich domain, four MTB repeats and an intact C-terminus.

Findings from the transgenic mouse model expressing Tau35 showed that these mice manifest several key features of tauopathies, including accumulation of abnormally phosphorylated tau along with deregulated GSK3β, autophagic dysfunction, and progressive cognitive and motor deficits (Bondulich et al., 2016). Follow up work carried out by Tong Guo (King's College London) in a cell model showed that Tau35 expression disrupts microtubule binding and compromises the cytoskeleton, as well as increasing activation of the UPR. Consequently, this study aims to extend studies on aged Tau35 mouse brain in order to further investigate underlying molecular mechanisms that give rise to a tauopathy phenotype. Using the Tau35 cell model, this study aimed to elucidate underlying processes involved in tau degradation that contribute to the potentially harmful effects of tau fragmentation.

The specific objectives of this study are to investigate cellular mechanisms affected by tau fragmentation in tauopathies by:

- Assessing changes in tau phosphorylation and UPR activation in different brain regions of aged Tau35 mice.
- Investigating the effects of tau fragmentation on cell viability and autophagic pathways in cells expressing Tau35.
- Determining the effects of Tau35 expression on lysosome biogenesis and lysosome functionality in cells.

Chapter 2 Materials and Methods

2.1 Materials

All reagents were from Sigma Aldrich and all solutions were prepared in ultra-high purity (UHP) water, unless otherwise stated.

2.1.1 **Animals**

Control mice used in this study were all male wild type (WT) C57BL/6J (Charles River, UK). All transgenic mice were bred on a 75%; 25% C57BL/6J; 129/Ola mice background reared in-house. Tau35 hemizygous male mice expressing Tau35 cDNA with a haemagglutinin (HA) tag under the control of the human tau promoter with targeted insertion into the *Hprt* locus were generated by genOway (Lyons, France) using "Quick Knock-in™" technology.

Mice were weaned at 3 weeks of age and had unlimited access to water and rodent chow (RM1 for all mice except breeders, which received RM3, Special Diet Services, Essex, UK). Mice were singly or group housed with a 12-hour light-dark cycle with constant room temperature. All of the studies were completed under appropriate Home Office Project and Personal Licenses.

2.1.2 **Plasmids**

cDNA sequences corresponding to human FL-tau (2N4R isoform) orTau35 (4R isoform, residues 187-441) were each inserted into the multiple cloning site of the pcDNA 3.1D/V5-His-TOPO vector (Invitrogen) for mammalian expression. These plasmids express FL-tau or Tau35 with a V5-His epitope tag fused to the C-terminus of the expressed protein.

A mammalian expression plasmid encoding human transcription factor EB (TFEB) fused to green fluorescent protein (EGFP) was obtained from Addgene.

2.1.3 **Primers used for polymerase chain reaction (PCR) genotyping**

Table 2-1 List of PCR primers

Primer	Primer sequence 5’ to 3’ (number of bases)
Forward Tau35	CGTATGTGATGGACATGGAGATGGAGG (27)
Reverse Tau35	GCCTCCCTCTTATTAAGGACGCTGAGG (27)
Forward HPRT	TGTCCTTAGAAAACACATATCCAGGGTTTAGG (32)
Reverse HPRT	CTGGCTTAAAGACAACATCTGCAGAAAAA (30)

2.1.4 **Buffer solutions**

Tris-buffered saline (TBS)

50mM Tris-HCl
150mM NaCl
pH 7.6

Phosphate-buffered saline (PBS)

137mM NaCl
2.7mM KCl
10mM disodium phosphate (Na_2HPO_4)
2mM monopotassium phosphate (KH_2PO_4)
pH 7.4

Extra strong lysis buffer (ESLB)

10mM Tris-HCl
75mM NaCl
0.5% (w/v) sodium dodecyl sulphate (SDS)
20mM sodium deoxycholate
1% (v/v) Triton X-100
2mM sodium orthovanadate
1.25mM NaF
1mM sodium pyrophosphate
10mM ethylenediaminetetraecetic acid (EDTA)
Complete Mini protease inhibitor cocktail,

	EDTA-free (Roche Diagnostics, 1 tablet/10ml buffer) 1% (w/v) PhosSTOP phosphatase inhibitor cocktail (Roche Diagnostics, 1 tablet/10ml buffer) pH 7.5
Isolation buffer	250mM mannitol 5mM HEPES 0.5mM EGTA Complete protease inhibitor cocktail, EDTA-free (Roche Diagnostics, 1 tablet/10ml buffer) pH 7.4

2.1.5 **Bicinchoninic acid Assay (BCA) protein assay**

BCA assay kit (Thermo Fisher Scientific)

Albumin standard (Thermo Fisher Scientific)

The kit was used according the manufacturer's instructions.

2.1.6 **Sodium dodecyl sulphate-polyacrylamide gel electrophoresis (SDS-PAGE) and western blotting (WB)**

Laemmli buffer (2x)	65.8mM Tris-HCl 2.1% (w/v) SDS 26.3% (w/v) glycerol 0.01% (w/v) bromophenol blue 5% (v/v) β-mercaptoethanol (BME) pH 6.8
Resolving gel	10% (w/v) acrylamide (National Diagnostics) 25% (v/v) resolving buffer (National

	Diagnostics) 0.01% (w/v) ammonium persulphate (APS, National Diagnostics) 0.1%(v/v) N,N,N',N'tetramethylethylendiamine (TEMED, National Diagnostics) pH 8.8
Stacking gel	4% (w/v) acrylamide (National Diagnostics) 25% (v/v) stacking buffer, (National Diagnostics) 0.075% (w/v) APS 0.15% (v/v) TEMED pH 6.8
Running buffer	25mM Tris base, (National Diagnostics) 192mM glycine (National Diagnostics) 0.1% (w/v) SDS pH 6.8
Electrophoresis molecular weight markers	Precision Plus Protein Standards, All Blue (Bio-Rad)
Transfer buffer	25mM Tris base 192mM glycine 20% (v/v) methanol pH 6.8
Precast gels	NuPAGE 4-12% Bis-Tris gels (Thermo Fisher Scientific)
Running buffer for precast gels	NuPAGE Novex 4-12% Bis-Tris Protein gels, 1.5 mm, 15 well (Thermo Fisher Scientific)

Blocking solution (milk)	3% (w/v) skimmed milk powder in TBS + 0.1% (v/v) Tween 20
Blocking solutions (Odyssey)	Odyssey (TBS) blocking buffer (Li-Cor)
Blocking solution (BSA)	2% (w/v) bovine serum albumin (BSA) in TBS
Wash solution	TBS + 0.1% (v/v) Tween 20

2.1.7 **Immunocytochemistry (ICC)**

Fixation solution (PFA)	4% paraformaldehyde (PFA) in PBS pH 7.4
Blocking solution (BSA)	2% (w/v) bovine serum albumin (BSA) in PBS
Blocking solution (serum)	10% (v/v) goat serum in 0.5% (w/v) Triton-X100 in PBS
Permeabilising solution	0.5% (v/v) Triton-X100 in PBS
Hoechst solution	0.5% (v/v) Hoechst 33342 in PBS
Mounting medium	Fluorescence mounting medium (DAKO)

2.1.8 **Primary antibodies for WB and ICC**

Antibody	Species	Epitope	Dilution	Source
β-Actin	Mouse monoclonal	β-Actin	WB: 1/5000	Sigma Aldrich
β-Actin	Rabbit polyclonal	β-Actin	WB: 1/3000	Abcam
12E8	Mouse monoclonal	Tau phosphorylated at Ser262/Ser356	WB: 1/40000	Prothena Corporation
AT-180	Mouse monoclonal	Tau phosphorylated at Thr231	WB: 1/1000	Invitrogen
PHF-1	Mouse monoclonal	Tau phosphorylated at Ser396/Ser404	WB: 1/1000	Peter Davies (Albert Einstein College of Medicine)
Tau	Rabbit polyclonal	Tau residues (amino acids 243-441)	WB: 1/5000 ICC: 1/1000	DAKO
Tau-1	Mouse monoclonal	Tau dephosphorylated at Ser195, 198, 199, and 202	WB: 1/1000	Merck Millipore

Anti-V5	Mouse monoclonal	V5 tag (GKPIPNPLLGLDST)	WB: 1/5000	Invitrogen
Atg 13	Rabbit polyclonal	Atg 13	WB: 1/1000	Cell Signalling Technology
Atg 5	Rabbit polyclonal	Atg 5	WB: 1/500	Cell Signalling Technology
Atg 7	Rabbit polyclonal	Atg 7	WB: 1/1000	Sigma Aldrich
Beclin 1	Rabbit polyclonal	Beclin 1	WB: 1/500	Cell Signalling Technology
Cathepsin D	Goat polyclonal	Cathepsin D	ICC: 1/100	Santa Cruz Biotechnology
Cathepsin L	Rabbit polyclonal	Cathepsin L	ICC: 1/100	Abcam
CHOP	Mouse monoclonal	CHOP	WB: 1/500	Cell Signalling Technology (CST)
GAPDH	Mouse monoclonal	GAPDH	WB: 1/500	Santa Cruz Biotechnology

GT1b	Mouse monoclonal	Ganglioside GT1b	ICC: 1/50	Developmental Studies Hybridoma Bank
HA	Mouse monoclonal	HA tag (YPYDVPDYA)	WB: 1/1000	Sigma Aldrich
Importin α7	Rabbit polyclonal	Importin α7	WB: 1/1000	Abcam
LAMP-2	Mouse monoclonal	LAMP-2	ICC: 1/50	Santa Cruz Biotechnology
LBPA	Mouse monoclonal	LBPA	ICC: 1/100	Merck Millipore
LC3-B	Rabbit polyclonal	LC3-B I and II	WB: 1/1000 ICC: 1/200	Sigma Aldrich
P62	Mouse monoclonal	P62	ICC: 1/100	Novus Biological
Phospho eIF2α	Rabbit polyclonal	Phosphorylated eIF2α at Ser51	WB: 1/500	Cell Signalling Technology
Phospho GSK3	Rabbit polyclonal	Phosphorylated (inactive) GSK3α and GSK3β	WB: 1/1000	Cell Signalling Technology

Phospho IRE-1	Rabbit polyclonal	IRE1 phosphorylated at Ser724	WB: 1/500	Novus Biologicals
Phospho mTOR	Rabbit polyclonal	mTOR phosphorylated at Ser2448	WB: 1/1000	Cell Signalling Technology
Phospho PERK	Rabbit polyclonal	Phosphorylated PERK at Thr980	WB: 1/500	Cell Signalling Technology
Phospho AMPK	Rabbit polyclonal	AMPK phosphorylated at Thr172	WB: 1/1000	Cell Signalling Technology
Phospho ERK	Rabbit polyclonal	Dually phosphorylated active forms of ERK (ERK1 and ERK2)	WB: 1/1000	Promega
Total AMPK	Rabbit polyclonal	Total AMPK	WB: 1/1000	Cell Signalling Technology
Total eIF2α	Mouse monoclonal	Total eIFf2α	WB: 1/1000	Cell Signalling Technology
Total ERK	Mouse monoclonal	Total ERK	WB: 1/1000	Cell Signalling Technology
Total GSK3	Mouse monoclonal	Total GSK3α and GSK3β	WB: 1/1000	Santa Cruz Biotechnology

Total IRE-1	Rabbit polyclonal	Total IRE-1	WB: 1/1000	Cell Signalling Technology
Total mTOR	Rabbit polyclonal	Total mTOR	WB: 1/500	Cell Signalling Technology
Total PERK	Rabbit polyclonal	Total PERK	WB: 1/500	Cell Signalling Technology

Abbreviations: AMPK: AMP-activated protein kinase, Atg-5: autophagy related gene 5, Atg-7: autophagy related gene 7, Atg-13: autophagy related gene 13, CHOP: C/EBP homologous protein, eIF2α: eukaryotic initiation factor 2α, ERK: extracellular signal–regulated kinase, GAPDH: glyceraldehyde 3-phosphate dehydrogenase, GSK3: glycogen synthase kinase 3, HA: hemagglutinin, IRE1: inositol-requiring enzyme 1, LAMP2: lysosomal associated membrane protein 2, LBPA: Lysobisphosphaditic acid: LC3, microtubule-=associated protein 1 light-chain 3; mTOR: mammalian target of rapamycin, PERK: protein kinase RNA (PKR)-like ER kinase.

Table 2-2 Secondary antibodies for WB

Antibody	Dilution	Source
Alexa Fluor 680 (goat, anti-mouse)	1/5,000	Invitrogen
IRDye 800 (goat anti-rabbit)	1/5,000	Invitrogen

Table 2-3 Secondary antibodies for ICC

Antibody	Dilution	Source
Alexa Fluor 488 (goat, anti-mouse)	1/1,000	Invitrogen
Alexa Fluor 568 (goat, anti-rabbit)	1/1,000	Invitrogen
Alexa Fluor 488 (donkey, anti-goat)	1/1,000	Invitrogen

2.1.9 **Agarose gel electrophoresis**

50x TAE buffer (Tris-acetate-EDTA)	40 mM Tris, pH 7.6 20 mM Acetic acid 1 mM EDTA pH 8.0
Nuclear acid molecular weight marker	1 kb DNA ladder (New England Biolabs) Molecular weight sizes: 0.5, 1, 2, 3, 4, 5, 6, 8 and 10kb

2.1.10 ***E. coli* culture**

LB	20 g/L Luria-Bertani (LB) powder sterilised by autoclaving

LB agar	32 g/L agar sterilised by autoclaving 100 µg/ml Ampicillin 50 µg/ml Kanamycin

2.1.11 **Plasmid DNA preparation**

Plasmid DNA was prepared using a QIAprep Maxiprep Kit (Qiagen).

2.1.12 **Cell culture**

Table 2-4 Cell culture reagents

CHO cell culture media	Ham's F-12 medium (PAA Laboratories Ltd) 10% (v/v) foetal bovine serum (FBS) (PAA Laboratories Ltd) 2mM L-glutamine (PAA Laboratories Ltd) 100 U/ml penicillin (PAA Laboratories Ltd) 100µg/ml streptomycin (PAA Laboratories Ltd)
Trypan blue	0.4% (w/v) Trypan blue solution
HBSS without Ca^{2+}/Mg^{2+} (Invitrogen)	Hank's Balanced Salt Solution without Ca^{2+}/Mg^{2+}
Trypsin	0.25% trypsin solution (PAA Laboratories Ltd)
Cell freezing media	10% (v/v) Dimethyl sulfoxide (DMSO) in Ham's F-12

Table 2-5 Cell culture treatments and stains

JetPEI transfection kit (Polyplus-transfection)	
HBSS with Ca^{2+}/Mg^{2+} (Invitrogen)	Hank's Balanced Salt Solution with Ca^{2+}/Mg^{2+}
Dithiothreitol (DTT) (Thermo Fisher)	Final concentration: 20 mM in Ham's F12
Thapsigargin (Thermo Fisher)	Final concentration: 1 µM in Ham's F12
Calcein AM cell viability (eBioscience)	500 nM – 1 µM
Rapamycin	Final concentration: 1 µM in Ham's F12
AR-A014418	Final concentration: 100 nM in Ham's F12
Trehalose	Final concentration: 100 mM in Ham's F12
Bafilomycin A1	Final concentration: WB: 400 nM in Ham's F12 ICC: 200 nM in Ham's F12
LysoTracker Red DND-99 (Thermo Fisher)	Final concentration: 800 nM in Ham's F12
BODIPY 493/503 (Invitrogen)	Final concentration: 2 µM in Ham's F12

2.2 Methods

2.2.1 Mouse brain dissection

Wild-type and Tau35 male mice aged 16-18 months were culled by cervical dislocation. The brains were extracted and dissected into 4 regions: hippocampus and associated cortex; amygdala and associated cortex; frontal region; and brainstem and cerebellum. Samples were frozen at -80 °C until required.

2.2.2 Preparation of brain homogenates

Samples of hippocampus and associated cortex; amygdala and associated cortex; frontal brain; and brainstem and cerebellum, from mice aged 16-18 months, were thawed on ice, weighed and homogenised in 4 volumes (w/v) ESLB using a Dounce homogeniser. The amount of protein present in each homogenate was measured using a BCA assay. Samples were diluted in the appropriate volume of 2X Laemmli sample buffer to provide 20 µg total protein/lane for analysis on western blots. For western blotting, n=6 for each genotype. Tau phosphorylation experiments had 3 technical replicates and UPR experiments had 6 technical replicates.

2.2.3 Genotyping and PCR

DNA was extracted from mouse ear notches using the KAPA mouse genotyping kit. Lysis and enzyme inactivation was then performed in a heating block at 75°C for 10 minutes, and 95°C for 5 minutes, respectively. Samples were centrifuged at 6000g for 1.5 minutes to pellet cellular debris and a 10-fold dilution with nuclease-free H_20, samples were cycled using primers for the transgene (Table 2-1). The following cycling conditions were used:

- One denaturing cycle at 94°C for 3 min
- 35 cycles of 95°C for 15 s, 55 ºC for 15 s, and 72°C for 1 min
- One extension cycle at 72°C for 5 min

PCR products were electrophoresed on 1.5% (w/v) agarose gels at 150V for 40-45 min and bands were detected by imaging with a benchtop 2UV transilluminator.

2.2.4 Generation of stable CHO cell lines

Mycoplasma negative Chinese hamster ovary (CHO) cells, acquired from the European Collection of Authenticated Cell Cultures were grown at 37°C with 5% CO_2 in Ham's F12 culture medium. 24 h before transfection, CHO cells were seeded at a density of 150,000

cells/well in a 12-well plate. CHO cells were transiently transfected with 2N4R tau or V5 tagged-Tau35 plasmids (1 µg plasmid/well for 12-well plate) using jetPEI™ (Polyplus Transfection) according to the manufacturer's instruction. 48 h after transfection the medium was replaced by Ham's F-12 medium, with the addition of 800 µg/mL G418 (Santa Cruz Biotechnology). After selection, G418-resistant cells were transferred to 145 mm diameter dishes for clonal isolation. Cell clusters were isolated using cloning cylinders and transferred to 6-well plates for clonal expansion. Further characterization of the G418-resistant cells was undertaken using western blots to examine the stable expression of tau protein and immunocytochemistry to assess the homogeneity of the cell lines. Clonal cells homogenously expressing 2N4R tau or Tau35, termed CHO-FL and CHO-Tau35, respectively, were selected and maintained in CHO cell growth medium without G418 at 37°C in 5% CO_2. This work was done by Tong Guo.

2.2.5 **Cell culture**

CHO cells stably expressing FL-tau (FL-CHO) or Tau35 (Tau35-CHO), and untransfected CHO cells were maintained as monolayer cultures in Ham's F-12 culture medium at 37°C in an atmosphere of 5% CO_2. Cells were passaged when they reached 80-90% confluence. After rinsing in HBSS, cells were trypsinised and counted prior transferring them into new flasks or plates using fresh CHO cell culture medium. To count CHO cells, 10 µl of cell suspension was added to 90 µl of Trypan blue solution and 10 µl was loaded into a haemocytometer. The cell density was determined using the following equation:

$$Cell\ density = \frac{total\ cell\ count}{squares\ counted}\ X\ 10^5/ml$$

For western blotting and cell viability experiments using CHO cells, n= independent cell cultures. For imaging experiments, n= independent experiments foe each cell line where 30 cells were quantified in each experiment.

2.2.6 **Transient transfection of CHO cells**

CHO cells were transfected using JetPEI transfection kit (Polyplus-transfection) according to the manufacturer's protocol. 100,000 cells/well were transferred to a 12-well plate 24 h prior to transfection. Immediately before transfection, media in the wells was replaced with fresh Ham's F-12 culture medium. For each well of a 12-well plate, 1 µg of DNA was

diluted in 150 mM NaCl to a final volume of 50 µl. In a separate tube, 3 µl of JetPEI was diluted in 150 mM NaCl to a final volume of 50 µl. The JetPEI solution was added to the DNA solution and incubated for 30 min at ambient temperature. The transfection complex was added to each well, followed by gentle swirling of the plate and the cells were incubated at 37°C in an atmosphere of 5% CO_2 for a further 24 h. Cells were rinsed twice with PBS and fixed with the fixation solution for 20 min for immunocytochemistry.

2.2.7 **DNA transformation**

Library Efficiency DH5α competent cells (Invitrogen) were used for DNA transformation, according to the manufacturer's protocol.

2.2.8 **Plasmid extraction**

Glycerol stocks of bacteria harbouring tau or TFEB plasmids were removed from -80°C storage and incubated in 200 ml autoclaved LB medium containing 100 µg/mL ampicillin or 50 µg/mL kanamycin, overnight at 37°C, with shaking at 220 rpm. Plasmids were prepared using the Plasmid Midi Kit (Qiagen), according to the manufacturer's protocol. The concentration and purity of the DNA was calculated by measuring absorbance at 260 nm and 280 nm (NanodropTM UV-Vis spectrophotometer).

2.2.9 **Freezing and recovery of CHO cells**

To freeze cells for long-term storage, CHO cells were trypsinised and resuspended in Ham's F-12 medium, as described above. Cell suspensions were centrifuged at 700 g(av) for 5 min at ambient temperature. The supernatant was discarded and the pellet was resuspended in pre-cooled 10% (v/v) DMSO containing Ham's F-12 media, at 4°C and dispensed into 1 ml aliquots in cryogenic tubes. Tubes were maintained at 4°C for 20-30 min, then at -20°C for 1 h, and finally at -80°C overnight, before being transferred to liquid nitrogen.

1ml aliquots of frozen CHO cells were thawed at 37°C and immediately transferred into 75cm^2 tissue culture flasks containing 10 ml pre-warmed Ham's F-12 culture medium. After 24 h incubation at 37°C, the medium was replaced with fresh Ham's F-12 culture medium.

2.2.10 **CHO cell treatments**

FL-CHO, Tau35-CHO and untransfected CHO cells were seeded at the following densities:

10 cm diameter dish	700,000 cells/well
6-well plate	300,000 cells/well
12-well plate	50,000 cells/well
96 well plate	10,000 cells/well

Treatments for cell viability assay

24 h after seeding CHO cells, the medium was replaced with 20 mM DTT or 1 µM thapsigargin in fresh culture medium. Cells were treated with DTT for 4 h or thapsigargin for either 6 h or 24 h. Following treatment, cells were washed with pre-cooled PBS at 4^{o}C.

Autophagy-modulating treatments

24 h after seeding CHO cells, autophagy was induced by replacing the medium with HBSS (with Ca^{2+} and Mg^{2+}) and cells were starved for 3 h. To activate autophagy through an mTOR-dependent route, cells were treated with 1 µM rapamycin for 6 h. To activate autophagy through an mTOR-independent route, cells were treated with 100 mM trehalose for 24 h. To block the fusion of autophagosomes with lysosomes by inhibiting v-ATPase, cells were treated with 200 nM bafilomycin A1 for 2 h and examined by immunocytochemistry, or were treated with 300 nM bafilomycin A1 for 2 h and examined on western blots.

Inhibition of glycogen synthase kinase-3β (GSK-3β)

24 hours after seeding CHO cells, the medium was replaced with the 100 nM AR-A014418 and cells were incubated for 16 h at 37°C

2.2.11 **Cell viability assay using a plate reader**

Calcein Violet 450 AM dye was diluted to 1 µM in 1X pre-warmed (37°C) Calcein AM DW buffer. CHO cells in a 96-well plate were washed 3 times with PBS. 100 µl of diluted calcein AM dye was added per well and from this point onwards the plate was protected from light. Cells were incubated at 37°C for 30 min, after which the fluorescence intensity was recorded using a 490/520 nm excitation/emission filters in an Omega plate reader.

2.2.12 **Cell viability assay using fluorescence activated cell sorting (FACS)**

For cell survival assay, CHO cells were grown on a 6-well plate for 24 h before the start of the experiment. F-12 medium from the plate was collected to account for floating/dying cells. Cells were trypsinised and resuspended in double the volume of F-12 medium and were pooled with previously collected medium. Cells were centrifuged at 700 g(av) for 5 min at ambient temperature. The supernatant was discarded and the pellet was stained with Calcein Violet 450 AM Viability Dye (500 nM, eBioscience) in PBS for 30 min at room temperature. After washing twice with PBS, cells were resuspended in PBS and analysed with the BD FACSCanto II (BD Biosciences).

2.2.13 **Nuclear and cytoplasmic fractionation**

Cells grown in 10 cm diameter tissue culture dishes were scraped into 1 ml PBS and centrifuged at 600 g(av) for 5 min at 4°C. The cell pellet was resuspended in 100 µl isolation buffer and sonicated at 40% intensity for 4 pulses (1 s per pulse). Nuclei were pelleted by centrifugation at 1,000 g(av) for 10 min at 4°C. The pellet (nuclear fraction) was resuspended in 100 µl PBS, centrifuged at 1,000 g(av) for 10 min at 4°C and the final pellet was resuspended in isolation buffer, discarding the wash supernatant. The first 1,000g(av) supernatant was centrifuged at 100,000 g(av) for 60 min at 4°C and the resulting supernatant corresponded to the cytoplasmic fraction, the final pellet was discarded.

2.2.14 **Preparation of cell lysates**

After removing the culture medium, cells were washed three times with cold PBS. To lyse the cells, they were scraped into 2X or 4X Laemmli sample buffer containing protease and phosphatase inhibitors (250 µl of buffer/well of a 6-well plate). Cell lysates were analysed on western blots.

2.2.15 **SDS-PAGE and western blots**

Samples of brain homogenates and CHO cell lysates were heated at 95°C for 5 min and centrifuged at 13,000 g(av) for 5 min at ambient temperature prior to loading on 7.5% (w/v), 10% (w/v) or 12% (w/v) polyacrylamide gels. 7.5% and 10% gels were run at 150 V for 55-60 min and 80-90 min, respectively, and 12% gels were run at 120 V for 100-110 min using the Bio-Rad system. Precast gels were run at 110 V fir 100-110 min using the Invitrogen system. Separated proteins were transferred onto 0.2 µm nitrocellulose membranes (GE Healthcare) using a wet transfer system (Bio-Rad) whereby the membrane

along with filter paper and sponges (Whatman) were pre-soaked in transfer buffer. Sponge, filter papers (4-5), gel, membrane, filter papers (4-5), and sponge were fitted into a transfer cassette. Proteins were transferred at 100 V for 60 min on ice, then blocked with either Odyssey (TBS) blocking buffer or milk blocking solution for 60 min to minimise non-specific binding of antibodies. All antibodies from Cell Signaling Technology were diluted in Odyssey blocking buffer. All other antibodies were diluted in 3% (w/v) milk solution. Blocked membranes were incubated in primary antibodies overnight at 4°C, then washed (3 x 10 min) in TBS + Tween 20 and incubated with secondary antibody for 60 minutes at ambient temperature in the dark. Blots were washed in TBS (3 x 10 minutes) and antigens were visualised using the Odyssey infrared imaging system (Li-Cor Biosciences).

2.2.16 **Immunocytochemistry for LC3**

Cells grown on coverslips in a 12-well plate were rinsed twice with pre-cooled PBS. Cells were fixed and permeablised using ice-cold methanol for 5 minutes at -20°C. Cells were blocked using 2% (v/v) BSA in PBS overnight at 4°C. Cells were then incubated with the LC3 antibody diluted in 2% (v/v) BSA in PBS for 1 hour at ambient temperature. Cells were washed with 2% (v/v) BSA in PBS (3 X 5 minutes), followed by incubation with the secondary antibody diluted in 2% (v/v) BSA in PBS for 30 minutes at ambient temperature. Cells were washed with 2% (v/v) BSA in PBS (3 X 5 minutes) and were incubated 0.5% (v/v) Hoechst in PBS for 2 min followed by washes with PBS, H_2O and a rinse with 70% ethanol. Fixed cells were mounted onto slides with mounting media (DAKO).

2.2.17 **Immunocytochemistry for other antibodies**

For immunocytochemistry, most experiments included cells cultured on coverslips in 12-well plates. Cells were washed with PBS and were fixed in 4% PFA for 20 min at ambient temperature. Cells were permeablised in 0.5% (v/v) Triton X-100 in PBS (3 x 5 minutes) and preincubated in blocking buffer (serum) for 30-60 min at ambient temperature. Cells were exposed to primary antibodies diluted in the blocking buffer (serum) overnight at 4°C. Cells were washed with 0.5% (w/v) Triton X-100 in PBS (3 x 5 min) and then incubated with the appropriate secondary antibody diluted in 0.5% (w/v) Triton X-100 in PBS for 1 h at ambient temperature. Cells were washed with 0.5% (w/v) Triton X-100 in PBS (3 x 5 min) and incubated 0.5% (v/v) Hoechst in PBS for 2 min, followed by brief washes with PBS, UHP

water and 70% (v/v) ethanol. Fixed cells were mounted onto slides using fluorescence mounting medium (DAKO).

2.2.18 **Lysotracker staining**

CHO cells grown on coverslips on 12-well plates were treated with 300 nM Bafilomycin A1 in Ham's F12 for 2 h at 37°C, as described above. Bafilomycin-treated cells serve as a negative control because Bafilomycin blocks autophagy by inhibiting V-ATPases and lysosomal acidification. After treatment, cells were incubated with 800 nM Lysotracker in Ham's F12 culture medium at 37°C for 10 min. Medium was replaced with fresh Ham's F12 and cells were incubated for 10 min at 37°C to avoid cell death. Cells were fixed with fixation solution for 30 min at 37°C. Cells were washed with PBS (2 X 5 min) and incubated in permeabilising solution for 10 min followed by washes with PBS (2 X 5 min). Cells were incubated 0.3% (v/v) Hoechst in PBS for 2 min followed by washes with PBS. Fixed cells were mounted onto slides with mounting media (DAKO).

2.2.19 **Boron-dipyrromethene (BODIPY) staining**

Cells grown on coverslips on 12-well plates were washed with PBS. To label intracellular lipids, cells were treated with 2 µM BODIPY 493/503 (Invitrogen) staining solution in PBS for 15 min at 37°C. Cells were washed with PBS 2 X 5 min and fixed with fixation solution for 30 min at ambient temperature. Cells were washed with PBS 3 X 5 min. Cells were incubated 0.3% (v/v) Hoechst in PBS for 2 min followed by washes with PBS. Fixed cells were mounted onto slides with mounting media (DAKO).

2.2.20 **Data analysis**

Western blot analysis

Western blots were quantified using Fiji-ImageJ (https://imagej.net/Fiji).

FACS data analysis

Data was analysed using FLOWJO-LLC software. Collected data points were subjected to 2 stages of gating to exclude unwanted cell populations.

- The first cell population (P1) was identified by excluding cellular debris.
- From P1, the second cell population (P2) was identified by excluding groups/clusters of cells (Figure 2-1).

Two parameters were used for gating cell populations:

- FSC (Forware Scatter) parameter. This parameter is a measurement of the amount of the laser beam that passes around the cell. This gives a relative size for the cell.
- SSC (Side Scatter) parameter. This parameter is a measurement of the amount of the laser beam that bounces off of particulates inside of the cell. This is a measurement of cell complexity.

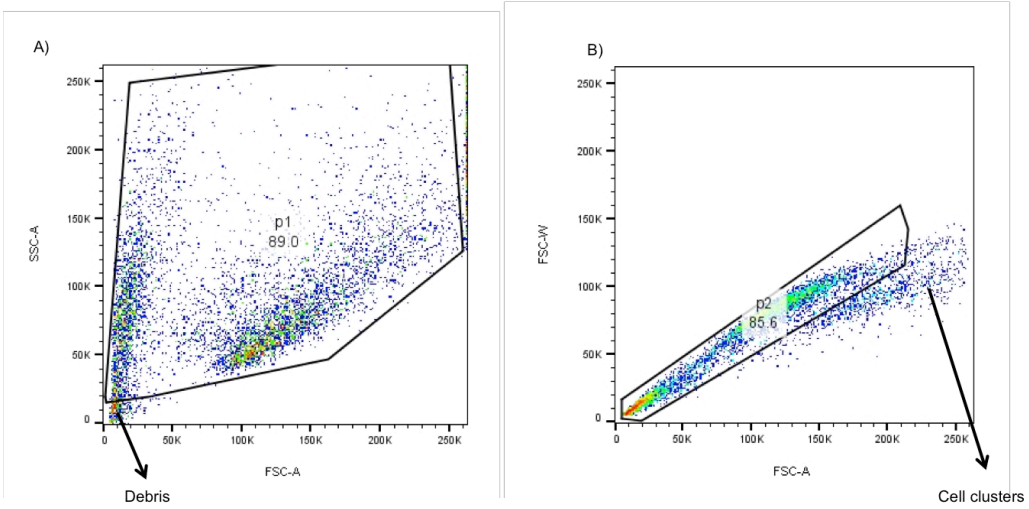

Figure 2-1 Example of identification of P1 and P2: Dot blot of A total cell population and the definition of P1, B P1 and the definition of P2.

Finally, the P2 cell population was plotted onto a histogram to determine the percentage of Calcein Violet 450 AM positive cells (viable cells).

Image analysis

The numbers, sizes and circularity of intracellular puncta were analysed using the GFP-LC3 macro (NIH) on Fiji-ImageJ. The number of puncta was normalised to cell area (μm^2). Signal intensity measurements were determined using Fiji-ImageJ.

Intensity distribution analysis of LC3 puncta was assessed using NIS-Elements Advanced Research software. This was done by firstly defining the nucleus and excluding this region from the analysis. Concentric circles were then drawn around the nucleus at intervals of 3 µm (Figure 2-2). The intensity signal was then measured within each ring.

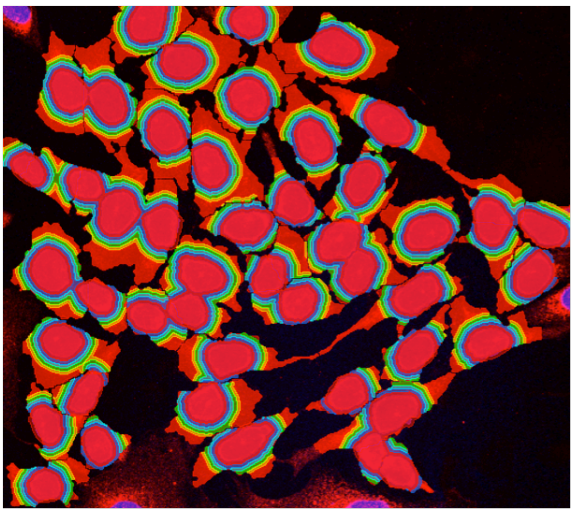

Figure 2-2 Example image of LC3 distribution analysis: Screenshot image of intensity distribution analysis of CHO cells stained with LC3 antibody. The red central circle is the defined nuclear region. The coloured rings surrounding this region are the intensity-analysis regions.

Colocalisation analysis was performed using NIS-Elements Advanced Research software. This was done by measuring the linear correlation between the GFP and RFP channels, thereby determining the Pearson correlation coefficient.

Statistical analysis

Data was collated using Microsoft Excel. Statistical analyses were performed using GraphPad Prism 7. Data were analysed using Student's t-test, one-way analysis of variance (ANOVA), or two-way ANOVA, as appropriate. Tukey's test (post-hoc analysis) was used in conjunction with ANOVA analyses. Differences were taken as statistically significant if $P<0.05$.

Chapter 3 Increased tau phosphorylation and activation of the unfolded protein response in Tau35 mice

3.1 Introduction

Neurodegenerative tauopathies exhibit several pathological characteristics including the accumulation of highly phosphorylated, aggregated and truncated forms of tau protein (Brandt et al., 2005). Truncation of tau can have detrimental effects as it leads to a build-up of toxic tau fragments that can lead to cellular dysfunction, neuronal loss and cell death (Amadoro et al., 2004). To validate the pathological role of truncated tau, this laboratory generated a Tau35 transgenic mouse expressing Tau35 fused to a HA tag under the control of the human tau promoter with targeted insertion into the *Hprt* locus. This model was developed following the discovery of the presence of the Tau35 fragment in post-mortem human brains of people affected by 4R tauopathies (Wray et al., 2008).

Numerous behavioural studies carried out on Tau35 mice revealed both motor and cognitive impairments. Tau35 mice exhibit clasping commencing at 4 months of age, increasing dramatically to include 25% of mice clasping at 5–6 months, and with all Tau35 mice showing paresis by 18 months of age (Bondulich et al., 2016). In addition, abnormal spine curvature was observed in Tau35 mice as early as 4 months of age. Testing on the accelerating rotarod revealed that Tau35 mice have a reduced latency to fall, which decreased with age, indicating an age-related defect in motor coordination. Tests carried out using the Morris water maze showed that by 8 months of age, Tau35 mice exhibit spatial learning and hippocampal-dependent memory deficits. Tau35 mice also have a life span of approximately 18-20 months, which is significantly reduced compared to that of their WT littermates (Bondulich et al., 2016).

immunohistochemical staining of hippocampal and cortical brain sections from groups of mice aged 2, 8, and 14-16 months revealed tau-positive labelling of inclusions in Tau35 mouse brain. The tau inclusions included dystrophic neurites and neuropil threads, which were labelled with tau antibodies PHF-1, TOC1, MC1, AT8 and TP007 in Tau35 mice aged 14-16 months (Bondulich et al., 2016). PHF-1 revealed increased cytoplasmic labelling at 2 months and tau-containing inclusions from 8 months, which were more abundant at 14–

16 months in Tau35 mouse brain, which was not apparent in WT hippocampal brain sections (Bondulich et al., 2016). Western blots of 14 month old Tau35 mouse hippocampal homogenates showed a progressive increase in tau phosphorylation at several sites including PHF-1, TG3 and AT270. Additionally, Tau-1 immunoreactivity was reduced, indicating increased tau phosphorylation at this epitope in Tau35 mice (Bondulich et al., 2016). There were no changes apparent in tau phosphorylation in other brain regions in Tau35 mice aged 14 months.

Protein degradation mechanisms are responsible for the re-establishment of homeostasis under conditions of cell stress. The ER uses these mechanisms to prevent the accumulation of toxic protein aggregates (Katayama, *et al*, 2004), including through activation of the UPR (Katayama et al., 2004; Nijholt et al., 2012a). Since it has previously been established that Tau35 mice exhibit increased tau phosphorylation at numerous disease-relevant epitopes, it is important to determine the underlying causes and/or consequence of the build-up of these abnormal tau inclusions. The effects of Tau35 expression on protein degradation have not previously been identified.

This chapter describes the effects of Tau35 expression on tau phosphorylation in different regions of aged Tau35 mouse brain. In parallel, molecular mechanisms such as the UPR, that may be responsible for the accumulation of phosphorylated tau species in Tau35 mice were also investigated.

3.2 Results

3.2.1 Changes in tau phosphorylation in aged Tau35 mouse brain

Since changes in tau phosphorylation in Tau35 mice were observed only in the hippocampus and associated cortex at 14 months, tau phosphorylation was examined in this and other brain regions (amygdala and associated cortex, brainstem and cerebellum, and the frontal brain region) in older Tau35 mice (aged 16-18 months).

Firstly, to confirm that Tau35 is expressed in the mice, western blots of homogenates prepared from hippocampus and associated cortex of Tau35 and WT mice aged 16-18

months were probed with an antibody recognising the HA tag (Figure 3-3-1). The results show that, as expected, HA is detected only in Tau35 mice and is absent in WT mice.

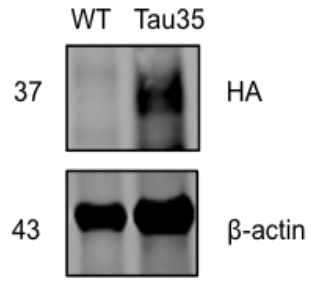

Figure 3-3-1 Verifying the presence of the HA-tagged Tau35 in mouse brain: Western blots of homogenates of hippocampus and associated cortex from wild-type (WT) and Tau35 mouse brain (aged 16-18 months) probed with antibodies to HA and β-actin (loading control). Molecular weights (kDa) are shown on the left.

To determine the effect of Tau35 expression on changes in tau pathology in aged animals (16-18 month), homogenates of hippocampus and associated cortex, amygdala and associated cortex, brainstem and cerebellum, and frontal region brain samples were prepared from 16-18 months old WT and Tau35 mice. Brain region homogenates were analysed on western blots probed with antibodies that detect disease-relevant tau epitopes: 12E8 (tau phosphorylated at Ser262/Ser356), AT180 (tau phosphorylated at Thr231), PHF-1 (tau phosphorylated at Ser396/Ser404) and Tau-1 (tau dephosphorylated at Ser195, 198, 199, and 202) and were normalised to total tau (phosphorylation-independent) (Figure 3-2). In the hippocampus and associated cortex, Tau35 mice exhibit significantly increased tau phosphorylation at the 12E8, AT180 and PHF-1 epitopes, compared to age matched WT mice (Figure 3-2A-C, $P<0.05$). Tau35 mice also exhibit reduced Tau-1 immunoreactivity, indicating a decrease in the amount of dephosphorylated tau, compared to age-matched WT mice (Figure 3-2D, $P<0.05$).

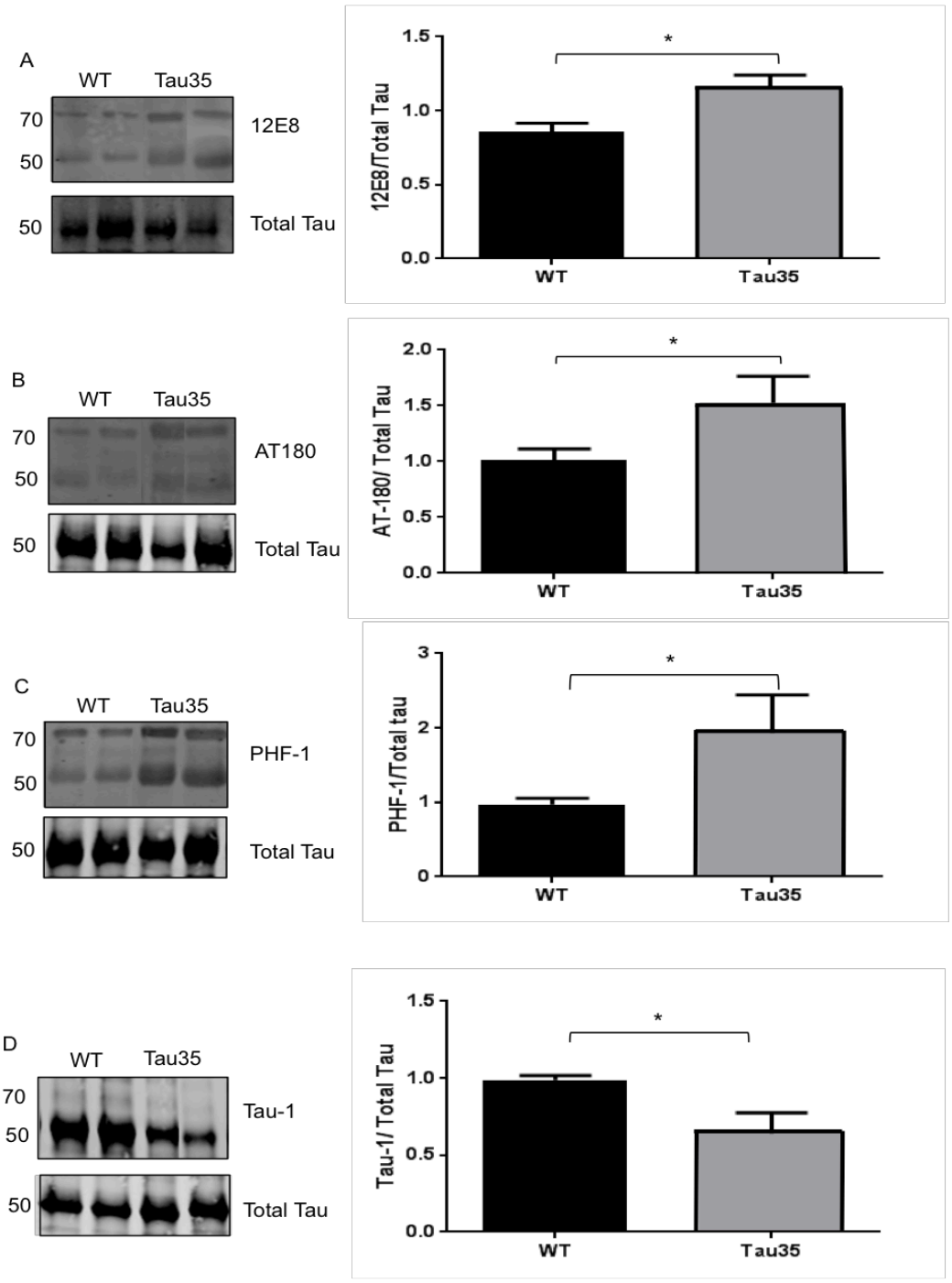

Figure 3-2 Tau phosphorylation in hippocampus and associated cortex of aged Tau35 mice: Western blots of homogenates prepared from wild-type (WT) and Tau35 mouse hippocampus and associated cortex (16-18 months), probed with antibodies **A** 12E8, **B** AT180, **C** PHF-1, **D** Tau-1 and total tau. Molecular weights (kDa) are shown on the left. Graphs show the amount of phosphorylated tau relative to total tau. Values represent mean ± SEM., n=6; Student's t-test, *P<0.05.

In contrast to the hippocampus and associated cortex, there were no significant changes in tau phosphorylation in the amygdala and associated cortex at the 12E8, AT180, or Tau-1 epitopes in Tau35 mice (Figure 3-3 A, B and D**,** $P>0.05$). However, Tau35 mice exhibited a statistically significant increase in tau phosphorylation at the PHF-1 site in the amygdala and associated cortex compared to WT mice (Figure 3-3 C, $P<0.01$).

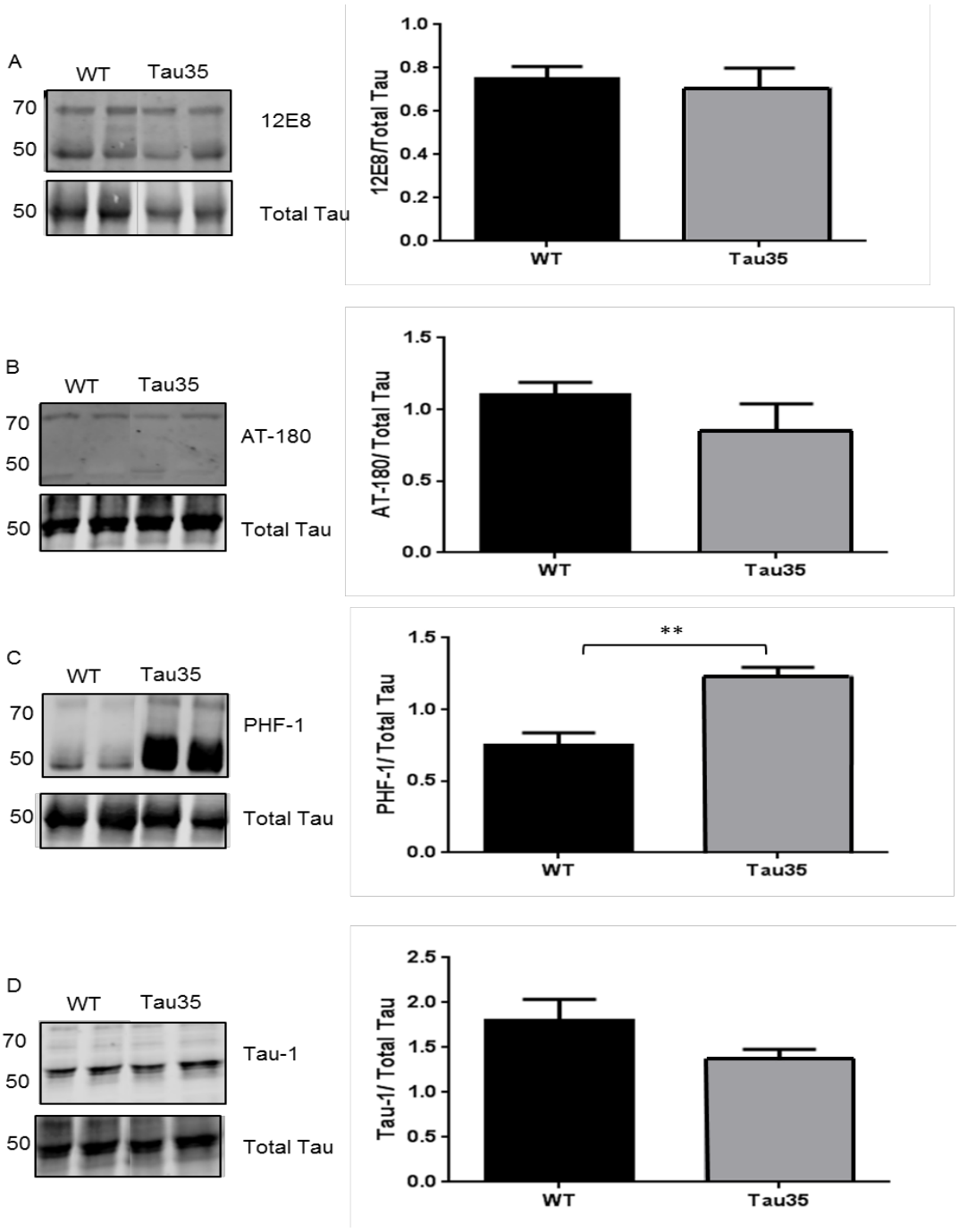

Figure 3-3 Tau phosphorylation in 16-18 month old amygdala and associated cortex of mice: Western blots of homogenates prepared from wild-type (WT) and Tau35 mouse amygdala and associated cortex (16-18 months), probed with antibodies **A** 12E8, **B** AT180, **C** PHF-1, **D** Tau-1 and total tau. Molecular weights (kDa) are shown on the left. Graphs show the quantitation of the different phospho tau sites relative to total tau. Values represent mean ± SEM, n=6; Student's t-test, **P<0.01.

Western blots of homogenates of brainstem and cerebellum revealed significantly increased tau phosphorylation at the 12E8 and AT180 epitopes (Figure 3-4 A and B $P<0.05$). In contrast, there were no significant differences in tau phosphorylation at the Tau-1 and PHF-1 epitopes (Figure 3-4 C and D, $P>0.05$).

Western blots of homogenates prepared from the frontal brain region of 16-18 month old WT and Tau35 mice show a significant elevation of phosphorylated tau at the 12E8 and Tau-1 epitopes compared to the age-matched WT mice (Figure 3-5 A and D, $P<0.01$). There was no significant difference in the amount of tau phosphorylated at the AT180 or PHF-1 epitopes (Figure 3-5 B and C, $P>0.05$).

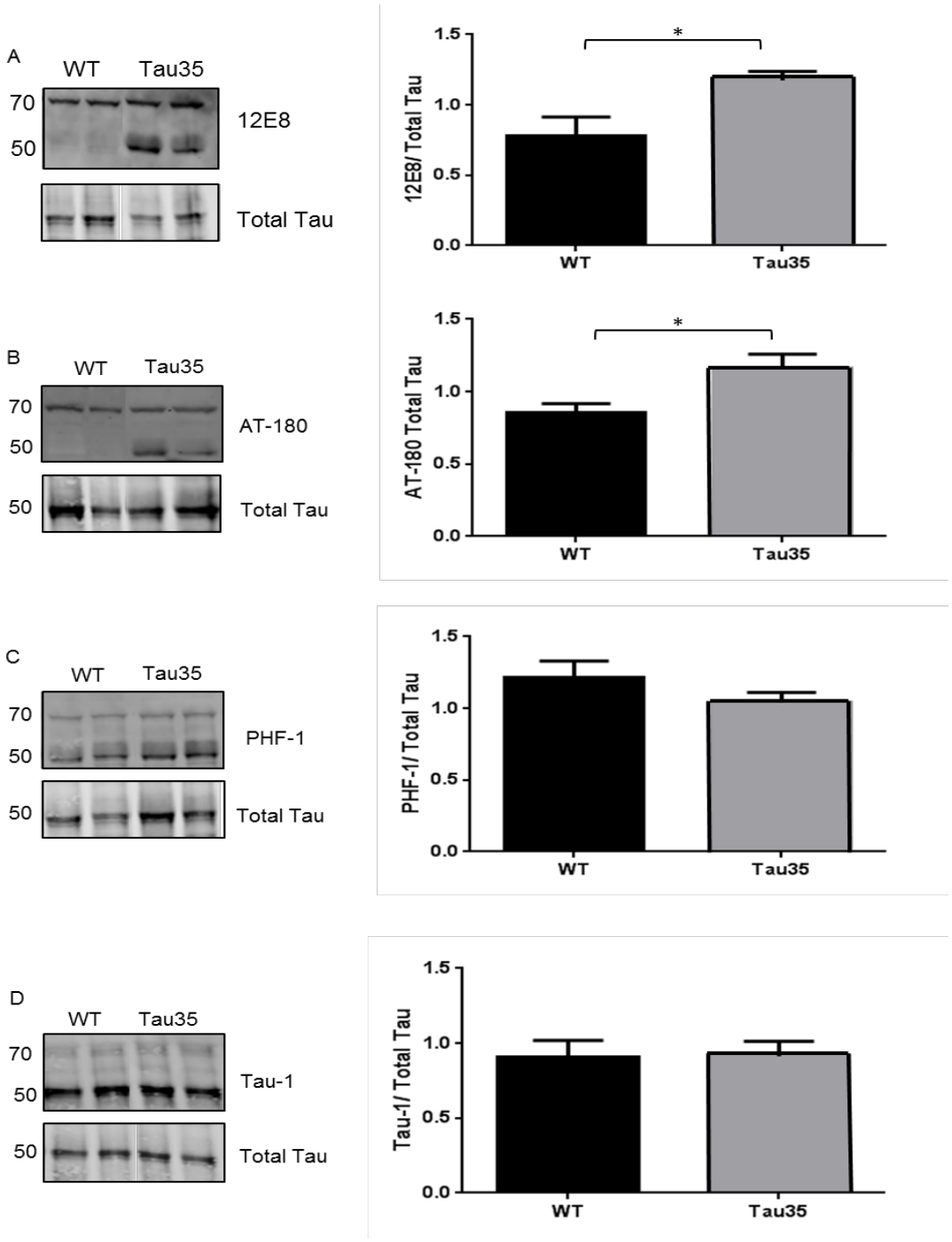

Figure 3-4 Tau phosphorylation in brainstem and cerebellum of mice aged 16-18 months: Western blots of homogenates prepared from wild-type (WT) and Tau35 mouse brainstem and cerebellum (16-18 months), probed with antibodies **A** 12E8, **B** AT180, **C** PHF-1, **D** Tau-1 and total tau. Molecular weights (kDa) are shown on the left. Graphs show the quantitation of the different phospho tau sites relative to total tau. Values represent mean ± SEM, n=6; Student's t-test, *P<0.05.

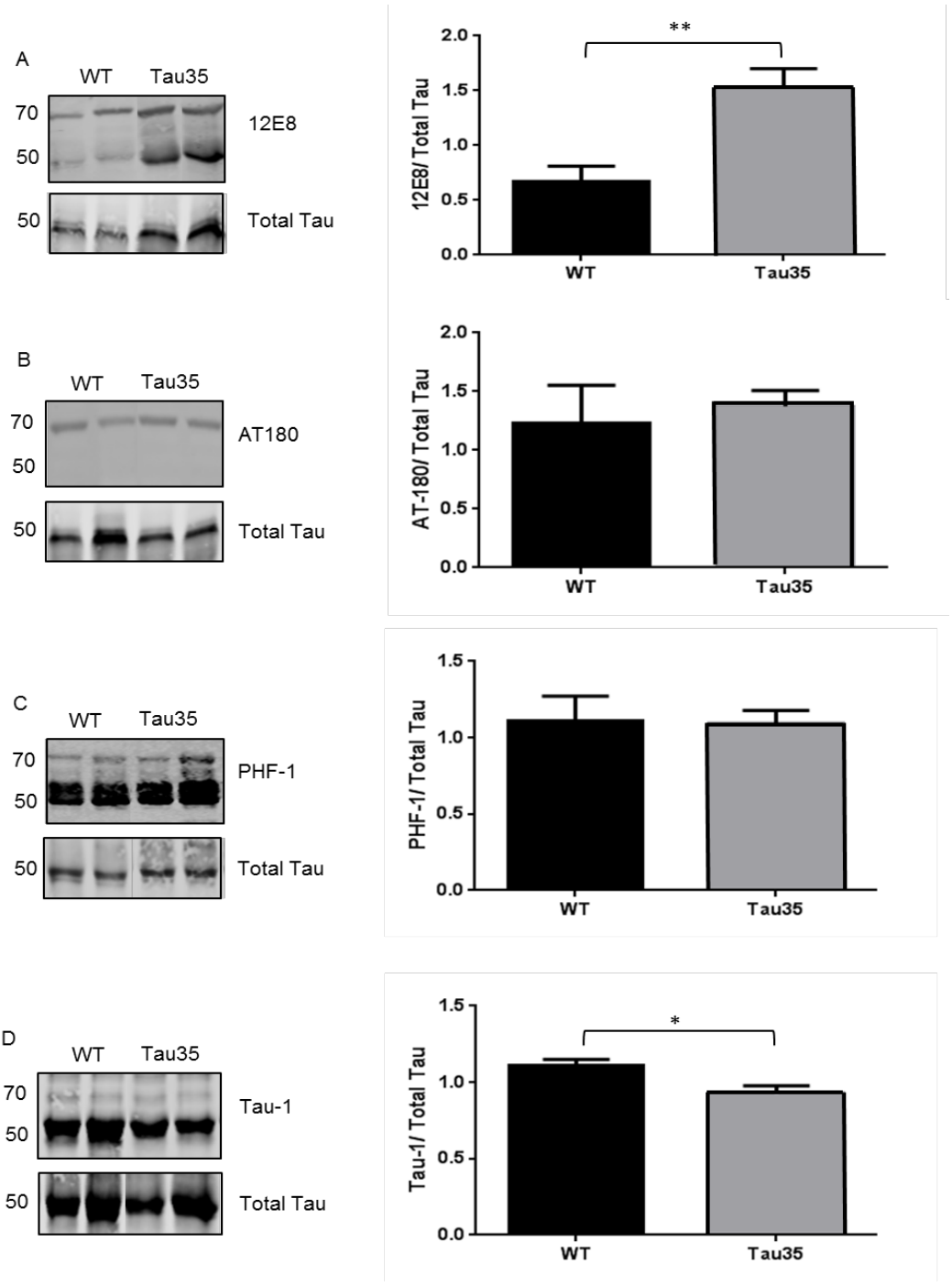

Figure 3-5 Tau phosphorylation in 16-18 month old frontal brain region of mice: Western blots of homogenates prepared from wild-type (WT) and Tau35 mouse frontal brain region (16-18 months), probed with antibodies **A** 12E8, **B** AT180, **C** PHF-1, **D** Tau-1 and total tau. Molecular weights (kDa) are shown on the left. Graphs show the quantitation of the different phospho tau sites relative to total tau. Values represent mean ± SEM, n=6; Student's t-test, *P<0.05, **P<0.01.

Table 3-1 below summarises the changes in Tau phosphorylation observed in the four different brain regions of Tau35 mice. Tau-1 was decreased in the hippocampus and associated cortex, and frontal region of aged Tau35 mice. AT180 levels were increased in the hippocampus and associated cortex, and in the brainstem and cerebellum. Increases in PHF-1 phosphorylation were exclusively noted in the hippocampus and associated cortex of Tau35 mice. Finally, 12E8 was increased in the hippocampus and associated cortex, and amygdala and associated cortex of Tau35 mice compared to age-matched WT mice.

Table 3-1 Summary of changes in tau phosphorylation in different brain regions of aged Tau35 mice: Changes in tau phosphorylation at the 12E8, AT180, PHF-1 and Tau-1 epitopes in the hippocampus and associated cortex, amygdala, brainstem and cerebellum and frontal regions in the brains of 16-18 Tau35 mice compared to age-matched WT mice.

Phospho-tau antibody	Hippocampus and associated cortex	Amygdala and associated cortex	Brainstem and cerebellum	Frontal region
Tau-1 (199/202)	Decreased	No change	No change	Decreased
AT180 (231)	Increased	No change	Increased	No change
12E8 (262/356)	Increased	No change	Increased	Increased
PHF-1 (396/404)	Increased	Increased	No change	No change

Taken together, the results from this section demonstrate that the expression of Tau35 has variable effects on tau phosphorylation in different brain regions of Tau35 mice aged 16-18 months. The hippocampus is the most affected brain region as changes in tau phosphorylation were detected using all of the four phosphorylation-dependent tau antibodies tested. Conversely, the amygdala is the least effected region with changes in tau phosphorylation only detected at the PHF-1 site.

3.2.2 **Investigating UPR activation in aged Tau35 mice**

The changes observed in tau phosphorylation between 16-18 month old WT and Tau35 mice are not consistent between the four brain regions examined (Table 3-1). In particular, the hippocampus and associated cortex (hereinafter referred to as hippocampus) in Tau35 mice harbours the most consistent increase in tau phosphorylation compared to WT mice, with changes in tau phosphorylation observed at all the four epitopes measured. In contrast, in the amygdala and associated cortex (hereinafter referred to as amygdala), increased tau phosphorylation is apparent only at PHF-1 epitope in Tau35 mice. The brainstem and cerebellum, and frontal region of Tau35 mice each showed changes in Tau phosphorylation at two out of the four epitopes measured (Table 3-1). However as in the amygdala, there were no changes in Tau phosphorylation at the PHF-1 site in either of these regions. Therefore, the hippocampus and amygdala were selected to examine the effects of Tau35 expression on the UPR to determine whether changes in tau phosphorylation correlate with UPR activation.

To assess the degree of activation of the PERK and IRE1 branches of the UPR, hippocampus and amygdala homogenates were prepared from 16-18 month old WT and Tau35 mice (n=6 for each genotype). Proteins were separated on either 7.5% (PERK and IRE1) or 10% (eIF2α and CHOP) SDS-PAGE. Western blots were probed with antibodies to total and phosphorylated PERK, total and phosphorylated eIF2α, CHOP, total and phosphorylated IRE1 to determine if there are any changes in these proteins that represent different points of the UPR pathway.

Once the PERK arm of the UPR becomes activated, PERK undergoes phosphorylation by dissociating from BiP (chapter 1, Figure 1-10) and hence phosphorylated PERK is an indicator of UPR activation. Figure 3-6 A shows that there is a statistically significant increase in the total amount of PERK relative to β-actin, in the hippocampus of Tau35 mice aged 16-18 months compared to WT mice ($P<0.05$). In contrast, phosphorylated PERK (relative to total PERK) in Tau35 mice is not significantly different from WT mice ($P=0.06$). PERK phosphorylation leads to the subsequent phosphorylation and activation of eIF2α. Western blots showed no difference in the amount of total eIF2α relative to the amount of

β-actin (Figure 3-6 B, P>0.05) and a marked reduction in the amount of phosphorylated to total eIF2α (Figure 3-6 B, P<0.01).

Finally, CHOP, the most downstream protein in the UPR pathway, was examined in order to determine if there is a difference in the amount of this protein in the hippocampus of 16-18 month old Tau35 mice. Western blots of CHOP showed a significant two-fold elevation in the amount of CHOP, relative to β-actin, in the hippocampus of Tau35 mice compared to WT mice (Figure 3-6 C, P<0.001).

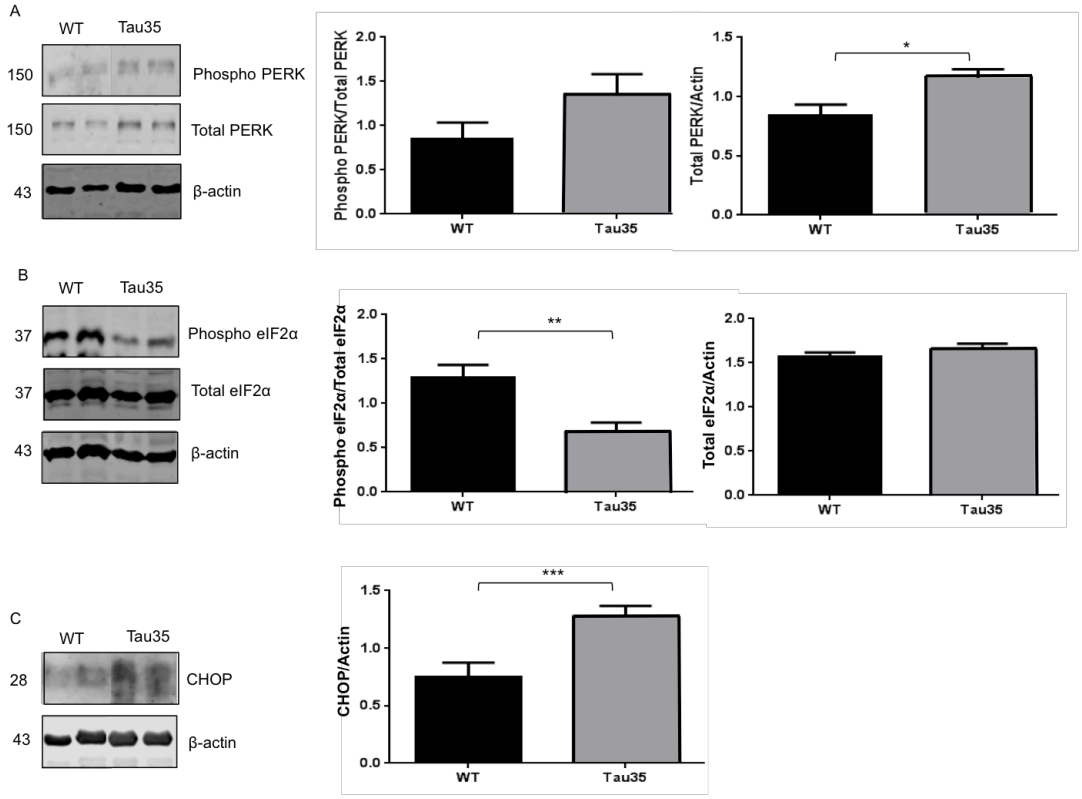

Figure 3-6 Activation of the PERK arm of the UPR in 16-18 month hippocampus and associated cortex mouse brain: Western blots of homogenates prepared from wild-type (WT) and Tau35 mouse hippocampus and associated cortex (16-18 months), probed with antibodies **A** phospho PERK and total PERK, **B** phospho eIF2α and total eIF2α, **C** CHOP and β-actin (loading control). Molecular weights (kDa) are shown on the left. Graphs show the quantitation of the western blots. Values represent mean ± SEM, n=6; Student's t-test, *P<0.05, **P<0.01, ***P<0.001.

The IRE1 branch of the UPR was next investigated in the hippocampus of Tau35 mice. In the absence of cell stress, IRE1 is bound to BiP; whereas under stress conditions, BiP dissociates from IRE1, which then autophosphorylates. Western blots of IRE1 show a statistically significant elevation in the amount of phosphorylated relative to total IRE1 (Figure 3-7, P<0.05), indicating activation of this arm of the UPR in aged Tau35 mice.

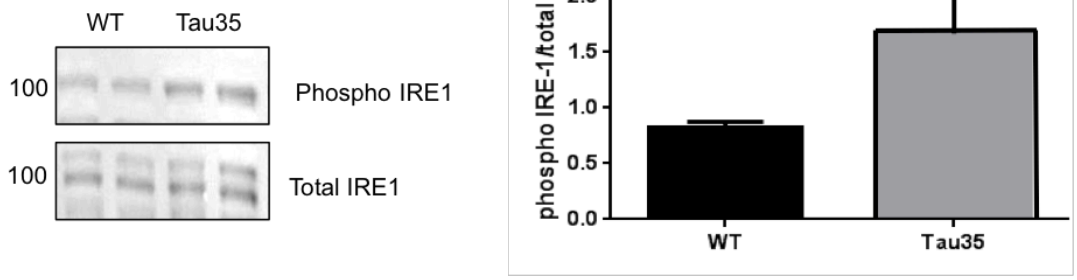

Figure 3-7 Activation of the IRE1 arm of the UPR in 16-18 month hippocampus and associated cortex of Tau35 mice: Western blots of homogenates prepared from wild-type (WT) and Tau35 mouse hippocampus and associated cortex (16-18 months), probed with antibodies phospho IRE1 and total IRE1. Molecular weights (kDa) are shown on the left. The graph shows the quantitation of the western blot. Values represent mean ± SEM, n=6; Student's t-test, *P<0.05.

In order to determine if UPR activation is localised to specific brain regions, the same components of the PERK arm of the pathway were measured on western blots of homogenates from the amygdala of 16-18 month WT and Tau35 mice (n=6). Western blots of the amygdala probed with total PERK and β-actin antibodies showed no statistically significant difference in the total amount of PERK in Tau35 mice compared to the WT mice (Figure 3-8 A, P>0.05). Bands corresponding to phosphorylated PERK were not detectable in the amygdala of either WT or Tau35 mice aged 16-18 months (not shown).

Figure 3-8 B shows western blots of the amygdala from WT and Tau35 mice aged 16-18 months probed with antibodies to total and phosphorylated eIF2α, and β-actin. The blots show no statistically significant difference in the total amount of eIF2α in the amygdala of

Tau35 mice compared to WT mice. In addition, the results revealed that that there is no statistically significant difference in the amount of phosphorylated eIF2α, relative to total eIF2α in Tau35 compared to WT mice (Fig. 3.8B, $P>0.05$). However, the amount of phosphorylated eIF2α detected in these samples was very low and barely detectable in the amygdala.

Western blots of the amygdala probed with antibody to CHOP showed no statistically significant difference between Tau35 and WT mice aged 16-18 months (Figure 3-8 C, $P>0.05$). The intensity of the band corresponding to CHOP was very weak in the amygdala of both WT and Tau35 mice, indicating very low CHOP expression in comparison to the amount of CHOP present in the hippocampus of Tau35 mice (Figure 3-6).

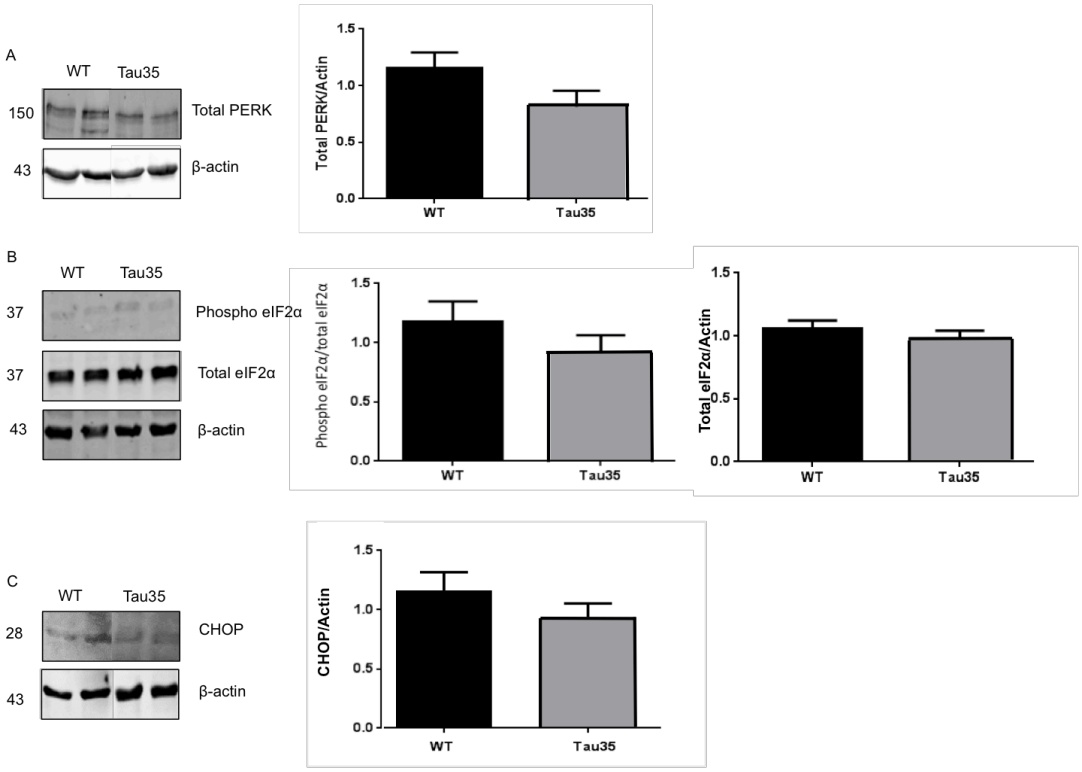

Figure 3-8 No change in the PERK arm of the UPR in the amygdala and associated cortex of Tau35 mice: Western blots of homogenates prepared from wild-type (WT) and Tau35 mouse amygdala and associated cortex (16-18 months), probed with antibodies **A** total PERK, and β-actin, **B** phospho eIF2α and total eIF2α, **C** CHOP and β-actin (loading control). Molecular weights (kDa) are shown on the left. Graphs show the quantitation of the western blots. Values represent mean ± SEM, n=6; Student's t-test.

3.3 Discussion

The overall aims of this chapter were to gain an understanding of the biochemical changes in tau phosphorylation in the brains of aged Tau35 mice. Moreover, since increased tau phosphorylation was noted only in the hippocampus and associated cortex of Tau35 mice aged 14 months (Bondulich *et al*, 2016), it was important to determine whether tau phosphorylation also occurred in different brain regions in older mice. In addition, since tau phosphorylation influences its ability to be degraded, it was of interest to identify whether underlying protein degradation mechanisms were affected as these may be responsible for the accumulation of phosphorylated tau in the brains of Tau35 mice.

The main findings of this chapter include the following changes in Tau35 mouse brain from animals aged 16-18 months:

- Increased phosphorylated tau in hippocampus at the 12E8, AT180, Tau-1, and PHF-1 epitopes.
- Increased tau phosphorylation detected solely at the PHF-1 epitope in the amygdala.
- Increased tau phosphorylation detected only at the 12E8 and AT180 epitopes in brainstem and cerebellum.
- Increased tau phosphorylation detected only at the 12E8 and Tau-1 epitopes in the frontal brain region.
- Evidence of increased activation of the PERK and IRE1 arms of the UPR in the hippocampus.
- No change in the PERK arm of the UPR in the amygdala.

3.3.1 **Brain region specific changes in tau phosphorylation in aged Tau35 mice**

It is well known that the accumulation of phosphorylated and abnormally modified tau can result from the presence of truncated tau species, leading to numerous neuropathological changes observed in human tauopathy (Delobel et al., 2008). Proteases including caspases, calpains, cathepsins, thrombin, asparagine endopeptidase (AEP), puromycin-sensitive aminopeptidase (PSA), human high temperature requirement serine protease A1 (HTRA1), and proteasomal proteases have been proposed as likely candidates that contribute to tau truncation, which in turn can generate potentially toxic fragments and even initiate the aggregation of tau (Hanger and Wray, 2010; Wang et al., 2010; Zhang et al., 2014). The results from this chapter provide evidence for a build-up of phosphorylated tau in the brains of Tau35 mice. In particular, the most affected region in Tau35 mice appears to be the hippocampus, whereas the amygdala is the least affected region.

There are substantial increases in tau phosphorylation in the hippocampus of Tau35 mice compared to age-matched WT control mice. In fact, elevation in tau phosphorylation at the PHF-1 epitope had been previously reported in Tau35 mice from as early as two months of age (Bondulich et al., 2016). The presence of phosphorylated tau inclusions in the hippocampus could also explain some of the cognitive changes previously described in Tau35 mice. Since the hippocampus is the brain region responsible for spatial learning (Clelland et al., 2009), the biochemical changes seen in this brain region could account for the observed memory deficits in Tau35 mice (Bondulich et al., 2016). Previous studies have shown a correlation between the presence of abnormally phosphorylated and aggregated tau species and cognitive decline in mouse models of tauopathy and also in human disease (Armstrong et al., 2009; Ramsden et al., 2005).

The amygdala appeared to be the least affected region in Tau35 mice aged 16-18 months as changes in tau phosphorylation were only detected at the PHF-1 site. An increase in tau phosphorylation at the PHF-1 site was not observed in the amygdala of Tau35 mice at 14 months of age (Bondulich et al., 2016). Therefore, the results from this chapter suggest that the expression of Tau35 drives changes in tau pathology at a later stage in the amygdala and associated cortex. A significant tau burden has been reported in the amygdala of rTg4510 mice, which harbour the P301L tau mutation (Cook et al., 2014b).

However, tau pathology in rTg4510 mice has predominantly been described in the hippocampus and studies have shown profound impairments in hippocampal-dependent learning and memory tests, including contextual fear conditioning in rTg4510 mice (Berger et al., 2007; O'Leary et al., 2010; Yue et al., 2011). To date, the Tau35 mice have been tested exclusively for motor and memory impairments, rather than for amygdala-dependent behaviours (Bondulich et al., 2016). However, rTg4510 mice also display an abnormal hyper-exploratory phenotype in the open-field, elevated plus maze, light-dark exploration, and cued fear conditioning, indicative of amygdala dysfunction (Cook et al., 2014b). In addition, another tau transgenic mouse that expresses human tau truncated at E391 (a fragment associated with the development of AD), shows increased tau phosphorylation in both the hippocampus and amygdala (McMillan et al., 2011). However, it is worth noting that, unlike in Tau35 mice in which truncated tau is expressed at <10% of endogenous mouse tau (Bondulich et al., 2016)., in E391 mice, total tau was 1.9-fold higher than endogenous mouse tau (McMillan et al., 2011), which corresponds to a significant overexpression of the transgenically expressed E391 tau fragment.

People with FTLD-tau present with a wide variety of clinical symptoms, that may include loss of social inhibition, inappropriate emotional responses, and restlessness (Lynch et al., 1994; Spillantini et al., 1997; Yamaoka et al., 1996). This suggests that the involvement of amygdala dysfunction is a possible contributing factor in some cases. Tau35 has been detected in several different 4R tauopathies including FTLD-tau, which may go some way towards explaining why tau pathology is observed in Tau35 mice.

The brainstem and cerebellum of Tau35 mice aged 16-18 months showed increased tau phosphorylation at two out of the four phosphorylated tau epitopes examined. These sites correspond to 12E8 (tau phosphorylated at Ser262/Ser356) and AT180 (tau phosphorylated at Thr231) sites. Similar to the amygdala, the brainstem and cerebellum has not been reported to be affected in the brains of Tau35 mice aged 14 months (Bondulich et al., 2016). Consequently, the changes detected here in older Tau35 mice could indicate a delay in tau phosphorylation in this brain region. The cerebellum controls motor activity, including voluntary movement, balance and motor co-ordination (Buckner, 2013). Tau35 mice exhibit a motor learning deficit on the accelerating rotarod, and they are more likely

to fall as they age, compared to WT mice (Bondulich et al., 2016). This suggests that the decline in motor co-ordination is progressive, and may explain the delayed changes seen in this region as perhaps there is a correlation between the decline in motor activity and tau phosphorylation in Tau35 mice.

It is common for other animal models of tauopathy to demonstrate more pronounced differences in tau phosphorylation as the mice age, which validates the results described in this chapter. One example of such age-dependent differences in tau phosphorylation is the pR5 P301L tau mouse model, where more brain regions show increased tau phosphorylation as the mice age. Similar to the Tau35 mice, the brain regions affected in pR5 P301L mice include the hippocampus as well as the amygdala and brainstem (Gotz *et al*, 2001; David *et al,* 2005; Pennanen *et al,* 2006). The results obtained from the frontal brain region of aged Tau35 mice revealed significant increases in tau phosphorylation at the 12E8 and Tau-1 epitopes, compared to age-matched WT control mice. The frontal region of Tau35 mice appears to be more affected by tau phosphorylation than the amygdala, although this is less than that seen in the hippocampus. As was the case for both the amygdala, and the brainstem and cerebellum, no change had been reported previously in the frontal brain region of Tau35 mice aged 14 months. Taken together, these results indicate an age-dependent increase in tau phosphorylation in Tau35 mice.

The changes in tau phosphorylation observed in the Tau35 mice may be explained at least in part, by differential Tau35 expression in each brain region. Work in this laboratory has shown that Tau35 protein expression in the mice is highest in the hippocampus, and brainstem and cerebellum, and lowest in the amygdala and frontal brain regions (Natalia Yankova, personal communication). Similar findings have been documented by Höfling et al, who found differential transgene expression patterns in an amyloid precursor protein (APP) mouse model of Alzheimer's disease (Hofling et al., 2016). Such observations are also noted in tauopathy models. For example, the regional vulnerability observed in the rTg4510 mouse brain, such as neuronal death and neurofibrillary lesions in the hippocampus, and neuronal loss of dentate gyrus granule cells, show some correlation with the regional vulnerability observed in human FTLD-tau, in which the subiculum and hippocampus are the most affected brain regions (Spires et al., 2006).

3.3.2 **Brain region specific activation of the UPR**

Investigation of UPR activation in the hippocampus and amygdala of aged Tau35 mice showed that the UPR is selectively activated in specific brain regions. Thus, UPR activation was observed in the hippocampus, but not in the amygdala of Tau35 mice aged 16-18 months. These findings are corroborated by a study of brain tissue from people with AD and PSP, in which UPR activation was observed exclusively in neuropathologically affected brain regions (Stutzbach et al., 2013). In PSP brain, the UPR was activated as indicated by increased staining of phosphorylated PERK and phosphorylated eIF2α, primarily in the pons and medulla, and to a much lesser extent in the hippocampus. In PSP neuropathological changes such as intracellular neurofibrillary and glial tangles made up of tau, and neuronal degeneration occur in the brainstem, particularly the pons and medulla, thereby revealing a correlation between neuropathology and UPR activation (Stutzbach et al., 2013). In AD on the other hand, the UPR was extensively activated in the hippocampus, which is consistent with this region being affected early in disease pathogenesis (Stutzbach et al., 2013). In Tau35 mice, abnormalities in motor, cognitive and pathological abnormities have been predominantly associated with changes in hippocampal-dependent activity. Notably, the build-up of misfolded proteins has been proposed to be a primary trigger of UPR activation in neurodegenerative diseases such as AD (Ho et al., 2012). Since there is a greater proportion of phosphorylated tau in the hippocampus of Tau35 mice compared to the amygdala, this may explain the differences in UPR activation between different regions as increased phosphorylated tau in the hippocampus may drive UPR activation. These findings therefore suggest that there may be a relationship between increased tau phosphorylation and aggregation, and activation of the UPR in the tauopathies.

Accumulation of tau in AD brain results in the eventual loss of neurons and cognitive dysfunction (LaFerla and Oddo, 2005; Selkoe, 2001). The number of dying neurons in AD brain exceeds the number of tau tangles (Ferreiro and Pereira, 2012b). This suggests the involvement of a secondary route that leads to cell death that may be initiated or accelerated by the accumulation of phosphorylated tau. Recently, it has been suggested that prolonged UPR activation could be a pathway through which soluble tau species contribute to neuronal death, thereby implying that activation of the UPR could contribute

to the progression of several neurodegenerative diseases (Ferreiro and Pereira, 2012b). Over-activation of the UPR in the hippocampus of Tau35 mice leads to the subsequent increase in the expression of CHOP (Figure 3-7 C), which may go on to activate apoptotic pathways in these cells (Tabas and Ron, 2011). However, there is no evidence of overt neuronal cell death in Tau35 mice up to the age of 16 months (Marie Bondulich, personal communication). Alternatively, elevated CHOP may have the opposite effect by activating sXBP1 (chapter 1, Figure 1-10), which targets several genes, including ER chaperones to facilitate refolding of misfolded proteins and reduce ER stress (Scheper and Hoozemans, 2015; Schonthal, 2012). XBP1 can also be activated by IRE1 activation which was shown to be increased in the brains of Tau35 mice as indicated by increased IRE1 phosphorylation. This observation may further contribute to the lack of changes seen in neuronal cell death in Tau35 mice.

Mitigation of global protein translation can lead to synaptic failure in the rTg4510 mouse model of frontotemporal dementia (Radford et al., 2015). Similarly, reductions in synapsin 1 and synaptobrevin, synaptic vesicle proteins involved in fusion and interaction with vesicle membranes and regulating the reserve pool of synaptic vesicles (Gitler et al., 2004) have been shown in Tau35 mice (Bondulich et al., 2016). Therefore, activation of the PERK branch of the UPR may be an important factor underlying the reduction in the levels of these synaptic proteins and the integrity of synapses.

These findings demonstrate that activation of the PERK and IRE1 branches of the UPR are brain region-dependent in Tau35 mice, and this activation may be related to the observed increases in tau phosphorylation in the same brain regions. Markers of UPR activation are also elevated in AD brain, particularly in the hippocampus, and UPR activation has also been reported in neurons with abnormally phosphorylated tau protein (Chang et al., 2002; Hoozemans et al., 2009; Unterberger et al., 2006). Taken together, this implies a possible relationship between the appearance of phosphorylated and misfolded tau, and activation of the UPR that could be involved in disease pathogenesis in human tauopathies.

Chapter 4 The effect of Tau35 expression on cell viability and autophagy activation

4.1 Introduction

A characteristic feature of neurodegenerative tauopathies is the build-up of abnormal inclusions, which contain misfolded and unfolded proteins. One system that is responsible for restoring homeostasis when such inclusions accumulate is the autophagy and lysosomal degradation system (Maiuri et al., 2007). Autophagy is a self-degradative process that clears protein aggregates and damaged organelles, such as mitochondria, the endoplasmic reticulum, and peroxisomes (Maiuri et al., 2007; Yu et al., 2018). Autophagy begins with an initiation phase, during which the proteins to be degraded are identified (chapter 1, Figure 1-7) (Yu et al., 2018). Initiation of autophagy is followed by the formation of a double-membrane structure known as the autophagosome, that sequesters the proteins to be degraded. The autophagosome then fuses with the lysosome to form an autolysosome and the degraded proteins are then recycled and fed back into the cell (Eskelinen, 2005). If autophagy fails to achieve homeostasis, this can lead to chronic ER stress, which ultimately results in the activation of cell death through apoptosis (Rao et al., 2001). Due to this, crosstalk between autophagic and apoptotic pathways determine the eventual fate of the cell. Beclin-1 has a prominent role in the initiation of autophagy, as it regulates the autophagy-promoting activity of Vps34, a Class III PI3-kinase. Beclin-1 additionally plays a role in the localisation of autophagic proteins to a pre-autophagosomal structure and is involved in membrane recruitment for the autophagosome, which is required for autophagosome formation (Criollo et al., 2007). Beclin-1 can also interact with Bcl-2 and is involved in the determination of cell survival (Chu et al., 2007).

There are several components upstream of the autophagy pathway that play a critical regulatory role. One such example is the primary nutrient-sensing complex, mammalian target of rapamycin complex 1 (mTORC1), including mTOR kinase, raptor, and mammalian lethal with SEC13 protein 8 (MLST8) (Hoeffer and Klann, 2010). Decreased mTORC1 activity is normally accompanied by upregulation of autophagy (Duran et al., 2011). Another component upstream of autophagy is adenosine monophosphate-activated protein kinase (AMPK), a conserved sensor of intracellular energy that is activated in

response to low nutrient availability and environmental stress, thereby activating autophagy (Hardie, 2011). The Atg1/ULK (autophagy related gene 1/Unc-51-like kinase) complex additionally plays an essential role in the initiation of autophagy as it receives signals of cellular nutrient status (Mizushima, 2010). When ULK1 senses an excess of nutrients, it recruits downstream Atg proteins to the autophagosome formation site, and increases autophagosome formation (Mizushima, 2010).

It is important to determine whether Tau35 expression affects protein degradation mechanisms, such as autophagy, as well as assessing the effect of Tau35 on cell survival. Some studies have reported that excess amounts of tau may be toxic to cells. For example, an excess of hTau induced mitotic arrest, with the presence of monopolar spindles, and apoptotic cell death in a *Drosophila* model (Bouge and Parmentier, 2016). Several studies have shown that a failure in autophagy in multiple neurodegenerative diseases including ALS, AD and PD, may be responsible for the build-up of proteins inside affected neurons (Chamoux et al., 2013; Fecto et al., 2011; Lee et al., 2010c). In particular, knockdown of *Atg5* and *Atg7* in mouse brain results in a neurodegenerative phenotype, with the accumulation of protein aggregates containing ubiquitin-positive inclusions in the absence of disease-causing proteins (Reggiori, 2012). In addition, autophagy was activated in brain regions in which the number of neurons containing tau inclusions was significantly reduced, as was the amount of insoluble tau, in transgenic mice expressing human P301S tau (Schaeffer et al., 2012a).

To examine the effects of Tau35 expression on the autophagy pathway and cell viability, CHO cell models that stably express either V5 tagged-Tau35, or the 2N4R isoform of human tau, were generated (Tong Guo, King's College London). These cell lines provide a means of understanding the molecular changes that occur along different stages of the autophagy pathway, as well as the opportunity to modify them using inhibitors and activators. Although CHO cells do not express tau, they have long been used to investigate changes in the cytoskeleton, including in relation to exogenous tau expression. For instance, they have been used to study physiological functions and pathological changes in tau (Gallo et al., 1992). Moreover, stable CHO cell lines have been used extensively to study the different roles of various microtubule-binding proteins such as human MAP4,

which also stabilises microtubules (Barlow et al., 1994). In addition, CHO cells stably expressing tau harbouring different frontotemporal dementia (FTLD-tau) mutations replicate several disease-associated pathological features, such as formation of insoluble filamentous tau aggregates and reduced interaction of tau with microtubules (Vogelsberg-Ragaglia et al., 2000). Therefore, stably transfected CHO cells represent a useful model in which to study the effects of tau and Tau35 on cellular functions.

4.2 Results

4.2.1 The effect of Tau35 expression on CHO cell viability

Firstly, to confirm the successful transfection and expression of FL-tau and Tau35 in CHO cells, western blots of total cell lysates were probed with an antibody recognising total tau. Figure 4-1 shows that CHO cells stably transfected with FL-tau show a band corresponding to tau just below 75kDa. Cells stably transfected with Tau35 show multiple bands when probed with the total tau antibody, ranging from 25kDa to 37kDa.

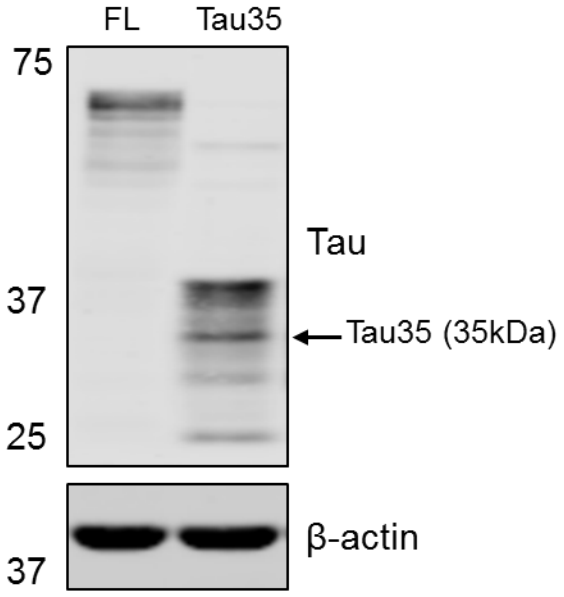

Figure 4-1 verifying the expression of FL-tau and Tau35 in CHO cells: Western blots of total cell lysates from CHO cells stably transfected with FL-tau or Tau35, probed with antibodies against total tau and β-actin (loading control). Molecular weights (kDa) are shown on the left.

To determine whether Tau35 expression impacts on cell survival, a cell viability assay was performed on CHO-Tau35, CHO-FL and untransfected CHO cells using calcein violet 450 AM. Calcein violet AM is a membrane-permeable dye that is taken up by live cells and hydrolysed by intracellular esterases into the green fluorescent, membrane-impermeable anion calcein. Non-viable cells are unable to retain the dye due to their compromised cell membrane integrity (Gillissen et al., 2016).

The first approach to measure cell viability involved using fluorescence activated cell sorting (FACS) in CHO-FL, CHO-Tau35 and untransfected CHO lines under basal conditions. Cells were exposed to 500 nM Calcein 450 AM for 30 min and calcein fluorescence was measured (BD FACSCanto II). Figure 4-2 shows representative histograms of calcein fluorescence recorded in the three cell lines. The peak corresponding to viable CHO-FL cells (Figure 4-2 A right) is almost two-fold higher than that corresponding to non-viable cells (Figure 4-2A left). Figure 4-2 B is the histogram corresponding to the count of Tau35-CHO cells. The peak corresponding to viable CHO-Tau35 cells (Figure 4-2 B right) is almost three-fold higher than that corresponding to non-viable cells (Figure 4-2 B left). Figure 4-2 C is a representative histogram for the data recorded for the untransfected CHO cells. The peak corresponding to viable CHO cells (Figure 4-2 C right) is approximately three-fold higher than that corresponding to non-viable cells (Figure 4-2 C left). Figure 4-2 D is data recorded from untransfected CHO cells without calcein AM (negative control). The single peak on the left shows the detection of a cell population. The results from this FACS analysis indicate that the population of viable cells far exceeds the number of non-viable cells in all three cell lines. The percentage of viable cells in each cell line (Figure 4-2E) shows that there is no statistically significant difference in the basal viability of CHO-FL, CHO-Tau35 or untransfected CHO cells.

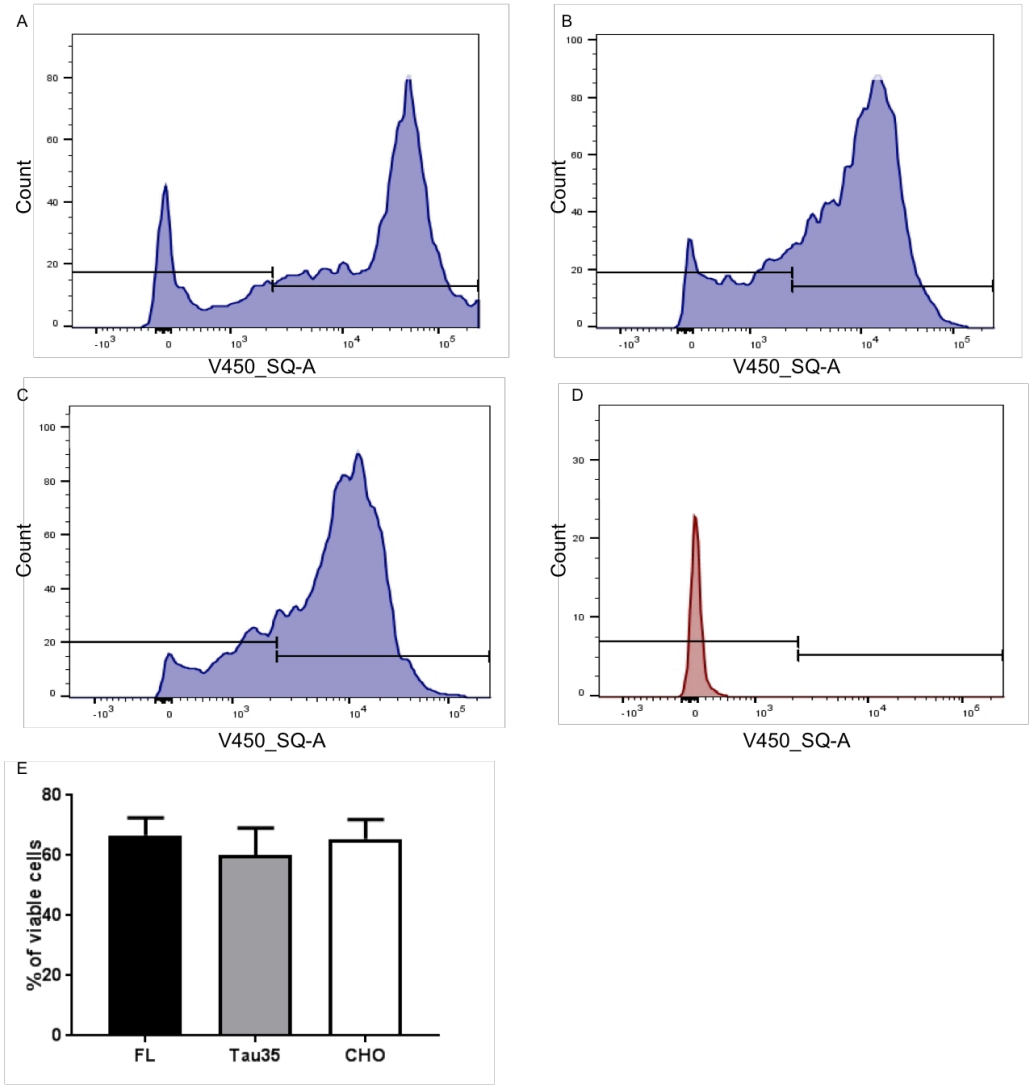

Figure 4-2 Calcein AM cell viability assay using FACS: A-D show histograms of cell viability assays performed on A CHO-FL, B CHO-Tau35, C CHO cells, D CHO cells without calcein (negative control). Calcein AM negative cells are shown with reduced fluorescent intensity for calcein AM (as gated). **E** Quantitation of viable cells, expressed as a percentage of the total number of cells analysed. Values represent mean ± SEM, n=3, one-way ANOVA.

A second approach used to measure cell viability was using a plate reader to detect the amount of calcein AM fluorescence taken up by each cell line. As had been previously shown using the FACS method (Figure 4-2), all three cell lines showed similar viability using this method (Figure 4-3A, $P>0.05$). This demonstrates that expression of either FL-tau or Tau35 does not induce cell death in CHO cells. These findings validate the previous results obtained from measuring calcein fluorescence in untreated cells using FACS and indicate that assay of cell viability by calcein AM uptake using the plate reader provides reliable and robust data.

The three CHO cell lines were subsequently treated with DTT or thapsigargin to determine how the cells respond to extrinsic UPR inducers. DTT is a strong reducing agent, which blocks the formation of disulfide bonds, thereby leading to ER stress (Carpio et al., 2015). Thapsigargin is a specific inhibitor of the sarcoplasmic/endoplasmic reticulum Ca^{2+}-ATPase that reduces ER calcium, thereby hindering the functionality of Ca^{2+}dependent ER chaperones, and causing the accumulation of unfolded proteins (Halliday et al., 2017). Measurement of cell viability using the plate reader method, after treating the CHO cell lines with 20 mM DTT for 4 h, showed a statistically significant increase in the viability of CHO-Tau35 cells compared to both CHO-FL and untransfected CHO cells (Figure 4-3 B, $P<0.05$). However, there was no significant difference between the number of viable CHO-FL and untransfected CHO cells (Figure 4-3 B). In CHO cells treated with thapsigargin (1 µM, 6 h), there was no statistically significant difference in cell viability between CHO-FL, CHO-Tau35 and untransfected CHO cells (Figure 4-3 C). Extending the time of thapsigargin treatment (1 µM, 24 h) showed a statistically significant increase in cell viability in CHO-FL and CHO-Tau35 cells, compared to untransfected CHO cells (Figure 4-3 D; $P<0.05$). However, there was no significant difference in cell viability between CHO-FL and CHO-Tau35 cells (Figure 4-3 D). Taken together, these results indicate that cell viability is significantly enhanced in CHO-Tau35 cells following induction of ER stress by DTT and also by extended thapsigargin treatment. In comparison, CHO-FL cells are not affected by ER stress in response to DTT as they respond similarly to untransfected CHO cells. However, CHO-FL cells are more sensitive than untransfected CHO cells to prolonged thapsigargin treatment and expression of FL-tau results in enhanced cell viability that is similar to that

of CHO-Tau35 cells under these conditions. The results suggest that at least in CHO cells, expression of tau, and especially Tau35, could have a protective role.

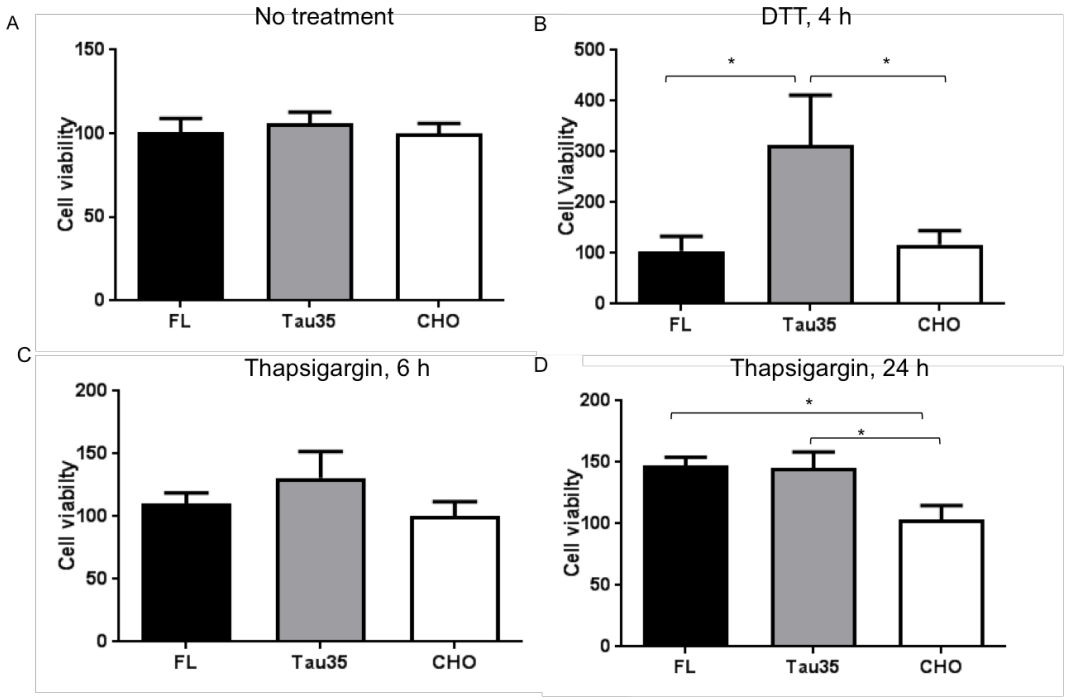

Figure 4-3 Cell viability assay using calcein AM: Cell viability assay performed on CHO-FL, CHO-Tau35 and untransfected CHO cells (%). **A** Untreated, **B** DTT (20 mM, 4 h), **C** Thapsigargin (1 µM, 6 h), **D** Thapsigargin (1 µM, 24 h). Values represent the percentage (%) of viable CHO-FL and CHO-Tau35 cells, relative to that of untransfected CHO cells (mean ± SEM, n=4; one-way ANOVA, *P<0.05).

4.2.2 **Early autophagy in CHO-Tau35 cells**

Previous work has shown that CHO-Tau35 cells exhibit increased tau phosphorylation at several different epitopes, including PHF-1 and AT180, compared to CHO-FL cells (Tong Guo, King's College London). This accumulation of phosphorylated tau suggests that autophagy might be disrupted in Tau35-CHO cells, thereby hindering protein clearance.

To measure changes in early autophagy, western blots of CHO-FL, CHO-Tau35 and CHO cell lysates were probed with an antibody against beclin-1. The amount of beclin-1 present in CHO-Tau35 cells, relative to β-actin, was decreased by approximately 30-40%, compared to CHO-FL and CHO cells (Figure 4-4; $P<0.01$ and $P<0.05$, respectively). In contrast, the amount of beclin-1 was unchanged in CHO-FL cells compared to CHO cells. These results show a selective loss of beclin-1 in CHO-Tau35 cells, suggesting that Tau35 expression induces a defect in early autophagy.

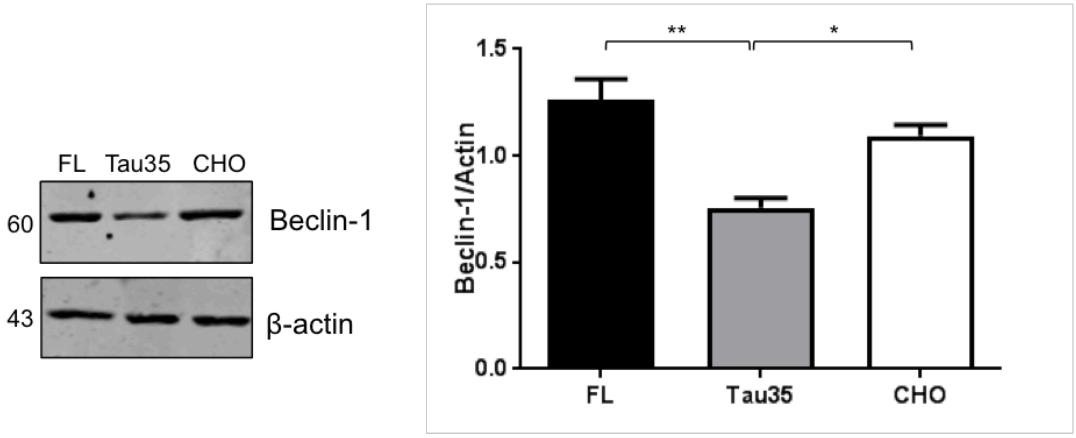

Figure 4-4 Early autophagy dysfunction indicated by reduced beclin-1 in CHO-Tau35 cells: Western blots of CHO-FL, CHO-Tau35 and untransfected CHO cell lysates probed with antibodies to beclin-1 and β-actin (loading control). Molecular weights (kDa) are shown on the left. The graph shows the quantitation of the western blot. Values represent mean ± SEM, n=4; one-way ANOVA, *P<0.05, **P<0.01.

To further investigate autophagy initiation in CHO-Tau35 cells, the amounts of three Atg proteins (Atg5, Atg7, and Atg13), each involved at different stages of autophagy activation,

were measured in the three cell lines. Western blots of CHO-FL, CHO-Tau35 and CHO cell lysates were probed with antibodies to Atg5, Atg7, or Atg13 and the amount of each protein was standardised to glyceraldehyde 3-phosphate dehydrogenase (GAPDH). The blots showed immunoreactive bands at the expected molecular weights for Atg5 (50 kDa), Atg7 (77 kDa) and Atg 13 (72 kDa) in all three CHO cell lines. The results showed no statistically significant differences in the amounts of Atg5, Atg7, or Atg13 in CHO-FL, CHO-Tau35 and CHO cells (Figure 4-5). Overall, these findings indicate that expression of either FL-tau or Tau35 does not influence autophagy initiation in CHO cells and that any effect of Tau35 on autophagy likely lies downstream.

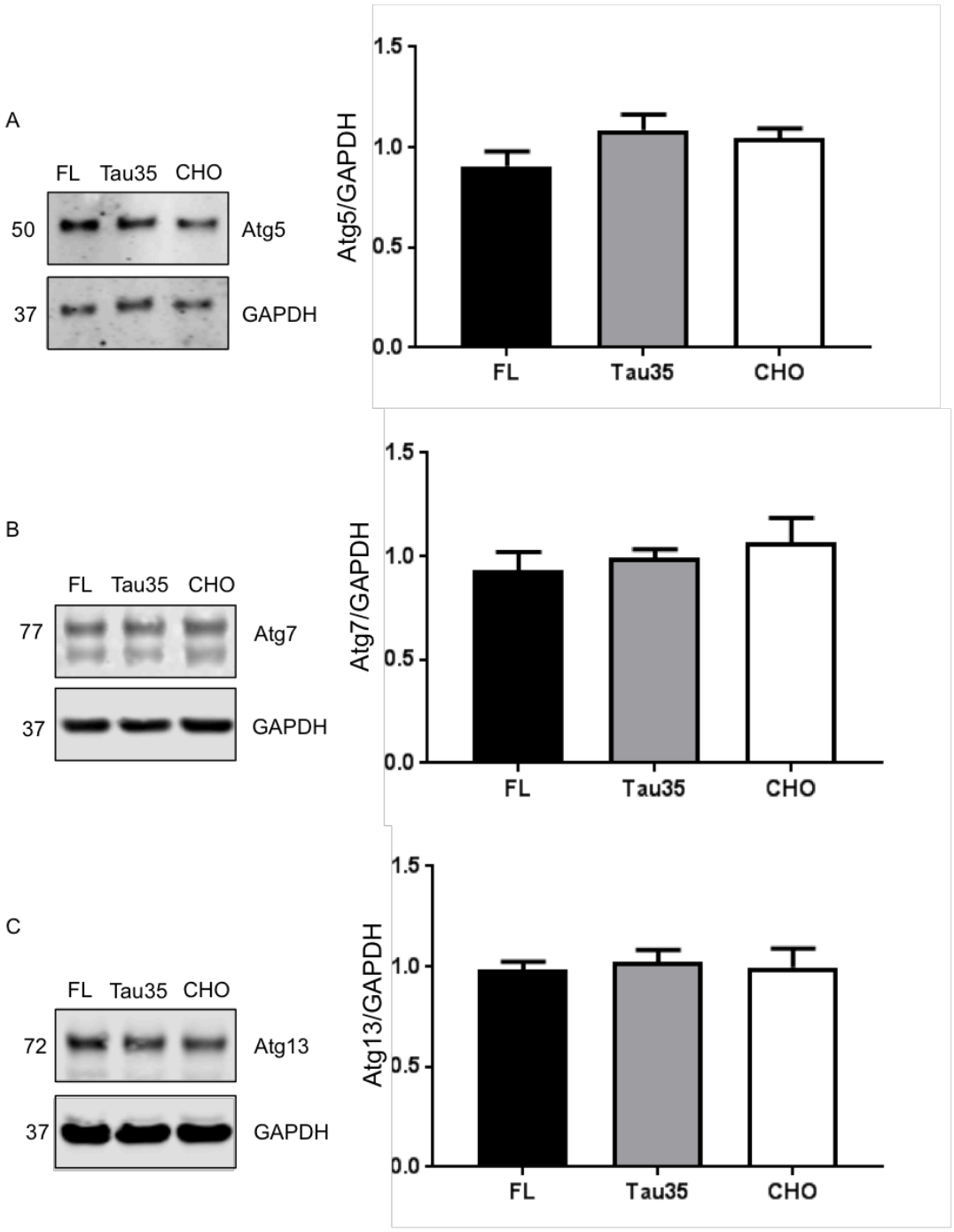

Figure 4-5 No changes in the amount of Atg5, Atg7, or Atg13 in CHO-Tau35 cells: Western blots of CHO-FL, CHO-Tau35 and untransfected CHO cell lysates probed with antibodies to **A** Atg5, **B** Atg7 **C** Atg13 and glyceraldehyde 3-phosphate dehydrogenase (GAPDH). Molecular weights (kDa) are shown on the left. The graphs show the quantitation of the Atg proteins on western blots, relative to GAPDH. Values represent mean ± SEM, n=3; one-way ANOVA.

4.2.3 **Autophagosome formation and maturation in CHO-Tau35 cells**

The amounts of LC3 in CHO-FL, CHO-Tau35 and CHO cells were measured to assess whether Tau35 expression induces changes in autophagosome formation. Western blots of lysates from each of the three cell lines were probed with an antibody detecting both LC3-I and LC3-II. The results showed a pronounced decrease in the basal amount of LC3-II in CHO-Tau35 cells, compared to CHO-FL and CHO cells (Figure 4-6 A; $P<0.01$ and $P<0.05$, respectively). Moreover, there was also a significant increase in the amount of LC3-II in CHO-FL compared to CHO cells ($P<0.05$). This implies that CHO-Tau35 cells contain fewer autophagosomes than CHO cells, whereas CHO-FL cells harbour an increased number of autophagosomes.

To confirm these effects of Tau35 and FL-tau expression on LC3-II, and to observe the cellular distribution of LC3 puncta CHO-FL, CHO-Tau35 and CHO cells were fixed in methanol and labelled with the same LC3 antibody used on the western blots. LC3 was visualised in the three cell lines using immunofluorescence and the fluorescence intensity of LC3 was determined. The results showed a marked reduction in LC3 immunofluorescence in CHO-Tau35 cells, compared to both CHO-FL and CHO cells (Figure 4-6 B; $P<0.01$ and $P<0.05$, respectively). Furthermore, there was a significant increase in LC3 intensity in CHO-FL cells compared to CHO cells (Figure 4-6 B, $P<0.05$). The findings from these experiments are consistent with those from the western blots, confirming the overall reduction in LC3 caused by Tau35 expression in CHO cells, indicating a deficit in basal autophagy.

The distribution of cytosolic LC3 puncta in CHO cells was determined for each cell line using a series of six concentric rings, positioned 3 µm apart, extending up to 18 µm out from the perimeter of the nucleus in each cell. The fluorescence intensity of LC3 inside each concentric ring was measured and plotted against the distance from the nucleus (Figure 4-7). Tau35-CHO cells showed a pronounced reduction in puncta compared to CHO-FL and CHO cells, at almost all distances from the nucleus. In comparison to untransfected CHO cells, CHO-Tau35 cells showed a mean significant reduction of 32% at the edge of the nucleus (0-3 µm distance), whereas CHO-FL cells only showed a 13% reduction, which was not significantly different from LC3 localisation in untransfected CHO

cells. Moreover, compared to CHO cells, CHO-Tau35 cells showed a mean reduction of 35% at a distance of18µm from the nucleus and CHO-FL cells showed a reduction of 10% in LC3 puncta at this distance. The results of the distribution of LC3 puncta in the three CHO cell lines are summarised in Table 4-1. Taken together, the distribution analysis results show that the number of LC3 puncta is reduced throughout the perimeter of CHO-Tau35 cells; however, the overall trend of LC3 puncta distribution appears to be similar across the three cell types.

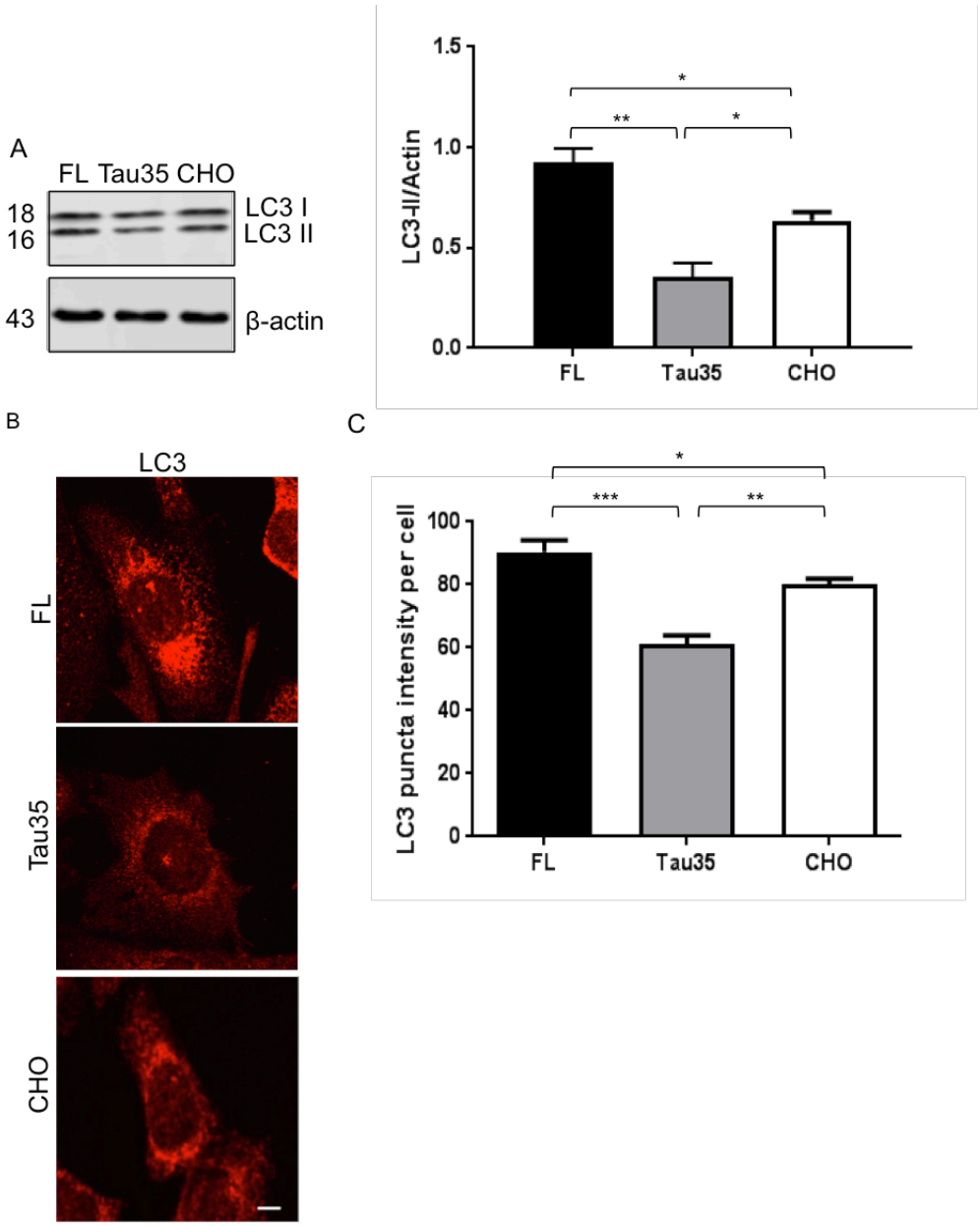

Figure 4-6 Reduced amount of the autophagosome marker LC3 in CHO-Tau35 cells: A Western blot and quantitation of LC3-I and LC3-II, relative to β-actin, in CHO-FL, CHO-Tau35 and CHO cell lysates, n=6. **B** immunofluorescence of methanol-fixed CHO-FL, CHO-Tau35 and CHO cells labelled with LC3 antibody, scale bar=10 µm. **C** Quantification of LC3 intensity. For the quantification, a total of 30 cells were analysed per condition, n=3 for each cell line. Values represent mean ± SEM, one-way ANOVA, *P<0.05, **P<0.01, ***P<0.001.

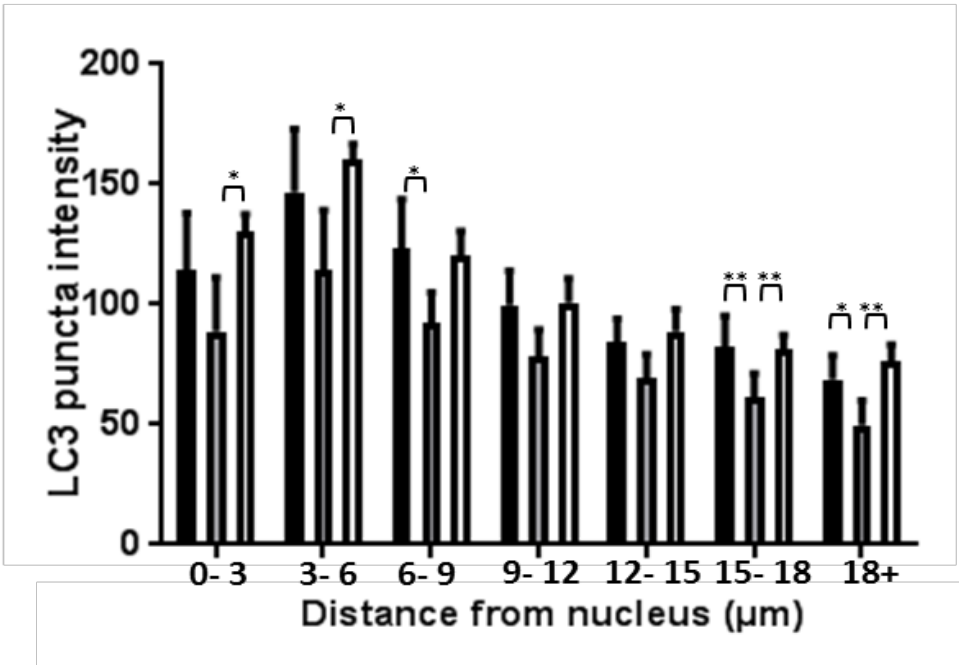

Figure 4-7 Trend of LC3 puncta distribution: Distribution analysis of LC3 immunofluorescence in CHO-FL, CHO-Tau35, and CHO cells. For each cell type, a total of 50 cells were counted. Values represent mean ± SEM, two-way ANOVA, *P<0.05, **P<0.01, ***P<0.001. Black bars: FL, grey bars: Tau35, white bars: CHO.

Table 4-1 Summary of the mean percentage reduction in puncta distribution in CHO-Tau35 and CHO-FL cells compared to CHO cells

Distance from nucleus (µm)	Percentage reduction in puncta intensity between CHO-Tau35 and CHO cells	Percentage reduction in puncta intensity between CHO-FL and CHO cells
0-3	32	13
3-6	29	9
6-9	23	-2
9-12	22	1
12-15	21	5
15-18	24	-1
18+	35	10

There are several different extrinsic autophagy activators that have been used to study autophagy in *in vitro* systems. One example is nutrient starvation, induced by depleting amino acids and/or growth factors, which is widely used to elicit an acute autophagic response by dephosphorylating ULK1. Therefore, to test the effects of inducing autophagy by effectively starving cells of nutrients, cell culture medium was replaced with HBSS (containing Mg^{2+} and $Ca^{2+)}$ in the three cell lines. Western blots of CHO-FL, CHO-Tau35 and CHO cells, either untreated or exposed to HBSS, were probed with antibodies to LC3 and β-actin to assess autophagy activation. The amount of LC3-II was significantly elevated in starved cells compared to untreated cells in all three cell lines (Figure 4-8, $P<0.05$). Furthermore, upon cell starvation, the amount of LC3-II in CHO-Tau35 cells reached approximately half of that in the CHO cells (Figure 4-8, $P<0.05$). In addition, the amount of LC3-II in CHO-FL cells was approximately three-fold higher than that of CHO-Tau35 cells upon starvation (Figure 4-8, $P<0.01$). HBSS also induced an increase in LC3-II in CHO-FL cells, compared to CHO cells (Figure 4-8, $P<0.05$). Taken together with the earlier finding of reduced basal LC3-II in CHO-Tau35 cells, these data suggest that Tau35 expression attenuates activation of autophagy in CHO cells, even after stimulation of autophagic processes induced by cell starvation. The expression of FL-tau in CHO cells does not have the same effect on the amount of LC3-II, indicating that the inhibition of autophagy activation is specific to Tau35.

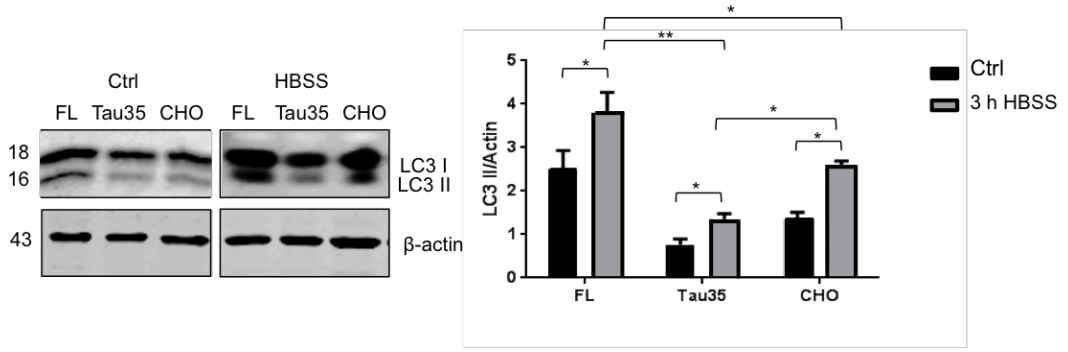

Figure 4-8 Reduced induction of LC3-II in CHO-Tau35 cells upon starvation: Western blots of CHO-FL, CHO-Tau35 and untransfected CHO cell lysates (untreated or treated with HBSS for 3 h to induce starvation) probed with antibodies to LC3 and β-actin (loading control). Molecular weights (kDa) are shown on the left. The graph shows the quantitation of the western blots. Values represent mean ± SEM, n=6; two-way ANOVA, *P<0.05, **P<0.01.

Autophagic flux measures the dynamic process of autophagy: autophagosome formation, maturation, fusion with lysosomes, subsequent breakdown and the release of macromolecules back into the cytosol (Zhang et al., 2013). Bafilomycin A1 inhibits V-ATPase, thereby preventing autophagosome-lysosome fusion and maturation of autophagic vacuoles, which results in the accumulation of autophagosomes (marked by LC3-II) in cells. Hence, one reliable method to determine if there are effects on autophagic flux is to expose cells to bafilomycin A1 and to measure the amount of LC3-II on western blots. Therefore, western blots of CHO-FL, CHO-Tau35 and CHO cell lysates, either untreated or exposed to bafilomycin (300 nM, 2 h), were probed with LC3 antibody (Figure 4-9). In all three cell types, bafilomycin caused a substantial build-up of LC3-II, compared to untreated cells ($P<0.01$). Despite this increase, the amount of LC3-II in CHO-Tau35 cells remained significantly lower than that in CHO-FL and CHO cells after bafilomycin treatment ($P<0.05$ and $P<0.001$, respectively). In contrast, there was no significant difference in the amount of LC3-II present in CHO-FL and CHO cells treated with bafilomycin under these conditions. These findings further support the autophagic deficit in CHO-Tau35 cells because the amount of LC3-II-postive autophagosomes in these cells remained substantially lower upon induction of autophagic flux.

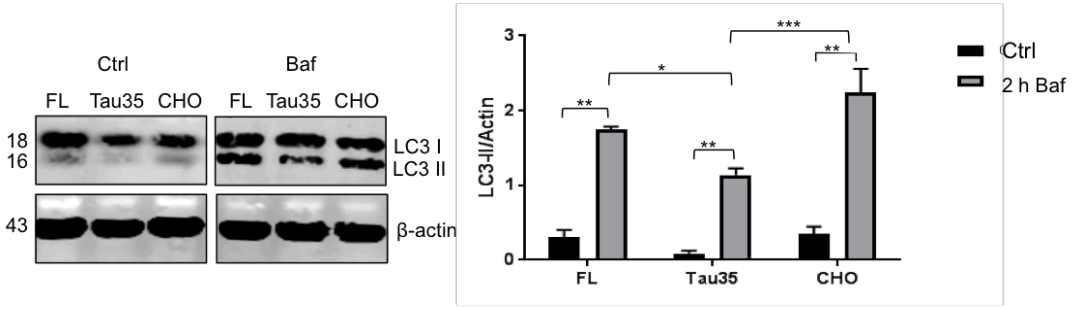

Figure 4-9 Reduced LC3-II in CHO-Tau35 cells upon induction of autophagic flux: Western blots of CHO-FL, CHO-Tau35 and untransfected CHO cell lysates probed with antibodies to LC3 and β-actin (loading control) in untreated and bafilomycin A1-treated (300 nM for 2 h) cells. Molecular weights (kDa) are shown on the left. The graph shows the quantitation of the western blots. Values represent mean ± SEM, n=6; two-way ANOVA, *P<0.05, **P<0.01, ***P<0.001.

4.2.4 **The effect of Tau35 expression on the size of CHO cells**

One of the defining functions of tau is to bind to microtubules, thereby promoting their stability and maintaining the structure of the cytoskeleton. In addition, tubulin acetylation is vital in modulating the function of microtubules (Perdiz et al., 2011). Acetylation of the Lys40 residue in α-tubulin is a key marker of polymer age and hence microtubule stability. Notably, deficits in tubulin acetylation at this site have been reported in a variety of neurodegenerative disorders, including Parkinson's disease and several tauopathies (Dubey et al., 2015; Zhang et al., 2015).

The immunofluorescence images used to analyse LC3 puncta intensity and distribution were additionally used to calculate cell size of CHO-FL, CHO-Tau35 and CHO cells. Previous work in this laboratory showed that Tau35 in CHO cells has a reduced ability to bind to microtubules, as well as a marked reduction in acetylated tubulin (Guo et al., 2019). Such disruptions in tubulin acetylation and microtubule binding could also impact on the size and morphology of CHO cells as CHO-Tau35 cells appear to be more rounded than CHO-FL and CHO cells. Therefore, the area occupied by CHO-Tau35, CHO-FL and CHO cells was determined (Figure 4-10). The results showed that CHO-Tau35 cells occupy approximately 35% less area compared to CHO cells (P<0.001), and they are approximately 25% smaller than CHO-FL cells (P<0.01). Additionally, CHO-FL cells exhibited a slight reduction of

approximately 16% in cell area compared to CHO cells (P<0.05). These results show that expression of both FL-tau and Tau35 has an impact on the size of CHO cells.

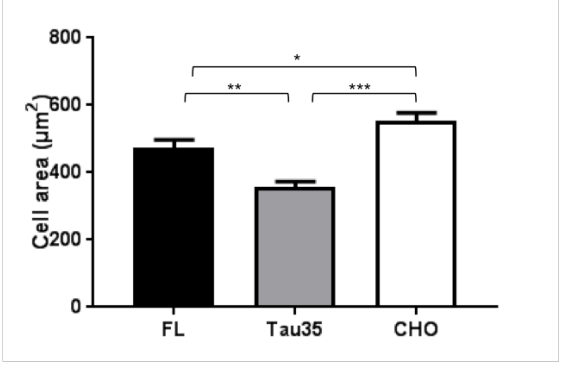

Figure 4-10 Reduced cell size in CHO-Tau35 cells: Quantification of cell area in CHO-FL, CHO-Tau35 and CHO cells from immunofluorescence images of LC3. For each cell type, a total of 50 cells were counted. Values represent mean ± SEM one-way ANOVA, *P<0.05, **P<0.01, ***P<0.001.

4.2.5 **Exploring upstream targets of autophagy in CHO-Tau35 cells**

mTORC1 negatively regulates autophagy in mammals (Ravikumar et al., 2004b). Rapamycin and other mTOR kinase inhibitors have been widely used to induce autophagy, including under nutrient-rich conditions, in order to study the impact of mTORC1 inhibition on pathways such as autophagy. Reducing mTOR activity increases lifespan (Finkel, 2015; Weichhart, 2018) and, conversely, mTOR signaling is upregulated in AD brain (Bockaert and Marin, 2015; Sun et al., 2014). Specifically, phosphorylated mTOR and its downstream targets, including p70S6 kinase and ribosomal protein S6, have been reported to be increased in AD (Pei et al., 2008). Moreover, direct interaction between raptor (a subunit of mTORC1) and ULK1 can be detected under nutrient-rich conditions (chapter 1, Figure 1-8). In addition, AMPK phosphorylation of raptor on two well-conserved serine residues inhibits mTORC1 and cell cycle arrest induced by energy stress (Gwinn et al., 2008). Notably, rapamycin-mediated induction of autophagy has also been shown to ameliorate Aβ and tau pathology in the brains of 3xTg-AD mice (Caccamo et al., 2010a).

Therefore, the state of mTORC1 activation was investigated in the three CHO cell lines, with the aim of understanding the molecular mechanism that leads to the apparent deficit

in autophagy induced by Tau35 expression. mTORC1 activity was measured by probing western blots of CHO-FL, CHO-Tau35 and CHO cell lysates with antibodies to total and phosphorylated mTOR, S6 and raptor. Each CHO cell line was either untreated or exposed to rapamycin (1 μM, 6 h) to induce autophagy (Figure 4-11). The basal level of phosphorylated/total mTOR in CHO-Tau35 cells was significantly higher than that of CHO-FL cells (Figure 4-10A, $P<0.01$), although this did not reach statistical significance when compared to mTOR activation in CHO cells ($P=0.056$). There was no difference between phosphorylated/total mTOR in CHO-FL and CHO cells. Rapamycin significantly reduced the amount of phosphorylated/total mTOR in all three CHO cell lines ($P<0.01$ in all cases). Notably, after rapamycin treatment, there were no significant differences in phosphorylated/total mTOR between CHO-FL, CHO-Tau35 and CHO cells ($P>0.05$). These results show that in comparison to the effects of FL-tau in CHO cells, Tau35 activates mTOR and this difference is repressed on induction of autophagy with rapamycin.

To investigate the impact of mTORC1 on autophagy activation in CHO-Tau35 cells, western blots of untreated and rapamycin treated (1 μM for 6 h) CHO-FL, CHO-Tau35 and CHO cells were probed with LC3 antibody (Figure 4-11 B). As expected, rapamycin induced a statistically significant increase in LC3-II in CHO-FL cells ($P<0.01$), CHO-Tau35 cells ($P<0.05$) and CHO cells ($P<0.001$) compared to untreated cells. There was a marked reduction in LC3-II in CHO-Tau35 cells compared to CHO-FL and CHO cells ($P<0.001$). These results indicate that, in relation to autophagosome formation, CHO-Tau35 cells are less responsive to rapamycin than are the other two CHO cell lines.

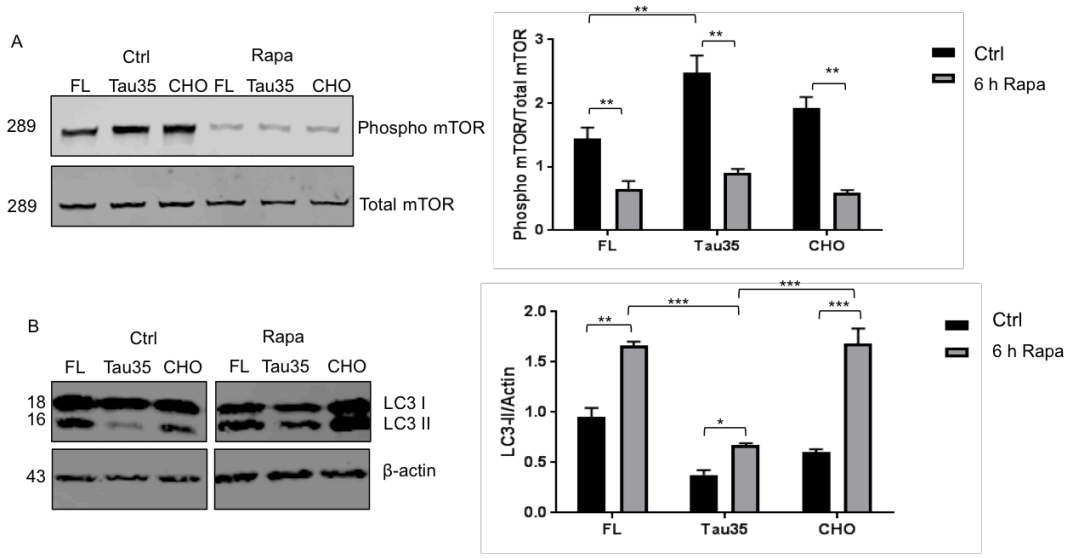

Figure 4-11 Activation of mTORC1 reduces autophagosome formation in CHO Tau35 cells: Western blots of cell lysates prepared from CHO-FL, CHO-Tau35 and untransfected CHO cells, either untreated or rapamycin-treated (1 μM for 6 h), and probed with antibodies **A** phospho mTOR (ser2448) and total mTOR, **B** LC3-I, LC3-II and β-actin (loading control). Molecular weights (kDa) are shown on the left. The graphs show the quantitation of the western blots. Values represent mean ±SEM, n=6; two-way ANOVA, *P<0.05, **P<0.01, ***P<0.001.

To confirm the observed activation of mTORC1 in CHO-Tau35 cells, phosphorylation of the mTORC1 substrate, S6 ribosomal protein (Ser240/244) and raptor (Ser792) were each assessed on western blots of the CHO cell lysates (Figure 4-12). The amount of phosphorylated/total S6 was dramatically increased in CHO-Tau35 cells compared to both CHO-FL and CHO cells, which exhibited little to no S6 phosphorylation (P<0.05). The amount of phosphorylated/total raptor was markedly decreased in CHO-Tau35 cells compared to CHO-FL (P<0.01) and CHO cells (P<0.05), indicating a lack of repression of mTORC1 by raptor in CHO-Tau35 cells. There was no significant difference in phosphorylated/total raptor at this site between CHO-FL and CHO cells. Taken together, these results show that multiple components of the mTORC1 complex are activated by the expression of Tau35 in CHO cells.

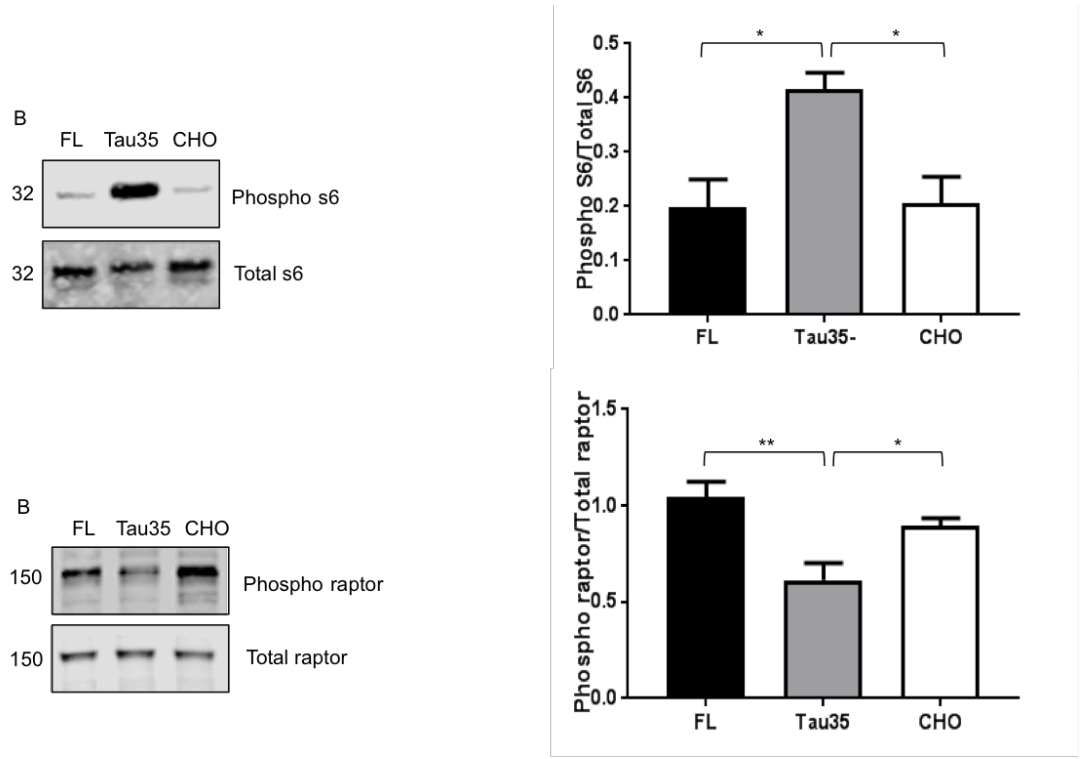

Figure 4-12 Confirmation of mTORC1 activation in CHO-Tau35 cells: Western blots of cell lysates prepared from CHO-FL, CHO-Tau35 and untransfected CHO cells probed with antibodies **A** phosphorylated (Ser240/244) and total S6, **B** phosphorylated (Ser792) and total raptor. Molecular weights (kDa) are shown on the left. The graphs show the quantitation of the western blots. Values represent mean ± SEM, n=6; one-way ANOVA, *P<0.05, **P<0.01.

Trehalose is a non-toxic, naturally occurring disaccharide that induces autophagy and has been reported to aid degradation of mutant huntingtin and α-synuclein (Sarkar et al., 2014). Trehalose activates autophagy through an mTOR-independent pathway, without stimulating ERK activation (Sarkar et al., 2007a). Administration of trehalose leads to degradation of mutant huntingtin in Neuro 2a cells exogenously expressing GFP-Htt (human huntingtin) (Q74), without affecting extracellular signal-regulated kinase (ERK) activity.

To gain further insight into the autophagic dysfunction apparent in CHO-Tau35 cells, trehalose was used to assess the activation of autophagy by a mechanism independent of

mTOR. CHO-FL, CHO-Tau35 and CHO cell lysates, either untreated or treated with trehalose (100 mM, 24 h), were probed on western blots with antibodies to LC3, and phosphorylated (active) and total ERK to assess the effect of this activator on autophagosome formation and ERK activity in CHO cells (Figure 4-13). The results show a significant increase in LC3-II in CHO-FL ($P<0.001$), CHO-Tau35 ($P<0.01$) and CHO cells following trehalose treatment. Figure 4-13 B shows a reduction in phosphorylated/total ERK in CHO-Tau35 cells compared to CHO-FL ($P<0.001$) and CHO cells ($P<0.05$). However, there was no difference in phosphorylated/total ERK between CHO-FL and CHO cells ($P>0.05$). Overall, these results indicate that CHO-Tau35 cells are more sensitive to trehalose treatment compared to CHO-FL and CHO cells, indicating that they have an increased ability to activate autophagy via an mTOR-independent route. Furthermore, the basal amount of activated ERK is markedly lower in these cells and an increase in ERK activity is associated with increased autophagy activation.

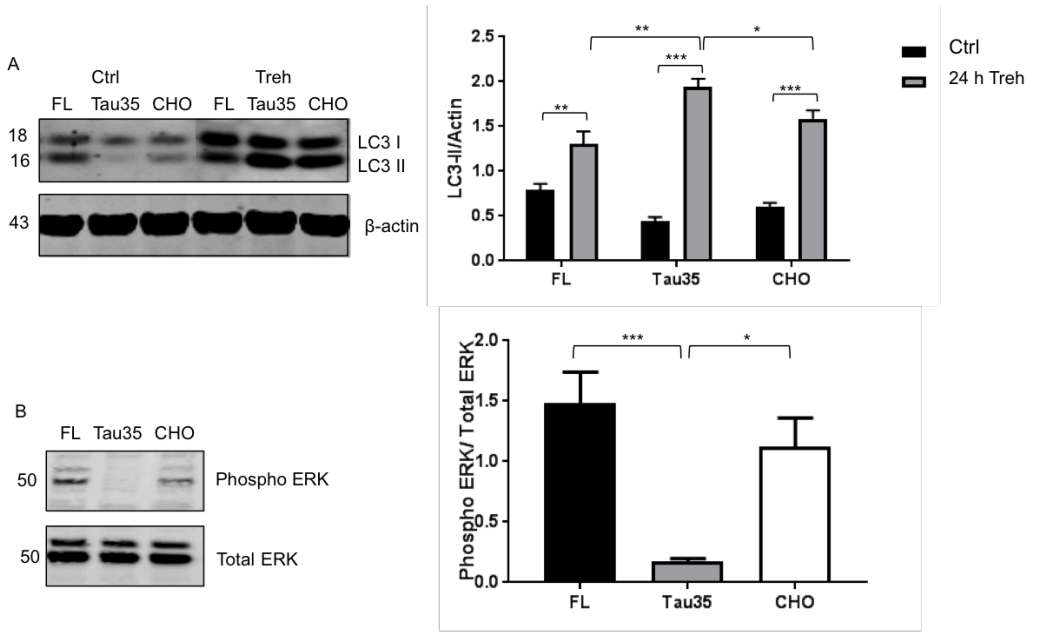

Figure 4-13 Increased autophagy activation in CHO-Tau35 cells upon activation of an mTOR-independent pathway: Western blots of cell lysates prepared from CHO-FL, CHO-Tau35 and untransfected CHO cells probed with antibodies **A** LC3 I, LC3 II and β-actin (loading control) in untreated and 100 mM trehalose (Treh) treated for 24 h, **B** phospho ERK (dually phosphorylated active forms of ERK: ERK1 and ERK2) and total ERK in untreated cells. Molecular weights (kDa) are shown on the left. The graphs show the quantitation of the western blots. Values represent mean ± SEM, n=6 for panel A and n=3 for panel B; one-way and two-way ANOVA, *P<0.05, **P<0.01, ***P<0.001.

AMPK is activated by nutrient deprivation, thereby activating ULK1-dependent autophagy and apoptosis (Dite et al., 2017). However, AMPK may also trigger autophagy through an indirect mechanism by phosphorylating raptor at several sites, including Ser792, which inhibits mTORC1 (see Figure 4-11). A large body of evidence suggests that AMPK downregulation might participate in neurodegenerative diseases such as AD, Parkinson's disease, Huntington's disease and ALS (Herrero-Martin et al., 2009; Liang et al., 2007).

Since AMPK plays a central role in a number of key cellular processes, AMPK activity was assessed in CHO-Tau35 cells by measuring the amount of phosphorylation at Thr172 relative to total AMPK. Figure 4-14 shows that there was a statistically significant reduction

in phosphorylated/total AMPK in CHO-Tau35 cells compared to both CHO-FL ($P<0.01$) and CHO cells ($P<0.05$). There was no change in the amount of phosphorylated/total AMPK between CHO-FL and CHO cells ($P>0.05$). Overall, these results indicate that there is a reduction in the basal activity of AMPK in CHO-Tau35 cells which may be a further reason behind the autophagic deficit observed in these cells.

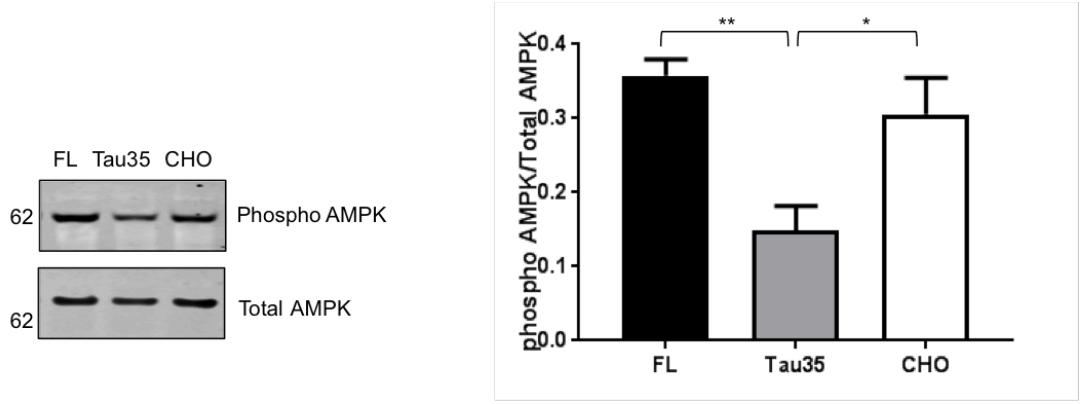

Figure 4-14 Reduced AMPK activity in CHO-Tau35 cells: Western blot of cell lysates prepared from CHO-FL, CHO-Tau35 and untransfected CHO cells probed with antibodies to phosphorylated (Thr172) and total AMPK. Molecular weights (kDa) are shown on the left. The graph shows the quantitation of the western blots. Values represent mean ± SEM, n=3; one-way ANOVA, *P<0.05, **P<0.01.

The activity of the ULK1 complex was investigated by measuring ULK1 phosphorylation on western blots of CHO-Tau35 cells. Data in Figure 4-15 A reveals a pronounced elevation in the total amount of ULK1 relative to GAPDH, in CHO-Tau35 cells compared to both CHO-FL ($P<0.01$) and CHO cells ($P<0.05$), while no difference was detected between CHO-FL and CHO cells ($p>0.05$). Figure 4-15 B (left graph) shows that there is no statistically significant difference in the amount of phosphorylated ULK1 at Ser555 between CHO-FL, CHO-Tau35 and CHO cells ($P>0.05$). Figure 4-15 B (right graph) shows that there is no significant difference in the amount of phosphorylated ULK1 at this site, relative to the amount of total ULK1 between CHO-Tau35 and CHO cells, or between CHO-FL and CHO cells. However, there was a significant increase in the amount of phosphorylated ULK1 at Ser555 in CHO-FL cells compared to CHO-Tau35 cells ($P<0.05$). Finally, Figure 4-15 C (left graph) shows similar results with phosphorylated ULK1 at Ser757, as there was no statistically

significant difference between CHO-FL, CHO-Tau35 and CHO cells (P>0.05). Moreover Figure 4-15 (right graph) shows that there is no statistically significant difference in the amount of phosphorylated ULK1 at Ser757 relative to total ULK1, between CHO-FL, CHO-Tau35 and CHO cells. Taken together, these data indicate that there are no differences in the activity of the ULK1 complex between CHO-Tau35 and CHO cells as there are no differences in phosphorylation levels, even though there is an increase of total ULK1 in CHO-Tau35 cells. However, there was a significant increase in phosphorylated ULK1 at Ser55 in CHO-FL compared to CHO-Tau35 cells which is elusive of increased ULK1 activation in CHO-FL cells.

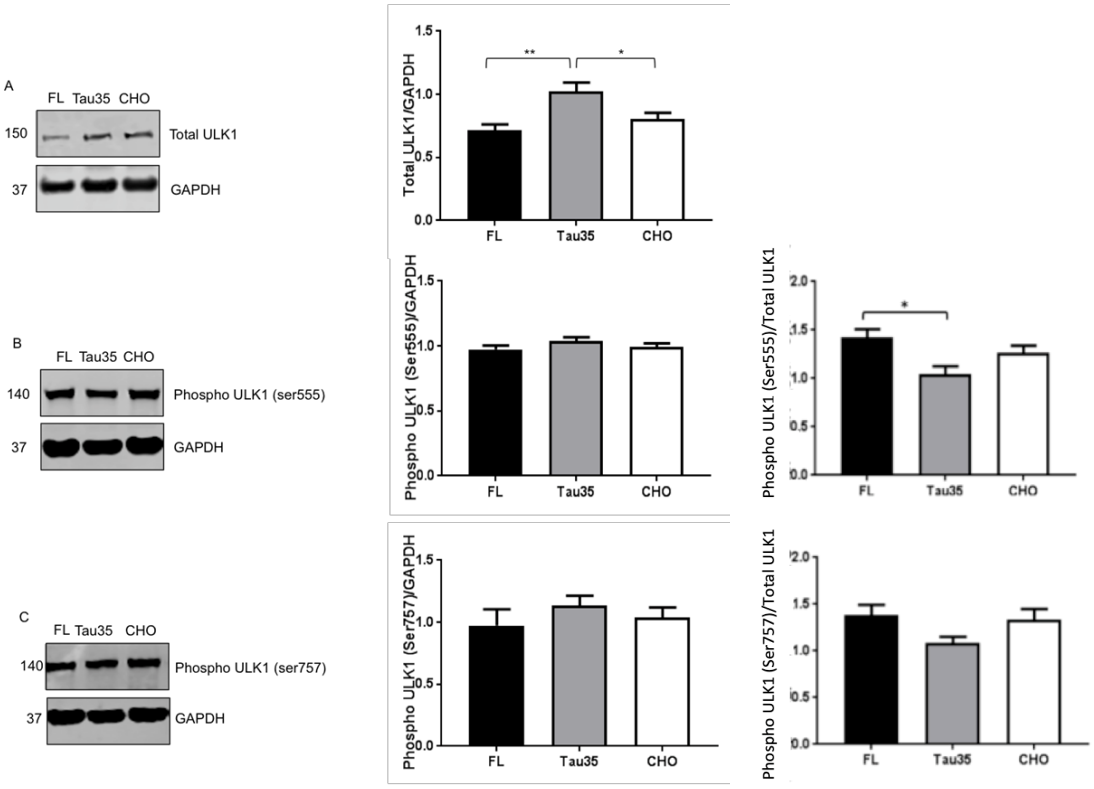

Figure 4-15 Changes in the activation of the ULK1 complex in CHO-Tau35 cells: Western blots of cell lysates of CHO-FL, CHO-Tau35 and untransfected CHO cells probed with antibodies **A** total ULK1 and GAPDH (loading control) **B** phospho ULK1 (Ser555) and GAPDH **C** phospho ULK1 (Ser757) and GAPDH. Molecular weights (kDa) are shown on the left. The graphs show the quantitation of the western blots. Values represent mean ± SEM, n=3; one-way ANOVA, *P<0.05, **P<0.01.

4.2.6 **Investigating Tau35 expression on the autophagy substrate p62**

The p62 protein is a common component of inclusion bodies found in protein aggregation diseases affecting the brain. Bjorkoy and colleagues (2005; 2006) found that p62 forms two types of bodies in the cytoplasm of cells. One is a type of inclusion bodies, known as sequestosomes, which are membrane-free p62-containing protein aggregates (Bjorkoy et al., 2005; Bjorkoy et al., 2006). The other p62 bodies are membrane-confined autophagosomal and lysosomal structures. Moreover, p62 is also found in nuclear bodies. The polyubiquitin-binding ability of the ubiquitin-associated domain is needed to form inclusion bodies. These ubiquitin-containing p62 bodies are degraded by autophagy (Bjorkoy et al., 2005).

The amount of p62 was assessed in CHO-FL, CHO-Tau35 and CHO cells using confocal immunofluorescence microscopy. The numbers of p62-positive puncta were counted in each cell type and normalised to the area of each cell (Figure 4-16 A, B). A significant increase was found in the number of p62 puncta in CHO-Tau35 cells compared to both CHO-FL and CHO cells ($P<0.001$), whereas there was no difference in the number of p62 puncta between CHO-FL and CHO cells. Since a previous study showed a substantial reduction in p62 in areas of e P301S tau transgenic mouse brain in which the number of neurons containing tau inclusions was significantly reduced (Schaeffer et al., 2012a), the colocalisation of p62 with tau was determined. Figure 4-16 C shows that although there was a substantial amount of colocalisation of p62 in CHO-FL and CHO-Tau35 cells, there was no significant difference between the two cell lines.

The pattern of p62 immunolabelling suggested a differential distribution of p62 puncta in the three CHO cell lines. Therefore, an analysis of p62 puncta distribution was performed by quantifying the number of p62-positive puncta at intervals of 3µm from the perimeter of the nucleus, as described for LC3, above (Figure 4-17). In untransfected CHO cells, p62 puncta are evenly distributed throughout the perinuclear and more distal regions of the cell. Conversely, there appears to be a significant increase of 42% (Table 4-2) in the clustering of the puncta towards the perinuclear region of the cell (0-3 µm from the nucleus) in CHO-FL cells compared to CHO cells. This increased perinuclear distribution of p62 puncta is also seen in the CHO-Tau35 cells, in which there is an increase of 59% in the

clustering of the puncta around the perinuclear region (0-3 μm) compared to CHO cells. The puncta distribution intensity further out in the cells (at 12, 15 and 18 μm distances) remained significantly higher in the CHO-Tau35 cells compared to the CHO-FL and CHO cells. Conversely, there were no significant differences between CHO-FL and CHO cells at these distances. Results summarising the percentage increase in puncta distribution are shown in Table 4-2. These findings indicate that expression of either FL-tau or Tau35 both increases the number of p62 puncta and alters their distribution in CHO cells.

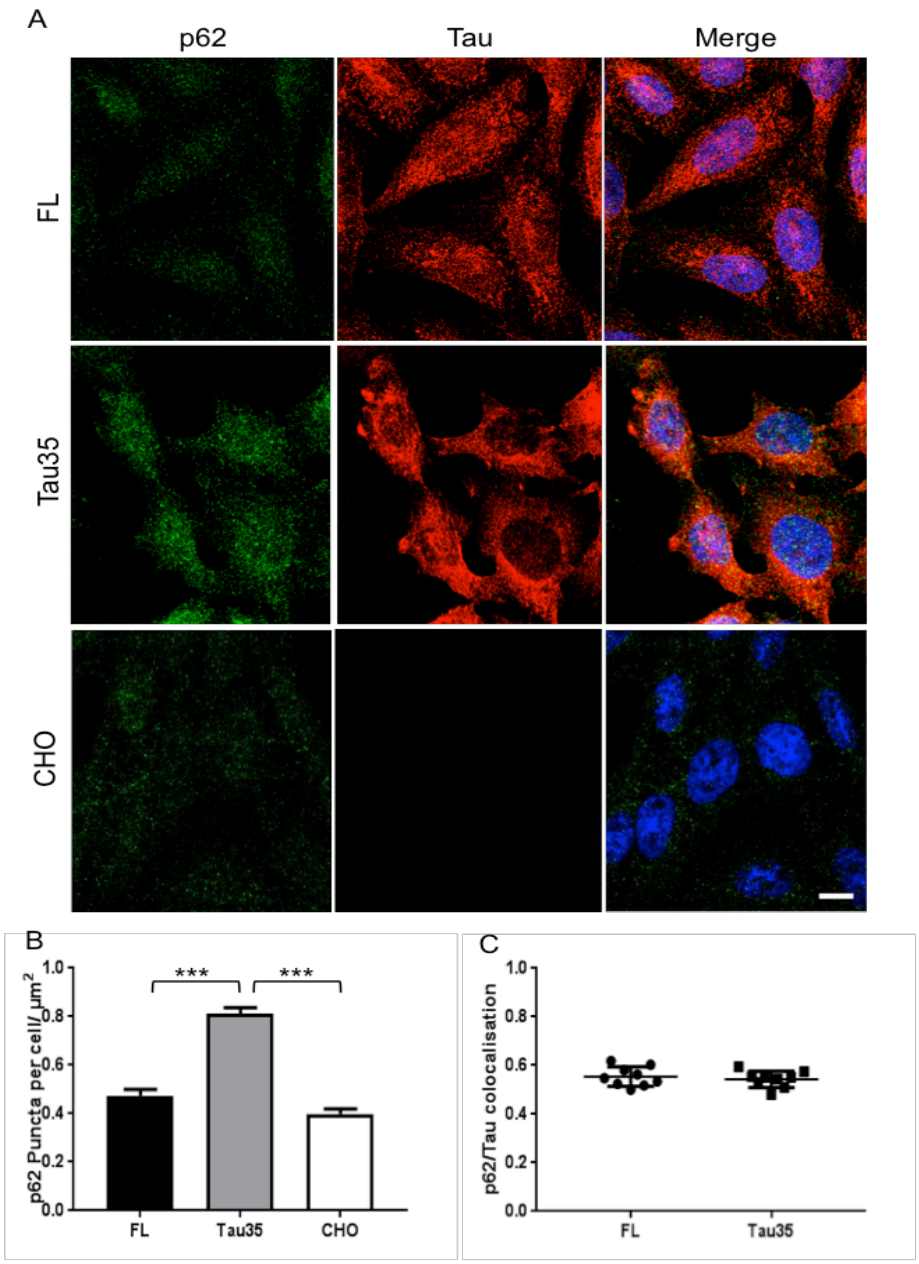

Figure 4-16 Increased p62 in CHO-Tau35 cells: A immunofluorescence of 4% PFA fixed CHO-FL, CHO-Tau35 and CHO cells co-stained with p62 antibody (green) and total tau antibody (red). Scale bar=10 µm. **B** Quantification of p62 puncta number normalised to cell area (μm^2). **C** Quantification of the colocalisation of p62 puncta with tau. For the quantification, a total of 30 cells were analysed per condition. Values represent mean ±SEM, n=3; one-way ANOVA or Student's t-test, **P<0.01, ***P<0.001.

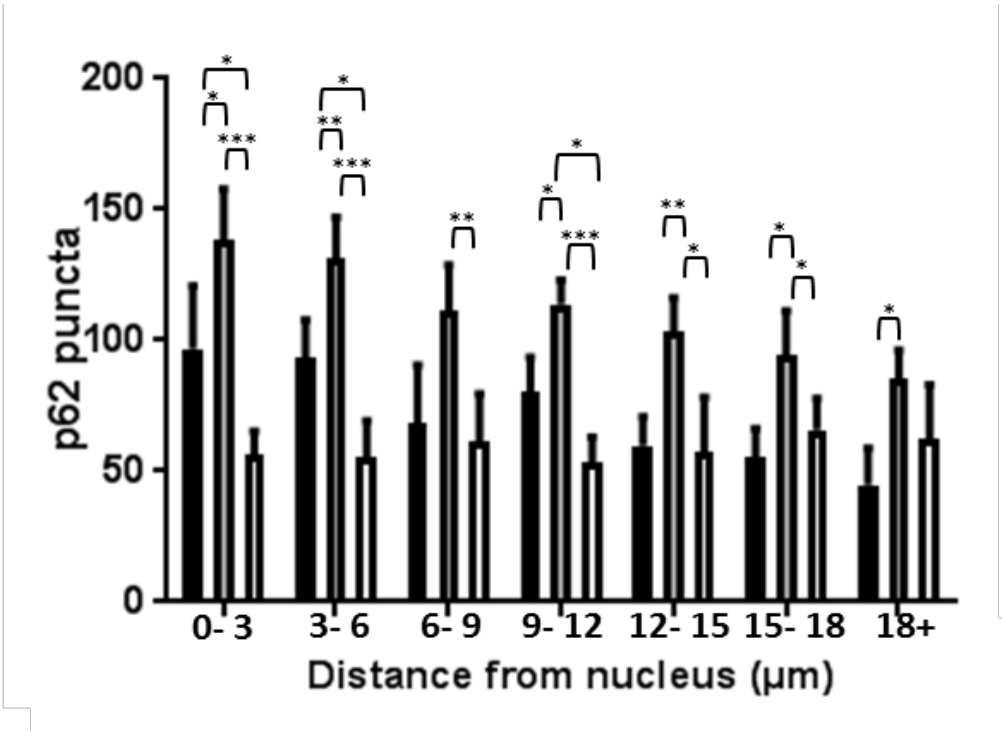

Figure 4-17 Trend of p62 puncta distribution: Data of distribution analysis carried on p62 immunofluorescence images. For each cell type, a total of 50 cells were counted. Values represent mean ± SEM, two-way ANOVA, *P<0.05, **P<0.01, ***P<0.001. Black bars: FL, grey bars: Tau35, white bars: CHO.

Table 4-2: Summary of the p62 puncta distribution in CHO-Tau35 and CHO-FL cells

Distance from nucleus (µm)	Percentage increase in puncta intensity between CHO-Tau35 and CHO cells	Percentage increase in puncta intensity between CHO-FL and CHO cells
0-3	59	42
3-6	58	41
6-9	45	10
9-12	53	34
12-15	44	4
15-18	30	-18
18+	27	-40

4.2.7 **The effect of autophagy activation on tau phosphorylation**

To investigate whether the elevation in phosphorylated tau in CHO-Tau35 cells may be due to the observed deficit in autophagy, CHO-FL and CHO-Tau35 cells were treated with rapamycin (1 μM for 6 h) and phosphorylated/total tau was assessed on western blots probed with PHF1 and total tau antibodies compared to untreated cells. There was a significant increase in PHF1 immunoreactivity in CHO-Tau35 compared to CHO-FL cells (Figure 4-18 A, $P<0.001$) and this was not affected by rapamycin treatment for 6 h. These results indicate that under these conditions, rapamycin does not affect the clearance of tau phosphorylated at the PHF1 epitope (Ser396/Ser404).

Since clearance of phosphorylated tau may be delayed following activation of autophagy, CHO-FL and CHO-Tau35 cells were exposed to 1 μM rapamycin for an extended period of 15 h and tau phosphorylation was assessed on western blots probed with PHF1, Tau-1, and total tau antibodies (Figure 4-18 B). After 15 h rapamycin treatment, there was a significant reduction in the amount of PHF1 tau in CHO-FL cells ($P<0.01$), indicating that phosphorylated FL-tau may be degraded by autophagy. However, the amount of tau phosphorylated at the PHF1 epitope was significantly increased in CHO-Tau35 cells following 15 h rapamycin treatment ($P<0.01$), indicating a failure to remove phosphorylated Tau35. The amount of Tau-1 (dephosphorylated tau) was also measured in CHO-FL and CHO-Tau35 cells with and without 1 μM rapamycin treatment for 15 h (Figure 4-18 B). The results reveal a significant decrease in the amount of Tau-1 in untreated CHO-Tau35 cells compared to CHO-FL cells ($p<0.01$), again indicating that tau phosphorylation is induced by Tau35 expression. Rapamycin treatment resulted in a significant increase in Tau-1 in CHO-FL cells compared to their untreated counterparts ($P<0.01$), demonstrating that, similar to PHF-1, phosphorylation of FL-tau at the Tau-1 epitope is reduced by the induction of autophagy. In contrast, in CHO-Tau35 cells, although there was a modest reduction in Tau-1 immunoreactivity, suggesting increased tau phosphorylation, this was not significantly different from untreated CHO-Tau35 cells. These results show the differential effects of rapamycin-induced autophagy activation on FL-tau and Tau35, and suggest that when expressed in CHO cells, Tau35 may be more resistant to both dephosphorylation and degradation.

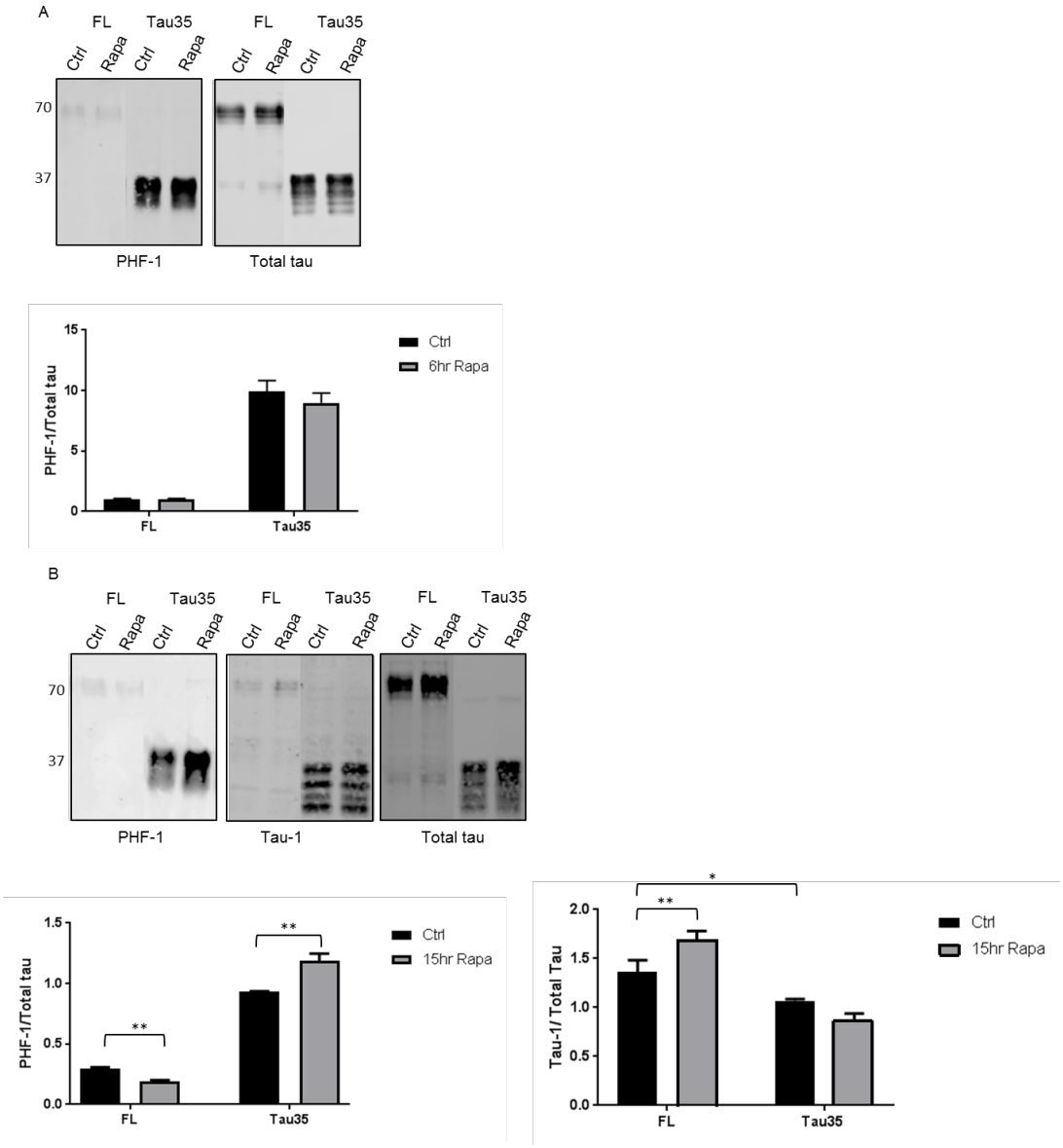

Figure 4-18 Changes in tau phosphorylation following autophagy activation by rapamycin: Western blots of cell lysates prepared from CHO-FL and CHO-Tau35 cells probed with antibodies **A** PHF-1 (Ser396/404) and total tau (loading control) in untreated and 1 µM rapamycin (Rapa) treated for 6 h. **B** PHF-1 (Ser396/404), Tau-1 (Ser195, 198, 199, and 202) and total tau in untreated and 1 µM rapamycin treated for 15 h. Molecular weights (kDa) are shown on the left of the blots. The graphs show the quantitation of the western blots. Values represent mean ± SEM, n=3; two-way ANOVA, *P<0.05, **P<0.01, ***P<0.001.

4.2.8 **Rescue of autophagy by inhibiting GSK3β**

GSK3 activity has been directly linked with impairments in the autophagy pathway and the development of tauopathies. For example, GSK3 inhibition reduces Aβ through the activation of the lysosomal/autophagy pathway, which increases the degradation of APP and its carboxy-terminal fragment (Parr et al., 2012b).

To investigate the effect of GSK3 inhibition on autophagy activation, CHO-FL, CHO-Tau35 and CHO cells were treated with the GSK3 inhibitor AR-A014418 (100 nM for 16 h). Western blots of treated and untreated cells were probed with antibodies against phosphorylated (Ser21/9, inactive) and total GSK3α/β (Figure 4-19 A). Under basal conditions, CHO-Tau35 cells showed a significant decrease in phosphorylated GSK3β compared to CHO-FL and CHO cells ($P<0.05$), indicating GSK3 activation, whereas there was no significant difference in phosphorylated/total GSK3β between CHO-FL and CHO cells. Following GSK3 inhibition with AR-A014418, there were significant increases in phosphorylated/total GSK3β in all of the three cell lines compared to their controls, indicating successful inhibition of GSK3β. In addition, there were no significant changes in phosphorylated GSK3β between CHO-FL, CHO-Tau35 and CHO cells following AR-A014418 treatment. These results demonstrate that, unlike the situation in CHO-FL cells, GSK3β is more active in CHO-Tau35 cells, implicating this kinase as a candidate for the increased tau phosphorylation observed following Tau35 expression. Additionally, this could explain the deficit in basal autophagy observed in CHO-Tau35 cells.

In parallel, western blots of untreated and AR-A014418-treated CHO-FL, CHO-Tau35 and CHO cells were probed with an antibody to LC3 to determine the effect of GSK3 on autophagy activation (Figure 4-19 B). Upon GSK3 inhibition, there were no significant changes in LC3-II between CHO-FL, CHO-Tau35 and CHO cells. Taken together, these results reveal that the inhibition of activated GSK3β rescues the initial deficit in autophagy seen in CHO-Tau35 cells. Notably, these results differ from the previous observations with HBSS and bafilomycin (Figure 4-8 and Figure 4-9, respectively), in which LC3-II remained significantly lower in CHO-Tau35 cells following activation of autophagy, indicating that those treatments were not able to rescue the basal autophagic deficits, while GSK3 inhibition may be able to rescue basal autophagic deficits.

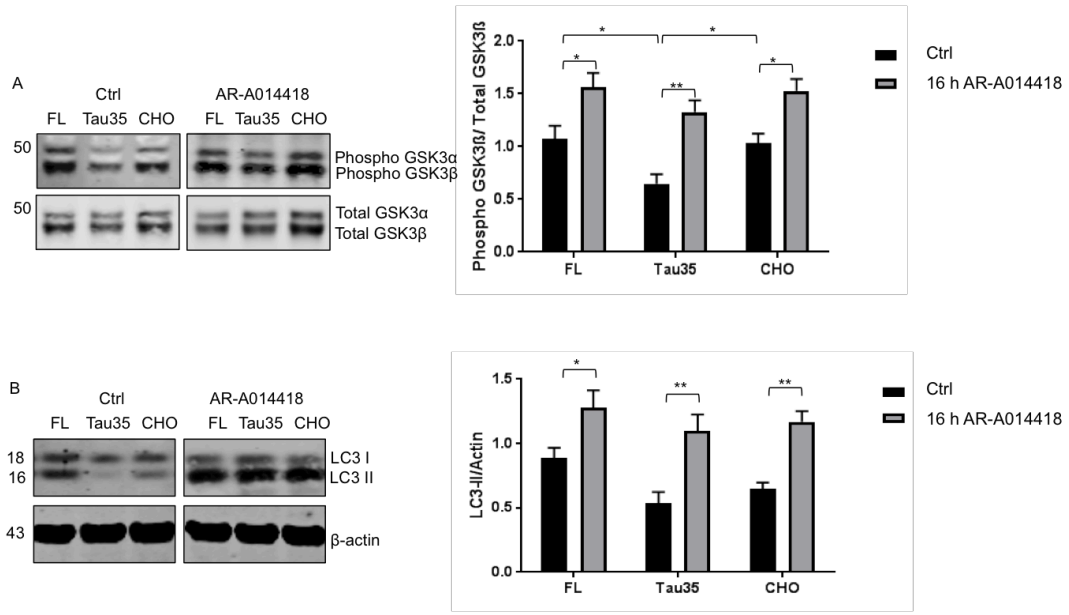

Figure 4-19 GSK3β inhibition rescues autophagy deficit in CHO-Tau35 cells: Western blots of cell lysates prepared from CHO-FL, CHO-Tau35 and untransfected CHO cells probed with antibodies **A** phosphorylated GSK3 (inactive GSK3α/β phosphorylated at Ser21/Ser9) and total GSK3 (loading control) in untreated and 100 nM AR-A014418 treated for 16 h. **B** LC3-I, LC3-II and β-actin (loading control) in untreated and 100 nM AR-A014418 treated for 16 h. Molecular weights (kDa) are shown on the left. The graphs show the quantitation of the western blots. Values represent mean ± SEM, n=6; two-way ANOVA, *P<0.05, **P<0.01.

4.3 Summary and discussion

The overall aims of this chapter were to determine the effect of Tau35 expression on (1) cell viability and (2) early autophagy activation, autophagosome formation and maturation. To address these aims, experiments were carried out on CHO cells stably expressing Tau35 or FL-tau to distinguish the effects of FL-tau expression from those of Tau35.

The main findings of this chapter include:

- No differences in cell viability between CHO-FL, CHO-Tau35, and CHO cells.
- Increased resistance to DTT in CHO-Tau35 cells compared to both CHO-FL and CHO cells.
- Increased resistance to extended thapsigargin exposure in both CHO-FL and CHO-Tau35 cells compared to CHO cells.
- A reduction in the early autophagy marker beclin-1 in CHO-Tau35 cells compared to CHO-FL and CHO cells. No changes in Atg proteins in the three CHO cell lines.
- Decreased LC3-II in CHO-Tau35 cells compared to CHO-FL and CHO cells under basal conditions, nutrient starvation and after induction of autophagic flux. Increased activity of mTORC1 in CHO-Tau35 cells.
- Increased LC3-II in CHO-Tau35 cells compared to CHO-FL and CHO cells following autophagy induction via an mTOR-independent route.
- Reduced ERK and AMPK activity in CHO-Tau35 cells compared to CHO-FL and CHO cells. No changes in phosphorylated ULK1, but an increased amount of total ULK1 in CHO-Tau35 cells compared to CHO-FL and CHO cells.
- Increased p62 in CHO-Tau35 cells compared to CHO-FL and CHO cells. No difference in p62/total tau colocalisation between CHO-FL and CHO-Tau35 cells.
- Autophagy activation enhanced removal of phosphorylated tau in CHO-FL cells but not in CHO-Tau35 cells.
- Inhibition of GSK3α/β rescues the autophagy deficit in CHO-Tau35 cells.

4.3.1 **The effect of Tau35 expression on cell viability**

Neurodegeneration in the tauopathies is characterised by the accumulation of highly phosphorylated tau as) NFTs, and other tau-positive lesions, that are a key neuropathological hallmark of AD and related tauopathies (Nelson et al., 2012). Although the mechanisms that underlie neurodegeneration remain elusive, the ultimate outcome is neuronal loss. In AD for example, the build-up of toxic stimuli, such as β-amyloid, causes cell death through the up-regulation of apoptotic markers (Friedlander, 2003). However, multiple studies report that apoptosis accounts for only a small proportion of neurons lost in AD and other tauopathies. A study using HEK293 cells demonstrated that cells overexpressing tau exhibit marked resistance to apoptosis induced by various apoptotic stimuli, and correlated with an increase in tau phosphorylation and elevated GSK3 activation (Li et al., 2007). Furthermore, in the same study, neuroblastoma cells harbouring highly phosphorylated tau showed an inverse staining pattern of PHF-1 to activated caspase-3, which is involved in the execution phase of apoptosis (Li et al., 2007). These findings may explain at least in part why CHO-Tau35 cells are able to bypass cell death, as these cells exhibit increasing amounts of phosphorylated tau as well as increased GSK3 activity.

In order to further validate this finding, CHO-FL, CHO-Tau35 and CHO cells were treated with DTT and thapsigargin to induce the UPR and cell viability was assessed. After DTT treatment, there was a marked increase in cell viability and/or sensitivity to DTT in CHO-Tau35 compared to CHO-FL and CHO cells. Due to the enhanced activation of the UPR in these cells, the increase in cell viability under these conditions is justified, as prolonged activation of PERK and increased CHOP can lead to the activation of potentially protective factors such as sXBP1, thereby promoting cell survival (Ron and Walter, 2007). On the other hand, cells behaved differently in response to thapsigargin treatment, where 6 hours of treatment at a concentration of 1 μM (which was sufficient to activate the UPR) led to no differences in cell viability between the three cell lines. However prolonged exposure to the drug led to a significant reduction in cell death in CHO-FL and CHO-Tau35 cells compared to CHO cells. The changes in response to both treatments can be explained by the differences in the mechanism of action between DTT and thapsigargin. While DTT disrupts protein disulfide bonding, thapsigargin inhibits the ER Ca2-dependent ATPase.

This may therefore imply that upon treatment with DTT, CHO-Tau35 cells are increasingly sensitive to DTT compared to CHO-FL and CHO cells. Conversely, prolonged treatment with thapsigargin renders CHO-Tau35 and CHO-FL more sensitive in comparison to CHO cells.

4.3.2 **Regulation of early autophagy and autophagosome formation/maturation**

The overt reduction in beclin-1 in CHO-Tau35 cells compared to CHO-FL and CHO cells is indicative of early autophagic dysfunction in these cells. These findings are corroborated by work carried out by Pickford et al. (2008), who showed that heterozygous deletion of the beclin-1 gene in mice decreased neuronal autophagy and caused a disruption in lysosomes, which led to a severe neurodegeneration phenotype. Furthermore, levels of beclin-1 were reportedly decreased in affected brain regions of patients with AD (Pickford et al., 2008b).

Beclin-1 complexes with class III PI-3 kinases, notably Vps34 during autophagy. Additional regulatory proteins couple with Vps34 and beclin-1 to either promote autophagy, such as UVRAG, BIF-1, Atg14L and Ambra (Liang et al., 2008; Young et al., 2009), or to inhibit autophagy, such as Bcl-2 (Zhong et al., 2009). The interaction of beclin-1 with Bcl-2 disrupts the interaction of beclin-1 with Vps34 (Patingre et al, 2005]. Thus, beclin-1 activity in autophagy is inhibited by interaction with Bcl-2 (and Bcl-XL) at the ER (Maiuri et al., 2007). This interaction is disrupted by JNK1-mediated phosphorylation of Bcl-2 in response to starvation-induced signaling (Maiuri et al., 2007). Therefore, due to reduced beclin-1 in CHO-Tau35 cells, it is possible that less beclin-1 is able to interact with proteins such as Vps34, thereby hindering activation of autophagy (chapter 1, Figure 1-7). Concurrently, reduced beclin-1 could also result in a decreased interaction with Bcl-2, which could further explain why differences in cell viability were not observed upon Tau35 expression. However, more experimental work is required to understand if these are viable hypotheses.

No changes in the amounts of Atg5, Atg7 and Atg13 were found in CHO-FL, CHO-Tau35 and CHO cells. These three proteins have vital functions in the autophagy initiation process as outlined earlier in Chapter 1 (p55). However, Atg5-Atg12 conjugation is not always dependent on autophagy activation because, once the autophagosome is formed, these proteins together with Atg16L rapidly dissociate from the autophagosomal membrane and

their low abundance makes them difficult to detect, rendering them poor markers of autophagy (Barth et al., 2010). Atg7 facilitates the activation of Atg12 prior to its conjugation with Atg5. However, the lack of changes seen in Atg7 can be disregarded in this scenario by the fact that there are overt reductions in the basal levels of LC3 (which occurs downstream of Atg7 activation) in CHO-Tau35 cells.

The decreased amount of LC3 observed is a robust marker of reduced autophagosome formation in CHO-Tau35 cells. This result is in contrast to the increase in LC3 detected in CHO-FL cells, indicating increased autophagosome formation in cells harbouring FL-tau. In other studies in this laboratory, CHO-Tau35 cells have been shown to have a reduced microtubule binding ability and a compromised cytoskeleton compared to CHO-FL cells (Guo et al., 2019). Since maximal autophagosome formation and efficient autophagosome motility require an intact microtubule network, it is plausible that these findings are inter-related (Kochl et al., 2006). For instance, upon amino acid starvation, disassembling microtubules with high doses of nocodazole prevents autophagosome formation (Geeraert et al., 2010). This could explain why CHO-Tau35 cells are less sensitive to HBSS-mediated starvation compared to CHO-FL and CHO cells; due to the disruption in their microtubule network as well as reductions in acetylated tubulin. The prominent cytoskeletal changes previously detected in CHO-Tau35 cells could also explain the significant reduction in cell size that is also observed herein. Furthermore, the stimulation of autophagic flux with bafilomycin illustrated the marked reduction in LC3-II in CHO-Tau35 cells compared to CHO-FL and CHO cells. Overall, these findings indicate that CHO-Tau35 cells have a reduced capacity to produce autophagosomes and support the view that Tau35 expression induces a deficit in autophagy.

The profound increases seen in markers of mTORC1 activity in CHO-Tau35 cells could contribute to the deficits observed in beclin-1 and LC3-II, as the mTORC1 complex acts as an inhibitor of autophagy. Enhanced mTORC1 activity could also account for the increase in phosphorylated tau noted in CHO-Tau35 cells, which is corroborated by previous findings showing that mTOR is able to regulate tau phosphorylation and degradation in 3xTg-AD mice. This effect is ameliorated by rapamycin, which also attenuates age-dependent cognitive decline in wild-type mice (Caccamo et al., 2010a). Treating P301S tau

transgenic mice with rapamycin also reduces tau phosphorylation at the AT180 and AT270 epitopes, as well as the associated behavioural deficits (Caccamo et al., 2013a). The fact that CHO-Tau35 cells exhibit significantly reduced LC3-II following rapamycin treatment indicates that these cells are less responsive to autophagy activation. Consequently, this reduced sensitivity could explain why tau phosphorylation at the PHF-1 and Tau-1 epitopes is not reduced by extended rapamycin treatment, which contrasts with the effects of autophagy activation in CHO-FL cells.

In addition to raptor being a component of the mTORC1 complex, it is also a substrate of AMPK. Phosphorylation of raptor by AMPK is required for suppression of mTORC1 activity induced by energetic stress (Howell et al., 2017). Moreover, raptor phosphorylation is necessary for the full engagement of an AMPK-mediated metabolic checkpoint (Gwinn et al., 2008). Therefore, the marked decrease in AMPK phosphorylation in CHO-Tau35 cells directly correlates with the observed reduction in raptor phosphorylation. AMPK additionally activates ULK1 by a coordinated cascade (Kim et al., 2011). In this chapter, the amounts of total ULK1 and ULK1 phosphorylated at Ser555 and Ser757 were measured in CHO-FL, CHO-Tau35 and CHO cells. No changes were detected at either of these two phosphorylation sites between CHO-Tau35 and CHO cells, however there was a modest increase in the amount of phosphorylated ULK1 at ser555 relative to total ULK1 in CHO-FL cells compared to CHO-Tau35 cells which indicates increased ULK1 activation in CHO-FL cells which may further contribute to the increased amounts of LC3 in these cells. Moreover, a substantial increase in the amount of total ULK1 in CHO-Tau35 cells compared to CHO-FL and CHO cells. Multiple other phosphorylation sites of the ULK1 complex are regulated by either mTORC1 or AMPK. For example, AMPK phosphorylates ULK1 at Ser317 and Ser777. Therefore, the total increase in ULK1 in CHO-Tau35 cells could be due to changes in phosphorylation at these sites or other sites. However, further work screening numerous phosphorylation sites is required to identify changes in the complex that result in early autophagy impairments.

The reduction in active ERK1/2 in CHO-Tau35 cells could also help to explain the decreased basal levels of LC3-II in these cells, because activation of ERK is reported to be a necessary step in the mTOR-independent route of autophagy activation (Wei et al., 2015). Notably

this reduction in active ERK1/2 rules out the likelihood of ERK1/2 activity being responsible for increased tau phosphorylation in CHO-Tau35 cells Phosphorylation (activation) of ERK1/2 plays an important role in the degradation of autophagy cargo, including p62 and mutant huntingtin protein aggregates (Wei et al., 2015). Therefore, the reduced ERK1/2 activity could potentially contribute to the build-up of both phosphorylated tau and p62 in CHO-Tau35 cells. However, trehalose treatment of Neuro 2a and HeLa cells showed no effect on the expression or phosphorylation of ERK1/2 (Wei et al, 2015). Trehalose treatment led to a significant increase in the amount of LC3-II in CHO-Tau35 cells compared to CHO-FL and CHO cells, indicating enhanced sensitivity of CHO-Tau35 cells to trehalose. These findings are consistent with a study showing that trehalose administration reduces disease burden in the P301S mouse model of tauopathy (Schaeffer et al., 2012). Additionally, trehalose was able to both stimulate autophagy, as assessed by increased LC3-II formation, and reduce sarkosyl-insoluble, disease-associated tau in the brains of P301S tau transgenic mice (Schaeffer et al., 2012a).

In addition to interacting with ERK, p62 also impinges on mTORC1 activity by interacting directly with raptor, thereby facilitating mTORC1 activation in response to the stimulation of pathway activation by amino acids (Sarkar, 2013). In NIH 3T3 cells lacking p62, autophagy is upregulated, which is similar to the upregulation of autophagy that accompanies decreased mTORC1 activity (Duran et al., 2011). Therefore, the increase in the number of p62 puncta observed in CHO-Tau35 cells further supports the view that Tau35 expression results in decreased basal autophagy and increased mTORC1 activity in this cell line.

In HeLa cells, p62 puncta were mainly found in the cytoplasm, with much less staining in the nuclei. Moreover, it was noted that nuclear p62 had a more speckled appearance and a minority of cells (~0.5%) displayed nuclear accumulation of p62 (Bjorkoy et al., 2005). This pattern of p62 staining has been observed in several other cell lines, including HEK293, MDCK II, HT1080, TERT fibroblasts, and NIH3T3 fibroblasts (Bjorkoy et al., 2005). These observations might explain the differences in the distribution of p62 puncta intensity in CHO-FL, CHO-Tau35 and CHO cells, as the more prominent perinuclear p62 staining in the CHO-Tau35 cells compared to CHO-FL and CHO cells could indicate an

abnormality in p62 degradation in these cells. Furthermore, since p62 is degraded by autophagy, the perinuclear puncta in CHO-Tau35 cells may not be able to be degraded efficiently because autophagosomes may accumulate in the cytosol. In contrast, the distribution pattern of LC3 puncta exhibited a similar pattern in CHO-FL, CHO-Tau35 and CHO cells indicating that Tau35 did not induce any overt abnormality in the distribution of autophagosomes.

Since increased colocalisation of p62 with tau inclusions has been shown in P301S tau transgenic mice (Schaeffer et al., 2012a), the colocalisation of p62 and tau was examined in the CHO cell lines. There was no change in the colocalisation of p62 and tau in CHO-Tau35 cells when compared to CHO-FL cells. However, the study in P301S tau mice showed similar amounts of p62 in transgenic mice and wild-type controls, indicating that p62 synthesis and basal autophagy were not affected by P301S tau expression in the transgenic mice. In contrast, the CHO cell models reported here exhibited significant differences in the amount of p62, suggesting that the increased p62 in CHO-Tau35 cells could potentially impact on its colocalisation with tau.

Inhibition of GSK3 activity reduces tau phosphorylation, enhances binding of tau to microtubules, and promotes microtubule assembly (Hanger et al., 2009a). In a study using Tg601 mice (transgenic mice expressing wild-type human tau), the GSK3 inhibitor AR-A014418 decreased p62 levels (Kambe *et al,* 2011). AR-A014418 also reduced the activity of GSK3β in CHO-Tau35 cells to a similar level as that observed in CHO-FL and CHO cells. Notably, GSK3 inhibition rescued the basal deficit in LC3-II that was observed in the CHO-Tau35 cells, which differed from the results obtained following HBSS and bafilomycin treatments.

Taken together, these results demonstrate that CHO-Tau35 cells exhibit a significant deficit in early autophagy as well as in markers of autophagosomes, that could not be rescued by amino acid starvation. It seems likely that these Tau35-induced changes may be mediated through increased activity of mTORC1 (possibly in combination with reduced activity of ERK and AMPK), activation of GSK3, and increased p62. Activation of autophagy with either trehalose or AR-A014418 rescued the basal reduction in LC3-II in CHO-Tau35 cells,

whereas rapamycin failed to do so. Overall, these findings indicate that CHO-Tau35 cells are more responsive to autophagy induction that does not directly target mTORC1 and that this new mechanistic insight may be important in the design of new therapeutics for the tauopathies.

Chapter 5 The effect of Tau35 expression on lysosomal biogenesis and functionality

5.1 Introduction

Autophagy is essential for neuronal survival and, in most disease states, is considered to be neuroprotective as it may be induced to alleviate cellular stress, such as nutrient deprivation and protein aggregation (Nixon and Yang, 2012). Initial studies suggested that the rate of autophagy in neurons is low (Nixon and Yang, 2012). However, more recent studies have indicated that neuronal autophagy is constitutively active and efficient in clearing autophagosomal cargoes (Boland et al., 2008a). In neurons, autophagic clearance depends on optimally functioning lysosomal proteolysis to maintain the retrograde delivery of autophagosomes to lysosomes in the cell body (Lee et al., 2010b).

The increase in mTORC1 activation, and the deficits in early autophagy and autophagosome formation seen in CHO-Tau35 cells suggested the possibility of differences in late stages of autophagy involving the lysosome. Degradation of previously sequestered cargo (Chapter 4) only occurs once autophagosomes fuse with either endosomes or lysosomes (Wong and Cuervo, 2010). Lysosomal dysfunction triggers the development of characteristic features of the aged human brain including the accumulation of Aβ and NFTs. Moreover, a recent study in BE(2)-M17D neuroblastoma cells inducibly expressing human tau, showed that the autophagic-lysosomal, as well as endosomal systems play a role in tau clearance, whereas dysfunction of these systems results in the formation of insoluble tau aggregates in lysosomes (Hamano et al., 2008b).

The production of lysosomes is closely regulated by TFEB through coordinated expression of autophagy and lysosomal target genes including lysosomal hydrolases, lysosome membrane proteins, and components of the V-ATPase complex that participate in lysosomal acidification (Settembre et al., 2011). Thus, TFEB positively regulates genes that are key to cellular degradative pathways. TFEB has been identified as a major player in coordinating autophagy through positively regulating autophagosome formation and autophagosome–lysosome fusion (Settembre et al., 2011). In addition, TFEB enhances protein clearance through lysosomal exocytosis, mediated by the lysosomal Ca^{2+} channel

MCOLN1 (Medina et al., 2011). Multiple mouse models of AD have demonstrated the beneficial effects mediated by TFEB, in relation to both Aβ and tau pathology (Parr et al., 2012b; Xiao et al., 2014b; Xiao et al., 2015b). With respect to tau, enhancing the activity of the autophagy lysosomal pathway through exogenous TFEB expression in the brain, dramatically reduces tau pathology, neurodegeneration, and behavioural deficits in the rTg4510 mouse model of tauopathy (Polito et al., 2014). The proposed mechanism of action was through a TFEB–PTEN–Akt–mTOR–TFEB regulatory feedback loop, in which TFEB induces the autophagy lysosomal pathway through upregulation of PTEN and inhibition of Akt and mTOR, which further activates TFEB (Polito et al., 2014).

Starvation activates autophagy and once this occurs, cellular lipids stored as triglycerides in lipid droplets are hydrolysed into fatty acids for energy (Lee et al., 2010b). Degradation of lipids and previously sequestered cargo, such as proteins and organelles is undertaken by lysosomes. The enzymatic degradation that occurs in lysosomes is highly dependent on them maintaining an acidic pH. Impaired lysosomal activity has been noted in hereditary lysosomal storage disorders, and recent studies have demonstrated a link between lysosomal dysfunction and neurodegenerative diseases such as AD and PD. (Boya, 2012). Abnormally elevated lysosomal pH and disruption of lysosomal proteolysis are major contributors to autophagy failure and its pathological consequences in AD (Nixon, 2013).

The main class of lysosomal proteases are the cathepsins, which are essential for lysosomes to perform their degradative function effectively (Guo et al., 2017). Several different cathepsins exist (Chapter 1) and cathepsin D in particular, is associated with the development of neurodegeneration, including processing of APP, tau and apolipoprotein E (Fernandez-Montoya and Perez, 2015; Khurana et al., 2010). Studies in transgenic mice expressing human tau with three FTDP-17 missense mutations (TauVLW mice), showed increased cathepsin D and partial colocalization of cathepsin D with human mutant tau in the hippocampi of these mice (region where human mutant tau accumulates). Other work showed that cathepsin D is upregulated with age in a *Drosophila* model of AD and related tauopathies (expressing the human tau mutant R406W). Genetic analysis in this study showed that cathepsin D plays a neuroprotective role because genetic ablation of cathepsin D markedly potentiates tau-induced neurotoxicity, as well as in the nervous

tissue of transgenic *Drosophila* (Fernandez-Montoya and Perez, 2015; Khurana et al., 2010).

This chapter describes the influence of Tau35 expression on the biogenesis and function of lysosomes.

5.2 Results

5.2.1 Effect of Tau35 expression on lysosome biogenesis

To begin to understand the effect of Tau35 expression on lysosome biogenesis, CHO-FL, CHO-Tau35 and CHO cells were labelled with an antibody recognising LAMP2 (a lysosomal membrane marker) to determine the lysosome load.

There was a pronounced reduction in the number of LAMP2 puncta (lysosomes) per cell, standardised to cell area (μm^2) in CHO-Tau35 cells compared to both CHO-FL and CHO cells (Figure 5-1 A and B, $P<0.01$ and $P<0.05$, respectively). There was no significant difference in the number of LAMP2 puncta between CHO-FL and CHO cells. Qualitative observations show an evident difference in the distribution of LAMP2 puncta between CHO-Tau35 cells, and CHO-FL and CHO cells. In CHO-FL and CHO cells, puncta appear to be evenly distributed across the cytoplasm, while in CHO-Tau35 cells, puncta are more apparent in the perinuclear region (Figure 5-1 A). The area of individual LAMP2 puncta was then quantified in each cell type (Figure 5-1 C). There were no significant differences between the size of the LAMP2 puncta in CHO-FL and CHO cells ($P>0.05$), or between CHO-Tau35 and CHO cells, although in the latter case, the mean size appeared to be modestly reduced ($P=0.065$). There was a significant increase of 42% in the area of individual LAMP2 puncta in CHO-FL cells compared to CHO-Tau35 ($P<0.001$). The circularity of the individual LAMP2 puncta (corresponding to lysosomes) was measured and no significant differences were found between CH-FL, CHO-Tau35 and CHO cells ($P>0.05$) Figure 5-1 D), indicating that the morphology of lysosomes is not affected by expression of either Tau35 or FL-Tau. These results show that expression of Tau35 leads to a reduction in the number of lysosomes and that FL-tau increases the area of individual lysosomes. These findings suggest that these two forms of tau have differing effects on lysosomal degradation in CHO cells and that Tau35 might impair the biogenesis of lysosomes.

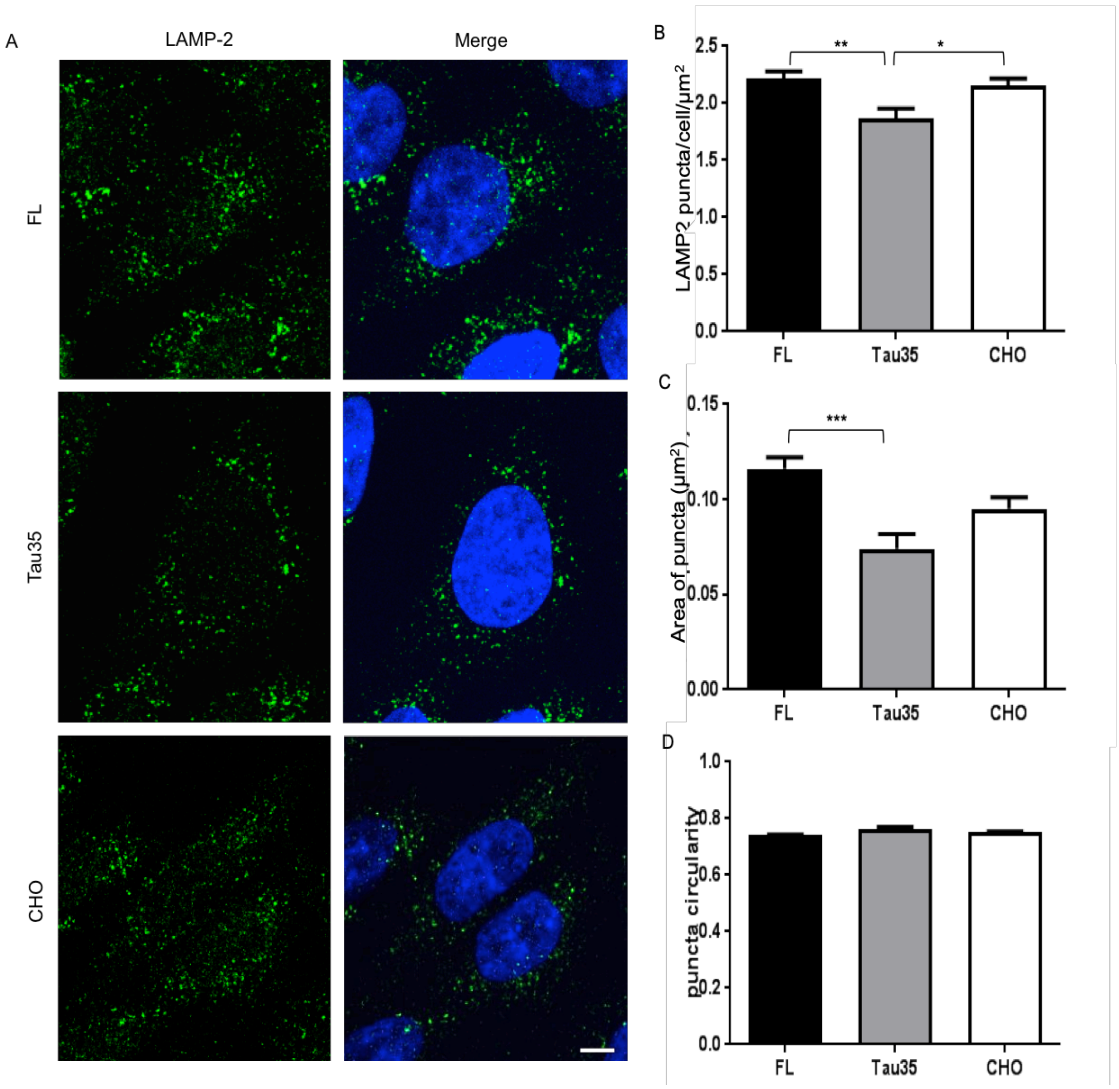

Figure 5-1 Reduction in the number of lysosomes and the area occupied by individual lysosomes in CHO-Tau35 cells: A Immunofluorescence of PFA-fixed CHO-FL, CHO-Tau35 and CHO cells labelled with LAMP2 antibody (green) and Hoescht 33342 (blue), scale bar=10 µm. **B** Quantification of the number of LAMP2 puncta/cell/µm^2. **C** Quantification of puncta area (µm^2). **D** Quantification of puncta circularity (scale of 0-1 where 1 indicates a full circle). For the quantification, a total of 30 cells were analysed per condition. Values represent mean ± SEM, n=3 for each cell line; one-way ANOVA, *P<0.05, **P<0.01, ***P<0.001.

Due to the modest reduction in the number of LAMP2 puncta in CHO-Tau35 cells, the nuclear/cytoplasmic localisation of TFEB, which regulates lysosomal biogenesis was examined by immunofluorescence in the three cell lines. There was a statistically significant decrease of 26% in the nuclear localisation of TFEB in CHO-Tau35 cells compared to that in CHO cells (Figure 5-2 A and B, $P<0.01$). Furthermore, compared to CHO-FL cells, the CHO-Tau35 cells exhibited an 18%reduction in nuclear TFEB ($P<0.05$). There was no statistically significant difference in the number of CHO-FL and CHO cells harbouring nuclear TFEB ($P>0.05$). Taken together, these results indicate a substantial reduction in nuclear TFEB in CHO-Tau35 cells and hence the likelihood of an elevated amount of TFEB retained in the cytoplasm due to Tau35 expression compared to that in CHO-FL and CHO cells. This finding could contribute to the previously observed increase in mTORC1 activity (Chapter 4) as well as the reduced number of lysosomes (Figure 5-1) caused by Tau35 expression.

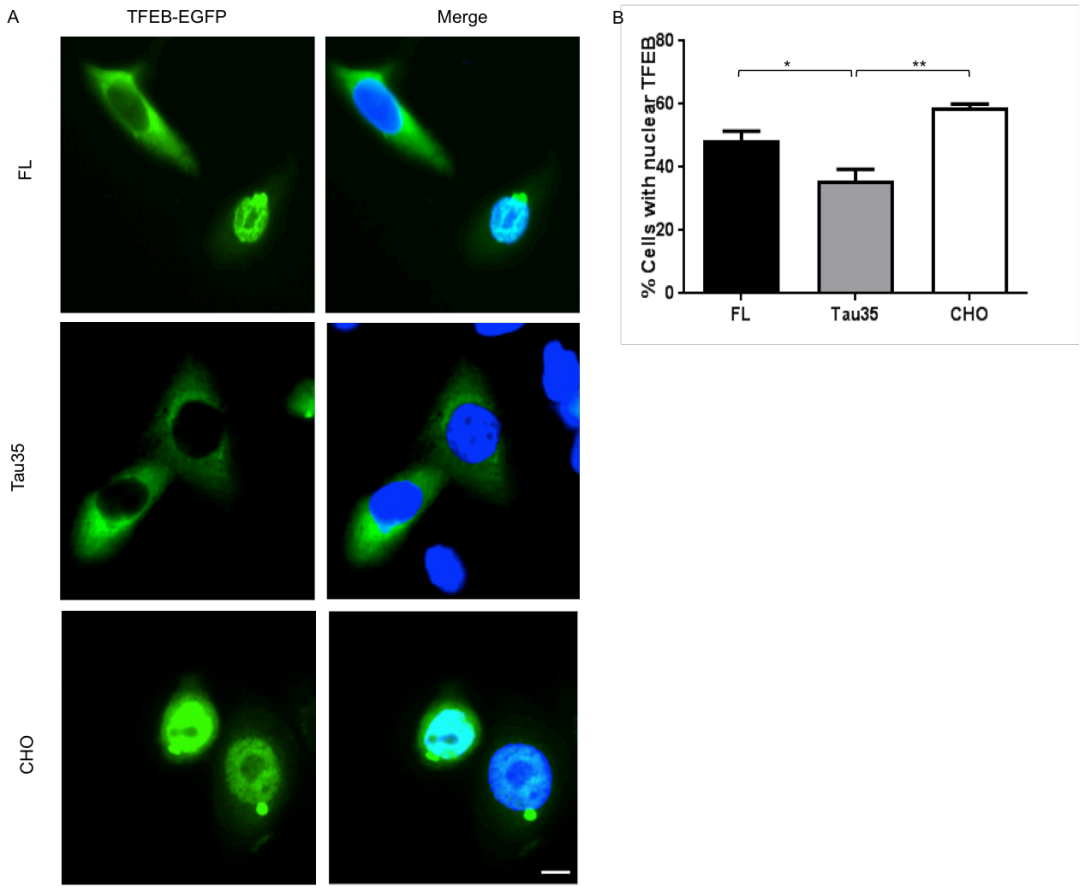

Figure 5-2 Reduced nuclear translocation of TFEB in CHO-Tau35 cells: A immunofluorescence of PFA-fixed CHO-FL, CHO-Tau35 and CHO cells expressing EGFP-TFEB (green) and labelled with Hoescht 33342 (blue), scale bar=10 µm. **B** Quantification of the percentage of cells with nuclear TFEB. For the quantification, a total of 30 cells were analysed per condition. Values represent mean ± SEM, n=3; one-way ANOVA, *P<0.05, **P<0.01.

Next, the amount of importin α7 was measured in different cell fractions of CHO-FL, CHO-Tau35 and CHO cells to determine its subcellular localisation. There was no significant difference in the amounts of importin α7 relative to GAPDH, in the total cell lysates of CHO-FL, CHO-Tau35 and CHO cells (Figure 5-3 A, $P>0.05$). Similarly, there were no significant changes in importin α7 relative to GAPDH, in the cytoplasmic fractions of the three cell types (Figure 5-3 B, $P>0.05$). In contrast, there were marked decreases of 66% and 63%, respectively in the amount of importin α7 relative to histone H3, in the nuclear fraction of CHO-Tau35 cells compared to both CHO-FL and CHO cells (Figure 5-3 C, $P<0.05$). Notably, expression of FL-tau did not affect the amount of nuclear importin α7 compared to CHO cells (Figure 5-3 C, $P>0.05$).

Taken together, these results illustrate that Tau35 selectively reduces the amount of importin α7 in the nucleus when expressed in CHO cells, which could explain the deficit in nuclear translocation of TFEB caused by Tau35 expression.

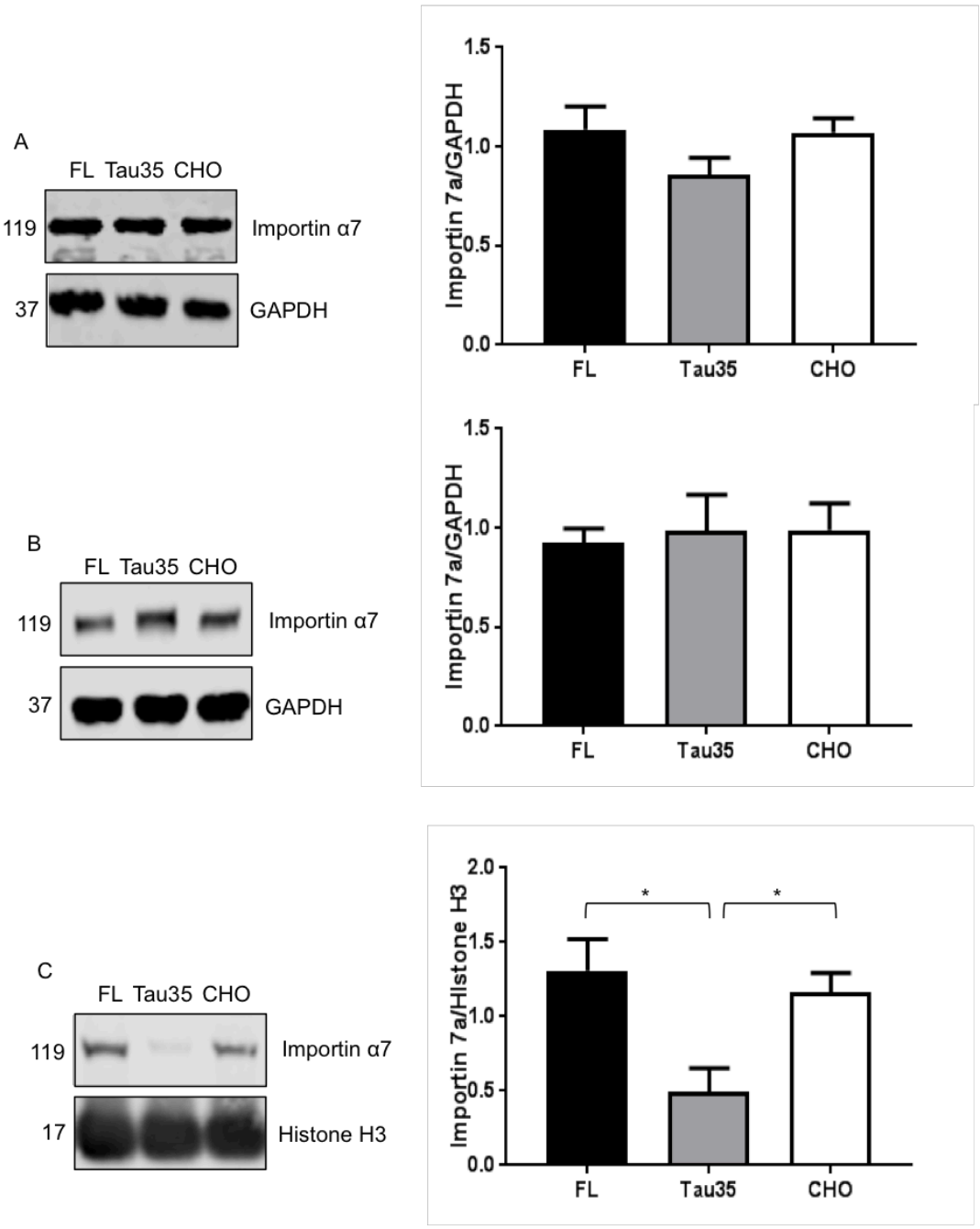

Figure 5-3 Reduced importin in the nuclear fraction of CHO-Tau35 cells: Western blots of CHO-FL, CHO-Tau35 and untransfected CHO cells. **A** Total cell lysates, **B** Cytosol, **C** Nuclei, probed with antibodies to importin α7, and glyceraldehyde 3-phosphate dehydrogenase (GAPDH) or histone H3. Molecular weights (kDa) are shown on the left of the blots. The graphs show the quantitation of importin α7, relative to GAPDH or histone H3. Values represent mean ± SEM, n=3. One-way ANOVA. *P<0.05.

5.2.2 **The effect of Tau35 expression on lysosome functionality**

The maintenance of a highly acidic (pH 4–5) environment, generated mainly by v-ATPase, is essential for normal functioning of lysosomes. Altered v-ATPase activity and lysosomal pH dysregulation have been implicated in cellular aging, longevity, and adult-onset neurodegenerative diseases, including PD and AD (Colacurcio and Nixon, 2016). Therefore, the acidity of lysosomes was measured in CHO-FL, CHO-Tau35 and CHO cells. LysoTracker probes are used to label acidic organelles in the cells, including lysosomes, late-stage endosomes and peroxisomes as they are highly selective for acidic organelles and are freely membrane permeant at a neutral pH (Chazotte, 2011).

Qualitative observations from the raw data images of LysoTracker labelling in Figure 5-4 illustrate that the distribution of LysoTracker puncta in CHO-FL and CHO cells is predominantly perinuclear. In contrast, the LysoTracker-labelled puncta in CHO-Tau35 cells were less intense and appeared to be slightly more prominent at opposite poles of the CHO cells. Notably, the LysoTracker labelled puncta in CHO-FL cells appeared to be larger than those in CHO and CHO-Tau35 cells. These observations were confirmed in the quantitative analysis in which LysoTracker labelling revealed a 49% increase in the number of acidic structures in CHO-FL cells, compared to CHO-Tau35 and CHO cells (Figure 5-4, Figure 5-5, $P<0.01$). Although the number of Lysotracker-positive (acidic) puncta in CHO-Tau35 cells appeared to be slightly reduced relative to CHO cells (37%), this difference was not statistically significant (Figure 5-5), indicating that Tau35 expression does not affect the number of acidic structures under basal conditions. Inhibition of V-ATPase with bafilomycin (200 nM for 2 h) significantly reduced the number of acidic structures in all three cell lines ($P<0.01$ for CHO-FL, and $P<0.001$ for CHO-Tau35 and CHO cells) (Figure 5-5), as expected. In CHO and CHO-Tau35 cells, bafilomycin treatment resulted in almost complete removal of LysoTracker-positive structures. In contrast, approximately 30% of the puncta remained in CHO-FL cells after bafilomycin treatment. Figure 5-5 C reveals that there were no significant differences between the areas of individual LysoTracker-positive puncta in CHO-FL and CHO cells ($P>0.05$), or between CHO-Tau35 and CHO cells. However, there was a significant increase in the area of individual LysoTracker puncta in CHO-FL cells compared to CHO-Tau35 cells ($P<0.01$).

In summary, these results demonstrate that under basal conditions, CHO-Tau35 cells exhibit a significant reduction in the number of acidic structures compared to CHO-FL cells, and show a slight but not significant reduction compared to that in CHO cells. This indicates a likely impairment in lysosome functionality induced by Tau35 expression in cells. The presence of an increased number of acidic puncta in CHO-FL cells following bafilomycin could suggest the presence of additional acidic structures in these cells, such as late-stage endosomes or peroxisomes, although this needs to be explored further. Furthermore, the reduction in the area of individual LysoTracker puncta in CHO-Tau35 cells compared to CHO-FL cells could indicate that full-length tau might have a propensity to cluster these acidic structures, and that this capacity is absent from Tau35. Overall, these findings demonstrate a reduction in the number of acidic structures induced by Tau35 expression in CHO cells. Furthermore, qualitative observations demonstrate that the intracellular localisation of acidic structures is similar between CHO-FL and CHO cells, but may be more polarised in CHO-Tau35 cells.

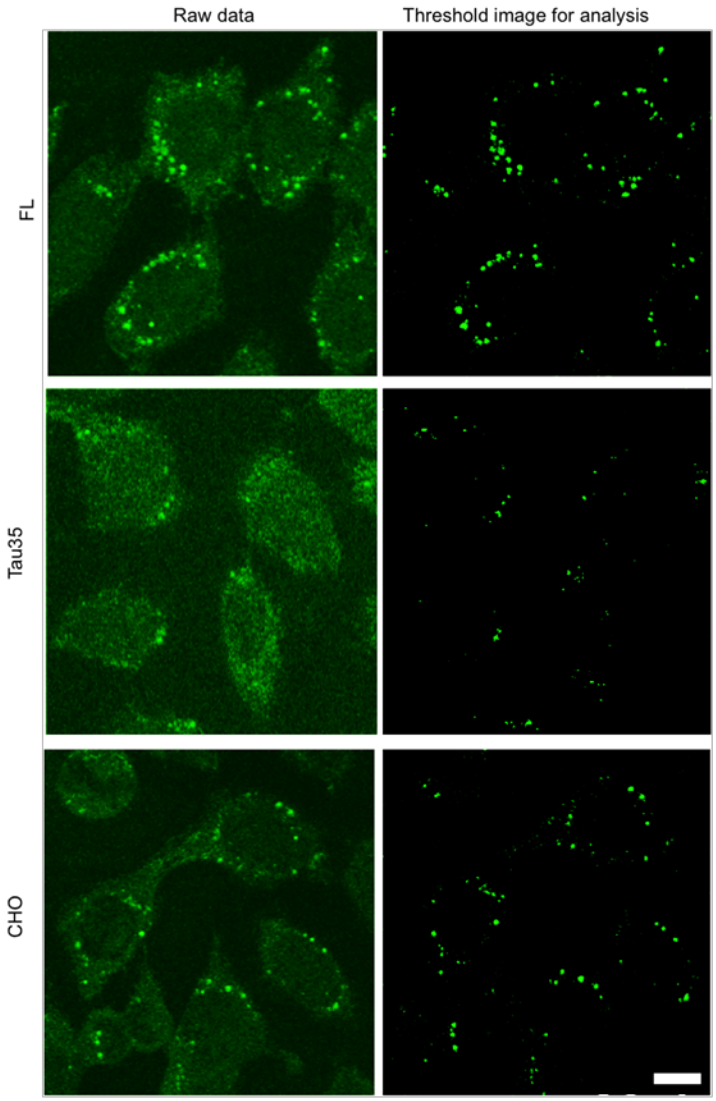

Figure 5-4 Raw data and thresholded images of LysoTracker Deep Red stained cells: LysoTracker staining of PFA-fixed untreated CHO-FL, CHO-Tau35 and CHO cells. Panels on the left show the raw images before thresholding. Panels on the right show images after thresholding for image analysis. Scale bar=10 µm.

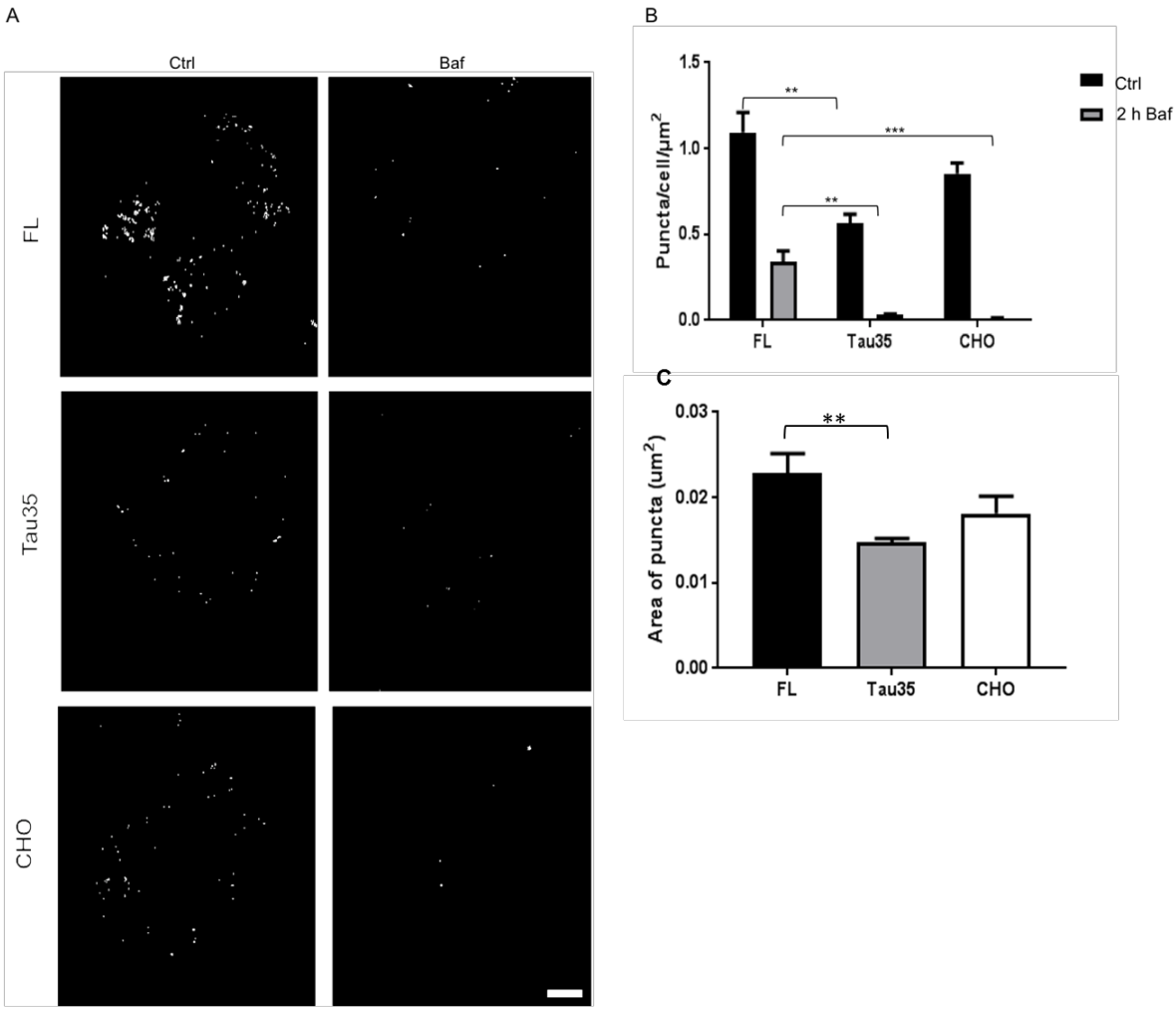

Figure 5-5 Reduced number of acidic structures in CHO-Tau35 cells: A LysoTracker staining of PFA-fixed CHO-FL, CHO-Tau35 and CHO cells, untreated and bafilomycin (Baf)-treated (200 nM for 2 h). Scale bar=10 µm. **B** Quantification of LysoTracker puncta/cell/µm^2. **C** Quantification of the area of LysoTracker (µm^2). For the quantification, a total of 30 cells were analysed per condition. Values represent mean ± SEM, n=3 for each cell line; one-way ANOVA, **P<0.01, ***P<0.001.

To further explore the effect of Tau35 expression on lysosome functionality, cathepsin D and cathepsin L were assessed in CHO-FL, CHO-Tau35 and CHO cells using immunofluorescence. Cathepsin D deficiency is associated with the accumulation of Lewy bodies in PD, and with the appearance of amyloid plaques and NFT in AD. It is well established that this aspartic protease functions optimally at an acidic pH (Turk et al., 1999). The role of cathepsin L is less well elucidated than that of cathepsin D in relation to neurodegeneration however, cathepsin L and B deficient mice reveal a degree of brain atrophy not previously seen in mice. Greatest activity is obtained close to pH 5-6 and 30-40% of the enzyme remains activated at pH 7 (Turk et al, 1999).

The number of cathepsin D puncta was quantified in each of the three cell lines. The results revealed a statistically significant decrease in the number of cathepsin D puncta in CHO-Tau35 cells compared to both CHO-FL and CHO cells (Figure 5-6A and B, $P<0.001$ for both). However, there were no differences in the number of cathepsin D puncta in CHO-FL and CHO cells ($P>0.05$), indicating that tau expression *per se* was not responsible for the reduction of puncta in Tau35-expressing cells.

The mean colocalisation of LAMP2 and cathepsin D in the CHO cells exceeded 92% in all three cell lines, indicating an overall high degree of colocalisation of these two proteins, as expected from the primary association of cathepsin D with lysosomes (Figure 5-6 C). Comparison of the cells showed a small but significant reduction in the colocalisation of LAMP2 and cathepsin D puncta in CHO-Tau35 cells compared to CHO-FL and CHO cells (reductions of 3% and 4% in colocalisation, respectively) ($P<0.05$). There were no significant changes in LAMP2 and cathepsin D colocalisation in CHO-FL compared to CHO cells ($P>0.05$). The reduced colocalisation of cathepsin D and LAMP2 in Tau35-expressing cells may be related to the fact that lysosomal degradation capacity is impaired by expression of Tau35 as the location of this enzyme within lysosomes in pivotal for the degradative function of lysosomes.

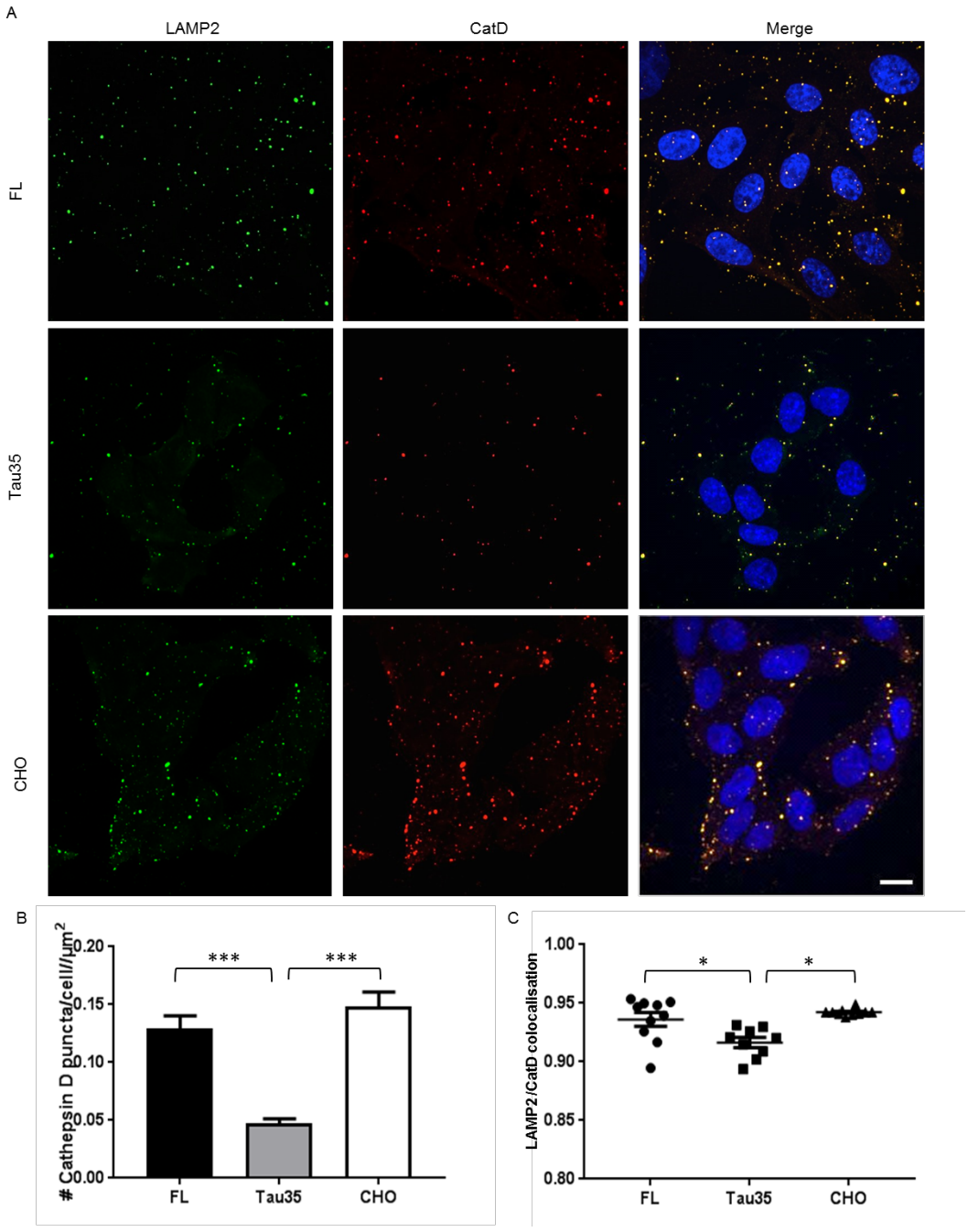

Figure 5-6 Reduction in cathepsin D puncta and LAMP2/Cathepsin D colocalisation in CHO-Tau35 cells: A immunofluorescence of PFA-fixed CHO-FL, CHO-Tau35 and CHO cells labelled with LAMP2 (green) and cathepsin D (red) antibodies, and Hoescht 33342 (blue), scale bar=10 µm. **B** Quantification of number of cathepsin D puncta/cell/µm^2, n=3 for each cell line. **C** Quantification of LAMP2/cathepsin D colocalisation, n=3 for each cell line. For the quantification, a total of 30 cells were analysed per condition. Values represent mean ± SEM; one-way ANOVA, *P<0.05, ***P<0.001.

The amount of cathepsin L was determined in CHO-FL, CHO-Tau35 and CHO cells (Figure 5-7 A and B). The results showed no differences in the number of cathepsin L puncta in any of the three cell lines ($P>0.05$). Notably, in contrast to the results obtained with cathepsin D, there was a significant increase in the colocalisation of LAMP2 and cathepsin L in CHO-Tau35 cells compared to both CHO-FL (8%) and CHO cells (10%) (Figure 5-7, $P<0.05$ and $P<0.01$, respectively). There were no significant differences in LAMP2/cathepsin L colocalisation between CHO-FL and CHO cells ($P>0.05$). Unlike the observations made for LAMP2/cathepsin D colocalisation, the colocalisation of LAMP2/cathepsin L puncta was less in all three cell lines (67% in CHO-FL, 72% in CHO-Tau35 and 64% in CHO cells). This indicates that the overall colocalisation of lysosomes with cathepsin L is relatively reduced compared to cathepsin D in all the three cell lines.

In summary, these results demonstrate a decrease in cathepsin D and a marked reduction in the degree of colocalisation of cathepsin D with lysosomes (LAMP2) caused by Tau35 expression in CHO cells. Both changes could indicate a Tau35-induced impairment in lysosomal function. The increased colocalisation of cathepsin L with lysosomes in CHO-Tau35 cells may be a further indicator of lysosomal dysfunction as this may correlate with an increased pH of the lysosomes as cathepsin L has been shown to be active at a pH of up to 6.5, which is substantially higher than the optimum pH activity of cathepsin D. The increase in cathepsin L colocalisation in CHO-Tau35 cells may also be an underlying reason behind the reduced cathepsin D in these cells as cathepsin L specifically degrades the single-chain isoform of cathepsin D (Streubel et al., 2018). Moreover the increased colocalisation of cathepsin L with lysosomes in CHO-Tau35 cells may be related to the function of this enzyme as it is responsible for degrading aggregating proteins like synuclein, so increased colocalisation with lysosomes might be enhanced by Tau35 expression in an attempt to degrade it (Wille et al., 2004).

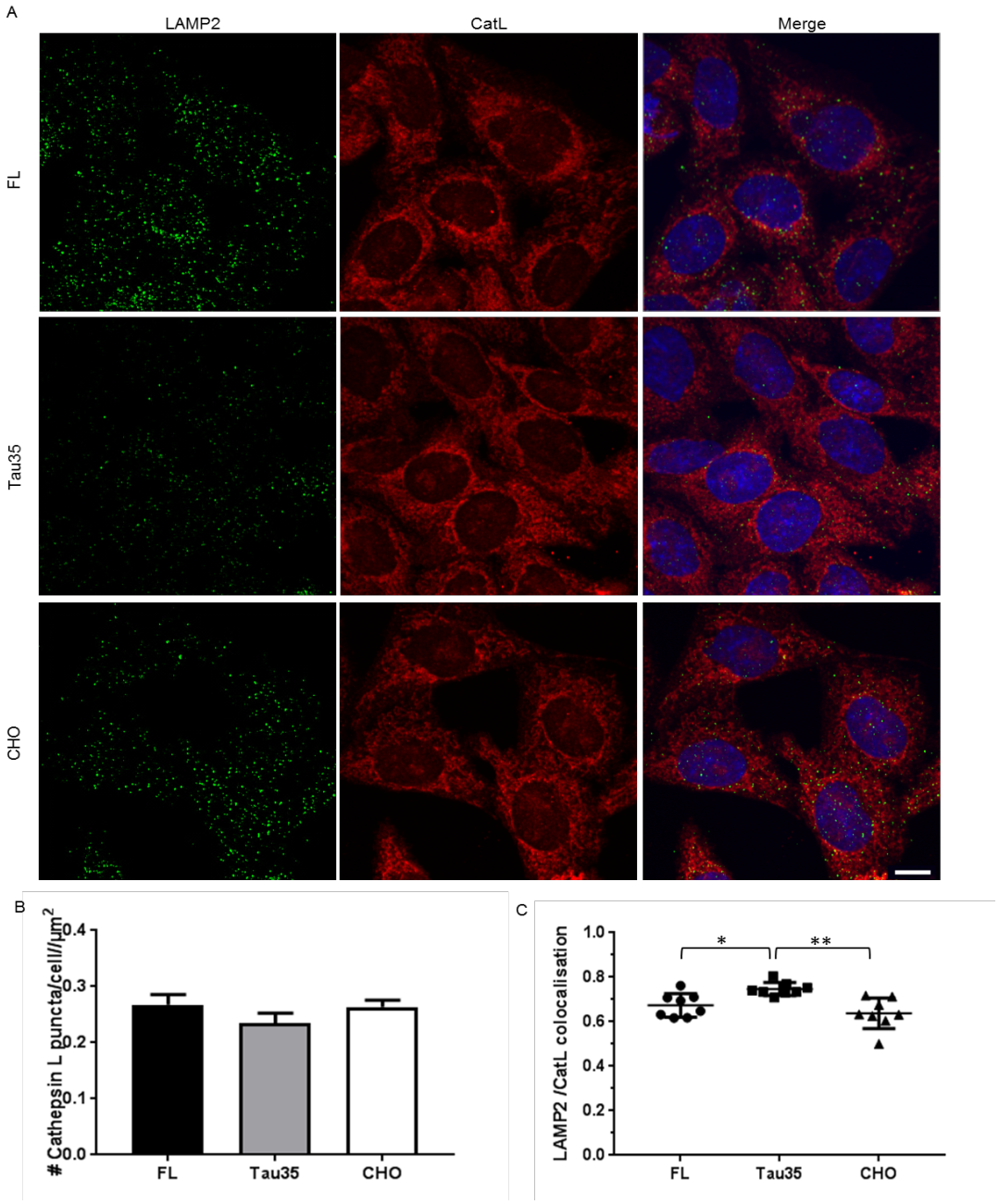

Figure 5-7 Figure 5 7 No change in Cathepsin L, but increased LAMP2/Cathepsin L colocalisation in CHO-Tau35 cells: A immunofluorescence of PFA-fixed CHO-FL, CHO-Tau35 and CHO cells labelled with LAMP2 (green) and cathepsin L (red) antibodies, and Hoescht 33342 (blue), scale bar=10 µm. **B** Quantification of number of cathepsin L puncta/cell/µm^2, n=3 for each cell line. **C** Quantification of LAMP2/cathepsin L colocalisation, n=3 for each cell line. For the quantification, a total of 30 cells were analysed per condition. Values represent mean ± SEM; one-way ANOVA, *P<0.05, **P<0.01.

5.2.3 **The impact of Tau35 expression on lipid clearance in CHO cells**

Lysosomes play an important role in lipid degradation and a wide range of different lipids including glycosphingolipids (GSLs), phospholipids and cholesterol, accumulate in cells as a consequence of lysosome dysfunction. Therefore, to further investigate lysosome fubction, CHO-FL, CHO-Tau35 and CHO cells were stained with BODIPY to fluorescently label intracellular neutral lipids, and the number of BODIPY-positive puncta were counted. The results of this analysis showed a marked, two-fold increase in the number of BODIPY puncta in CHO-Tau35 cells compared to CHO cells when normalised to cell area (Figure 5-8 A and B, $P<0.05$). Although the number of BODIPY-positive lipid droplets in CHO-FL cells also appeared to be increased compared to CHO cells, this was not statistically significant. The area of individual BODIPY puncta was also significantly increased in CHO-Tau35 cells compared to that in CHO cells (Figure 5-8 C, $P<0.01$). Notably, the area of individual BODIPY puncta in CHO-FL cells was significantly increased compared to both CHO-Tau35 and CHO cells ($P<0.05$ and $P<0.001$, respectively).

Taken together, these findings demonstrate that expression of Tau35 in CHO cells leads to an increase both in the overall accumulation of neutral lipids and in the area occupied by individual lipid droplets compared to CHO cells. Expression of FL-tau did not affect the amount of neutral lipid puncta but their area was dramatically increased by FL-tau expression. This indicates that both FL-tau and Tau35 have an increased propensity to cause lipid clustering in CHO cells, although FL-tau has a greater propensity to result in the fusion of lipid droplets than Tau35.

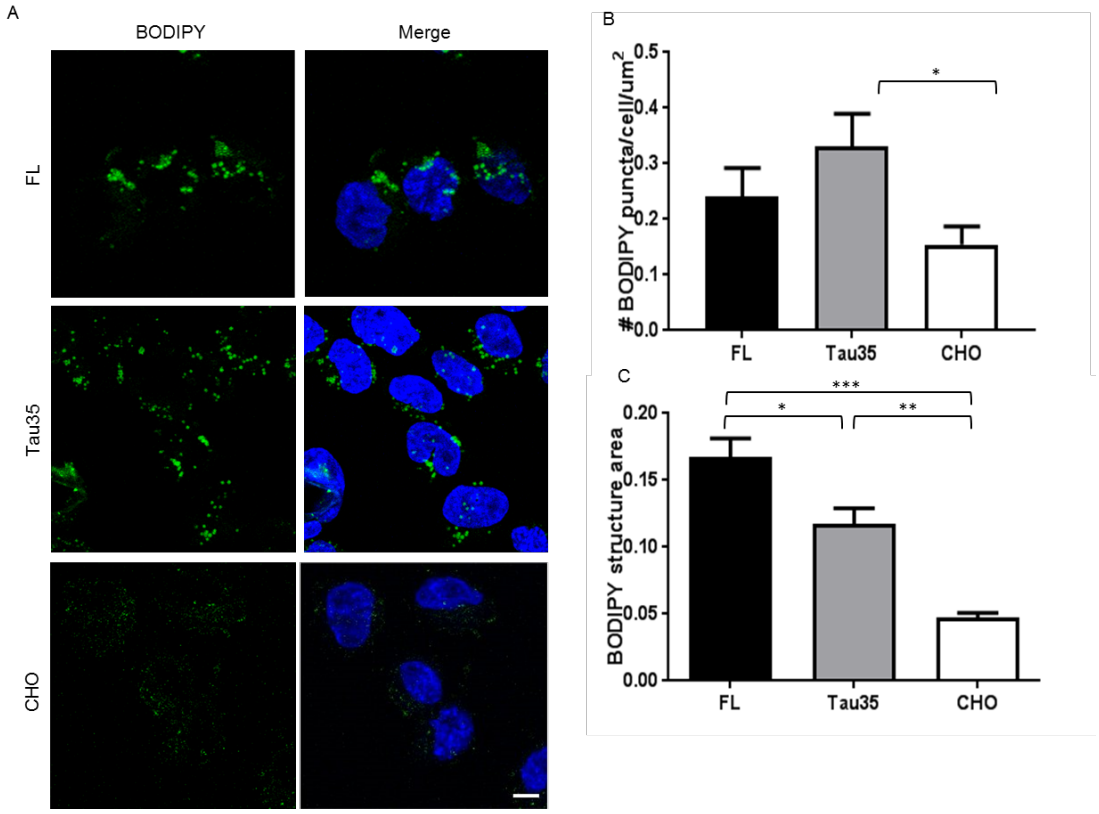

Figure 5-8 Increased lipid accumulation in CHO-Tau35 cells: A immunofluorescence of BODIPY stained followed by PFA-fixation of CHO-FL, CHO-Tau35 and CHO cells (green) and Hoescht 33342 (blue), scale bar=10 µm. **B** Quantification of the number of BODIPY puncta/cell/µm^2. **C** Quantification of BODIPY puncta area (µm^2). For the quantification, a total of 30 cells were analysed per condition. Values represent mean ± SEM, n=3 for each cell line; one-way ANOVA, *P<0.05, **P<0.01, ***P<0.001.

Since BODIPY labels a wide variety of intracellular lipid populations, CHO-FL, CHO-Tau35 and CHO cells were subsequently immunolabelled with a specific lipid antibody to gain a more detailed understanding of which populations of lipids are altered by expression of Tau35 and FL-tau. Therefore, CHO-FL, CHO-Tau35 and CHO cells were immunolabelled with lysobisphosphatidic acid (LBPA), which is a lipid marker of late-stage endosomes. Visualising potential changes in LBPA is of interest because abnormalities in endosomes, and/or dysfunctional endosomal-lysosomal trafficking has been shown to play a pivotal role in neurodegenerative diseases such as AD.

There was no change in the amount of LBPA puncta in CHO-Tau35 cells compared to CHO cells (Figure 5-9). In contrast, there was a statistically significant decrease in the number of LBPA puncta in CHO-FL cells compared to both CHO-Tau35 and CHO cells ($P<0.001$). The results also show no change in the area of individual LBPA puncta in CHO-Tau35 cells compared to CHO cells. However, the area of LBPA puncta in CHO-FL cells was significantly increased compared to both CHO-Tau35 and CHO cells ($P<0.05$ and $P<0.01$, respectively).

Taken together these findings indicate that the number and size of LBPA puncta is equivalent in CHO-Tau35 and CHO cells, indicating that this marker of late-stage endosomes is not affected by Tau35 expression. In contrast, expression of FL-tau caused a significant reduction in the number of LBPA puncta, implying that tau expression either reduced the number of late-stage endosomes in CHO cells or led to the fusion of late-stage endosomes, which may explain the increase in LBPA area. The increased area of LBPA puncta in CHO-FL cells is consistent with the previous observations with BODIPY labelling in CHO-FL cells (Figure 5-8). This confirms the increased propensity for lipid clustering induced by FL-tau expression in cells.

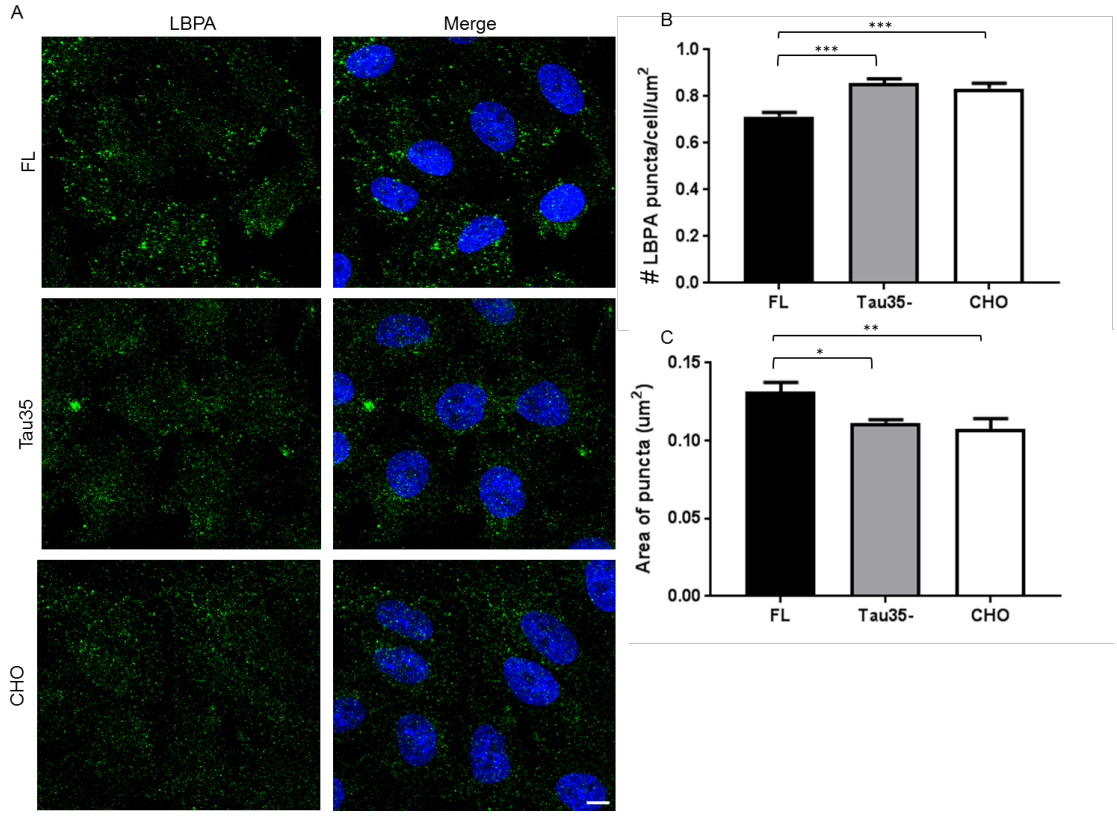

Figure 5-9 Lysophosphatidic acid in CHO-FL, CHO-Tau35 and CHO cells: A Immunofluorescence of PFA-fixed CHO-FL, CHO-Tau35 and CHO cells labelled with LBPA (green) antibody, and Hoescht 33342 (blue), scale bar=10 µm. **B** Quantification of the number of LBPA puncta/cell/µm^2. **C** Quantification of the area of individual LBPA puncta (µm^2). For the quantification, a total of 30 cells were analysed per condition. Values represent mean ± SEM, n=3 for each cell line; one-way ANOVA, *P<0.05, **P<0.01, ***P<0.001.

5.2.4 **The effect of Tau35 expression on lysosome interaction with tau**

Next, the association of tau with lysosomes was assessed in CHO-FL and CHO-Tau35 cells by determining the degree of tau colocalisation with LAMP2 following PFA fixation. There is a significant increase in the colocalisation of tau and LAMP2 in CHO-Tau35 cells (64%) compared to CHO-FL cells (37%) (Figure 5-10, $P<0.001$). These results demonstrate that tau in CHO-Tau35 cells associates with lysosomes, which may in part, be due to the apparent build-up of phosphorylated tau in CHO-Tau35 cells compared to CHO-FL cells (Chapter 4).

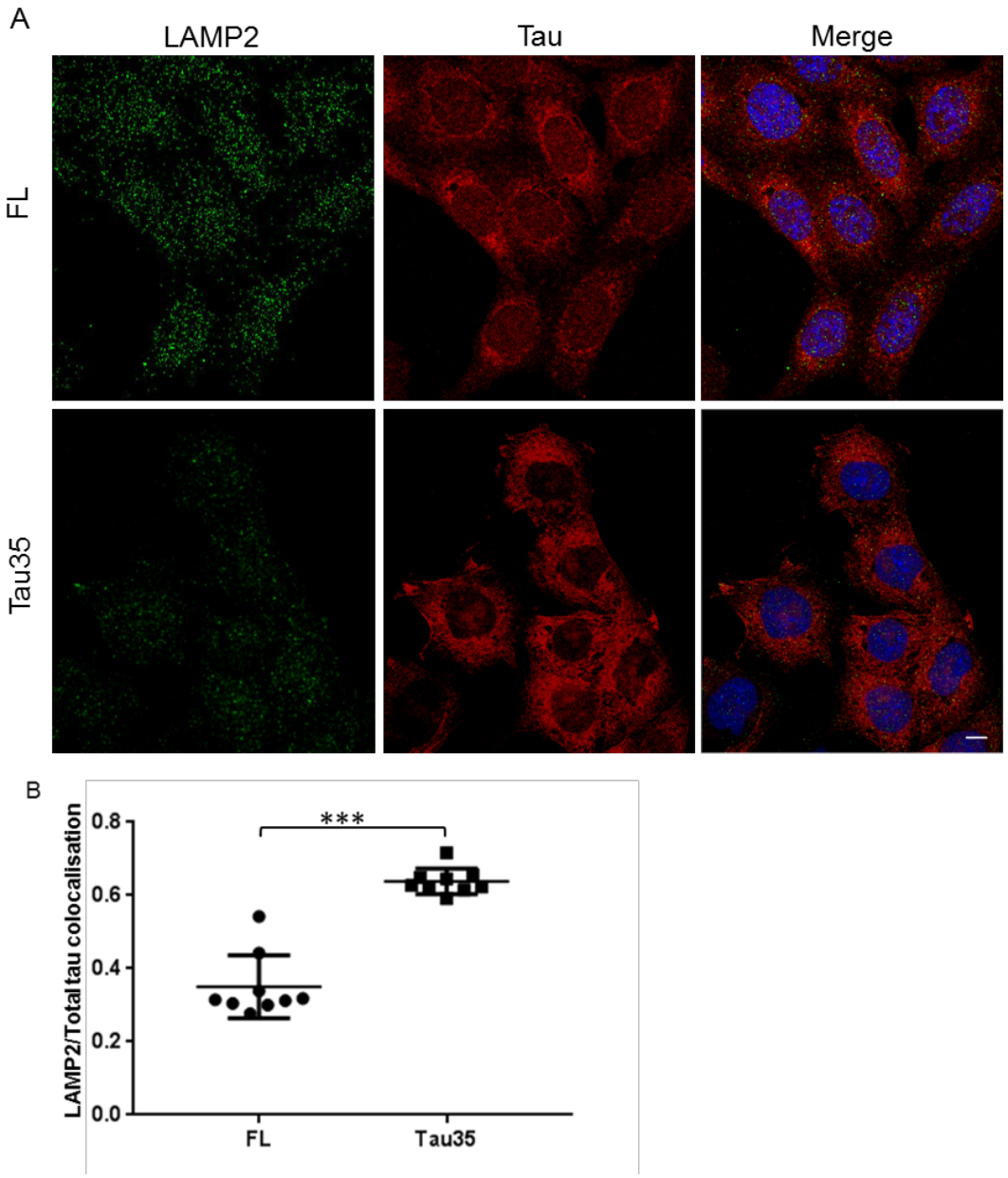

Figure 5-10 Increased colocalisation of tau with LAMP2 in CHO-Tau35 cells: A Immunofluorescence of PFA-fixed CHO-FL, CHO-Tau35 and CHO cells labelled with LAMP2 (green) and total tau (red) antibodies, and Hoescht 33342 (blue), scale bar=10 µm. **B** Quantification of LAMP2/total tau colocalisation. For the quantification, a total of 30 cells were analysed per condition. Values represent mean ± SEM, n=3 for each cell line; student's t-test, ***P<0.001.

5.3 Summary and discussion

The overall aim of this chapter was to determine the relative effects of expressing Tau35 and FL-tau on lysosome biogenesis and lysosomal functionality in CHO cells.

The main findings of this chapter include:

- Reduced number of lysosomes in CHO-Tau35 cells compared to CHO-FL and CHO cells, and decreased area of individual lysosomes in CHO-Tau35 cells compared to CHO-FL cells.
- Decreases in the nuclear translocation of TFEB and importin α7 (in the nuclear fraction) in CHO-Tau35 cells compared to CHO-FL and CHO cells.
- Fewer acidic structures in CHO-Tau35 cells compared to CHO-FL and CHO cells.
- Decrease in the number of cathepsin D puncta and cathepsin D/LAMP2 colocalisation in CHO-Tau35 cells compared to CHO-FL and CHO cells. Conversely, there were no changes in the number of cathepsin L puncta in the three cell types. However, cathepsin L/LAMP2 colocalisation was increased in CHO-Tau35 cells compared to CHO-FL and CHO cells.
- Increased number and area of individual BODIPY neutral lipid droplets in CHO-Tau35 cells compared to CHO cells. CHO-FL cells exhibited an increase in the area of individual BODIPY droplets compared to both CHO-Tau35 and CHO cells.
- Decrease in the number of LBPA puncta in CHO-FL cells compared to the other two cell types. LBPA puncta area was increased in CHO-FL cells compared to CHO cells, but similar to CHO-Tau35 cells.
- There was an increase in LAMP2/total tau colocalisation in CHO-Tau35 cells compared to CHO-FL cells.

5.3.1 **Effect of Tau35 on lysosome biogenesis**

Lysosomal biogenesis is tightly regulated by TFEB (Sardiello et al., 2009). The attenuated nuclear translocation of TFEB in CHO-Tau35 cells may contribute to the reduction in LAMP2 puncta, due to the inability of TFEB to facilitate the transcription of genes involved in lysosomal biogenesis. Increased retention of TFEB in the cytosol may be due to activation of mTOR signalling in CHO-Tau35 cells since, although phosphorylated mTOR was not significantly increased (P=0.055), phosphorylated ribosomal protein S6, a downstream target of mTOR, was increased, and raptor phosphorylation was reduced by Tau35 expression (Chapter 4). The findings reported here in CHO-Tau35 cells are supported by those of other groups investigating lysosomal abnormalities in neurodegenerative disease. For example, lysosomal deficiency is evident in a variety of *in vitro* and rodent models of PD and AD, such as CHO cells inducibly expressing the C-terminal fragment of APP (APP-CTF) and APP/PS1 transgenic mice (Decressac et al., 2013; Dehay et al., 2010; Parr et al., 2012b; Xiao et al., 2015b). Furthermore, overexpressing TFEB or inducing nuclear translocation of TFEB improves PD symptoms and ameliorates α-synuclein pathology in the *in vivo* 1-methyl-4-phenyl-1,2,3,6-tetrahydropyridine mouse model of α-synuclein toxicity (Dehay et al., 2010). Therefore, the decreased amount of nuclear TFEB in CHO-Tau35 cells may further contribute to the toxic effects of Tau35.

In AD, there is aberrant localisation of nuclear proteins involved in cell cycle activation including mislocalised cyclins and cyclin-dependent kinases, as well as components of mitogenic signal transduction pathways (McShea et al., 1997; Ogawa et al., 2003). For example, phosphorylated histone-3 has been reported to be mislocalised to the cytoplasm of AD neurons (Ogawa et al., 2003). The shuttling of a large number of nuclear proteins into the nucleus is mediated by importins (Macara, 2001). Shuttling of importin α1 between the cytoplasm and the nucleus, and the subsequent importin α1-mediated cytoplasmic-nuclear transport, was demonstrated to be hindered in AD neurons compared to controls by immunohistochemistry (Lee et al., 2006). The overt decrease in importin α7 observed in the nuclear fraction of CHO-Tau35 cells could therefore support the view that aberrant tau fragmentation could have a negative impact on nuclear-cytoplasmic trafficking. Furthermore, our finding may correlate with and potentially explain the increased cytoplasmic retention of TFEB apparent in CHO-Tau35 cells. However, it will be

important to examine additional components of the nuclear pore complex to validate this hypothesis and examine potential additional factors behind the cytoplasmic retention of TFEB in CHO-Tau35 cells.

5.3.2 **The effect of Tau35 on lysosome functionality**

A reduction in the number of acidic structures, including endosomes and lysosomes, labelled by LysoTracker in CHO-Tau35 cells compared to CHO-FL and CHO cells suggests compromised lysosomal functionality induced by Tau35 expression. The decline in the number of these acidic structures could be an underlying cause that would contribute to the autophagic abnormalities noted in CHO-Tau35 cells. Defective lysosomal function is now recognised as a primary factor in the pathogenesis of AD (Nixon and Yang, 2012; Zare-Shahabadi et al., 2015), PD (Dehay et al., 2013), and FTLD (Gotzl et al., 2014). A study of PS1KO cells showed that defective lysosomal acidification is one of the main reasons for autophagic dysregulation under these conditions (Li et al., 2013; Wolfe et al., 2013). The results from that study revealed elevated lysosomal pH using ratiometric pH sensing dyes and decrease of LysoTracker signal, similar to the results obtained using LysoTracker in CHO-Tau35 cells. Moreover, lysosomal acidification defects were also demonstrated in the brains of PS1 hypomorphic and conditional PS1/2 knockout mice (Lee et al., 2010b).

The apparent reduction in the number of cathepsin D puncta in CHO-Tau35 cells is a further indication of impaired lysosome function upon Tau35 expression. This is supported by previous findings showing that the complete loss of cathepsin D in mice results in the lysosomal neurodegenerative disorder, neuronal ceroid lipofuscinosis (Siintola et al., 2006; Steinfeld et al., 2006). Furthermore, cathepsin inhibition in mouse hippocampal slice and cell culture studies has previously been shown to affect tau proteolysis and solubility. Work by Khurana et al, using a *Drosophila* model of AD (UAS-tau1–^{421}) , determined that removing cathepsin D substantially potentiated tau-induced neurotoxicity (Khurana et al., 2010). Moreover, the presence of a neurotoxic C-terminally truncated tau fragment, that had previously been detected in AD brain is increased in the absence of cathepsin D in mice (Khurana et al., 2010). Therefore, the reduction in cathepsin D in CHO-Tau35 cells could potentially contribute to the elevation in the amount of phosphorylated tau observed in this cell model (Guo et al., 2019).

The significant decrease in cathepsin D/LAMP2 colocalisation in CHO-Tau35 cells further reveals disruptions and abnormalities in the lysosomes. This observation is consistent with previous findings that report mislocalisation of cathepsin D in neurodegenerative disease. For example, cathepsin D immunoreactivity in AD brain is concentrated extracellularly within amyloid plaques, rather than being confined to lysosomes (Gowrishankar et al., 2015).

Although there were no changes detected in the numbers of cathepsin L puncta in CHO-FL, CHO-Tau35 and CHO cells, there was a significant increase in cathepsin L/LAMP2 colocalisation in CHO-Tau35 cells compared to CHO-FL and CHO cells. As previously outlined, cathepsin L activity has a higher pH optimum than cathepsin D, and since there were less acidic structures observed in CHO-Tau35 cells, this may explain the increased ability of cathepsin L to associate with the lysosomes upon the expression of Tau35. The increase in cathepsin L/LAMP2 colocalisation could additionally explain the build-up of phosphorylated tau upon the expression of Tau35 as it cathepsin L has been shown to be involved in the cleavage of the mutant tau construct $Tau_{RD}\Delta K280$, generating a fragment which strongly promotes tau aggregation (Wang et al., 2009).

The apparent elevation in both the number and size of BODIPY lipid droplets in CHO-Tau35 cells is further evidence of lysosomal dysfunction caused by expression of Tau35 as lipids have been known to accumulate in a wide range of LSDs such as Niemann Pick type C (Walkley and Vanier, 2009).. Increased lipid accumulation in CHO-Tau35 cells could also be explained by the increased activity of GSK3β observed in these cells (Chapter 4), a phenomenon also observed in AD (Jazvinscak Jembrek et al., 2015).. It has been hypothesised that Aβ may increase tau phosphorylation by a mechanism dependent on GSK-3β. Consequently, there is often a correlation seen between the elevation of phosphorylated tau and the build-up of lipids (Jazvinscak Jembrek et al., 2015).

The decreased number of LBPA puncta in CHO-FL cells suggests a reduction in late-stage endosomes in these cells. This reduction may be due to the elevated levels of Beclin 1 previously detected in CHO-FL cells (Chapter 4). It was reported that a beclin-1-binding

autophagic tumour suppressor, UV radiation resistance-associated gene protein (UVRAG), interacts with the class C Vps complex of the endosomal fusion machinery. This interaction stimulates Rab7 GTPase activity and autophagosome maturation and fusion with late endosomes/lysosomes, thereby enhancing delivery and degradation of autophagic cargo. Furthermore, the UVRAG-class-C-Vps complex accelerates endosome–endosome fusion, resulting in rapid degradation of endocytic cargo (Liang et al., 2008). Therefore, the reduction in LBPA could potentially be due to enhanced degradation by the UVRAG complex. Furthermore, the findings in Chapter 4 show elevated LC3 in CHO-FL cells, indicating an increase in autophagosomes, which could further help to explain the observed decrease in LBPA in these cells.

5.3.3 **The link between lysosomes and tau**

The increased colocalisation of LAMP2 with total tau in CHO-tau35 cells relative to CHO-FL cells could provide a justification for the accumulation of phosphorylated tau caused by Tau35 expression. Monomeric tau is actively cleared through the proteasome (Brown et al., 2005), whereas the higher order tau oligomers and aggregates found in tauopathies, are preferentially degraded by the lysosome. In fact, proteasomal activity appears to be reduced in AD brain, and PHF-tau isolated from human AD brain was not degraded by the proteasome. In fact, aggregated tau was shown to inhibit the proteasome (Keck et al., 2003; Rubinsztein, 2006). Therefore, upon Tau35 expression, highly phosphorylated tau would colocalise with lysosomes in an attempt to enhance tau degradation. However, due to the observed impairment in lysosome biogenesis, the reduced number of lysosomes present in CHO-Tau35 cells may lack the capacity to degrade the accumulating phosphorylated and aggregated tau.

Taken together, the results from this chapter reveal that Tau35 expression in CHO cells causes a deficiency in lysosome biogenesis which may result from the reduction in nuclear translocation of TFEB, as well as a reduction in importin α7 and increased activity of mTORC1 (Chapter 4). In addition, reduced lysosome functionality is apparent due to Tau35 expression in these cells through reduced numbers of acidic structures, cathepsin D, colocalisation of lysosomes with cathepsin D and enhanced lipid accumulation. Together, these cellular abnormalities and lack of effective lysosomal degradation, could contribute

to a vicious cycle that accelerates the build-up of phosphorylated and aggregated tau in CHO-Tau35 cells.

Chapter 6 Discussion

6.1 Summary of results

The overall aims and objectives of this study were:

- To assess changes in tau phosphorylation and UPR activation in different brain regions of aged Tau35 mice.
- To investigate the effect of Tau35 expression on cell viability and autophagy activation using a Tau35 cell model.
- To determine if Tau35 expression affects lysosome biogenesis and functionality in the cell model of Tau35.

The primary findings of this thesis are summarised as follows:

Tau35-expressing transgenic mouse brain exhibits region-dependent increases in tau phosphorylation and UPR activation

In the Tau35 mouse model of tauopathy, expressing a C-terminal tau fragment associated with human tauopathy (Tau35), there were increases in tau phosphorylation that were brain region-dependent. The hippocampus was the most affected area in terms of tau phosphorylation, while the amygdala was the least affected. Furthermore, increased activation of the UPR was also brain region-dependent and this correlated with increased tau phosphorylation, with increased UPR activation observed in the hippocampus and no changes detected in the amygdala of Tau35 mice.

Tau35 causes autophagic dysfunction without affecting viability of CHO cells

To further elucidate the molecular mechanisms affected by Tau35 expression, a CHO cell model in which Tau35 is stably expressed was used to determine the effect of Tau35 expression on cell viability and autophagic/lysosomal degradation. Tau35 did not induce cell death in CHO cells. Reductions in beclin-1 and LC3 indicate deficits in early autophagy/phagophore formation and a deficit in the number of autophagosomes, respectively. This induction of autophagic dysfunction by Tau35 is supported by the finding of increased p62 in CHO-Tau35 cells. Possible mechanisms underlying the deficits observed

in the autophagy pathway in CHO-Tau35 cells include increased activation of mTORC1 and decreased activity of AMPK.

Lysosome biogenesis and functionality is impaired in CHO-Tau35 cells

Reduced numbers of LAMP2 puncta were found in CHO-Tau35 cells, demonstrating that the there are fewer lysosomes in these cells. Increased cytoplasmic retention of TFEB and decreased importin α7 in CHO-Tau35 cells could be possible underlying reason for these Tau35-induced changes. Reductions in LysoTracker and cathepsin D labelling, as well as increased BODIPY staining in CHO-Tau35 cells support the view that Tau35 expression results in compromised lysosome functionality.

A summary of all the changes in markers of autophagy and lysosomal degradation pathways is illustrated in Table 6-1.

Table 6-1 Summary of the changes in markers of autophagy and lysosomal degradation in CHO-FL and CHO-Tau35 cells

Marker	CHO-FL cells	CHO-Tau35 cells
Beclin-1	-	Decreased
Atg proteins (Atg5, Atg7 and Atg13)	-	-
LC3	Increased	Decreased
Phospho mTOR (Ser2448)	-	-
Phospho S6	-	Increased
Phospho raptor	-	Decreased
Phospho ERK1/2	-	Decreased
Phospho AMPK (Thr172)	-	Decreased
ULK1	-	Increased
Phospho ULK1 (Ser555 and Ser757)	-	-
p62	-	Increased
LAMP2 (number)	-	Decreased
Nuclear TFEB	-	Decreased
LysoTracker (number)	-	Decreased
Cathepsin D (number)	-	Decreased
Cathepsin L (number)	-	-
BODIPY (number)	-	Increased
LBPA (number)	Decreased	-

The table illustrates the changes in markers of autophagy and lysosomal degradation in CHO-FL and CHO-Tau35 cells in comparison with CHO cells. (-) indicates no change.

6.2 Changes in Tau35 mouse and cell models

In 2008, this laboratory identified a 35 kDa C-terminal tau fragment (Tau35), lacking the N-terminus of tau but containing four microtubule-binding repeats (4R), that was readily detectable in PSP, CBD degeneration and 4R tau-related forms of FTLD, but was absent from healthy controls (Wray et al., 2008). Consequently, a Tau35-expressing mouse model was developed to study the effect of this fragment *in vivo*. Results showed that minimal expression of this tau fragment (<10%, relative to endogenous mouse tau) was sufficient to recapitulate key features of human tauopathies (Bondulich et al., 2016). Thus, Tau35 mice exhibit progressive cognitive (associated with hippocampal-dependent learning) and motor deficits. Moreover, Tau35 mice exhibit Increased tau phosphorylation in the hippocampus, loss of synaptic protein, and reduced life span (Bondulich et al., 2016). Tau35 mice express a truncated species of WT human tau at a very low level making this model the first of its kind to date. No other mice expressing low amounts of WT human tau have been reported to exhibit tauopathy. These mice therefore represent a novel and highly relevant animal model of sporadic tauopathy. Furthermore, Tau35 accurately represents the spectrum of sporadic human tauopathies in the absence of significantly increased tau expression or the presence of any tau mutation.

In this study N-terminal truncation of tau was shown to result in changes in tau phosphorylation in four different brain regions of 16-18 month old (aged) Tau35 mice. In a previous report, Bondulich et al (2016) reported increased tau phosphorylation at several different epitopes, but only in the hippocampus of mice aged up to 14 months (Bondulich et al., 2016). Therefore, the findings from the present study extend this work and demonstrate that Tau35 expression commences by affecting the hippocampus, but goes on to subsequently affect other brain regions as the mice age. This potentially indicates a spreading of tau pathology with increasing age, which parallels the findings in human tauopathy brain (Clavaguera et al., 2013; Iqbal et al., 2005). Overall, the results herein show that the hippocampus is the most affected brain region in Tau35 mice, followed by the brainstem and cerebellum, and frontal regions, with the amygdala being the least affected brain region. Notably, Zilka and colleagues found that the higher the expression level of truncated tau, the earlier the onset of tangle pathology and NFT formation (Zilka et al., 2006b). Therefore, considering the low-level expression of Tau35, it is not surprising

that increased tau phosphorylation is more prominent in older mice and spreads to brain regions other than the hippocampus once the mice age since this demonstrates the progression of disease.

Tau35 mice exhibited increased activation of the UPR in the hippocampus compared to WT mice. This was apparent from the activation of PERK, a key component of one branch of the UPR, as well as increased CHOP, a pro-apoptotic executioner of the UPR, and also IRE1 activation in the hippocampus of Tau35 mice. In contrast, activation of the PERK branch of the UPR was not apparent in the amygdala. Thus, these findings demonstrate that UPR activation is brain region-dependent in Tau35 mice and that this occurs in conjunction with tau phosphorylation. A large body of evidence has demonstrated a correlation between activation of the UPR and the development of several tauopathies, including AD and FTLD-tau (Höglinger et al., 2011; Pereira et al., 2014). Recent reports show that disrupted tau phosphorylation upon UPR activation was found in P301L tau transgenic mice (Radford et al., 2015). Moreover, increases in BiP are present in temporal cortex and hippocampus in AD compared with nondemented controls (Hoozemans et al., 2009). However, the mechanisms underlying this disruption in tau phosphorylation have not been well elucidated. One proposed mechanism in relation to the UPR and AD is that UPR activation precedes the widespread occurrence of neurofibrillary degeneration, as the protein expression levels of BiP are increased at an early stage of AD pathology in the temporal cortex (Hoozemans et al., 2009). The results from the present study therefore, show that abnormal truncation of tau abolishes its physiological function, as well as exerting a toxic effect via activation of branches of the UPR pathway.

A growing link between the UPR and autophagy has been substantiated. For example, the PERK–eIF2α pathway is essential for autophagy induction after unfolded or misfolded proteins accumulate in the ER lumen (B'chir et al., 2013). Specifically, ATF4 and CHOP were shown to transcriptionally regulate more than a dozen Atg genes (B'chir et al., 2013). In addition, it is notable that IRE1 is also implicated in the activation of autophagy (Ogata et al., 2006). Tumour necrosis factor (TNF) receptor-associated factor 2 (TRAF2)-dependent activation of IRE1 and JNK leads to Bcl-2 phosphorylation, enabling the dissociation of beclin-1 leading to the activation of the PI3K complex (Deegan et al., 2013).

Alongside this murine model of tauopathy, a CHO cell model of Tau35 was developed to identify key molecular mechanisms that may be responsible for phenotypic changes in the mice. Initial studies on this cell line revealed that Tau35 has a reduced ability to bind to and stabilise microtubules and has reduced acetylated tubulin and increased activity of GSK3β (Guo et al., 2019). Due to the crosstalk that occurs between the UPR and autophagy pathways, the effect of Tau35 expression on the autophagy and lysosomal degradation pathway was investigated in order to examine the underlying mechanistic changes of these pathways in CHO-Tau35 cells.

An overt reduction in the amount of beclin-1 was apparent in CHO-Tau35 cells compared to CHO-FL and CHO cells, demonstrating an early impairment in the autophagy pathway. Several recent studies have implicated decreases in beclin-1 in the pathogenesis of AD (Jaeger et al., 2010; Lucin et al., 2013). Specifically, neuronal expression of beclin-1 gradually reduces during ageing but this rate of decline is faster in AD-affected brains (Jaeger et al., 2010; Pickford et al., 2008a). One consequence of the depletion of beclin-1 is an increase in cleaved (active) capsase-3 which may subsequently lead to apoptosis (Rohn et al., 2011). However, no differences were found in cell death between CHO-FL, CHO-Tau35 and CHO cells. Therefore, in CHO-Tau35 cells, the observed decrease in beclin-1 may occur through an alternative route. It is likely that the decrease in beclin-1 is a result of a reduction in activated AMPK in CHO-Tau35 cells, as AMPK mediates its pro-autophagic effects through beclin-1 (Zhang et al., 2016). As a consequence, these observed deficits in CHO-Tau35 cells lead to reduced formation of autophagosomes, as indicated by a reduction in LC3-II. This autophagy deficit was not rescued when autophagic flux was induced with bafilomycin A1, indicating that CHO-Tau35 cells are less efficient than untransfected CHO cells in forming autophagosomes.

There now appears to be a growing link between autophagic function and the tauopathies. Phosphorylated tau accumulation is increased in brain-specific *Atg7* knockout mice compared to WT control mice (Inoue et al., 2012), indicating that phosphorylated tau is a substrate of autophagy. Consistently, phosphorylated tau colocalises with LC3 and p62 in post-mortem human brain from AD, PSP, and CBD, likely because both LC3 and p62 become engulfed into autophagosomes but are not degraded by autolysosomes (Piras et

al., 2016b). The build-up of phosphorylated tau in CHO-Tau35 cells could therefore partially be accounted for by the deficits observed in the autophagy pathway. Although increased colocalisation between p62 and tau was not evident in CHO-Tau35 cells, there was a significant increase in the number of p62 puncta, which supports the concept of defective autophagy induced by Tau35. There was additionally a marked increase in the colocalisation of LAMP2 puncta with tau in CHO-Tau35 cells compared to both CHO-FL and CHO cells. This finding supports the observation of increasingly phosphorylated tau (as seen in CHO-Tau35 cells) is a substrate of autophagy.

Increased mTORC1 activity was apparent in the CHO-Tau35 cell model as illustrated by increased phosphorylated ribosomal S6 protein, decreased phosphorylated raptor, although the increase in mTOR was not found to be significant (P=0.056). Enhanced mTOR signaling has been implicated in AD pathogenesis. Evidence from post-mortem human AD brains indicates that the levels of phospho-mTOR and its downstream target p70S6K, are increased compared to age-matched control cases, suggesting higher mTOR activity in AD brains (An et al., 2003; Pei and Hugon, 2008). Additional studies show that mTOR is implicated in tau-mediated pathogenesis in AD and related tauopathies as the mTORC1 complex induces tau expression and promotes its GSK3β-dependent phosphorylation (Caccamo et al., 2013b). Therefore, it is likely that the increased activity of GSK3β noted in CHO-Tau35 cells and the resulting increase in tau phosphorylation, are both a consequence of increased mTORC1 activity. Inhibition of GSK3β activity using the specific inhibitor AR-A014418, ameliorated the decline in LC3-II in CHO-Tau35 cells, implicating both mTORC1 and GSK3β in the impairment in autophagy. On the other hand, inhibition of mTORC1 using rapamycin was not able to restore the deficits in LC3-II or to reverse the increased tau phosphorylation in CHO-Tau35 cells. Although rapamycin is considered to be the canonical inhibitor of mTOR, some functions that regulate cap-dependent translation and autophagy are resistant to inhibition by rapamycin. This may explain why rapamycin treatment was not able to rescue the autophagy deficit observed in CHO-Tau35 cells.

There is also significant interplay between mTORC1 and TFEB. TFEB is considered as being the master regulator of autophagy as it influences the expression of genes encoding proteins of the autophagy-lysosome pathway. Furthermore, the nuclear abundance of this

transcription factor can be altered to match cellular demand for lysosome biogenesis and autophagosome-lysosome function (Roczniak-Ferguson et al., 2012a). The cytoplasmic retention of TFEB in CHO-Tau35 cells is a possible underlying reason for the reduced number of lysosomes and impairment in early autophagy activation. The beneficial effect of TFEB has been demonstrated in multiple models of AD including N2a cells stably expressing APP carrying the Swedish mutation, and APP/PS1 mice (Parr et al., 2012a; Xiao et al., 2014a; Xiao et al., 2015a). With respect to tau, enhancing the autophagy pathway through exogenous TFEB expression in the brain dramatically reduces tau pathology, neurodegeneration, and behavioural deficits in the rTg4510 mouse model (Martini-Stoica et al., 2016b). Moreover, activation of TFEB by fisetin, a naturally occurring flavonol, increases degradation of phosphorylated tau in neurons (Polito et al., 2014). The levels of TFEB expression and phosphorylation status have not yet been established in CHO-Tau35 cells so future work is required to gain further insight of the effect of Tau35 on TFEB.

The decreased number of acidic structures in CHO-Tau35 cells is an indication of impairment in lysosome functionality. Alterations in the pH of lysosomes have been observed in tauopathies (Gomez-Suaga et al., 2011; Lim et al., 2001). Presenilin 1 mutations in AD have been shown to result in failure of V-ATPase V0a1 subunit maturation and assembly of the V-ATPase complex, which is necessary for lysosomal acidification and protease activity (Lee et al., 2015; Lee et al., 2010a). Future work on understanding the reason behind the decrease in acidic structures in CHO-Tau35 cells is required.

A vast array of evidence indicates that disruption of the proteolytic clearance of autophagic vesicles by lysosomes is the principal basis for the neuronal accumulation of autophagic vesicles in AD brain. Even when autophagy is strongly induced in primary cortical neurons by rapamycin, autophagosomes can rapidly mature to autolysosomes without a major build-up of autophagic vacuoles (Boland et al., 2008b). In contrast, the autophagic vacuoles that accumulate in AD brain are autolysosomes and autophagosomes that have been reported to be filled with undigested or partially digested substrates (Nixon et al., 2005b). A similar pattern of autophagic vacuole accumulation and neuritic dystrophy is observed when lysosomal degradation is inhibited by deleting one or more cathepsins (Koike et al., 2000; Koike et al., 2005), by using cysteine protease inhibitors, or

general lysosomal enzyme inhibitors *in vivo* (Boland et al., 2008b; Ivy et al., 1989; Ivy et al., 1984). The reduction in cathepsin D puncta and the colocalisation of cathepsin D with LAMP2 in CHO-Tau35 cells is a further indication of impaired lysosome functionality and this may contribute further to the build-up of phosphorylated tau and lipids in these cells.

AD has long been recognised pathologically by the presence of long-lived protein aggregates such as amyloid plaques and neurofibrillary tangles, that accumulate as the disease progresses. Oxidatively modified proteins, lipids, and DNA additionally accumulate in AD brain (Kamat et al., 2008). As highlighted here, work from this study provides several lines of evidence that indicate a substantial reduction in lysosomal functionality in CHO-Tau35 cells. The accumulation of neutral lipids, further reinforces this finding, illustrating the decline in the degradative capacity of lysosomes. Lipid accumulation was initially identified as being a primary consequence of LSDs, such as Niemann Pick type C disease, in which increased tau phosphorylation is also apparent. (Lieberman et al., 2012; Menzies et al., 2015). Accumulation of lipids ultimately leads to defective lysosomal and non-lysosomal proteins, resulting in the build-up of autophagic and endosomal substrates. Interestingly, on the other hand, the late endosomal lipid marker LBPA was not increased in CHO-Tau35 cells which may indicate normal function of this pathway. However, future work is required to examine the effect of Tau35 expression on the late endocytic pathway.

Overall, the findings from this study provide a detailed understanding of some of the molecular mechanisms of protein degradation that are adversely affected by Tau35 expression. These findings are summarised in Figure 6-1.

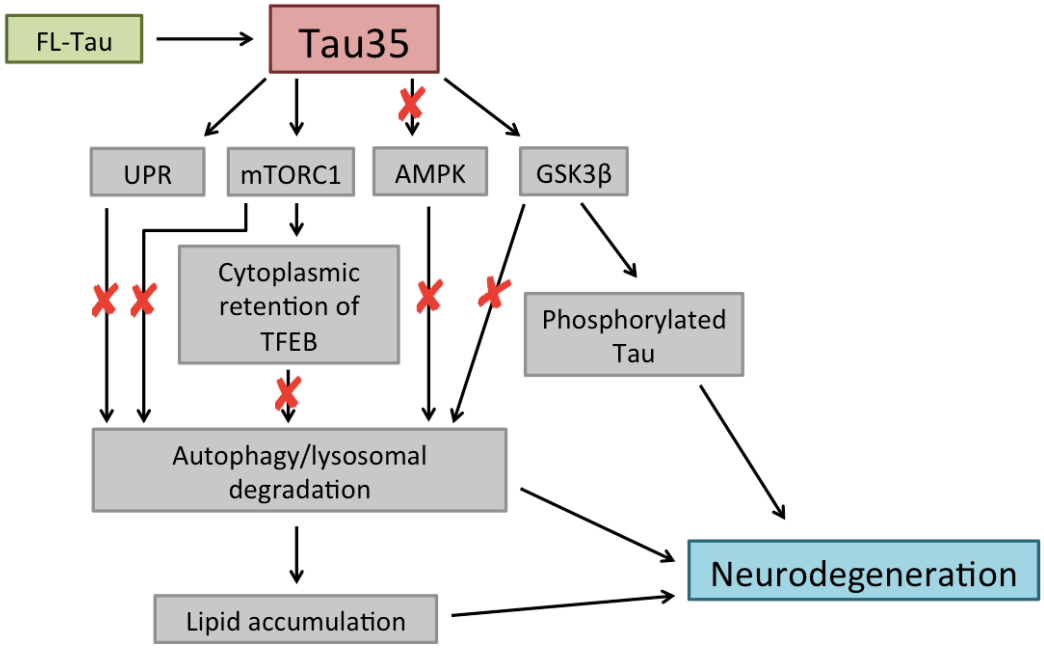

Figure 6-1 Schematic representation of the effects of Tau35 expression in cells: The diagram shows potential mechanisms by which Tau35 could be involved in the development of neurodegenerative disease. Tau35 expression leads to increased activation of the UPR, mTORC1, GSK3β, and inhibits AMPK. These changes lead to reduced activation of the autophagy and lysosomal degradation system, leading to lipid accumulation and neurodegeneration. Increased mTORC1 activation also leads to the cytoplasmic retention of TFEB, which reduces autophagy activation and lysosome biogenesis yielding the same outcome. Increased GSK3β activity causes an accumulation of phosphorylated tau also leading to neurodegeneration. Red crosses indicate inhibition.

6.3 Therapeutic perspectives of this study

Currently there is no cure for the human tauopathies. A great deal of research has been devoted to the identification of therapeutic treatments for AD and other tauopathies. The primary therapeutic approaches that have been considered include increasing microtubule stabilisation, inhibiting tau phosphorylation, enhancing clearance of misfolded tau or NFTs, inhibiting propagation of tau pathology, tau immunotherapy, and attenuating inflammatory pathways (Yoshiyama et al., 2012). Although the evidence for tau-based treatments for AD shows promise, they have not yet been successful. Therefore, alternative treatment strategies that are safe and effective are pivotal for combating these disorders.

In recent years modulating components of the UPR pathway as potential treatment for neurodegenerative disease has received a great deal of attention (C Stefani et al., 2012; Ma and Klann, 2014; Salminen et al., 2009; Scheper and Hoozemans, 2013). Of the three UPR branches, the PERK and IRE1 branches have been extensively described as being involved in AD, PD, HD and ALS (Ferreiro and Pereira, 2012a). On the other hand, given that upstream signals of the UPR may be amplified during the activation process of the UPR, a subtle inhibition of factors involved in the initiation stage of UPR (targets that are more upstream in the pathway) is believed to be able to induce significant therapeutic effects. Hence, inhibition of PERK and IRE1 have been proposed as a potential therapeutic strategy for neurodegenerative disease (Maly and Papa, 2014).

The inhibition of PERK has been attempted via different avenues to reverse the effects of neurodegeneration. The first of these approaches was through the direct knockout of the PERK gene (Ma and Klann, 2014). Deletion of the PERK gene restores the defect in the translation of synaptic proteins and rescues the neurodegenerative phenotype, such as neuronal cell death, and memory impairments in PERK knockout mice (Ma et al., 2013b; Moreno et al., 2012). Furthermore, inhibition of PERK activity has also been targeted by small molecules. Treatment with GSK2606414, an ATP-competitive small molecule inhibitor of PERK, rescued neurodegeneration, similar to genetic interference with the PERK pathway (Moreno et al., 2012). These findings provide a promising proof-of-concept for the effectiveness of PERK inhibition as a feasible therapeutic intervention in disorders

in which the PERK branch of the UPR is activated. However, although such approaches ameliorated neurodegeneration, they also resulted in some severe side effects. For example, homozygous $PERK^{-/-}$ mice displayed severe phenotypic abnormalities, similar to those of people affected by Wolcott–Rallison syndrome, including hepatic and renal dysfunction caused by mutations in the gene encoding PERK (Delépine et al., 2000). Severe abnormalities in the function of the endocrine and exocrine pancreas leading to systemic problems and early mortality were also evident following the knockdown of PERK (Harding et al., 2001; Zhang et al., 2012). Treatment with GSK2606414 also led to severe pancreatic abnormalities (Moreno et al., 2013). Considering increased PERK activation was apparent in the hippocampus of 16-18 month old Tau35 mice, this suggests that inhibiting PERK may be a compelling method to reverse the effects of Tau35 in human tauopathies, but only if the detrimental side effects can be avoided.

Targeting of IRE1 and XBP1 have also been attempted to reduce UPR activation. Given the dual functions of IRE1 as both an RNase and a protein kinase, three types of inhibitors have been developed. Type I kinase inhibitors that inhibit autophosphorylation of IRE1, but have no effect on RNase activity, have yet to show any promise (Wang and Mandelkow, 2012b). Type II inhibitors inhibit both kinase and RNase activities and therefore block all signaling through IRE1 (Ghosh et al., 2014). Type III inhibitors function by inhibiting RNase activity of IRE1 (Cross et al., 2012; Sanches et al., 2014), and these inhibitors could exert protective effects through blocking the generation of activated XBP1. With regards to XBP1, a study of a transgenic model of HD, showed that deletion of XBP1 was protective and accompanied by increased autophagic clearance of the huntingtin aggregates (Vidal et al., 2012). Overall these findings suggest a potential therapeutic strategy through the use of type III IRE1 inhibitors and lowering XBP1 expression in order to reverse over-activation of the UPR

Autophagy upregulation has been shown to have a neuroprotective and anti-ageing role in animal models. Its upregulation as a putative treatment of neurodegeneration, could potentially improve symptoms of neurodegeneration, as it promotes cell survival, improves mitochondrial function and resistance to oxidative stress. Several autophagy-inducing drugs have been shown to decrease the accumulation of protein aggregates and

improve neurodegenerative pathologies. In AD mouse models, long-term rapamycin treatment reduces Aβ42 and rescues cognitive deficits (Boland et al., 2008b; Caccamo et al., 2010b). Furthermore, rapamycin reduces the accumulation of huntingtin and cell death in HD cell models (Ravikumar et al., 2004a; Sarkar et al., 2009), as well as decreasing aberrant protein aggregation in two models of ALS (Wang et al., 2012). The induction of autolysosome formation appears to be a feasible therapeutic strategy for the tauopathies. Indeed, inducing autolysosome formation through rapamycin or temsirolimus, an analogue of rapamycin, has proven to be effective and alleviated tau phosphorylation in neurons and reversed the progression of tau pathology in P301S tau transgenic mice (Jiang et al., 2014; Ozcelik et al., 2013). In CHO-Tau35 cells, rapamycin treatment successfully inhibited activation of mTOR, but failed to rescue the autophagy deficit in these cells. Moreover, phosphorylated tau was not cleared in CHO-Tau35 cells following rapamycin, possibly due to some mTOR-resistant properties of rapamycin (Thoreen and Sabatini, 2009). Therefore, attempting to reverse the autophagic deficit in CHO-Tau35 cells using rapamycin is not a suitable treatment. Treatment with torin 1 may be a better approach to increase autophagic activity through inhibition of mTOR, as this drug does not have the mTOR-resistant properties of rapamycin (Thoreen and Sabatini, 2009).

Tackling deficits in autophagy by targeting mTOR-independent mechanisms has shown promise as a desirable proof of concept. GTM-1, a novel mTOR-independent autophagy inducer, has been shown to ameliorate Aβ pathology in mice (Chu et al., 2013). In addition, trehalose, an mTOR-independent activator of autophagy, has been shown to reduce Aβ accumulation (Rodríguez-Navarro et al., 2010) and facilitate the clearance of mutant α-synuclein *in vitro* (Rodríguez-Navarro et al., 2010). *In vivo,* trehalose has been shown to rescue dopaminergic activity in PD mouse models, to delay pathology in HD mouse models (Hebron et al., 2013; Vidoni et al., 2018), and to prolong lifespan in ALS mice (Castillo et al., 2013). Trehalose has also been shown to reduce tau aggregates and improve neuronal survival in several mouse models of the tauopathies (Congdon et al., 2012; Schaeffer et al., 2012b). Trehalose treatment proved to be effective in CHO-Tau35 cells and rescued the deficits observed in LC3-II. Therefore, the results herein demonstrate that activating autophagy via an mTOR-independent route may be a promising approach to counteract

the reduction of autophagy caused by Tau35 expression, and hence may be of use in human tauopathies.

A drug that has shown great promise for PD treatment is resveratrol. This drug induces autophagy through the AMPK pathway, and has neuroprotective effects in a rodent model of PD (6-OHDA-induced PD rat) (Jin et al., 2008). The mechanism of action of resveratrol has been proposed to involve the rescue of ATG4-mediated autophagosome formation (Vidoni et al., 2018). The anti-diabetic drug metformin and berberine have additionally been shown to modulate autophagy activity through AMPK-dependent mechanisms, although their exact mechanisms of action remain poorly understood. Metformin improves neurodegeneration in AD and HD models (the R6/2 line with ~150 glutamine repeats) (Ma et al., 2007; Song, 2016) and berberine has been shown to induce beneficial effects in the AD P301S transgenic mouse model (Haghani et al., 2015; Jiang et al., 2015).

Direct intracerebral delivery of beclin-1 has also been attempted in PD models in order to enhance the production of autophagosomes. One study resulted in a rescue of neurodegenerative phenotypes observed in a transgenic mouse of PD overexpressing α synuclein. (Spencer et al., 2009). Such findings show potential promise in the use of beclin-1 mimetics or other autophagy inducers for the treatment of neurodegenerative disease. Another therapeutic approach to enhance autophagy activation has been attempted through targeting cathepsins. In this avenue, the use of cystatin B inhibitors is promising, since it ameliorates cognitive decline in AD mouse models (Sun et al., 2008). The proposed mechanism of these inhibitors is to promote lysosomal activity by activating cathepsins, thereby leading to the effective clearance of autophagosomes.

Lithium treatment has also shown some promise for the treatment of neurodegenerative disease (Feng et al., 2008). Lithium suppresses tau phosphorylation in mice via GSK3β inhibition and reduces cell death (Zhang et al., 2011). Moreover, lithium also decreases the levels of inositol 3-phosphates (IP3), which inhibit autophagy (Sade et al., 2016). In this study inhibition of GSK3β activity in CHO-Tau35 cells rescued the decreased activity of autophagy. Inhibiting GSK3β activity has additionally been shown to promote α-tubulin acetylation (Nakakura et al., 2015), which has been noted as a consequence of Tau35

expression in Tau35 mice (Bondulich et al., 2016) and in CHO-Tau35 cells (Guo et al., 2019).

While all of these proposed potential treatment strategies may prevent neurodegeneration, it is important to note that autophagy-enhancing agents may also be detrimental due to over activation of these pathways. Hence, treatment with autophagy-modifying agents will likely require careful consideration of the degree to which these mechanisms are activated/inhibited. Therefore, the dose and times of treatment must be carefully monitored to achieve the optimal balance of autophagy activation.

6.4 Concluding remarks

In conclusion, in this study, a mouse and cell model expressing a disease-associated and N-terminally truncated tau fragment (Tau35) were used. Several important and disease-relevant pathological changes had been previously detected due to expression of Tau35 in mice. The findings from this study provide important insight into some of the underlying molecular mechanisms that lead to tau-mediated neurodegeneration as a consequence of tau truncation. Both the animal and cell models used in this study could serve as useful tools to further elucidate the detrimental effects of Tau35, and could aid in the identification of novel therapeutic interventions.

References

Aguado, C., Sarkar, S., Korolchuk, V.I., Criado, O., Vernia, S., Boya, P., Sanz, P., de Cordoba, S.R., Knecht, E., and Rubinsztein, D.C. (2010). Laforin, the most common protein mutated in Lafora disease, regulates autophagy. Hum Mol Genet *19*, 2867-2876.

Alers, S., Loffler, A.S., Wesselborg, S., and Stork, B. (2012). Role of AMPK-mTOR-Ulk1/2 in the regulation of autophagy: cross talk, shortcuts, and feedbacks. Mol Cell Biol *32*, 2-11.

Allen, B., Ingram, E., Takao, M., Smith, M.J., Jakes, R., Virdee, K., Yoshida, H., Holzer, M., Craxton, M., Emson, P.C.*, et al.* (2002). Abundant tau filaments and nonapoptotic neurodegeneration in transgenic mice expressing human P301S tau protein. J Neurosci *22*, 9340-9351.

Alvarez-Erviti, L., Rodriguez-Oroz, M.C., Cooper, J.M., Caballero, C., Ferrer, I., Obeso, J.A., and Schapira, A.H. (2010). Chaperone-mediated autophagy markers in Parkinson disease brains. Arch Neurol *67*, 1464-1472.

Amadoro, G., Corsetti, V., Ciotti, M., Florenzano, F., Capsoni, S., Amato, G., and Calissano, P. (2011). Endogenous Aβ causes cell death via early tau hyperphosphorylation. Neurobiology of aging *32*, 969-990.

Amadoro, G., Corsetti, V., Stringaro, A., Colone, M., D'Aguanno, S., Meli, G., Ciotti, M., Sancesario, G., Cattaneo, A., and Bussani, R. (2010). A NH 2 tau fragment targets neuronal mitochondria at AD synapses: possible implications for neurodegeneration. Journal of Alzheimer's Disease *21*, 445-470.

Amadoro, G., Serafino, A.L., Barbato, C., Ciotti, M.T., Sacco, A., Calissano, P., and Canu, N. (2004). Role of N-terminal tau domain integrity on the survival of cerebellar granule neurons. Cell Death Differ *11*, 217-230.

An, W.-L., Cowburn, R.F., Li, L., Braak, H., Alafuzoff, I., Iqbal, K., Iqbal, I.-G., Winblad, B., and Pei, J.-J. (2003). Up-regulation of phosphorylated/activated p70 S6 kinase and its relationship to neurofibrillary pathology in Alzheimer's disease. The American journal of pathology *163*, 591-607.

Arai, T., Ikeda, K., Akiyama, H., Nonaka, T., Hasegawa, M., Ishiguro, K., Iritani, S., Tsuchiya, K., Iseki, E., Yagishita, S.*, et al.* (2004). Identification of amino-terminally cleaved tau fragments that distinguish progressive supranuclear palsy from corticobasal degeneration. Ann Neurol *55*, 72-79.

Armstrong, R.A., Lantos, P.L., and Cairns, N.J. (2009). Hippocampal pathology in progressive supranuclear palsy (PSP): a quantitative study of 8 cases. Clin Neuropathol *28*, 46-53.

Avila, J., Lucas, J.J., Pérez, M., and Hernández, F. (2004). Role of Tau Protein in Both Physiological and Pathological Conditions. Physiological Reviews *84*, 361-384.

Axe, E.L., Walker, S.A., Manifava, M., Chandra, P., Roderick, H.L., Habermann, A., Griffiths, G., and Ktistakis, N.T. (2008). Autophagosome formation from membrane compartments enriched in phosphatidylinositol 3-phosphate and dynamically connected to the endoplasmic reticulum. J Cell Biol *182*, 685-701.

B'chir, W., Maurin, A.-C., Carraro, V., Averous, J., Jousse, C., Muranishi, Y., Parry, L., Stepien, G., Fafournoux, P., and Bruhat, A. (2013). The eIF2α/ATF4 pathway is essential for stress-induced autophagy gene expression. Nucleic acids research *41*, 7683-7699.

Barlow, S., Gonzalez-Garay, M.L., West, R.R., Olmsted, J.B., and Cabral, F. (1994). Stable expression of heterologous microtubule-associated proteins (MAPs) in Chinese hamster ovary cells: evidence for differing roles of MAPs in microtubule organization. J Cell Biol *126*, 1017-1029.

Barth, S., Glick, D., and Macleod, K.F. (2010). Autophagy: assays and artifacts. J Pathol *221*, 117-124.

Basurto-Islas, G., Luna-Munoz, J., Guillozet-Bongaarts, A.L., Binder, L.I., Mena, R., and Garcia-Sierra, F. (2008). Accumulation of aspartic acid421- and glutamic acid391-cleaved tau in neurofibrillary tangles correlates with progression in Alzheimer disease. J Neuropathol Exp Neurol *67*, 470-483.

Bedford, L., Paine, S., Sheppard, P.W., Mayer, R.J., and Roelofs, J. (2010). Assembly, structure, and function of the 26S proteasome. Trends Cell Biol *20*, 391-401.

Bendiske, J., and Bahr, B.A. (2003). Lysosomal activation is a compensatory response against protein accumulation and associated synaptopathogenesis--an approach for slowing Alzheimer disease? J Neuropathol Exp Neurol *62*, 451-463.

Berger, Z., Roder, H., Hanna, A., Carlson, A., Rangachari, V., Yue, M., Wszolek, Z., Ashe, K., Knight, J., Dickson, D*., et al.* (2007). Accumulation of pathological tau species and memory loss in a conditional model of tauopathy. J Neurosci *27*, 3650-3662.

Bergeron, C., Pollanen, M.S., Weyer, L., and Lang, A.E. (1997). Cortical degeneration in progressive supranuclear palsy. A comparison with cortical-basal ganglionic degeneration. J Neuropathol Exp Neurol *56*, 726-734.

Bhaskar, K., Yen, S.H., and Lee, G. (2005). Disease-related modifications in tau affect the interaction between Fyn and Tau. J Biol Chem *280*, 35119-35125.

Bhattacharyya, S., Yu, H., Mim, C., and Matouschek, A. (2014). Regulated protein turnover: snapshots of the proteasome in action. Nat Rev Mol Cell Biol *15*, 122-133.

Bi, X., Haque, T.S., Zhou, J., Skillman, A.G., Lin, B., Lee, C.E., Kuntz, I.D., Ellman, J.A., and Lynch, G. (2000). Novel cathepsin D inhibitors block the formation of hyperphosphorylated tau fragments in hippocampus. J Neurochem *74*, 1469-1477.

Biernat, J., and Mandelkow, E.M. (1999). The development of cell processes induced by tau protein requires phosphorylation of serine 262 and 356 in the repeat domain and is inhibited by phosphorylation in the proline-rich domains. Mol Biol Cell *10*, 727-740.

Billingsley, M.L., and Kincaid, R.L. (1997). Regulated phosphorylation and dephosphorylation of tau protein: effects on microtubule interaction, intracellular trafficking and neurodegeneration. Biochemical Journal *323*, 577-591.

Bjorkoy, G., Lamark, T., Brech, A., Outzen, H., Perander, M., Overvatn, A., Stenmark, H., and Johansen, T. (2005). p62/SQSTM1 forms protein aggregates degraded by autophagy and has a protective effect on huntingtin-induced cell death. J Cell Biol *171*, 603-614.

Bjorkoy, G., Lamark, T., and Johansen, T. (2006). p62/SQSTM1: a missing link between protein aggregates and the autophagy machinery. Autophagy *2*, 138-139.

Bockaert, J., and Marin, P. (2015). mTOR in Brain Physiology and Pathologies. Physiol Rev *95*, 1157-1187.

Boland, B., Kumar, A., Lee, S., Platt, F.M., Wegiel, J., Yu, W.H., and Nixon, R.A. (2008). Autophagy induction and autophagosome clearance in neurons: relationship to autophagic pathology in Alzheimer's disease. J Neurosci *28*, 6926-6937.

Boman, A., Svensson, S., Boxer, A., Rojas, J.C., Seeley, W.W., Karydas, A., Miller, B., Kagedal, K., and Svenningsson, P. (2016). Distinct Lysosomal Network Protein Profiles in Parkinsonian Syndrome Cerebrospinal Fluid. J Parkinsons Dis *6*, 307-315.

Bondulich, M.K., Guo, T., Meehan, C., Manion, J., Rodriguez Martin, T., Mitchell, J.C., Hortobagyi, T., Yankova, N., Stygelbout, V., Brion, J.P*., et al.* (2016). Tauopathy induced by low level expression of a human brain-derived tau fragment in mice is rescued by phenylbutyrate. Brain *139*, 2290-2306.

Borroni, B., Agosti, C., Alberici, A., Premi, E., Locatelli, P., and Padovani, A. (2007). "Alien face" in corticobasal degeneration syndrome: extending clinical features. Int Psychogeriatr *19*, 1175-1177.

Botez, G., Probst, A., Ipsen, S., and Tolnay, M. (1999). Astrocytes expressing hyperphosphorylated tau protein without glial fibrillary tangles in argyrophilic grain disease. Acta Neuropathol *98*, 251-256.

Bouge, A.L., and Parmentier, M.L. (2016). Tau excess impairs mitosis and kinesin-5 function, leading to aneuploidy and cell death. Dis Model Mech *9*, 307-319.

Boutajangout, A., Boom, A., Leroy, K., and Brion, J.P. (2004). Expression of tau mRNA and soluble tau isoforms in affected and non-affected brain areas in Alzheimer's disease. FEBS Lett *576*, 183-189.

Boutajangout, A., Sigurdsson, E.M., and Krishnamurthy, P.K. (2011). Tau as a therapeutic target for Alzheimer's disease. Curr Alzheimer Res *8*, 666-677.

Boya, P. (2012). Lysosomal function and dysfunction: mechanism and disease. Antioxid Redox Signal *17*, 766-774.

Braak, E., Arai, K., and Braak, H. (1999). Cerebellar involvement in Pick's disease: affliction of mossy fibers, monodendritic brush cells, and dentate projection neurons. Exp Neurol *159*, 153-163.

Braak, H., and Braak, E. (1991). Neuropathological stageing of Alzheimer-related changes. Acta Neuropathol *82*, 239-259.

Braak, H., and Braak, E. (1995). Staging of Alzheimer's disease-related neurofibrillary changes. Neurobiol Aging *16*, 271-278; discussion 278-284.

Brandt, R., Hundelt, M., and Shahani, N. (2005). Tau alteration and neuronal degeneration in tauopathies: mechanisms and models. Biochim Biophys Acta *1739*, 331-354.

Brookmeyer, R., Johnson, E., Ziegler-Graham, K., and Arrighi, H.M. (2007). Forecasting the global burden of Alzheimer's disease. Alzheimers Dement *3*, 186-191.

Brown, M.R., Bondada, V., Keller, J.N., Thorpe, J., and Geddes, J.W. (2005). Proteasome or calpain inhibition does not alter cellular tau levels in neuroblastoma cells or primary neurons. J Alzheimers Dis *7*, 15-24.

Buckner, R.L. (2013). The cerebellum and cognitive function: 25 years of insight from anatomy and neuroimaging. Neuron *80*, 807-815.

Buee, L., Bussiere, T., Buee-Scherrer, V., Delacourte, A., and Hof, P.R. (2000). Tau protein isoforms, phosphorylation and role in neurodegenerative disorders. Brain Res Brain Res Rev *33*, 95-130.

Bukar Maina, M., Al-Hilaly, Y.K., and Serpell, L.C. (2016). Nuclear Tau and Its Potential Role in Alzheimer's Disease. Biomolecules *6*, 9.

C Stefani, I., Wright, D., M Polizzi, K., and Kontoravdi, C. (2012). The role of ER stress-induced apoptosis in neurodegeneration. Current Alzheimer Research *9*, 373-387.

Caccamo, A., Magri, A., Medina, D.X., Wisely, E.V., Lopez-Aranda, M.F., Silva, A.J., and Oddo, S. (2013a). mTOR regulates tau phosphorylation and degradation: implications for Alzheimer's disease and other tauopathies. Aging Cell *12*, 370-380.

Caccamo, A., Magrì, A., Medina, D.X., Wisely, E.V., López‐Aranda, M.F., Silva, A.J., and Oddo, S. (2013b). mTOR regulates tau phosphorylation and degradation: implications for Alzheimer's disease and other tauopathies. Aging cell *12*, 370-380.

Caccamo, A., Majumder, S., Richardson, A., Strong, R., and Oddo, S. (2010a). Molecular interplay between mammalian target of rapamycin (mTOR), amyloid-beta, and Tau: effects on cognitive impairments. J Biol Chem *285*, 13107-13120.

Caccamo, A., Majumder, S., Richardson, A., Strong, R., and Oddo, S. (2010b). Molecular interplay between mTOR, Aβ and tau: effects on cognitive impairments. Journal of Biological Chemistry, jbc. M110. 100420.

Caccamo, A., Oddo, S., Tran, L.X., and LaFerla, F.M. (2007). Lithium reduces tau phosphorylation but not Aβ or working memory deficits in a transgenic model with both plaques and tangles. American Journal of Pathology *170*, 1669-1675.

Canu, N., Dus, L., Barbato, C., Ciotti, M.T., Brancolini, C., Rinaldi, A.M., Novak, M., Cattaneo, A., Bradbury, A., and Calissano, P. (1998). Tau cleavage and dephosphorylation in cerebellar granule neurons undergoing apoptosis. Journal of Neuroscience *18*, 7061-7074.

Carpio, M.A., Michaud, M., Zhou, W., Fisher, J.K., Walensky, L.D., and Katz, S.G. (2015). BCL-2 family member BOK promotes apoptosis in response to endoplasmic reticulum stress. Proc Natl Acad Sci U S A *112*, 7201-7206.

Casarejos, M.J., Solano, R.M., Gomez, A., Perucho, J., de Yebenes, J.G., and Mena, M.A. (2011). The accumulation of neurotoxic proteins, induced by proteasome inhibition, is reverted by trehalose, an enhancer of autophagy, in human neuroblastoma cells. Neurochem Int *58*, 512-520.

Casas-Tinto, S., Zhang, Y., Sanchez-Garcia, J., Gomez-Velazquez, M., Rincon-Limas, D.E., and Fernandez-Funez, P. (2011). The ER stress factor XBP1s prevents amyloid-beta neurotoxicity. Hum Mol Genet *20*, 2144-2160.

Castillo, K., Nassif, M., Valenzuela, V., Rojas, F., Matus, S., Mercado, G., Court, F.A., van Zundert, B., and Hetz, C. (2013). Trehalose delays the progression of amyotrophic lateral sclerosis by enhancing autophagy in motoneurons. Autophagy *9*, 1308-1320.

Cataldo, A.M., Peterhoff, C.M., Schmidt, S.D., Terio, N.B., Duff, K., Beard, M., Mathews, P.M., and Nixon, R.A. (2004). Presenilin mutations in familial Alzheimer disease and transgenic mouse models accelerate neuronal lysosomal pathology. J Neuropathol Exp Neurol *63*, 821-830.

Chamoux, E., McManus, S., Laberge, G., Bisson, M., and Roux, S. (2013). Involvement of kinase PKC-zeta in the p62/p62(P392L)-driven activation of NF-kappaB in human osteoclasts. Biochim Biophys Acta *1832*, 475-484.

Chang, R.C., Suen, K.C., Ma, C.H., Elyaman, W., Ng, H.K., and Hugon, J. (2002). Involvement of double-stranded RNA-dependent protein kinase and phosphorylation of eukaryotic initiation factor-2alpha in neuronal degeneration. J Neurochem *83*, 1215-1225.

Chapel, A., Kieffer-Jaquinod, S., Sagne, C., Verdon, Q., Ivaldi, C., Mellal, M., Thirion, J., Jadot, M., Bruley, C., Garin, J*., et al.* (2013). An extended proteome map of the lysosomal membrane reveals novel potential transporters. Mol Cell Proteomics *12*, 1572-1588.

Chazotte, B. (2011). Labeling membrane glycoproteins or glycolipids with fluorescent wheat germ agglutinin. Cold Spring Harb Protoc *2011*, pdb prot5623.

Chen, J., Kanai, Y., Cowan, N.J., and Hirokawa, N. (1992). Projection domains of MAP2 and tau determine spacings between microtubules in dendrites and axons. Nature *360*, 674-677.

Cho, D.H., Jo, Y.K., Hwang, J.J., Lee, Y.M., Roh, S.A., and Kim, J.C. (2009). Caspase-mediated cleavage of ATG6/Beclin-1 links apoptosis to autophagy in HeLa cells. Cancer Lett *274*, 95-100.

Cho, J.H., and Johnson, G.V. (2004). Glycogen synthase kinase 3 beta induces caspase-cleaved tau aggregation in situ. J Biol Chem *279*, 54716-54723.

Chu, C., Zhang, X., Ma, W., Li, L., Wang, W., Shang, L., and Fu, P. (2013). Induction of autophagy by a novel small molecule improves aβ pathology and ameliorates cognitive deficits. PLoS One *8*, e65367.

Chu, C.T., Zhu, J., and Dagda, R. (2007). Beclin 1-independent pathway of damage-induced mitophagy and autophagic stress: implications for neurodegeneration and cell death. Autophagy *3*, 663-666.

Chung, C.W., Song, Y.H., Kim, I.K., Yoon, W.J., Ryu, B.R., Jo, D.G., Woo, H.N., Kwon, Y.K., Kim, H.H., Gwag, B.J*., et al.* (2001). Proapoptotic effects of tau cleavage product generated by caspase-3. Neurobiol Dis *8*, 162-172.

Ciechanover, A., and Brundin, P. (2003). The ubiquitin proteasome system in neurodegenerative diseases: sometimes the chicken, sometimes the egg. Neuron *40*, 427-446.

Ciechanover, A., and Kwon, Y.T. (2015). Degradation of misfolded proteins in neurodegenerative diseases: therapeutic targets and strategies. Exp Mol Med *47*, e147.

Clavaguera, F., Akatsu, H., Fraser, G., Crowther, R.A., Frank, S., Hench, J., Probst, A., Winkler, D.T., Reichwald, J., and Staufenbiel, M. (2013). Brain homogenates from human tauopathies induce tau inclusions in mouse brain. Proceedings of the National Academy of Sciences *110*, 9535-9540.

Clelland, C.D., Choi, M., Romberg, C., Clemenson, G.D., Jr., Fragniere, A., Tyers, P., Jessberger, S., Saksida, L.M., Barker, R.A., Gage, F.H*., et al.* (2009). A functional role for adult hippocampal neurogenesis in spatial pattern separation. Science *325*, 210-213.

Cohen, T.J., Guo, J.L., Hurtado, D.E., Kwong, L.K., Mills, I.P., Trojanowski, J.Q., and Lee, V.M. (2011). The acetylation of tau inhibits its function and promotes pathological tau aggregation. Nat Commun *2*, 252.

Colacurcio, D.J., and Nixon, R.A. (2016). Disorders of lysosomal acidification-The emerging role of v-ATPase in aging and neurodegenerative disease. Ageing Res Rev *32*, 75-88.

Congdon, E.E., Wu, J.W., Myeku, N., Figueroa, Y.H., Herman, M., Marinec, P.S., Gestwicki, J.E., Dickey, C.A., Yu, W.H., and Duff, K.E. (2012). Methylthioninium chloride (methylene blue) induces autophagy and attenuates tauopathy in vitro and in vivo. Autophagy *8*, 609-622.

Connell, J.W., Gibb, G.M., Betts, J.C., Blackstock, W.P., Gallo, J., Lovestone, S., Hutton, M., and Anderton, B.H. (2001). Effects of FTDP-17 mutations on the in vitro phosphorylation of tau by glycogen synthase kinase 3beta identified by mass spectrometry demonstrate certain mutations exert long-range conformational changes. FEBS Lett *493*, 40-44.

Cook, C., Carlomagno, Y., Gendron, T.F., Dunmore, J., Scheffel, K., Stetler, C., Davis, M., Dickson, D., Jarpe, M., DeTure, M.*, et al.* (2014a). Acetylation of the KXGS motifs in tau is a critical determinant in modulation of tau aggregation and clearance. Hum Mol Genet *23*, 104-116.

Cook, C., Dunmore, J.H., Murray, M.E., Scheffel, K., Shukoor, N., Tong, J., Castanedes-Casey, M., Phillips, V., Rousseau, L., Penuliar, M.S.*, et al.* (2014b). Severe amygdala dysfunction in a MAPT transgenic mouse model of frontotemporal dementia. Neurobiol Aging *35*, 1769-1777.

Corsetti, V., Amadoro, G., Gentile, A., Capsoni, S., Ciotti, M.T., Cencioni, M.T., Atlante, A., Canu, N., Rohn, T.T., Cattaneo, A.*, et al.* (2008). Identification of a caspase-derived N-terminal tau fragment in cellular and animal Alzheimer's disease models. Molecular and cellular neurosciences *38*, 381-392.

Criollo, A., Vicencio, J.M., Tasdemir, E., Maiuri, M.C., Lavandero, S., and Kroemer, G. (2007). The inositol trisphosphate receptor in the control of autophagy. Autophagy *3*, 350-353.

Cross, B.C., Bond, P.J., Sadowski, P.G., Jha, B.K., Zak, J., Goodman, J.M., Silverman, R.H., Neubert, T.A., Baxendale, I.R., and Ron, D. (2012). The molecular basis for selective inhibition of unconventional mRNA splicing by an IRE1-binding small molecule. Proceedings of the National Academy of Sciences *109*, E869-E878.

Cross, D.A., Alessi, D.R., Cohen, P., Andjelkovich, M., and Hemmings, B.A. (1995). Inhibition of glycogen synthase kinase-3 by insulin mediated by protein kinase B. Nature *378*, 785-789.

Crowther, T., Goedert, M., and Wischik, C.M. (1989). The repeat region of microtubule-associated protein tau forms part of the core of the paired helical filament of Alzheimer's disease. Ann Med *21*, 127-132.

Crump, C.J., Johnson, D.S., and Li, Y.M. (2013). Development and mechanism of gamma-secretase modulators for Alzheimer's disease. Biochemistry *52*, 3197-3216.

Cuervo, A.M., and Dice, J.F. (2000). Regulation of lamp2a levels in the lysosomal membrane. Traffic *1*, 570-583.

Curcio-Morelli, C., Charles, F.A., Micsenyi, M.C., Cao, Y., Venugopal, B., Browning, M.F., Dobrenis, K., Cotman, S.L., Walkley, S.U., and Slaugenhaupt, S.A. (2010). Macroautophagy is defective in mucolipin-1-deficient mouse neurons. Neurobiol Dis *40*, 370-377.

Czabotar, P.E., Lessene, G., Strasser, A., and Adams, J.M. (2014). Control of apoptosis by the BCL-2 protein family: implications for physiology and therapy. Nature reviews Molecular cell biology *15*, 49.

Damme, M., Suntio, T., Saftig, P., and Eskelinen, E.L. (2015). Autophagy in neuronal cells: general principles and physiological and pathological functions. Acta Neuropathol *129*, 337-362.

Dantuma, N.P., and Bott, L.C. (2014). The ubiquitin-proteasome system in neurodegenerative diseases: precipitating factor, yet part of the solution. Front Mol Neurosci *7*, 70.

David, D.C., Layfield, R., Serpell, L., Narain, Y., Goedert, M., and Spillantini, M.G. (2002). Proteasomal degradation of tau protein. J Neurochem *83*, 176-185.

Davies, S.W., Turmaine, M., Cozens, B.A., DiFiglia, M., Sharp, A.H., Ross, C.A., Scherzinger, E., Wanker, E.E., Mangiarini, L., and Bates, G.P. (1997). Formation of neuronal intranuclear inclusions underlies the neurological dysfunction in mice transgenic for the HD mutation. Cell *90*, 537-548.

de Barreda, E.G., and Avila, J. (2010). Is tau a suitable therapeutical target in tauopathies? World J Biol Chem *1*, 81-84.

de Silva, R., Lashley, T., Strand, C., Shiarli, A.M., Shi, J., Tian, J., Bailey, K.L., Davies, P., Bigio, E.H., Arima, K.*, et al.* (2006). An immunohistochemical study of cases of sporadic and inherited frontotemporal lobar degeneration using 3R- and 4R-specific tau monoclonal antibodies. Acta Neuropathol *111*, 329-340.

De Strooper, B. (2010). Proteases and proteolysis in Alzheimer disease: a multifactorial view on the disease process. Physiological reviews *90*, 465-494.

Decressac, M., Mattsson, B., Weikop, P., Lundblad, M., Jakobsson, J., and Bjorklund, A. (2013). TFEB-mediated autophagy rescues midbrain dopamine neurons from alpha-synuclein toxicity. Proc Natl Acad Sci U S A *110*, E1817-1826.

Deegan, S., Saveljeva, S., Gorman, A.M., and Samali, A. (2013). Stress-induced self-cannibalism: on the regulation of autophagy by endoplasmic reticulum stress. Cellular and Molecular Life Sciences *70*, 2425-2441.

Dehay, B., Bove, J., Rodriguez-Muela, N., Perier, C., Recasens, A., Boya, P., and Vila, M. (2010). Pathogenic lysosomal depletion in Parkinson's disease. J Neurosci *30*, 12535-12544.

Dehay, B., Martinez-Vicente, M., Caldwell, G.A., Caldwell, K.A., Yue, Z., Cookson, M.R., Klein, C., Vila, M., and Bezard, E. (2013). Lysosomal impairment in Parkinson's disease. Mov Disord *28*, 725-732.

Delacourte, A., Robitaille, Y., Sergeant, N., Buee, L., Hof, P.R., Wattez, A., Laroche-Cholette, A., Mathieu, J., Chagnon, P., and Gauvreau, D. (1996). Specific pathological Tau protein variants characterize Pick's disease. J Neuropathol Exp Neurol *55*, 159-168.

Delépine, M., Nicolino, M., Barrett, T., Golamaully, M., Lathrop, G.M., and Julier, C. (2000). EIF2AK3, encoding translation initiation factor 2-α kinase 3, is mutated in patients with Wolcott-Rallison syndrome. Nature genetics *25*, 406.

Delobel, P., Lavenir, I., Fraser, G., Ingram, E., Holzer, M., Ghetti, B., Spillantini, M.G., Crowther, R.A., and Goedert, M. (2008). Analysis of tau phosphorylation and truncation in a mouse model of human tauopathy. Am J Pathol *172*, 123-131.

Deming, Y., Xia, J., Cai, Y., Lord, J., Holmans, P., Bertelsen, S., Holtzman, D., Morris, J.C., Bales, K., Pickering, E.H.*, et al.* (2016). A potential endophenotype for Alzheimer's disease: cerebrospinal fluid clusterin. Neurobiol Aging *37*, 208 e201-208 e209.

Deng, Z., Purtell, K., Lachance, V., Wold, M.S., Chen, S., and Yue, Z. (2017). Autophagy Receptors and Neurodegenerative Diseases. Trends Cell Biol *27*, 491-504.

Dhanasekaran, D.N., and Reddy, E.P. (2008). JNK signaling in apoptosis. Oncogene *27*, 6245-6251.

Diao, J., Liu, R., Rong, Y., Zhao, M., Zhang, J., Lai, Y., Zhou, Q., Wilz, L.M., Li, J., Vivona, S.*, et al.* (2015). ATG14 promotes membrane tethering and fusion of autophagosomes to endolysosomes. Nature *520*, 563-566.

Ding, H., Dolan, P.J., and Johnson, G.V. (2008). Histone deacetylase 6 interacts with the microtubule-associated protein tau. J Neurochem *106*, 2119-2130.

Dite, T.A., Ling, N.X.Y., Scott, J.W., Hoque, A., Galic, S., Parker, B.L., Ngoei, K.R.W., Langendorf, C.G., O'Brien, M.T., Kundu, M.*, et al.* (2017). The autophagy initiator ULK1 sensitizes AMPK to allosteric drugs. Nat Commun *8*, 571.

Dixit, R., Ross, J.L., Goldman, Y.E., and Holzbaur, E.L. (2008). Differential regulation of dynein and kinesin motor proteins by tau. Science *319*, 1086-1089.

Dolan, P.J., and Johnson, G.V. (2010). The role of tau kinases in Alzheimer's disease. Curr Opin Drug Discov Devel *13*, 595-603.

Dubey, J., Ratnakaran, N., and Koushika, S.P. (2015). Neurodegeneration and microtubule dynamics: death by a thousand cuts. Front Cell Neurosci *9*, 343.

Duran, A., Amanchy, R., Linares, J.F., Joshi, J., Abu-Baker, S., Porollo, A., Hansen, M., Moscat, J., and Diaz-Meco, M.T. (2011). p62 is a key regulator of nutrient sensing in the mTORC1 pathway. Mol Cell *44*, 134-146.

Egan, D.F., Shackelford, D.B., Mihaylova, M.M., Gelino, S., Kohnz, R.A., Mair, W., Vasquez, D.S., Joshi, A., Gwinn, D.M., Taylor, R*., et al.* (2011). Phosphorylation of ULK1 (hATG1) by AMP-activated protein kinase connects energy sensing to mitophagy. Science *331*, 456-461.

Eidenmuller, J., Fath, T., Maas, T., Pool, M., Sontag, E., and Brandt, R. (2001). Phosphorylation-mimicking glutamate clusters in the proline-rich region are sufficient to simulate the functional deficiencies of hyperphosphorylated tau protein. Biochem J *357*, 759-767.

Elrick, G. (2002). Less whingeing on pay or we alienate the public. Nurs Stand *16*, 30.

Engel, T., Goñi-Oliver, P., Lucas, J.J., Avila, J., and Hernández, F. (2006). Chronic lithium administration to FTDP-17 tau and GSK-3β overexpressing mice prevents tau hyperphosphorylation and neurofibrillary tangle formation, but pre-formed neurofibrillary tangles do not revert. Journal of neurochemistry *99*, 1445-1455.

Eskelinen, E.L. (2005). Maturation of autophagic vacuoles in Mammalian cells. Autophagy *1*, 1-10.

Fang, X., Yu, S.X., Lu, Y., Bast, R.C., Jr., Woodgett, J.R., and Mills, G.B. (2000). Phosphorylation and inactivation of glycogen synthase kinase 3 by protein kinase A. Proc Natl Acad Sci U S A *97*, 11960-11965.

Fasulo, L., Ugolini, G., Visintin, M., Bradbury, A., Brancolini, C., Verzillo, V., Novak, M., and Cattaneo, A. (2000). The neuronal microtubule‐associated protein tau is a substrate for caspase‐3 and an effector of apoptosis. Journal of neurochemistry *75*, 624-633.

Fath, T., Eidenmuller, J., and Brandt, R. (2002). Tau-mediated cytotoxicity in a pseudohyperphosphorylation model of Alzheimer's disease. J Neurosci *22*, 9733-9741.

Fecto, F., and Siddique, T. (2011). SIGMAR1 mutations, genetic heterogeneity at the chromosome 9p locus, and the expanding etiological diversity of amyotrophic lateral sclerosis. Ann Neurol *70*, 867-870.

Fecto, F., Yan, J., Vemula, S.P., Liu, E., Yang, Y., Chen, W., Zheng, J.G., Shi, Y., Siddique, N., Arrat, H*., et al.* (2011). SQSTM1 mutations in familial and sporadic amyotrophic lateral sclerosis. Arch Neurol *68*, 1440-1446.

Felbor, U., Kessler, B., Mothes, W., Goebel, H.H., Ploegh, H.L., Bronson, R.T., and Olsen, B.R. (2002). Neuronal loss and brain atrophy in mice lacking cathepsins B and L. Proc Natl Acad Sci U S A *99*, 7883-7888.

Feng, H.-L., Leng, Y., Ma, C.-H., Zhang, J., Ren, M., and Chuang, D.-M. (2008). Combined lithium and valproate treatment delays disease onset, reduces neurological deficits and prolongs survival in an amyotrophic lateral sclerosis mouse model. Neuroscience *155*, 567-572.

Fernandez-Montoya, J., and Perez, M. (2015). Cathepsin D in a murine model of frontotemporal dementia with Parkinsonism-linked to chromosome 17. J Alzheimers Dis *45*, 1-14.

Ferreiro, E., and Pereira, C.M. (2012a). Endoplasmic reticulum stress: a new playER in tauopathies. The Journal of pathology *226*, 687-692.

Ferreiro, E., and Pereira, C.M. (2012b). Endoplasmic reticulum stress: a new playER in tauopathies. J Pathol *226*, 687-692.

Ferrucci, M., Fulceri, F., Toti, L., Soldani, P., Siciliano, G., Paparelli, A., and Fornai, F. (2011). Protein clearing pathways in ALS. Arch Ital Biol *149*, 121-149.

Feuillette, S., Blard, O., Lecourtois, M., Frebourg, T., Campion, D., and Dumanchin, C. (2005). Tau is not normally degraded by the proteasome. J Neurosci Res *80*, 400-405.

Filipcik, P., Zilka, N., Bugos, O., Kucerak, J., Koson, P., Novak, P., and Novak, M. (2012). First transgenic rat model developing progressive cortical neurofibrillary tangles. Neurobiology of aging *33*, 1448-1456.

Finkel, T. (2015). The metabolic regulation of aging. Nat Med *21*, 1416-1423.

Flament, S., Delacourte, A., Verny, M., Hauw, J.J., and Javoy-Agid, F. (1991). Abnormal Tau proteins in progressive supranuclear palsy. Similarities and differences with the neurofibrillary degeneration of the Alzheimer type. Acta Neuropathol *81*, 591-596.

Fontaine, S.N., Sabbagh, J.J., Baker, J., Martinez-Licha, C.R., Darling, A., and Dickey, C.A. (2015). Cellular factors modulating the mechanism of tau protein aggregation. Cell Mol Life Sci *72*, 1863-1879.

Forman, M.S., Trojanowski, J.Q., and Lee, V.M. (2004). Neurodegenerative diseases: a decade of discoveries paves the way for therapeutic breakthroughs. Nat Med *10*, 1055-1063.

Friedlander, R.M. (2003). Apoptosis and caspases in neurodegenerative diseases. N Engl J Med *348*, 1365-1375.

Gallo, J.M., Hanger, D.P., Twist, E.C., Kosik, K.S., and Anderton, B.H. (1992). Expression and phosphorylation of a three-repeat isoform of tau in transfected non-neuronal cells. Biochem J *286 (Pt 2)*, 399-404.

Galluzzi, L., Kepp, O., Zitvogel, L., and Kroemer, G. (2010). Bacterial invasion: linking autophagy and innate immunity. Curr Biol *20*, R106-108.

Gamblin, T.C., Chen, F., Zambrano, A., Abraha, A., Lagalwar, S., Guillozet, A.L., Lu, M., Fu, Y., Garcia-Sierra, F., LaPointe, N.*, et al.* (2003). Caspase cleavage of tau: linking amyloid and neurofibrillary tangles in Alzheimer's disease. Proc Natl Acad Sci U S A *100*, 10032-10037.

Ganley, I.G., Lam du, H., Wang, J., Ding, X., Chen, S., and Jiang, X. (2009). ULK1.ATG13.FIP200 complex mediates mTOR signaling and is essential for autophagy. J Biol Chem *284*, 12297-12305.

Ganley, I.G., Wong, P.M., Gammoh, N., and Jiang, X. (2011). Distinct autophagosomal-lysosomal fusion mechanism revealed by thapsigargin-induced autophagy arrest. Mol Cell *42*, 731-743.

Garcia-Sierra, F., Mondragon-Rodriguez, S., and Basurto-Islas, G. (2008). Truncation of tau protein and its pathological significance in Alzheimer's disease. J Alzheimers Dis *14*, 401-409.

Garg, S., Timm, T., Mandelkow, E.-M., Mandelkow, E., and Wang, Y. (2011). Cleavage of Tau by calpain in Alzheimer's disease: the quest for the toxic 17 kD fragment. Neurobiology of aging *32*, 1-14.

Garwood, C.J., Pooler, A.M., Atherton, J., Hanger, D.P., and Noble, W. (2011). Astrocytes are important mediators of Abeta-induced neurotoxicity and tau phosphorylation in primary culture. Cell Death Dis *2*, e167.

Geeraert, C., Ratier, A., Pfisterer, S.G., Perdiz, D., Cantaloube, I., Rouault, A., Pattingre, S., Proikas-Cezanne, T., Codogno, P., and Pous, C. (2010). Starvation-induced hyperacetylation of tubulin is required for the stimulation of autophagy by nutrient deprivation. J Biol Chem *285*, 24184-24194.

Ghosh, R., Wang, L., Wang, E.S., Perera, B.G.K., Igbaria, A., Morita, S., Prado, K., Thamsen, M., Caswell, D., and Macias, H. (2014). Allosteric inhibition of the IRE1α RNase preserves cell viability and function during endoplasmic reticulum stress. Cell *158*, 534-548.

Giacomini, C., Koo, C.-Y., Yankova, N., Tavares, I.A., Wray, S., Noble, W., Hanger, D.P., and Morris, J.D. (2018). A new TAO kinase inhibitor reduces tau phosphorylation at sites associated with neurodegeneration in human tauopathies. Acta neuropathologica communications *6*, 37.

Gillissen, M.A., Yasuda, E., de Jong, G., Levie, S.E., Go, D., Spits, H., van Helden, P.M., and Hazenberg, M.D. (2016). The modified FACS calcein AM retention assay: A high throughput flow cytometer based method to measure cytotoxicity. J Immunol Methods *434*, 16-23.

Gipson, T.T., and Johnston, M.V. (2012). Plasticity and mTOR: towards restoration of impaired synaptic plasticity in mTOR-related neurogenetic disorders. Neural Plast *2012*, 486402.

Gitler, D., Takagishi, Y., Feng, J., Ren, Y., Rodriguiz, R.M., Wetsel, W.C., Greengard, P., and Augustine, G.J. (2004). Different presynaptic roles of synapsins at excitatory and inhibitory synapses. J Neurosci *24*, 11368-11380.

Glabe, C. (2001). Intracellular mechanisms of amyloid accumulation and pathogenesis in Alzheimer's disease. J Mol Neurosci *17*, 137-145.

Goedert, M. (2004). Tau protein and neurodegeneration. Semin Cell Dev Biol *15*, 45-49.

Goedert, M., and Jakes, R. (1990). Expression of separate isoforms of human tau protein: correlation with the tau pattern in brain and effects on tubulin polymerization. EMBO J *9*, 4225-4230.

Golde, T.E., Schneider, L.S., and Koo, E.H. (2011). Anti-aβ therapeutics in Alzheimer's disease: the need for a paradigm shift. Neuron *69*, 203-213.

Gomez-Suaga, P., Luzon-Toro, B., Churamani, D., Zhang, L., Bloor-Young, D., Patel, S., Woodman, P.G., Churchill, G.C., and Hilfiker, S. (2011). Leucine-rich repeat kinase 2 regulates autophagy through a calcium-dependent pathway involving NAADP. Human molecular genetics *21*, 511-525.

Gong, C.X., and Iqbal, K. (2008). Hyperphosphorylation of microtubule-associated protein tau: a promising therapeutic target for Alzheimer disease. Curr Med Chem *15*, 2321-2328.

Goode, N., Hughes, K., Woodgett, J.R., and Parker, P.J. (1992). Differential regulation of glycogen synthase kinase-3 beta by protein kinase C isotypes. J Biol Chem *267*, 16878-16882.

Gotzl, J.K., Mori, K., Damme, M., Fellerer, K., Tahirovic, S., Kleinberger, G., Janssens, J., van der Zee, J., Lang, C.M., Kremmer, E.*, et al.* (2014). Common pathobiochemical hallmarks of progranulin-associated frontotemporal lobar degeneration and neuronal ceroid lipofuscinosis. Acta Neuropathol *127*, 845-860.

Gowrishankar, S., Yuan, P., Wu, Y., Schrag, M., Paradise, S., Grutzendler, J., De Camilli, P., and Ferguson, S.M. (2015). Massive accumulation of luminal protease-deficient axonal lysosomes at Alzheimer's disease amyloid plaques. Proc Natl Acad Sci U S A *112*, E3699-3708.

Guillozet-Bongaarts, A.L., Cahill, M.E., Cryns, V.L., Reynolds, M.R., Berry, R.W., and Binder, L.I. (2006). Pseudophosphorylation of tau at serine 422 inhibits caspase cleavage: in vitro evidence and implications for tangle formation in vivo. J Neurochem *97*, 1005-1014.

Guillozet-Bongaarts, A.L., Garcia-Sierra, F., Reynolds, M.R., Horowitz, P.M., Fu, Y., Wang, T., Cahill, M.E., Bigio, E.H., Berry, R.W., and Binder, L.I. (2005). Tau truncation during neurofibrillary tangle evolution in Alzheimer's disease. Neurobiology of aging *26*, 1015-1022.

Guise, S., Braguer, D., Carles, G., Delacourte, A., and Briand, C. (2001). Hyperphosphorylation of tau is mediated by ERK activation during anticancer drug-induced apoptosis in neuroblastoma cells. J Neurosci Res *63*, 257-267.

Guo, H., Albrecht, S., Bourdeau, M., Petzke, T., Bergeron, C., and LeBlanc, A.C. (2004). Active caspase-6 and caspase-6-cleaved tau in neuropil threads, neuritic plaques, and neurofibrillary tangles of Alzheimer's disease. The American journal of pathology *165*, 523-531.

Guo, T., Dakkak, D., Rodriguez-Martin, T., Noble, W., and Hanger, D.P. (2019). A pathogenic tau fragment compromises microtubules, disrupts insulin signaling and induces the unfolded protein response. Acta Neuropathol Commun *7*, 2.

Guo, T., Noble, W., and Hanger, D.P. (2017). Roles of tau protein in health and disease. Acta Neuropathol *133*, 665-704.

Gwinn, D.M., Shackelford, D.B., Egan, D.F., Mihaylova, M.M., Mery, A., Vasquez, D.S., Turk, B.E., and Shaw, R.J. (2008). AMPK phosphorylation of raptor mediates a metabolic checkpoint. Mol Cell *30*, 214-226.

Haghani, M., Shabani, M., and Tondar, M. (2015). The therapeutic potential of berberine against the altered intrinsic properties of the CA1 neurons induced by Aβ neurotoxicity. European journal of pharmacology *758*, 82-88.

Halliday, M., and Mallucci, G.R. (2014). Targeting the unfolded protein response in neurodegeneration: A new approach to therapy. Neuropharmacology *76 Pt A*, 169-174.

Halliday, M., Radford, H., Zents, K.A.M., Molloy, C., Moreno, J.A., Verity, N.C., Smith, E., Ortori, C.A., Barrett, D.A., Bushell, M.*, et al.* (2017). Repurposed drugs targeting eIF2α-P-mediated translational repression prevent neurodegeneration in mice. Brain *140*, 1768-1783.

Hamano, T., Gendron, T.F., Causevic, E., Yen, S.H., Lin, W.L., Isidoro, C., Deture, M., and Ko, L.W. (2008). Autophagic-lysosomal perturbation enhances tau aggregation in transfectants with induced wild-type tau expression. Eur J Neurosci *27*, 1119-1130.

Hanger, D.P., Anderton, B.H., and Noble, W. (2009a). Tau phosphorylation: the therapeutic challenge for neurodegenerative disease. Trends Mol Med *15*, 112-119.

Hanger, D.P., Byers, H.L., Wray, S., Leung, K.Y., Saxton, M.J., Seereeram, A., Reynolds, C.H., Ward, M.A., and Anderton, B.H. (2007). Novel phosphorylation sites in tau from Alzheimer brain support a role for casein kinase 1 in disease pathogenesis. J Biol Chem *282*, 23645-23654.

Hanger, D.P., Seereeram, A., and Noble, W. (2009b). Mediators of tau phosphorylation in the pathogenesis of Alzheimer's disease. Expert Rev Neurother *9*, 1647-1666.

Hanger, D.P., and Wray, S. (2010). Tau cleavage and tau aggregation in neurodegenerative disease. Biochem Soc Trans *38*, 1016-1020.

Hardie, D.G. (2011). AMP-activated protein kinase: an energy sensor that regulates all aspects of cell function. Genes Dev *25*, 1895-1908.

Harding, H.P., Zeng, H., Zhang, Y., Jungries, R., Chung, P., Plesken, H., Sabatini, D.D., and Ron, D. (2001). Diabetes mellitus and exocrine pancreatic dysfunction in perk−/− mice reveals a role for translational control in secretory cell survival. Molecular cell *7*, 1153-1163.

Hawley, S.A., Pan, D.A., Mustard, K.J., Ross, L., Bain, J., Edelman, A.M., Frenguelli, B.G., and Hardie, D.G. (2005). Calmodulin-dependent protein kinase kinase-beta is an alternative upstream kinase for AMP-activated protein kinase. Cell Metab *2*, 9-19.

Hayashi-Nishino, M., Fujita, N., Noda, T., Yamaguchi, A., Yoshimori, T., and Yamamoto, A. (2009). A subdomain of the endoplasmic reticulum forms a cradle for autophagosome formation. Nat Cell Biol *11*, 1433-1437.

He, S., Wang, L., Miao, L., Wang, T., Du, F., Zhao, L., and Wang, X. (2009). Receptor interacting protein kinase-3 determines cellular necrotic response to TNF-alpha. Cell *137*, 1100-1111.

Hebron, M.L., Lonskaya, I., and Moussa, C.E.-H. (2013). Nilotinib reverses loss of dopamine neurons and improves motor behavior via autophagic degradation of α-synuclein in Parkinson's disease models. Human molecular genetics *22*, 3315-3328.

Herrero-Martin, G., Hoyer-Hansen, M., Garcia-Garcia, C., Fumarola, C., Farkas, T., Lopez-Rivas, A., and Jaattela, M. (2009). TAK1 activates AMPK-dependent cytoprotective autophagy in TRAIL-treated epithelial cells. EMBO J *28*, 677-685.

Hershko, A. (1991). The ubiquitin pathway for protein degradation. Trends in biochemical sciences *16*, 265-268.

Hetz, C., and Mollereau, B. (2014). Disturbance of endoplasmic reticulum proteostasis in neurodegenerative diseases. Nat Rev Neurosci *15*, 233-249.

Ho, Y.S., Yang, X., Lau, J.C., Hung, C.H., Wuwongse, S., Zhang, Q., Wang, J., Baum, L., So, K.F., and Chang, R.C. (2012). Endoplasmic reticulum stress induces tau pathology and forms a vicious cycle: implication in Alzheimer's disease pathogenesis. J Alzheimers Dis *28*, 839-854.

Hoeffer, C.A., and Klann, E. (2010). mTOR signaling: at the crossroads of plasticity, memory and disease. Trends Neurosci *33*, 67-75.

Hofling, C., Morawski, M., Zeitschel, U., Zanier, E.R., Moschke, K., Serdaroglu, A., Canneva, F., von Horsten, S., De Simoni, M.G., Forloni, G.*, et al.* (2016). Differential transgene

expression patterns in Alzheimer mouse models revealed by novel human amyloid precursor protein-specific antibodies. Aging Cell *15*, 953-963.

Höglinger, G.U., Melhem, N.M., Dickson, D.W., Sleiman, P.M., Wang, L.-S., Klei, L., Rademakers, R., De Silva, R., Litvan, I., and Riley, D.E. (2011). Identification of common variants influencing risk of the tauopathy progressive supranuclear palsy. Nature genetics *43*, 699.

Hoover, B.R., Reed, M.N., Su, J., Penrod, R.D., Kotilinek, L.A., Grant, M.K., Pitstick, R., Carlson, G.A., Lanier, L.M., and Yuan, L.-L. (2010). Tau mislocalization to dendritic spines mediates synaptic dysfunction independently of neurodegeneration. Neuron *68*, 1067-1081.

Hoozemans, J.J., van Haastert, E.S., Nijholt, D.A., Rozemuller, A.J., Eikelenboom, P., and Scheper, W. (2009). The unfolded protein response is activated in pretangle neurons in Alzheimer's disease hippocampus. Am J Pathol *174*, 1241-1251.

Hoozemans, J.J., van Haastert, E.S., Nijholt, D.A., Rozemuller, A.J., and Scheper, W. (2012). Activation of the unfolded protein response is an early event in Alzheimer's and Parkinson's disease. Neurodegener Dis *10*, 212-215.

Horowitz, P.M., Patterson, K.R., Guillozet-Bongaarts, A.L., Reynolds, M.R., Carroll, C.A., Weintraub, S.T., Bennett, D.A., Cryns, V.L., Berry, R.W., and Binder, L.I. (2004). Early N-terminal changes and caspase-6 cleavage of tau in Alzheimer's disease. J Neurosci *24*, 7895-7902.

Hosokawa, N., Hara, T., Kaizuka, T., Kishi, C., Takamura, A., Miura, Y., Iemura, S., Natsume, T., Takehana, K., Yamada, N.*, et al.* (2009). Nutrient-dependent mTORC1 association with the ULK1-Atg13-FIP200 complex required for autophagy. Mol Biol Cell *20*, 1981-1991.

Hou, W., Han, J., Lu, C., Goldstein, L.A., and Rabinowich, H. (2010). Autophagic degradation of active caspase-8: a crosstalk mechanism between autophagy and apoptosis. Autophagy *6*, 891-900.

Howell, J.J., Hellberg, K., Turner, M., Talbott, G., Kolar, M.J., Ross, D.S., Hoxhaj, G., Saghatelian, A., Shaw, R.J., and Manning, B.D. (2017). Metformin Inhibits Hepatic mTORC1 Signaling via Dose-Dependent Mechanisms Involving AMPK and the TSC Complex. Cell Metab *25*, 463-471.

Hyman, B.T., Van Hoesen, G.W., Damasio, A.R., and Barnes, C.L. (1984). Alzheimer's disease: cell-specific pathology isolates the hippocampal formation. Science *225*, 1168-1170.

Imaizumi, K., Miyoshi, K., Katayama, T., Yoneda, T., Taniguchi, M., Kudo, T., and Tohyama, M. (2001). The unfolded protein response and Alzheimer's disease. Biochim Biophys Acta *1536*, 85-96.

Inoue, K., Rispoli, J., Kaphzan, H., Klann, E., Chen, E.I., Kim, J., Komatsu, M., and Abeliovich, A. (2012). Macroautophagy deficiency mediates age-dependent neurodegeneration through a phospho-tau pathway. Molecular neurodegeneration *7*, 48.

Iqbal, K., Alonso, A.d.C., Chen, S., Chohan, M.O., El-Akkad, E., Gong, C.-X., Khatoon, S., Li, B., Liu, F., and Rahman, A. (2005). Tau pathology in Alzheimer disease and other tauopathies. Biochimica et Biophysica Acta (BBA)-Molecular Basis of Disease *1739*, 198-210.

Ittner, L.M., and Götz, J. (2011). Amyloid-β and tau—a toxic pas de deux in Alzheimer's disease. Nature Reviews Neuroscience *12*, 67.

Ivy, G., Kanai, S., Ohta, M., Smith, G., Sato, Y., Kobayashi, M., and Kitani, K. (1989). Lipofuscin-like substances accumulate rapidly in brain, retina and internal organs with cysteine protease inhibition. Advances in experimental medicine and biology *266*, 31-45; discussion 45-37.

Ivy, G., Schottler, F., Wenzel, J., Baudry, M., and Lynch, G. (1984). Inhibitors of lysosomal enzymes: accumulation of lipofuscin-like dense bodies in the brain. Science *226*, 985-987.

Jaeger, P.A., Pickford, F., Sun, C.-H., Lucin, K.M., Masliah, E., and Wyss-Coray, T. (2010). Regulation of amyloid precursor protein processing by the Beclin 1 complex. PloS one *5*, e11102.

Jaeger, P.A., and Wyss-Coray, T. (2010). Beclin 1 complex in autophagy and Alzheimer disease. Arch Neurol *67*, 1181-1184.

Jager, R., Bertrand, M.J., Gorman, A.M., Vandenabeele, P., and Samali, A. (2012). The unfolded protein response at the crossroads of cellular life and death during endoplasmic reticulum stress. Biology of the cell / under the auspices of the European Cell Biology Organization *104*, 259-270.

Jankowsky, J.L., Fadale, D.J., Anderson, J., Xu, G.M., Gonzales, V., Jenkins, N.A., Copeland, N.G., Lee, M.K., Younkin, L.H., Wagner, S.L*., et al.* (2004). Mutant presenilins specifically elevate the levels of the 42 residue beta-amyloid peptide in vivo: evidence for augmentation of a 42-specific gamma secretase. Hum Mol Genet *13*, 159-170.

Jazvinscak Jembrek, M., Hof, P.R., and Simic, G. (2015). Ceramides in Alzheimer's Disease: Key Mediators of Neuronal Apoptosis Induced by Oxidative Stress and Abeta Accumulation. Oxid Med Cell Longev *2015*, 346783.

Jeganathan, S., von Bergen, M., Brutlach, H., Steinhoff, H.J., and Mandelkow, E. (2006). Global hairpin folding of tau in solution. Biochemistry *45*, 2283-2293.

Jezegou, A., Llinares, E., Anne, C., Kieffer-Jaquinod, S., O'Regan, S., Aupetit, J., Chabli, A., Sagne, C., Debacker, C., Chadefaux-Vekemans, B*., et al.* (2012). Heptahelical protein PQLC2 is a lysosomal cationic amino acid exporter underlying the action of cysteamine in cystinosis therapy. Proc Natl Acad Sci U S A *109*, E3434-3443.

Jiang, T., Yu, J.-T., Zhu, X.-C., Zhang, Q.-Q., Cao, L., Wang, H.-F., Tan, M.-S., Gao, Q., Qin, H., and Zhang, Y.-D. (2014). Temsirolimus attenuates tauopathy in vitro and in vivo by targeting tau hyperphosphorylation and autophagic clearance. Neuropharmacology *85*, 121-130.

Jiang, W., Wei, W., Gaertig, M.A., Li, S., and Li, X.-J. (2015). Therapeutic effect of berberine on Huntington's disease transgenic mouse model. PLoS One *10*, e0134142.

Jin, F., Wu, Q., Lu, Y.-F., Gong, Q.-H., and Shi, J.-S. (2008). Neuroprotective effect of resveratrol on 6-OHDA-induced Parkinson's disease in rats. European journal of pharmacology *600*, 78-82.

Jucker, M., and Walker, L.C. (2011). Pathogenic protein seeding in Alzheimer disease and other neurodegenerative disorders. Ann Neurol *70*, 532-540.

Jung, C.H., Ro, S.-H., Cao, J., Otto, N.M., and Kim, D.-H. (2010). mTOR regulation of autophagy. FEBS letters *584*, 1287-1295.

Kabeya, Y., Mizushima, N., Ueno, T., Yamamoto, A., Kirisako, T., Noda, T., Kominami, E., Ohsumi, Y., and Yoshimori, T. (2000). LC3, a mammalian homologue of yeast Apg8p, is localized in autophagosome membranes after processing. EMBO J *19*, 5720-5728.

Kadowaki, H., Nishitoh, H., Urano, F., Sadamitsu, C., Matsuzawa, A., Takeda, K., Masutani, H., Yodoi, J., Urano, Y., Nagano, T*., et al.* (2005). Amyloid beta induces neuronal cell death through ROS-mediated ASK1 activation. Cell Death Differ *12*, 19-24.

Kamat, C.D., Gadal, S., Mhatre, M., Williamson, K.S., Pye, Q.N., and Hensley, K. (2008). Antioxidants in central nervous system diseases: preclinical promise and translational challenges. Journal of Alzheimer's Disease *15*, 473-493.

Kaneko, M., Niinuma, Y., and Nomura, Y. (2003). Activation signal of nuclear factor-kappa B in response to endoplasmic reticulum stress is transduced via IRE1 and tumor necrosis factor receptor-associated factor 2. Biol Pharm Bull *26*, 931-935.

Kang, R., Zeh, H.J., Lotze, M.T., and Tang, D. (2011). The Beclin 1 network regulates autophagy and apoptosis. Cell Death Differ *18*, 571-580.

Katayama, T., Imaizumi, K., Manabe, T., Hitomi, J., Kudo, T., and Tohyama, M. (2004). Induction of neuronal death by ER stress in Alzheimer's disease. J Chem Neuroanat *28*, 67-78.

Keck, S., Nitsch, R., Grune, T., and Ullrich, O. (2003). Proteasome inhibition by paired helical filament-tau in brains of patients with Alzheimer's disease. J Neurochem *85*, 115-122.

Khurana, V., Elson-Schwab, I., Fulga, T.A., Sharp, K.A., Loewen, C.A., Mulkearns, E., Tyynela, J., Scherzer, C.R., and Feany, M.B. (2010). Lysosomal dysfunction promotes cleavage and neurotoxicity of tau in vivo. PLoS Genet *6*, e1001026.

Kim, D.H., Sarbassov, D.D., Ali, S.M., King, J.E., Latek, R.R., Erdjument-Bromage, H., Tempst, P., and Sabatini, D.M. (2002). mTOR interacts with raptor to form a nutrient-sensitive complex that signals to the cell growth machinery. Cell *110*, 163-175.

Kim, J., Kundu, M., Viollet, B., and Guan, K.L. (2011). AMPK and mTOR regulate autophagy through direct phosphorylation of Ulk1. Nat Cell Biol *13*, 132-141.

Kim, R., Emi, M., Tanabe, K., and Murakami, S. (2006). Role of the unfolded protein response in cell death. Apoptosis : an international journal on programmed cell death *11*, 5-13.

Kim, S., Sato, Y., Mohan, P.S., Peterhoff, C., Pensalfini, A., Rigoglioso, A., Jiang, Y., and Nixon, R.A. (2016). Evidence that the rab5 effector APPL1 mediates APP-betaCTF-induced dysfunction of endosomes in Down syndrome and Alzheimer's disease. Mol Psychiatry *21*, 707-716.

Kim, Y.C., and Guan, K.L. (2015). mTOR: a pharmacologic target for autophagy regulation. J Clin Invest *125*, 25-32.

Kirkin, V., McEwan, D.G., Novak, I., and Dikic, I. (2009). A role for ubiquitin in selective autophagy. Mol Cell *34*, 259-269.

Kochl, R., Hu, X.W., Chan, E.Y., and Tooze, S.A. (2006). Microtubules facilitate autophagosome formation and fusion of autophagosomes with endosomes. Traffic *7*, 129-145.

Koike, M., Nakanishi, H., Saftig, P., Ezaki, J., Isahara, K., Ohsawa, Y., Schulz-Schaeffer, W., Watanabe, T., Waguri, S., and Kametaka, S. (2000). Cathepsin D deficiency induces lysosomal storage with ceroid lipofuscin in mouse CNS neurons. Journal of Neuroscience *20*, 6898-6906.

Koike, M., Shibata, M., Waguri, S., Yoshimura, K., Tanida, I., Kominami, E., Gotow, T., Peters, C., von Figura, K., and Mizushima, N. (2005). Participation of autophagy in storage of lysosomes in neurons from mouse models of neuronal ceroid-lipofuscinoses (Batten disease). The American journal of pathology *167*, 1713-1728.

Komatsu, M., Waguri, S., Chiba, T., Murata, S., Iwata, J., Tanida, I., Ueno, T., Koike, M., Uchiyama, Y., Kominami, E*., et al.* (2006). Loss of autophagy in the central nervous system causes neurodegeneration in mice. Nature *441*, 880-884.

Korte, M., Herrmann, U., Zhang, X., and Draguhn, A. (2012). The role of APP and APLP for synaptic transmission, plasticity, and network function: lessons from genetic mouse models. Exp Brain Res *217*, 435-440.

Kosik, K.S., Orecchio, L.D., Bakalis, S., and Neve, R.L. (1989). Developmentally regulated expression of specific tau sequences. Neuron *2*, 1389-1397.

Kouri, N., Murray, M.E., Hassan, A., Rademakers, R., Uitti, R.J., Boeve, B.F., Graff-Radford, N.R., Wszolek, Z.K., Litvan, I., Josephs, K.A*., et al.* (2011). Neuropathological features of corticobasal degeneration presenting as corticobasal syndrome or Richardson syndrome. Brain *134*, 3264-3275.

Krüger, U., Wang, Y., Kumar, S., and Mandelkow, E.-M. (2012). Autophagic degradation of tau in primary neurons and its enhancement by trehalose. Neurobiology of aging *33*, 2291-2305.

Kuperstein, I., Broersen, K., Benilova, I., Rozenski, J., Jonckheere, W., Debulpaep, M., Vandersteen, A., Segers-Nolten, I., Van Der Werf, K., Subramaniam, V*., et al.* (2010). Neurotoxicity of Alzheimer's disease Abeta peptides is induced by small changes in the Abeta42 to Abeta40 ratio. EMBO J *29*, 3408-3420.

LaFerla, F.M., and Oddo, S. (2005). Alzheimer's disease: Abeta, tau and synaptic dysfunction. Trends Mol Med *11*, 170-176.

Lalonde, R., and Strazielle, C. (2011). Genetic Models of Cerebellar Dysfunction. In Animal Models of Movement Disorders (Springer), pp. 241-262.

Lao, F., Chen, L., Li, W., Ge, C., Qu, Y., Sun, Q., Zhao, Y., Han, D., and Chen, C. (2009). Fullerene nanoparticles selectively enter oxidation-damaged cerebral microvessel endothelial cells and inhibit JNK-related apoptosis. ACS Nano *3*, 3358-3368.

Laws, N., and Hoey, A. (2004). Progression of kyphosis in mdx mice. Journal of Applied Physiology *97*, 1970-1977.

Lee, H.G., Ueda, M., Miyamoto, Y., Yoneda, Y., Perry, G., Smith, M.A., and Zhu, X. (2006). Aberrant localization of importin alpha1 in hippocampal neurons in Alzheimer disease. Brain Res *1124*, 1-4.

Lee, J.-H., McBrayer, M.K., Wolfe, D.M., Haslett, L.J., Kumar, A., Sato, Y., Lie, P.P., Mohan, P., Coffey, E.E., and Kompella, U. (2015). Presenilin 1 maintains lysosomal Ca2+ homeostasis via TRPML1 by regulating vATPase-mediated lysosome acidification. Cell reports *12*, 1430-1444.

Lee, J.H., Yu, W.H., Kumar, A., Lee, S., Mohan, P.S., Peterhoff, C.M., Wolfe, D.M., Martinez-Vicente, M., Massey, A.C., Sovak, G*., et al.* (2010). Lysosomal proteolysis and autophagy require presenilin 1 and are disrupted by Alzheimer-related PS1 mutations. Cell *141*, 1146-1158.

Lee, J.Y., Nagano, Y., Taylor, J.P., Lim, K.L., and Yao, T.P. (2010c). Disease-causing mutations in parkin impair mitochondrial ubiquitination, aggregation, and HDAC6-dependent mitophagy. J Cell Biol *189*, 671-679.

Lee, M.J., Lee, J.H., and Rubinsztein, D.C. (2013). Tau degradation: the ubiquitin–proteasome system versus the autophagy-lysosome system. Progress in neurobiology *105*, 49-59.

Lee, S.S. (2001). Effective screening for Alzheimer's disease in everyday practice. JAAPA *14*, 39-48.

Lee, V.M., Goedert, M., and Trojanowski, J.Q. (2001). Neurodegenerative tauopathies. Annu Rev Neurosci *24*, 1121-1159.

Leroy, K., Ando, K., Héraud, C., Yilmaz, Z., Authelet, M., Boeynaems, J.M., Buée, L., De Decker, R., and Brion, J.P. (2010). Lithium treatment arrests the development of neurofibrillary tangles in mutant tau transgenic mice with advanced neurofibrillary pathology. Journal of Alzheimer's Disease *19*, 705-719.

Leroy, K., Yilmaz, Z., and Brion, J.P. (2007). Increased level of active GSK-3beta in Alzheimer's disease and accumulation in argyrophilic grains and in neurones at different stages of neurofibrillary degeneration. Neuropathol Appl Neurobiol *33*, 43-55.

Lewis, J., McGowan, E., Rockwood, J., Melrose, H., Nacharaju, P., Van Slegtenhorst, M., Gwinn-Hardy, K., Paul Murphy, M., Baker, M., Yu, X.*, et al.* (2000). Neurofibrillary tangles, amyotrophy and progressive motor disturbance in mice expressing mutant (P301L) tau protein. Nat Genet *25*, 402-405.

Li, G., Zhu, D., Xue, L., and Jiang, H. (2013). Quinoline-based fluorescent probe for ratiometric detection of lysosomal pH. Organic letters *15*, 5020-5023.

Li, H.L., Wang, H.H., Liu, S.J., Deng, Y.Q., Zhang, Y.J., Tian, Q., Wang, X.C., Chen, X.Q., Yang, Y., Zhang, J.Y.*, et al.* (2007). Phosphorylation of tau antagonizes apoptosis by stabilizing beta-catenin, a mechanism involved in Alzheimer's neurodegeneration. Proc Natl Acad Sci U S A *104*, 3591-3596.

Liang, C., Lee, J.S., Inn, K.S., Gack, M.U., Li, Q., Roberts, E.A., Vergne, I., Deretic, V., Feng, P., Akazawa, C.*, et al.* (2008). Beclin1-binding UVRAG targets the class C Vps complex to coordinate autophagosome maturation and endocytic trafficking. Nat Cell Biol *10*, 776-787.

Liang, J., Shao, S.H., Xu, Z.X., Hennessy, B., Ding, Z., Larrea, M., Kondo, S., Dumont, D.J., Gutterman, J.U., Walker, C.L.*, et al.* (2007). The energy sensing LKB1-AMPK pathway regulates p27(kip1) phosphorylation mediating the decision to enter autophagy or apoptosis. Nat Cell Biol *9*, 218-224.

Lieberman, A.P., Puertollano, R., Raben, N., Slaugenhaupt, S., Walkley, S.U., and Ballabio, A. (2012). Autophagy in lysosomal storage disorders. Autophagy *8*, 719-730.

Lim, F., Hernandez, F., Lucas, J., Gomez-Ramos, P., Moran, M., and Avila, J. (2001). FTDP-17 mutations in tau transgenic mice provoke lysosomal abnormalities and Tau filaments in forebrain. Molecular and Cellular Neuroscience *18*, 702-714.

Lin, W.L., Lewis, J., Yen, S.H., Hutton, M., and Dickson, D.W. (2003). Filamentous tau in oligodendrocytes and astrocytes of transgenic mice expressing the human tau isoform with the P301L mutation. Am J Pathol *162*, 213-218.

Lin, X., Li, S., Zhao, Y., Ma, X., Zhang, K., He, X., and Wang, Z. (2013). Interaction domains of p62: a bridge between p62 and selective autophagy. DNA and cell biology *32*, 220-227.

Lipinski, M.M., Zheng, B., Lu, T., Yan, Z., Py, B.F., Ng, A., Xavier, R.J., Li, C., Yankner, B.A., Scherzer, C.R*., et al.* (2010). Genome-wide analysis reveals mechanisms modulating autophagy in normal brain aging and in Alzheimer's disease. Proc Natl Acad Sci U S A *107*, 14164-14169.

Liu, B., Du, H., Rutkowski, R., Gartner, A., and Wang, X. (2012). LAAT-1 is the lysosomal lysine/arginine transporter that maintains amino acid homeostasis. Science *337*, 351-354.

Liu, F., Grundke-Iqbal, I., Iqbal, K., and Gong, C.X. (2005a). Contributions of protein phosphatases PP1, PP2A, PP2B and PP5 to the regulation of tau phosphorylation. Eur J Neurosci *22*, 1942-1950.

Liu, F., Iqbal, K., Grundke-Iqbal, I., Rossie, S., and Gong, C.X. (2005b). Dephosphorylation of tau by protein phosphatase 5: impairment in Alzheimer's disease. J Biol Chem *280*, 1790-1796.

Liu, F., Li, B., Tung, E.J., Grundke-Iqbal, I., Iqbal, K., and Gong, C.X. (2007). Site-specific effects of tau phosphorylation on its microtubule assembly activity and self-aggregation. Eur J Neurosci *26*, 3429-3436.

Lloyd-Evans, E., and Haslett, L.J. (2016). The lysosomal storage disease continuum with ageing-related neurodegenerative disease. Ageing Res Rev *32*, 104-121.

Lourenco, M.V., Clarke, J.R., Frozza, R.L., Bomfim, T.R., Forny-Germano, L., Batista, A.F., Sathler, L.B., Brito-Moreira, J., Amaral, O.B., Silva, C.A*., et al.* (2013). TNF-alpha mediates PKR-dependent memory impairment and brain IRS-1 inhibition induced by Alzheimer's beta-amyloid oligomers in mice and monkeys. Cell Metab *18*, 831-843.

Lucin, K.M., O'Brien, C.E., Bieri, G., Czirr, E., Mosher, K.I., Abbey, R.J., Mastroeni, D.F., Rogers, J., Spencer, B., and Masliah, E. (2013). Microglial beclin 1 regulates retromer trafficking and phagocytosis and is impaired in Alzheimer's disease. Neuron *79*, 873-886.

Ludolph, A.C., Kassubek, J., Landwehrmeyer, B.G., Mandelkow, E., Mandelkow, E.M., Burn, D.J., Caparros-Lefebvre, D., Frey, K.A., de Yebenes, J.G., Gasser, T*., et al.* (2009). Tauopathies with parkinsonism: clinical spectrum, neuropathologic basis, biological markers, and treatment options. Eur J Neurol *16*, 297-309.

Lynch, T., Sano, M., Marder, K.S., Bell, K.L., Foster, N.L., Defendini, R.F., Sima, A.A., Keohane, C., Nygaard, T.G., Fahn, S*., et al.* (1994). Clinical characteristics of a family with

chromosome 17-linked disinhibition-dementia-parkinsonism-amyotrophy complex. Neurology *44*, 1878-1884.

Ma, T., and Klann, E. (2014). PERK: a novel therapeutic target for neurodegenerative diseases? Alzheimer's research & therapy *6*, 30.

Ma, T., Trinh, M.A., Wexler, A.J., Bourbon, C., Gatti, E., Pierre, P., Cavener, D.R., and Klann, E. (2013a). Suppression of eIF2alpha kinases alleviates Alzheimer's disease-related plasticity and memory deficits. Nat Neurosci *16*, 1299-1305.

Ma, T., Trinh, M.A., Wexler, A.J., Bourbon, C., Gatti, E., Pierre, P., Cavener, D.R., and Klann, E. (2013b). Suppression of eIF2α kinases alleviates Alzheimer's disease–related plasticity and memory deficits. Nature neuroscience *16*, 1299.

Ma, T.C., Buescher, J.L., Oatis, B., Funk, J.A., Nash, A.J., Carrier, R.L., and Hoyt, K.R. (2007). Metformin therapy in a transgenic mouse model of Huntington's disease. Neuroscience letters *411*, 98-103.

Macara, I.G. (2001). Transport into and out of the nucleus. Microbiol Mol Biol Rev *65*, 570-594, table of contents.

Mackenzie, I.R., Neumann, M., Bigio, E.H., Cairns, N.J., Alafuzoff, I., Kril, J., Kovacs, G.G., Ghetti, B., Halliday, G., Holm, I.E.*, et al.* (2010). Nomenclature and nosology for neuropathologic subtypes of frontotemporal lobar degeneration: an update. Acta Neuropathol *119*, 1-4.

Magnani, E., Fan, J., Gasparini, L., Golding, M., Williams, M., Schiavo, G., Goedert, M., Amos, L.A., and Spillantini, M.G. (2007). Interaction of tau protein with the dynactin complex. EMBO J *26*, 4546-4554.

Maiuri, M.C., Le Toumelin, G., Criollo, A., Rain, J.C., Gautier, F., Juin, P., Tasdemir, E., Pierron, G., Troulinaki, K., Tavernarakis, N.*, et al.* (2007). Functional and physical interaction between Bcl-X(L) and a BH3-like domain in Beclin-1. EMBO J *26*, 2527-2539.

Maly, D.J., and Papa, F.R. (2014). Druggable sensors of the unfolded protein response. Nature chemical biology *10*, 892.

Mandelkow, E.M., Schweers, O., Drewes, G., Biernat, J., Gustke, N., Trinczek, B., and Mandelkow, E. (1996). Structure, microtubule interactions, and phosphorylation of tau protein. Ann N Y Acad Sci *777*, 96-106.

Marchand, B., Arsenault, D., Raymond-Fleury, A., Boisvert, F.M., and Boucher, M.J. (2015). Glycogen synthase kinase-3 (GSK3) inhibition induces prosurvival autophagic signals in human pancreatic cancer cells. J Biol Chem *290*, 5592-5605.

Marcus, J.N., and Schachter, J. (2011). Targeting post-translational modifications on tau as a therapeutic strategy for Alzheimer's disease. J Neurogenet *25*, 127-133.

Martina, J.A., Diab, H.I., Lishu, L., Jeong-A, L., Patange, S., Raben, N., and Puertollano, R. (2014). The nutrient-responsive transcription factor TFE3 promotes autophagy, lysosomal biogenesis, and clearance of cellular debris. Sci Signal *7*, ra9-ra9.

Martini-Stoica, H., Xu, Y., Ballabio, A., and Zheng, H. (2016). The Autophagy-Lysosomal Pathway in Neurodegeneration: A TFEB Perspective. Trends Neurosci *39*, 221-234.

Matsumoto, S.E., Motoi, Y., Ishiguro, K., Tabira, T., Kametani, F., Hasegawa, M., and Hattori, N. (2015). The twenty-four KDa C-terminal tau fragment increases with aging in tauopathy mice: implications of prion-like properties. Hum Mol Genet *24*, 6403-6416.

Matus, S., Lisbona, F., Torres, M., Leon, C., Thielen, P., and Hetz, C. (2008). The stress rheostat: an interplay between the unfolded protein response (UPR) and autophagy in neurodegeneration. Curr Mol Med *8*, 157-172.

McEwan, D.G., Popovic, D., Gubas, A., Terawaki, S., Suzuki, H., Stadel, D., Coxon, F.P., Miranda de Stegmann, D., Bhogaraju, S., Maddi, K*., et al.* (2015). PLEKHM1 regulates autophagosome-lysosome fusion through HOPS complex and LC3/GABARAP proteins. Mol Cell *57*, 39-54.

McGowan, E., Eriksen, J., and Hutton, M. (2006). A decade of modeling Alzheimer's disease in transgenic mice. TRENDS in Genetics *22*, 281-289.

McKhann, G.M., Albert, M.S., Grossman, M., Miller, B., Dickson, D., Trojanowski, J.Q., Work Group on Frontotemporal, D., and Pick's, D. (2001). Clinical and pathological diagnosis of frontotemporal dementia: report of the Work Group on Frontotemporal Dementia and Pick's Disease. Arch Neurol *58*, 1803-1809.

McMillan, P.J., Kraemer, B.C., Robinson, L., Leverenz, J.B., Raskind, M., and Schellenberg, G. (2011). Truncation of tau at E391 promotes early pathologic changes in transgenic mice. J Neuropathol Exp Neurol *70*, 1006-1019.

McShea, A., Harris, P.L., Webster, K.R., Wahl, A.F., and Smith, M.A. (1997). Abnormal expression of the cell cycle regulators P16 and CDK4 in Alzheimer's disease. Am J Pathol *150*, 1933-1939.

Medina, D.L., Di Paola, S., Peluso, I., Armani, A., De Stefani, D., Venditti, R., Montefusco, S., Scotto-Rosato, A., Prezioso, C., Forrester, A*., et al.* (2015). Lysosomal calcium signalling regulates autophagy through calcineurin and TFEB. Nat Cell Biol *17*, 288-299.

Medina, D.L., Fraldi, A., Bouche, V., Annunziata, F., Mansueto, G., Spampanato, C., Puri, C., Pignata, A., Martina, J.A., Sardiello, M*., et al.* (2011). Transcriptional activation of lysosomal exocytosis promotes cellular clearance. Dev Cell *21*, 421-430.

Melis, V., Zabke, C., Stamer, K., Magbagbeolu, M., Schwab, K., Marschall, P., Veh, R.W., Bachmann, S., Deiana, S., Moreau, P.H*., et al.* (2015). Different pathways of molecular pathophysiology underlie cognitive and motor tauopathy phenotypes in transgenic models

for Alzheimer's disease and frontotemporal lobar degeneration. Cell Mol Life Sci *72*, 2199-2222.

Menzies, F.M., Fleming, A., and Rubinsztein, D.C. (2015). Compromised autophagy and neurodegenerative diseases. Nature Reviews Neuroscience *16*, 345.

Mercado, G., Valdes, P., and Hetz, C. (2013). An ERcentric view of Parkinson's disease. Trends Mol Med *19*, 165-175.

Meske, V., Albert, F., and Ohm, T.G. (2008). Coupling of mammalian target of rapamycin with phosphoinositide 3-kinase signaling pathway regulates protein phosphatase 2A- and glycogen synthase kinase-3 -dependent phosphorylation of Tau. J Biol Chem *283*, 100-109.

Metaxakis, A., Ploumi, C., and Tavernarakis, N. (2018). Autophagy in Age-Associated Neurodegeneration. Cells *7*.

Min, S.W., Cho, S.H., Zhou, Y., Schroeder, S., Haroutunian, V., Seeley, W.W., Huang, E.J., Shen, Y., Masliah, E., Mukherjee, C*., et al.* (2010). Acetylation of tau inhibits its degradation and contributes to tauopathy. Neuron *67*, 953-966.

Misiak, B., Cialkowska-Kuzminska, M., Frydecka, D., Chladzinska-Kiejna, S., and Kiejna, A. (2013). European studies on the prevalence of dementia in the elderly: time for a step towards a methodological consensus. Int J Geriatr Psychiatry *28*, 1211-1221.

Mizushima, N. (2007). Autophagy: process and function. Genes Dev *21*, 2861-2873.

Mizushima, N. (2010). The role of the Atg1/ULK1 complex in autophagy regulation. Curr Opin Cell Biol *22*, 132-139.

Mondragon-Rodriguez, S., Basurto-Islas, G., Santa-Maria, I., Mena, R., Binder, L.I., Avila, J., Smith, M.A., Perry, G., and Garcia-Sierra, F. (2008). Cleavage and conformational changes of tau protein follow phosphorylation during Alzheimer's disease. Int J Exp Pathol *89*, 81-90.

Mondragón‐Rodríguez, S., Basurto‐Islas, G., Santa‐Maria, I., Mena, R., Binder, L.I., Avila, J., Smith, M.A., Perry, G., and García‐Sierra, F. (2008). Cleavage and conformational changes of tau protein follow phosphorylation during Alzheimer's disease. International journal of experimental pathology *89*, 81-90.

Moreno, J.A., Halliday, M., Molloy, C., Radford, H., Verity, N., Axten, J.M., Ortori, C.A., Willis, A.E., Fischer, P.M., and Barrett, D.A. (2013). Oral treatment targeting the unfolded protein response prevents neurodegeneration and clinical disease in prion-infected mice. Science translational medicine *5*, 206ra138-206ra138.

Moreno, J.A., Radford, H., Peretti, D., Steinert, J.R., Verity, N., Martin, M.G., Halliday, M., Morgan, J., Dinsdale, D., and Ortori, C.A. (2012). Sustained translational repression by eIF2α-P mediates prion neurodegeneration. Nature *485*, 507.

Morishima-Kawashima, M., Hasegawa, M., Takio, K., Suzuki, M., Titani, K., and Ihara, Y. (1993). Ubiquitin is conjugated with amino-terminally processed tau in paired helical filaments. Neuron *10*, 1151-1160.

Mukai, F., Ishiguro, K., Sano, Y., and Fujita, S.C. (2002). Alternative splicing isoform of tau protein kinase I/glycogen synthase kinase 3beta. J Neurochem *81*, 1073-1083.

Nakakura, T., Asano-Hoshino, A., Suzuki, T., Arisawa, K., Tanaka, H., Sekino, Y., Kiuchi, Y., Kawai, K., and Hagiwara, H. (2015). The elongation of primary cilia via the acetylation of α-tubulin by the treatment with lithium chloride in human fibroblast KD cells. Medical molecular morphology *48*, 44-53.

Nakanishi, H. (2003). Neuronal and microglial cathepsins in aging and age-related diseases. Ageing Res Rev *2*, 367-381.

Nakashima, H., Ishihara, T., Suguimoto, P., Yokota, O., Oshima, E., Kugo, A., Terada, S., Hamamura, T., Trojanowski, J.Q., Lee, V.M.Y.*, et al.* (2005). Chronic lithium treatment decreases tau lesions by promoting ubiquitination in a mouse model of tauopathies. Acta neuropathologica *110*, 547-556.

Napolitano, G., and Ballabio, A. (2016). TFEB at a glance. J Cell Sci *129*, 2475-2481.

Nazio, F., Strappazzon, F., Antonioli, M., Bielli, P., Cianfanelli, V., Bordi, M., Gretzmeier, C., Dengjel, J., Piacentini, M., Fimia, G.M.*, et al.* (2013). mTOR inhibits autophagy by controlling ULK1 ubiquitylation, self-association and function through AMBRA1 and TRAF6. Nat Cell Biol *15*, 406-416.

Nelson, P.T., Alafuzoff, I., Bigio, E.H., Bouras, C., Braak, H., Cairns, N.J., Castellani, R.J., Crain, B.J., Davies, P., Del Tredici, K.*, et al.* (2012). Correlation of Alzheimer disease neuropathologic changes with cognitive status: a review of the literature. J Neuropathol Exp Neurol *71*, 362-381.

Nijholt, D.A., van Haastert, E.S., Rozemuller, A.J., Scheper, W., and Hoozemans, J.J. (2012). The unfolded protein response is associated with early tau pathology in the hippocampus of tauopathies. J Pathol *226*, 693-702.

Nishimura, I., Yang, Y., and Lu, B. (2004). PAR-1 kinase plays an initiator role in a temporally ordered phosphorylation process that confers tau toxicity in Drosophila. Cell *116*, 671-682.

Nixon, R.A. (2013). The role of autophagy in neurodegenerative disease. Nat Med *19*, 983-997.

Nixon, R.A., Wegiel, J., Kumar, A., Yu, W.H., Peterhoff, C., Cataldo, A., and Cuervo, A.M. (2005a). Extensive involvement of autophagy in Alzheimer disease: an immuno-electron microscopy study. J Neuropathol Exp Neurol *64*, 113-122.

Nixon, R.A., Wegiel, J., Kumar, A., Yu, W.H., Peterhoff, C., Cataldo, A., and Cuervo, A.M. (2005b). Extensive involvement of autophagy in Alzheimer disease: an immuno-electron microscopy study. Journal of Neuropathology & Experimental Neurology *64*, 113-122.

Nixon, R.A., and Yang, D.S. (2011). Autophagy failure in Alzheimer's disease--locating the primary defect. Neurobiol Dis *43*, 38-45.

Nixon, R.A., and Yang, D.S. (2012). Autophagy and neuronal cell death in neurological disorders. Cold Spring Harb Perspect Biol *4*.

Noble, W., Garwood, C., Stephenson, J., Kinsey, A.M., Hanger, D.P., and Anderton, B.H. (2009). Minocycline reduces the development of abnormal tau species in models of Alzheimer's disease. FASEB J *23*, 739-750.

Noble, W., Hanger, D.P., and Gallo, J.M. (2010). Transgenic mouse models of tauopathy in drug discovery. CNS Neurol Disord Drug Targets *9*, 403-428.

Noble, W., Planel, E., Zehr, C., Olm, V., Meyerson, J., Suleman, F., Gaynor, K., Wang, L., LaFrancois, J., Feinstein, B.*, et al.* (2005). Inhibition of glycogen synthase kinase-3 by lithium correlates with reduced tauopathy and degeneration in vivo. Proceedings of the National Academy of Sciences of the United States of America *102*, 6990-6995.

O'Leary, J.C., 3rd, Li, Q., Marinec, P., Blair, L.J., Congdon, E.E., Johnson, A.G., Jinwal, U.K., Koren, J., 3rd, Jones, J.R., Kraft, C.*, et al.* (2010). Phenothiazine-mediated rescue of cognition in tau transgenic mice requires neuroprotection and reduced soluble tau burden. Mol Neurodegener *5*, 45.

Ogata, M., Hino, S.-i., Saito, A., Morikawa, K., Kondo, S., Kanemoto, S., Murakami, T., Taniguchi, M., Tanii, I., and Yoshinaga, K. (2006). Autophagy is activated for cell survival after endoplasmic reticulum stress. Molecular and cellular biology *26*, 9220-9231.

Ogawa, O., Zhu, X., Lee, H.G., Raina, A., Obrenovich, M.E., Bowser, R., Ghanbari, H.A., Castellani, R.J., Perry, G., and Smith, M.A. (2003). Ectopic localization of phosphorylated histone H3 in Alzheimer's disease: a mitotic catastrophe? Acta Neuropathol *105*, 524-528.

Otomo, A., Kunita, R., Suzuki-Utsunomiya, K., Ikeda, J.E., and Hadano, S. (2011). Defective relocalization of ALS2/alsin missense mutants to Rac1-induced macropinosomes accounts for loss of their cellular function and leads to disturbed amphisome formation. FEBS Lett *585*, 730-736.

Ott, C., Konig, J., Hohn, A., Jung, T., and Grune, T. (2016). Macroautophagy is impaired in old murine brain tissue as well as in senescent human fibroblasts. Redox Biol *10*, 266-273.

Oyama, F., Murakami, N., and Ihara, Y. (1998). Chloroquine myopathy suggests that tau is degraded in lysosomes: implication for the formation of paired helical filaments in Alzheimer's disease. Neurosci Res *31*, 1-8.

Ozcelik, S., Fraser, G., Castets, P., Schaeffer, V., Skachokova, Z., Breu, K., Clavaguera, F., Sinnreich, M., Kappos, L., and Goedert, M. (2013). Rapamycin attenuates the progression of tau pathology in P301S tau transgenic mice. PloS one *8*, e62459.

Palmieri, M., Impey, S., Kang, H., di Ronza, A., Pelz, C., Sardiello, M., and Ballabio, A. (2011). Characterization of the CLEAR network reveals an integrated control of cellular clearance pathways. Hum Mol Genet *20*, 3852-3866.

Papasozomenos, S.C., and Binder, L.I. (1987). Phosphorylation determines two distinct species of Tau in the central nervous system. Cell Motil Cytoskeleton *8*, 210-226.

Park, S.Y., and Ferreira, A. (2005). The generation of a 17 kDa neurotoxic fragment: An alternative mechanism by which tau mediates β-amyloid-induced neurodegeneration. Journal of Neuroscience *25*, 5365-5375.

Parr, C., Carzaniga, R., Gentleman, S.M., Van Leuven, F., Walter, J., and Sastre, M. (2012). Glycogen synthase kinase 3 inhibition promotes lysosomal biogenesis and autophagic degradation of the amyloid-beta precursor protein. Mol Cell Biol *32*, 4410-4418.

Pattingre, S., Tassa, A., Qu, X., Garuti, R., Liang, X.H., Mizushima, N., Packer, M., Schneider, M.D., and Levine, B. (2005). Bcl-2 antiapoptotic proteins inhibit Beclin 1-dependent autophagy. Cell *122*, 927-939.

Pei, J.J., Bjorkdahl, C., Zhang, H., Zhou, X., and Winblad, B. (2008). p70 S6 kinase and tau in Alzheimer's disease. J Alzheimers Dis *14*, 385-392.

Pei, J.J., Braak, H., An, W.L., Winblad, B., Cowburn, R.F., Iqbal, K., and Grundke-Iqbal, I. (2002). Up-regulation of mitogen-activated protein kinases ERK1/2 and MEK1/2 is associated with the progression of neurofibrillary degeneration in Alzheimer's disease. Brain Res Mol Brain Res *109*, 45-55.

Pei, J.J., and Hugon, J. (2008). mTOR‐dependent signalling in Alzheimer's disease. Journal of cellular and molecular medicine *12*, 2525-2532.

Pemberton, L.F., and Paschal, B.M. (2005). Mechanisms of receptor‐mediated nuclear import and nuclear export. Traffic *6*, 187-198.

Perdiz, D., Mackeh, R., Pous, C., and Baillet, A. (2011). The ins and outs of tubulin acetylation: more than just a post-translational modification? Cell Signal *23*, 763-771.

Pereira, E.R., Frudd, K., Awad, W., and Hendershot, L.M. (2014). Endoplasmic reticulum (ER) stress and hypoxia response pathways interact to potentiate hypoxia-inducible factor 1 (HIF-1) transcriptional activity on targets like vascular endothelial growth factor (VEGF). The Journal of biological chemistry *289*, 3352-3364.

Pickford, F., Masliah, E., Britschgi, M., Lucin, K., Narasimhan, R., Jaeger, P.A., Small, S., Spencer, B., Rockenstein, E., and Levine, B. (2008a). The autophagy-related protein beclin

1 shows reduced expression in early Alzheimer disease and regulates amyloid β accumulation in mice. The Journal of clinical investigation *118*, 2190-2199.

Pickford, F., Masliah, E., Britschgi, M., Lucin, K., Narasimhan, R., Jaeger, P.A., Small, S., Spencer, B., Rockenstein, E., Levine, B.*, et al.* (2008b). The autophagy-related protein beclin 1 shows reduced expression in early Alzheimer disease and regulates amyloid beta accumulation in mice. J Clin Invest *118*, 2190-2199.

Piras, A., Collin, L., Gruninger, F., Graff, C., and Ronnback, A. (2016a). Autophagic and lysosomal defects in human tauopathies: analysis of post-mortem brain from patients with familial Alzheimer disease, corticobasal degeneration and progressive supranuclear palsy. Acta Neuropathol Commun *4*, 22.

Piras, A., Collin, L., Grüninger, F., Graff, C., and Rönnbäck, A. (2016b). Autophagic and lysosomal defects in human tauopathies: analysis of post-mortem brain from patients with familial Alzheimer disease, corticobasal degeneration and progressive supranuclear palsy. Acta neuropathologica communications *4*, 22.

Polito, V.A., Li, H., Martini-Stoica, H., Wang, B., Yang, L., Xu, Y., Swartzlander, D.B., Palmieri, M., di Ronza, A., Lee, V.M.*, et al.* (2014). Selective clearance of aberrant tau proteins and rescue of neurotoxicity by transcription factor EB. EMBO Mol Med *6*, 1142-1160.

Radford, H., Moreno, J.A., Verity, N., Halliday, M., and Mallucci, G.R. (2015). PERK inhibition prevents tau-mediated neurodegeneration in a mouse model of frontotemporal dementia. Acta Neuropathol *130*, 633-642.

Ramsden, M., Kotilinek, L., Forster, C., Paulson, J., McGowan, E., SantaCruz, K., Guimaraes, A., Yue, M., Lewis, J., Carlson, G.*, et al.* (2005). Age-dependent neurofibrillary tangle formation, neuron loss, and memory impairment in a mouse model of human tauopathy (P301L). J Neurosci *25*, 10637-10647.

Rao, R.V., Hermel, E., Castro-Obregon, S., del Rio, G., Ellerby, L.M., Ellerby, H.M., and Bredesen, D.E. (2001). Coupling endoplasmic reticulum stress to the cell death program. Mechanism of caspase activation. J Biol Chem *276*, 33869-33874.

Ravikumar, B., Vacher, C., Berger, Z., Davies, J.E., Luo, S., Oroz, L.G., Scaravilli, F., Easton, D.F., Duden, R., and O'Kane, C.J. (2004a). Inhibition of mTOR induces autophagy and reduces toxicity of polyglutamine expansions in fly and mouse models of Huntington disease. Nature genetics *36*, 585.

Ravikumar, B., Vacher, C., Berger, Z., Davies, J.E., Luo, S., Oroz, L.G., Scaravilli, F., Easton, D.F., Duden, R., O'Kane, C.J.*, et al.* (2004b). Inhibition of mTOR induces autophagy and reduces toxicity of polyglutamine expansions in fly and mouse models of Huntington disease. Nat Genet *36*, 585-595.

Reddy, P.H. (2011). Abnormal tau, mitochondrial dysfunction, impaired axonal transport of mitochondria, and synaptic deprivation in Alzheimer's disease. Brain Res *1415*, 136-148.

Reggiori, F. (2012). Autophagy: New Questions from Recent Answers. ISRN Mol Biol *2012*, 738718.

Reimann, O. (2017). Tag-free semisynthetic tau proteins and novel antibodies targeted against phospho-tau.

Reits, E., Griekspoor, A., Neijssen, J., Groothuis, T., Jalink, K., van Veelen, P., Janssen, H., Calafat, J., Drijfhout, J.W., and Neefjes, J. (2003). Peptide diffusion, protection, and degradation in nuclear and cytoplasmic compartments before antigen presentation by MHC class I. Immunity *18*, 97-108.

Reyes, J.F., Reynolds, M.R., Horowitz, P.M., Fu, Y., Guillozet-Bongaarts, A.L., Berry, R., and Binder, L.I. (2008). A possible link between astrocyte activation and tau nitration in Alzheimer's disease. Neurobiol Dis *31*, 198-208.

Ritz, D., Vuk, M., Kirchner, P., Bug, M., Schutz, S., Hayer, A., Bremer, S., Lusk, C., Baloh, R.H., Lee, H.*, et al.* (2011). Endolysosomal sorting of ubiquitylated caveolin-1 is regulated by VCP and UBXD1 and impaired by VCP disease mutations. Nat Cell Biol *13*, 1116-1123.

Robert, M., and Mathuranath, P. (2007). Tau and tauopathies. Neurology India *55*, 11-16.

Rockenstein, E., Ubhi, K., Mante, M., Florio, J., Adame, A., Winter, S., Brandstaetter, H., Meier, D., and Masliah, E. (2015). Neuroprotective effects of Cerebrolysin in triple repeat Tau transgenic model of Pick's disease and fronto-temporal tauopathies. BMC Neurosci *16*, 85.

Roczniak-Ferguson, A., Petit, C.S., Froehlich, F., Qian, S., Ky, J., Angarola, B., Walther, T.C., and Ferguson, S.M. (2012a). The transcription factor TFEB links mTORC1 signaling to transcriptional control of lysosome homeostasis. Sci Signal *5*, ra42-ra42.

Roczniak-Ferguson, A., Petit, C.S., Froehlich, F., Qian, S., Ky, J., Angarola, B., Walther, T.C., and Ferguson, S.M. (2012b). The transcription factor TFEB links mTORC1 signaling to transcriptional control of lysosome homeostasis. Sci Signal *5*, ra42.

Rodriguez-Martin, T., Cuchillo-Ibanez, I., Noble, W., Nyenya, F., Anderton, B.H., and Hanger, D.P. (2013). Tau phosphorylation affects its axonal transport and degradation. Neurobiol Aging *34*, 2146-2157.

Rodríguez-Navarro, J.A., Rodríguez, L., Casarejos, M.J., Solano, R.M., Gómez, A., Perucho, J., Cuervo, A.M., de Yébenes, J.G., and Mena, M.A. (2010). Trehalose ameliorates dopaminergic and tau pathology in parkin deleted/tau overexpressing mice through autophagy activation. Neurobiology of disease *39*, 423-438.

Rohn, T.T., Wirawan, E., Brown, R.J., Harris, J.R., Masliah, E., and Vandenabeele, P. (2011). Depletion of Beclin-1 due to proteolytic cleavage by caspases in the Alzheimer's disease brain. Neurobiology of disease *43*, 68-78.

Ron, D., and Hubbard, S.R. (2008). How IRE1 reacts to ER stress. Cell *132*, 24-26.

Roux, P.P., and Blenis, J. (2004). ERK and p38 MAPK-activated protein kinases: a family of protein kinases with diverse biological functions. Microbiology and molecular biology reviews *68*, 320-344.

Rubinsztein, D.C. (2006). The roles of intracellular protein-degradation pathways in neurodegeneration. Nature *443*, 780-786.

Rubinsztein, D.C., Gestwicki, J.E., Murphy, L.O., and Klionsky, D.J. (2007). Potential therapeutic applications of autophagy. Nat Rev Drug Discov *6*, 304-312.

Rudrabhatla, P., and Pant, H.C. (2010). Phosphorylation-specific peptidyl-prolyl isomerization of neuronal cytoskeletal proteins by pin1: Implications for therapeutics in neurodegeneration. Journal of Alzheimer's Disease *19*, 389-403.

Russell, C.L., Koncarevic, S., and Ward, M.A. (2014). Post-translational modifications in Alzheimer's disease and the potential for new biomarkers. J Alzheimers Dis *41*, 345-364.

Sade, Y., Toker, L., Kara, N.Z., Einat, H., Rapoport, S., Moechars, D., Berry, G., Bersudsky, Y., and Agam, G. (2016). IP3 accumulation and/or inositol depletion: two downstream lithium's effects that may mediate its behavioral and cellular changes. Translational psychiatry *6*, e968.

Salminen, A., Kauppinen, A., Suuronen, T., Kaarniranta, K., and Ojala, J. (2009). ER stress in Alzheimer's disease: a novel neuronal trigger for inflammation and Alzheimer's pathology. Journal of neuroinflammation *6*, 41.

Sanches, M., Duffy, N.M., Talukdar, M., Thevakumaran, N., Chiovitti, D., Canny, M.D., Lee, K., Kurinov, I., Uehling, D., and Al-Awar, R. (2014). Structure and mechanism of action of the hydroxy–aryl–aldehyde class of IRE1 endoribonuclease inhibitors. Nature communications *5*, 4202.

Sardi, S.P., Clarke, J., Kinnecom, C., Tamsett, T.J., Li, L., Stanek, L.M., Passini, M.A., Grabowski, G.A., Schlossmacher, M.G., Sidman, R.L*., et al.* (2011). CNS expression of glucocerebrosidase corrects alpha-synuclein pathology and memory in a mouse model of Gaucher-related synucleinopathy. Proc Natl Acad Sci U S A *108*, 12101-12106.

Sardiello, M., Palmieri, M., di Ronza, A., Medina, D.L., Valenza, M., Gennarino, V.A., Di Malta, C., Donaudy, F., Embrione, V., Polishchuk, R.S*., et al.* (2009). A gene network regulating lysosomal biogenesis and function. Science *325*, 473-477.

Sarkar, S. (2013). Regulation of autophagy by mTOR-dependent and mTOR-independent pathways: autophagy dysfunction in neurodegenerative diseases and therapeutic application of autophagy enhancers. Biochem Soc Trans *41*, 1103-1130.

Sarkar, S., Chigurupati, S., Raymick, J., Mann, D., Bowyer, J.F., Schmitt, T., Beger, R.D., Hanig, J.P., Schmued, L.C., and Paule, M.G. (2014). Neuroprotective effect of the chemical

chaperone, trehalose in a chronic MPTP-induced Parkinson's disease mouse model. Neurotoxicology *44*, 250-262.

Sarkar, S., Davies, J.E., Huang, Z., Tunnacliffe, A., and Rubinsztein, D.C. (2007a). Trehalose, a novel mTOR-independent autophagy enhancer, accelerates the clearance of mutant huntingtin and alpha-synuclein. J Biol Chem *282*, 5641-5652.

Sarkar, S., Perlstein, E.O., Imarisio, S., Pineau, S., Cordenier, A., Maglathlin, R.L., Webster, J.A., Lewis, T.A., O'Kane, C.J., Schreiber, S.L*., et al.* (2007b). Small molecules enhance autophagy and reduce toxicity in Huntington's disease models. Nat Chem Biol *3*, 331-338.

Sarkar, S., Ravikumar, B., Floto, R., and Rubinsztein, D. (2009). Rapamycin and mTOR-independent autophagy inducers ameliorate toxicity of polyglutamine-expanded huntingtin and related proteinopathies. Cell death and differentiation *16*, 46.

Sarkar, S., and Rubinsztein, D.C. (2008). Huntington's disease: degradation of mutant huntingtin by autophagy. The FEBS journal *275*, 4263-4270.

Schaeffer, V., Lavenir, I., Ozcelik, S., Tolnay, M., Winkler, D.T., and Goedert, M. (2012). Stimulation of autophagy reduces neurodegeneration in a mouse model of human tauopathy. Brain *135*, 2169-2177.

Scheper, W., and Hoozemans, J. (2013). A new PERKspective on neurodegeneration. Sci Transl Med *5*, 206fs237.

Scheper, W., and Hoozemans, J.J. (2015). The unfolded protein response in neurodegenerative diseases: a neuropathological perspective. Acta Neuropathol *130*, 315-331.

Schonthal, A.H. (2012). Endoplasmic reticulum stress: its role in disease and novel prospects for therapy. Scientifica *2012*, 857516.

Selkoe, D.J. (2001). Alzheimer's disease: genes, proteins, and therapy. Physiol Rev *81*, 741-766.

Serenó, L., Coma, M., Rodríguez, M., Sánchez-Ferrer, P., Sánchez, M.B., Gich, I., Agulló, J.M., Pérez, M., Avila, J., Guardia-Laguarta, C*., et al.* (2009). A novel GSK-3β inhibitor reduces Alzheimer's pathology and rescues neuronal loss in vivo. Neurobiology of disease *35*, 359-367.

Settembre, C., De Cegli, R., Mansueto, G., Saha, P.K., Vetrini, F., Visvikis, O., Huynh, T., Carissimo, A., Palmer, D., Klisch, T.J*., et al.* (2013). TFEB controls cellular lipid metabolism through a starvation-induced autoregulatory loop. Nat Cell Biol *15*, 647-658.

Settembre, C., Di Malta, C., Polito, V.A., Garcia Arencibia, M., Vetrini, F., Erdin, S., Erdin, S.U., Huynh, T., Medina, D., Colella, P*., et al.* (2011). TFEB links autophagy to lysosomal biogenesis. Science *332*, 1429-1433.

Settembre, C., Zoncu, R., Medina, D.L., Vetrini, F., Erdin, S., Erdin, S., Huynh, T., Ferron, M., Karsenty, G., Vellard, M.C*., et al.* (2012). A lysosome-to-nucleus signalling mechanism senses and regulates the lysosome via mTOR and TFEB. EMBO J *31*, 1095-1108.

Shahani, N., and Brandt, R. (2002). Functions and malfunctions of the tau proteins. Cell Mol Life Sci *59*, 1668-1680.

Shibata, M., Lu, T., Furuya, T., Degterev, A., Mizushima, N., Yoshimori, T., MacDonald, M., Yankner, B., and Yuan, J. (2006). Regulation of intracellular accumulation of mutant Huntingtin by Beclin 1. J Biol Chem *281*, 14474-14485.

Siintola, E., Partanen, S., Stromme, P., Haapanen, A., Haltia, M., Maehlen, J., Lehesjoki, A.E., and Tyynela, J. (2006). Cathepsin D deficiency underlies congenital human neuronal ceroid-lipofuscinosis. Brain *129*, 1438-1445.

Simic, G., Babic Leko, M., Wray, S., Harrington, C., Delalle, I., Jovanov-Milosevic, N., Bazadona, D., Buee, L., de Silva, R., Di Giovanni, G*., et al.* (2016). Tau Protein Hyperphosphorylation and Aggregation in Alzheimer's Disease and Other Tauopathies, and Possible Neuroprotective Strategies. Biomolecules *6*, 6.

Sjoberg, M.K., Shestakova, E., Mansuroglu, Z., Maccioni, R.B., and Bonnefoy, E. (2006). Tau protein binds to pericentromeric DNA: a putative role for nuclear tau in nucleolar organization. J Cell Sci *119*, 2025-2034.

Smith, H.L., and Mallucci, G.R. (2016). The unfolded protein response: mechanisms and therapy of neurodegeneration. Brain *139*, 2113-2121.

Sokolow, S., Henkins, K.M., Bilousova, T., Gonzalez, B., Vinters, H.V., Miller, C.A., Cornwell, L., Poon, W.W., and Gylys, K.H. (2015). Pre‐synaptic C‐terminal truncated tau is released from cortical synapses in Alzheimer's disease. Journal of neurochemistry *133*, 368-379.

Song, R. (2016). Mechanism of metformin: a tale of two sites. Diabetes Care *39*, 187-189.

Spencer, B., Potkar, R., Trejo, M., Rockenstein, E., Patrick, C., Gindi, R., Adame, A., Wyss-Coray, T., and Masliah, E. (2009). Beclin 1 gene transfer activates autophagy and ameliorates the neurodegenerative pathology in α-synuclein models of Parkinson's and Lewy body diseases. Journal of Neuroscience *29*, 13578-13588.

Spillantini, M.G., and Goedert, M. (2013). Tau pathology and neurodegeneration. Lancet Neurol *12*, 609-622.

Spillantini, M.G., Goedert, M., Crowther, R.A., Murrell, J.R., Farlow, M.R., and Ghetti, B. (1997). Familial multiple system tauopathy with presenile dementia: a disease with abundant neuronal and glial tau filaments. Proc Natl Acad Sci U S A *94*, 4113-4118.

Spires, T.L., Orne, J.D., SantaCruz, K., Pitstick, R., Carlson, G.A., Ashe, K.H., and Hyman, B.T. (2006). Region-specific dissociation of neuronal loss and neurofibrillary pathology in a mouse model of tauopathy. Am J Pathol *168*, 1598-1607.

Steele, J.C., Richardson, J.C., and Olszewski, J. (1964). Progressive Supranuclear Palsy. A Heterogeneous Degeneration Involving the Brain Stem, Basal Ganglia and Cerebellum with Vertical Gaze and Pseudobulbar Palsy, Nuchal Dystonia and Dementia. Arch Neurol *10*, 333-359.

Steinfeld, R., Reinhardt, K., Schreiber, K., Hillebrand, M., Kraetzner, R., Bruck, W., Saftig, P., and Gartner, J. (2006). Cathepsin D deficiency is associated with a human neurodegenerative disorder. Am J Hum Genet *78*, 988-998.

Streubel, M.K., Bischof, J., Weiss, R., Duschl, J., Liedl, W., Wimmer, H., Breitenbach, M., Weber, M., Geltinger, F., and Richter, K. (2018). Behead and live long or the tale of cathepsin L. Yeast *35*, 237-249.

Stutzbach, L.D., Xie, S.X., Naj, A.C., Albin, R., Gilman, S., Group, P.S.P.G.S., Lee, V.M., Trojanowski, J.Q., Devlin, B., and Schellenberg, G.D. (2013). The unfolded protein response is activated in disease-affected brain regions in progressive supranuclear palsy and Alzheimer's disease. Acta Neuropathol Commun *1*, 31.

Sueda, T., Sakai, D., Kawamoto, K., Konno, M., Nishida, N., Koseki, J., Colvin, H., Takahashi, H., Haraguchi, N., Nishimura, J.*, et al.* (2016). BRAF V600E inhibition stimulates AMP-activated protein kinase-mediated autophagy in colorectal cancer cells. Sci Rep *6*, 18949.

Suh, K.S., Tanaka, T., Sarojini, S., Nightingale, G., Gharbaran, R., Pecora, A., and Goy, A. (2013). The role of the ubiquitin proteasome system in lymphoma. Critical reviews in oncology/hematology *87*, 306-322.

Sultan, A., Nesslany, F., Violet, M., Begard, S., Loyens, A., Talahari, S., Mansuroglu, Z., Marzin, D., Sergeant, N., Humez, S.*, et al.* (2011). Nuclear tau, a key player in neuronal DNA protection. J Biol Chem *286*, 4566-4575.

Sun, B., Zhou, Y., Halabisky, B., Lo, I., Cho, S.-H., Mueller-Steiner, S., Devidze, N., Wang, X., Grubb, A., and Gan, L. (2008). Cystatin C-cathepsin B axis regulates amyloid beta levels and associated neuronal deficits in an animal model of Alzheimer's disease. Neuron *60*, 247-257.

Sun, L., Liu, S.Y., Zhou, X.W., Wang, X.C., Liu, R., Wang, Q., and Wang, J.Z. (2003). Inhibition of protein phosphatase 2A- and protein phosphatase 1-induced tau hyperphosphorylation and impairment of spatial memory retention in rats. Neuroscience *118*, 1175-1182.

Sun, Y.X., Ji, X., Mao, X., Xie, L., Jia, J., Galvan, V., Greenberg, D.A., and Jin, K. (2014). Differential activation of mTOR complex 1 signaling in human brain with mild to severe Alzheimer's disease. J Alzheimers Dis *38*, 437-444.

Sutherland, C., Campbell, D.G., and Cohen, P. (1993). Identification of insulin-stimulated protein kinase-1 as the rabbit equivalent of rskmo-2. Identification of two threonines phosphorylated during activation by mitogen-activated protein kinase. Eur J Biochem *212*, 581-588.

Tabas, I., and Ron, D. (2011). Integrating the mechanisms of apoptosis induced by endoplasmic reticulum stress. Nat Cell Biol *13*, 184-190.

Tamagnini, F., Walsh, D.A., Brown, J.T., Bondulich, M.K., Hanger, D.P., and Randall, A.D. (2017). Hippocampal neurophysiology is modified by a disease-associated C-terminal fragment of tau protein. Neurobiology of aging *60*, 44-56.

Tang, D., Kang, R., Cheh, C.W., Livesey, K.M., Liang, X., Schapiro, N.E., Benschop, R., Sparvero, L.J., Amoscato, A.A., Tracey, K.J.*, et al.* (2010). HMGB1 release and redox regulates autophagy and apoptosis in cancer cells. Oncogene *29*, 5299-5310.

Tavares, I.A., Touma, D., Lynham, S., Troakes, C., Schober, M., Causevic, M., Garg, R., Noble, W., Killick, R., Bodi, I.*, et al.* (2013). Prostate-derived sterile 20-like kinases (PSKs/TAOKs) phosphorylate tau protein and are activated in tangle-bearing neurons in Alzheimer disease. J Biol Chem *288*, 15418-15429.

Tenreiro, S., Eckermann, K., and Outeiro, T.F. (2014). Protein phosphorylation in neurodegeneration: friend or foe? Front Mol Neurosci *7*, 42.

Thoreen, C.C., and Sabatini, D.M. (2009). Rapamycin inhibits mTORC1, but not completely. Autophagy *5*, 725-726.

Tian, Y., Wang, L., and Ou, J.H. (2015). Autophagy, a double-edged sword in hepatocarcinogenesis. Mol Cell Oncol *2*, e1004968.

Trabzuni, D., Wray, S., Vandrovcova, J., Ramasamy, A., Walker, R., Smith, C., Luk, C., Gibbs, J.R., Dillman, A., Hernandez, D.G.*, et al.* (2012). MAPT expression and splicing is differentially regulated by brain region: relation to genotype and implication for tauopathies. Hum Mol Genet *21*, 4094-4103.

Tresse, E., Salomons, F.A., Vesa, J., Bott, L.C., Kimonis, V., Yao, T.P., Dantuma, N.P., and Taylor, J.P. (2010). VCP/p97 is essential for maturation of ubiquitin-containing autophagosomes and this function is impaired by mutations that cause IBMPFD. Autophagy *6*, 217-227.

Turk, B., Dolenc, I., Lenarcic, B., Krizaj, I., Turk, V., Bieth, J.G., and Bjork, I. (1999). Acidic pH as a physiological regulator of human cathepsin L activity. Eur J Biochem *259*, 926-932.

Unterberger, A., Andrews, S.D., Weaver, I.C., and Szyf, M. (2006). DNA methyltransferase 1 knockdown activates a replication stress checkpoint. Mol Cell Biol *26*, 7575-7586.

van der Kallen, C.J.H., van Greevenbroek, M.M.J., Stehouwer, C.D.A., and Schalkwijk, C.G. (2009). Endoplasmic reticulum stress-induced apoptosis in the development of diabetes: is

there a role for adipose tissue and liver? Apoptosis : an international journal on programmed cell death *14*, 1424-1434.

van Swieten, J.C., Rosso, S.M., van Herpen, E., Kamphorst, W., Ravid, R., and Heutink, P. (2004). Phenotypic variation in frontotemporal dementia and parkinsonism linked to chromosome 17. Dementia and geriatric cognitive disorders *17*, 261-264.

Vidal, R., Caballero, B., Couve, A., and Hetz, C. (2011). Converging pathways in the occurrence of endoplasmic reticulum (ER) stress in Huntington's disease. Curr Mol Med *11*, 1-12.

Vidal, R.L., Figueroa, A., Court, F.A., Thielen, P., Molina, C., Wirth, C., Caballero, B., Kiffin, R., Segura-Aguilar, J., and Cuervo, A.M. (2012). Targeting the UPR transcription factor XBP1 protects against Huntington's disease through the regulation of FoxO1 and autophagy. Human molecular genetics *21*, 2245-2262.

Vidoni, C., Secomandi, E., Castiglioni, A., Melone, M.A., and Isidoro, C. (2018). Resveratrol protects neuronal-like cells expressing mutant Huntingtin from dopamine toxicity by rescuing ATG4-mediated autophagosome formation. Neurochemistry international *117*, 174-187.

Violet, M., Delattre, L., Tardivel, M., Sultan, A., Chauderlier, A., Caillierez, R., Talahari, S., Nesslany, F., Lefebvre, B., and Bonnefoy, E. (2014). A major role for Tau in neuronal DNA and RNA protection in vivo under physiological and hyperthermic conditions. Frontiers in cellular neuroscience *8*, 84.

Vogelsberg-Ragaglia, V., Bruce, J., Richter-Landsberg, C., Zhang, B., Hong, M., Trojanowski, J.Q., and Lee, V.M. (2000). Distinct FTDP-17 missense mutations in tau produce tau aggregates and other pathological phenotypes in transfected CHO cells. Mol Biol Cell *11*, 4093-4104.

von Bergen, M., Friedhoff, P., Biernat, J., Heberle, J., Mandelkow, E.M., and Mandelkow, E. (2000). Assembly of tau protein into Alzheimer paired helical filaments depends on a local sequence motif ((306)VQIVYK(311)) forming beta structure. Proc Natl Acad Sci U S A *97*, 5129-5134.

Walkley, S.U., and Vanier, M.T. (2009). Secondary lipid accumulation in lysosomal disease. Biochim Biophys Acta *1793*, 726-736.

Wang, I.-F., Guo, B.-S., Liu, Y.-C., Wu, C.-C., Yang, C.-H., Tsai, K.-J., and Shen, C.-K.J. (2012). Autophagy activators rescue and alleviate pathogenesis of a mouse model with proteinopathies of the TAR DNA-binding protein 43. Proceedings of the National Academy of Sciences *109*, 15024-15029.

Wang, J.Z., Grundke-Iqbal, I., and Iqbal, K. (2007). Kinases and phosphatases and tau sites involved in Alzheimer neurofibrillary degeneration. Eur J Neurosci *25*, 59-68.

Wang, Y., and Mandelkow, E. (2012). Degradation of tau protein by autophagy and proteasomal pathways (Portland Press Limited).

Wang, Y., and Mandelkow, E. (2016). Tau in physiology and pathology. Nat Rev Neurosci *17*, 5-21.

Wang, Y., Martinez-Vicente, M., Kruger, U., Kaushik, S., Wong, E., Mandelkow, E.M., Cuervo, A.M., and Mandelkow, E. (2009). Tau fragmentation, aggregation and clearance: the dual role of lysosomal processing. Hum Mol Genet *18*, 4153-4170.

Wang, Z.F., Yin, J., Zhang, Y., Zhu, L.Q., Tian, Q., Wang, X.C., Li, H.L., and Wang, J.Z. (2010). Overexpression of tau proteins antagonizes amyloid-beta-potentiated apoptosis through mitochondria-caspase-3 pathway in N2a cells. J Alzheimers Dis *20*, 145-157.

Wei, P.F., Jin, P.P., Barui, A.K., Hu, Y., Zhang, L., Zhang, J.Q., Shi, S.S., Zhang, H.R., Lin, J., Zhou, W*., et al.* (2015). Differential ERK activation during autophagy induced by europium hydroxide nanorods and trehalose: Maximum clearance of huntingtin aggregates through combined treatment. Biomaterials *73*, 160-174.

Wei, Y., Pattingre, S., Sinha, S., Bassik, M., and Levine, B. (2008). JNK1-mediated phosphorylation of Bcl-2 regulates starvation-induced autophagy. Mol Cell *30*, 678-688.

Weichhart, T. (2018). mTOR as Regulator of Lifespan, Aging, and Cellular Senescence: A Mini-Review. Gerontology *64*, 127-134.

Wider, C., and Wszolek, Z.K. (2008). Rapidly progressive familial parkinsonism with central hypoventilation, depression and weight loss (Perry syndrome)--a literature review. Parkinsonism Relat Disord *14*, 1-7.

Wille, A., Gerber, A., Heimburg, A., Reisenauer, A., Peters, C., Saftig, P., Reinheckel, T., Welte, T., and Bühling, F. (2004). Cathepsin L is involved in cathepsin D processing and regulation of apoptosis in A549 human lung epithelial cells. Biological chemistry *385*, 665-670.

Wimo, A., Reed, C.C., Dodel, R., Belger, M., Jones, R.W., Happich, M., Argimon, J.M., Bruno, G., Novick, D., Vellas, B*., et al.* (2013). The GERAS Study: a prospective observational study of costs and resource use in community dwellers with Alzheimer's disease in three European countries--study design and baseline findings. J Alzheimers Dis *36*, 385-399.

Winslow, A.R., Chen, C.W., Corrochano, S., Acevedo-Arozena, A., Gordon, D.E., Peden, A.A., Lichtenberg, M., Menzies, F.M., Ravikumar, B., Imarisio, S*., et al.* (2010). alpha-Synuclein impairs macroautophagy: implications for Parkinson's disease. J Cell Biol *190*, 1023-1037.

Wirawan, E., Vande Walle, L., Kersse, K., Cornelis, S., Claerhout, S., Vanoverberghe, I., Roelandt, R., De Rycke, R., Verspurten, J., Declercq, W*., et al.* (2010). Caspase-mediated cleavage of Beclin-1 inactivates Beclin-1-induced autophagy and enhances apoptosis by promoting the release of proapoptotic factors from mitochondria. Cell Death Dis *1*, e18.

Wold, M.S., Lim, J., Lachance, V., Deng, Z., and Yue, Z. (2016). ULK1-mediated phosphorylation of ATG14 promotes autophagy and is impaired in Huntington's disease models. Mol Neurodegener *11*, 76.

Wolfe, D.M., Lee, J.h., Kumar, A., Lee, S., Orenstein, S.J., and Nixon, R.A. (2013). Autophagy failure in A lzheimer's disease and the role of defective lysosomal acidification. European Journal of Neuroscience *37*, 1949-1961.

Wong, E., and Cuervo, A.M. (2010). Autophagy gone awry in neurodegenerative diseases. Nat Neurosci *13*, 805-811.

Woodgett, J.R. (1991). cDNA cloning and properties of glycogen synthase kinase-3. Methods Enzymol *200*, 564-577.

Woods, A., Dickerson, K., Heath, R., Hong, S.P., Momcilovic, M., Johnstone, S.R., Carlson, M., and Carling, D. (2005). Ca2+/calmodulin-dependent protein kinase kinase-beta acts upstream of AMP-activated protein kinase in mammalian cells. Cell Metab *2*, 21-33.

Wray, S., Saxton, M., Anderton, B.H., and Hanger, D.P. (2008). Direct analysis of tau from PSP brain identifies new phosphorylation sites and a major fragment of N-terminally cleaved tau containing four microtubule-binding repeats. J Neurochem *105*, 2343-2352.

Wu, G., Sankaranarayanan, S., Wong, J., Tugusheva, K., Michener, M.S., Shi, X., Cook, J.J., Simon, A.J., and Savage, M.J. (2012). Characterization of plasma β -secretase (BACE1) activity and soluble amyloid precursor proteins as potential biomarkers for Alzheimer's disease. Journal of neuroscience research *90*, 2247-2258.

Wu, J., and Kaufman, R.J. (2006). From acute ER stress to physiological roles of the Unfolded Protein Response. Cell Death Differ *13*, 374-384.

Wyttenbach, A. (2004). Role of heat shock proteins during polyglutamine neurodegeneration: mechanisms and hypothesis. J Mol Neurosci *23*, 69-96.

Xiao, Q., Yan, P., Ma, X., Liu, H., Perez, R., Zhu, A., Gonzales, E., Burchett, J.M., Schuler, D.R., Cirrito, J.R*., et al.* (2014). Enhancing astrocytic lysosome biogenesis facilitates Abeta clearance and attenuates amyloid plaque pathogenesis. J Neurosci *34*, 9607-9620.

Xiao, Q., Yan, P., Ma, X., Liu, H., Perez, R., Zhu, A., Gonzales, E., Tripoli, D.L., Czerniewski, L., Ballabio, A*., et al.* (2015). Neuronal-Targeted TFEB Accelerates Lysosomal Degradation of APP, Reducing Abeta Generation and Amyloid Plaque Pathogenesis. J Neurosci *35*, 12137-12151.

Yamaguchi, H., Ishiguro, K., Uchida, T., Takashima, A., Lemere, C.A., and Imahori, K. (1996). Preferential labeling of Alzheimer neurofibrillary tangles with antisera for tau protein

kinase (TPK) I/glycogen synthase kinase-3 beta and cyclin-dependent kinase 5, a component of TPK II. Acta Neuropathol *92*, 232-241.

Yamaoka, L.H., Welsh-Bohmer, K.A., Hulette, C.M., Gaskell, P.C., Jr., Murray, M., Rimmler, J.L., Helms, B.R., Guerra, M., Roses, A.D., Schmechel, D.E.*, et al.* (1996). Linkage of frontotemporal dementia to chromosome 17: clinical and neuropathological characterization of phenotype. Am J Hum Genet *59*, 1306-1312.

Yang, D.S., Stavrides, P., Mohan, P.S., Kaushik, S., Kumar, A., Ohno, M., Schmidt, S.D., Wesson, D.W., Bandyopadhyay, U., Jiang, Y.*, et al.* (2011). Therapeutic effects of remediating autophagy failure in a mouse model of Alzheimer disease by enhancing lysosomal proteolysis. Autophagy *7*, 788-789.

Yao, X.Q., Zhang, X.X., Yin, Y.Y., Liu, B., Luo, D.J., Liu, D., Chen, N.N., Ni, Z.F., Wang, X., Wang, Q.*, et al.* (2011). Glycogen synthase kinase-3beta regulates Tyr307 phosphorylation of protein phosphatase-2A via protein tyrosine phosphatase 1B but not Src. Biochem J *437*, 335-344.

Yin, Y.Y., Liu, H., Cong, X.B., Liu, Z., Wang, Q., Wang, J.Z., and Zhu, L.Q. (2010). Acetyl-L-carnitine attenuates okadaic acid induced tau hyperphosphorylation and spatial memory impairment in rats. J Alzheimers Dis *19*, 735-746.

Yla-Anttila, P., Vihinen, H., Jokitalo, E., and Eskelinen, E.L. (2009). 3D tomography reveals connections between the phagophore and endoplasmic reticulum. Autophagy *5*, 1180-1185.

Yoneda, T., Imaizumi, K., Oono, K., Yui, D., Gomi, F., Katayama, T., and Tohyama, M. (2001). Activation of caspase-12, an endoplastic reticulum (ER) resident caspase, through tumor necrosis factor receptor-associated factor 2-dependent mechanism in response to the ER stress. J Biol Chem *276*, 13935-13940.

Yoshiyama, Y., Higuchi, M., Zhang, B., Huang, S.M., Iwata, N., Saido, T.C., Maeda, J., Suhara, T., Trojanowski, J.Q., and Lee, V.M. (2007). Synapse loss and microglial activation precede tangles in a P301S tauopathy mouse model. Neuron *53*, 337-351.

Yoshiyama, Y., Lee, V.M., and Trojanowski, J.Q. (2012). Therapeutic strategies for tau mediated neurodegeneration. J Neurol Neurosurg Psychiatry, jnnp-2012-303144.

Young, A.R., Narita, M., Ferreira, M., Kirschner, K., Sadaie, M., Darot, J.F., Tavare, S., Arakawa, S., Shimizu, S., Watt, F.M.*, et al.* (2009). Autophagy mediates the mitotic senescence transition. Genes Dev *23*, 798-803.

Yu, L., Chen, Y., and Tooze, S.A. (2018). Autophagy pathway: Cellular and molecular mechanisms. Autophagy *14*, 207-215.

Yu, W.H., Kumar, A., Peterhoff, C., Shapiro Kulnane, L., Uchiyama, Y., Lamb, B.T., Cuervo, A.M., and Nixon, R.A. (2004). Autophagic vacuoles are enriched in amyloid precursor

protein-secretase activities: implications for beta-amyloid peptide over-production and localization in Alzheimer's disease. Int J Biochem Cell Biol *36*, 2531-2540.

Yue, M., Hanna, A., Wilson, J., Roder, H., and Janus, C. (2011). Sex difference in pathology and memory decline in rTg4510 mouse model of tauopathy. Neurobiol Aging *32*, 590-603.

Zare-Shahabadi, A., Masliah, E., Johnson, G.V., and Rezaei, N. (2015). Autophagy in Alzheimer's disease. Rev Neurosci *26*, 385-395.

Zatloukal, K., Stumptner, C., Fuchsbichler, A., Heid, H., Schnoelzer, M., Kenner, L., Kleinert, R., Prinz, M., Aguzzi, A., and Denk, H. (2002). p62 Is a common component of cytoplasmic inclusions in protein aggregation diseases. Am J Pathol *160*, 255-263.

Zhang, C.E., Tian, Q., Wei, W., Peng, J.H., Liu, G.P., Zhou, X.W., Wang, Q., Wang, D.W., and Wang, J.Z. (2008). Homocysteine induces tau phosphorylation by inactivating protein phosphatase 2A in rat hippocampus. Neurobiol Aging *29*, 1654-1665.

Zhang, D., Wang, W., Sun, X., Xu, D., Wang, C., Zhang, Q., Wang, H., Luo, W., Chen, Y., and Chen, H. (2016). AMPK regulates autophagy by phosphorylating BECN1 at threonine 388. Autophagy *12*, 1447-1459.

Zhang, F., Su, B., Wang, C., Siedlak, S.L., Mondragon-Rodriguez, S., Lee, H.G., Wang, X., Perry, G., and Zhu, X. (2015). Posttranslational modifications of alpha-tubulin in alzheimer disease. Transl Neurodegener *4*, 9.

Zhang, H., Zhang, Y.-w., Chen, Y., Huang, X., Zhou, F., Wang, W., Xian, B., Zhang, X., Masliah, E., and Chen, Q. (2012). Appoptosin is a novel pro-apoptotic protein and mediates cell death in neurodegeneration. Journal of Neuroscience *32*, 15565-15576.

Zhang, L., Nosak, C., Sollazzo, P., Odisho, T., and Volchuk, A. (2014). IRE1 inhibition perturbs the unfolded protein response in a pancreatic beta-cell line expressing mutant proinsulin, but does not sensitize the cells to apoptosis. BMC Cell Biol *15*, 29.

Zhang, L., Sheng, R., and Qin, Z. (2009a). The lysosome and neurodegenerative diseases. Acta Biochim Biophys Sin (Shanghai) *41*, 437-445.

Zhang, X., Heng, X., Li, T., Li, L., Yang, D., Zhang, X., Du, Y., Doody, R.S., and Le, W. (2011). Long-term treatment with lithium alleviates memory deficits and reduces amyloid-β production in an aged Alzheimer's disease transgenic mouse model. Journal of Alzheimer's Disease *24*, 739-749.

Zhang, X.J., Chen, S., Huang, K.X., and Le, W.D. (2013). Why should autophagic flux be assessed? Acta Pharmacol Sin *34*, 595-599.

Zhang, Y., Tian, Q., Zhang, Q., Zhou, X., Liu, S., and Wang, J.Z. (2009b). Hyperphosphorylation of microtubule-associated tau protein plays dual role in neurodegeneration and neuroprotection. Pathophysiology *16*, 311-316.

Zhong, Y., Wang, Q.J., Li, X., Yan, Y., Backer, J.M., Chait, B.T., Heintz, N., and Yue, Z. (2009). Distinct regulation of autophagic activity by Atg14L and Rubicon associated with Beclin 1-phosphatidylinositol-3-kinase complex. Nat Cell Biol *11*, 468-476.

Zilka, N., Filipcik, P., Koson, P., Fialova, L., Skrabana, R., Zilkova, M., Rolkova, G., Kontsekova, E., and Novak, M. (2006). Truncated tau from sporadic Alzheimer's disease suffices to drive neurofibrillary degeneration in vivo. FEBS Lett *580*, 3582-3588.

.